Getting past the barrier:

New insights into the uptake mechanisms of cell-penetrating peptides and applications to the delivery of macromolecules

Proefschrift

ter verkrijging van de graad van doctor
aan de Radboud Universiteit Nijmegen
op gezag van de rector magnificus prof. mr. S.C.J.J. Kortmann,
volgens besluit van het college van decanen
in het openbaar te verdedigen op maandag 22 oktober 2012
om 10.30 uur precies

door
Wouter Peter Rita Verdurmen
geboren op 8 maart 1983
te Hulst

I

Promotor: Prof. dr. R.E. Brock

Copromotor: Mevr. dr. ir. Merel Adjobo-Hermans

Manuscriptcommissie:
Prof. dr. ir. J.C.M. van Hest
Prof. dr. O.C. Boerman
Mevr. prof. dr. A.S. Ulrich (Karlsruhe Institute of Technology)

Table of contents

IV

General introduction

1 General introduction

1.1 A dripping pipeline in drug discovery

The number of well-validated therapeutic targets has increased substantially over the last decade. However, despite considerably increased investments in drug research and development in the same period, the number of new targets that are exploited by drugs that make it to the market is still only three to four per year [1]. In addition, total numbers of drug approvals on a yearly basis have not improved. This last fact can be easily distilled from the number of FDA approved biologics license applications (i.e. biological medicines) and new molecular entities (i.e. small molecule drugs) from 1993 till 2011 (Figure 1.1). Regrettably, the combination of the increased investment and the relatively stable number of new drug approvals implies that the average cost per approved medicine has increased considerably [2, 3].
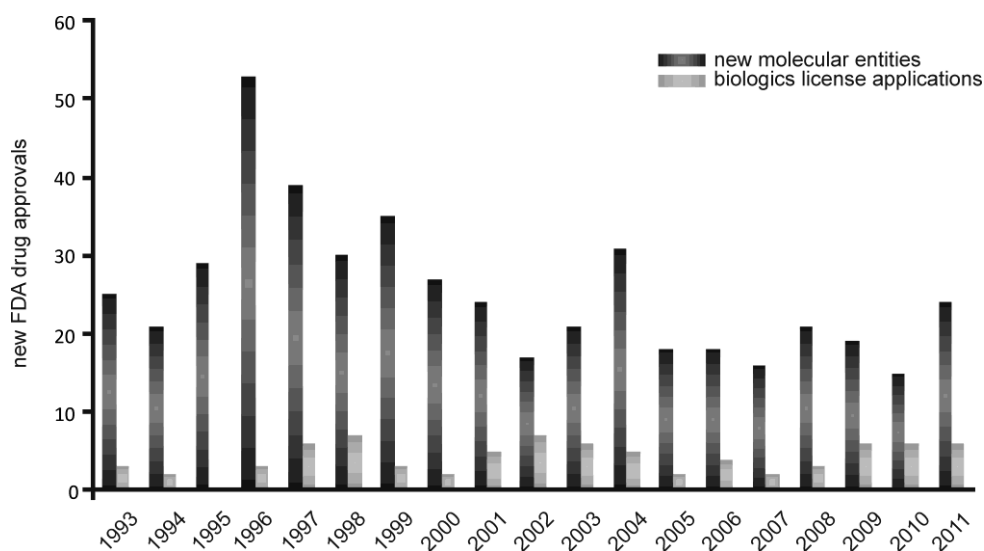
Figure 1.1. New FDA approvals from the period from 1993 to 2011. Adapted from Mullard [4].

Part of the reason for this reduced return on investment can be found in the strategies that are currently being applied in drug discovery. These strategies have changed several times over the course of modern history. Whereas initial discoveries were often the result of fortuitous accidents, such as Alexander Fleming's serendipitous discovery of penicillin, in more recent times drug discovery has been pursued through a wide array of strategies encompassing: high-throughput screening; structure-based design; fragment screening, i.e.

the testing of parts of molecules; and virtual screening, i.e. the computerized generation and testing of virtual libraries against drug target structures [5]. During the last couple of years, efforts to improve the quality of chemical compound libraries in order to make them more structurally diverse have also been growing. Moreover, there is also more interest in including compounds from the very beginning of the drug discovery process that have drug-like physicochemical properties [6]. In addition, the development of protein therapeutics has come to the fore and is playing an increasingly important role in medicine. Although protein therapeutics are on the market for a wide variety of indications and are used for their enzymatic or regulatory activity, their protein-binding activity or as protein vaccines, their use is largely restricted to extracellular applications [7]. Exceptions are few and include therapeutic enzymes that are trafficked to endocytic compartments via the mannose-6-phosphate receptors [8] and denileukin difitox (trade name: Ontak), a bacterial toxin of which the target resides in the cytosol [9].

Whereas these strategies have already proven their merits through the development of numerous clinically important drugs and will continue to play an important role in drug discovery in the foreseeable future, the number of targets that are amenable to being targeted by small molecules and/or extracellularly acting protein therapeutics remains low. For protein therapeutics, the reason is that the large pool of intracellular therapeutic targets has so far remained untapped. The bottleneck for developing small molecule drugs against many targets can be explained by the concept of so-called undruggable proteins, which are proteins that are extremely difficult to target with small molecules in a highly specific manner. Given the rise of protein therapeutics, the term undruggable proteins has become somewhat inadequate and/or fluid, but is still widely used because of its conceptual value. Frequently, undruggable proteins are involved in protein-protein interactions and do not contain any clefts or other structural characteristics that can be potently and specifically targeted by small molecules. Hence, most pharmaceutical companies aim to develop small molecule drugs against the same established and highly druggable targets, which represent only a small fraction of known therapeutically relevant proteins. Although precise numbers regarding druggable and undruggable proteins are continuously being disputed, an analysis by Hopkins and Groom showed that druggable proteins make up only a minor fraction of the disease-modifying genes (Figure 1.2) [10]. Of the estimated 600-1500 available human target proteins, an estimated 435 are being targeted by experimental, approved and withdrawn small molecule drugs [2]. Noteworthy is that attempts are being made to expand the number of targets that can be addressed with small molecules, mainly via targeting protein-protein interaction that exhibit hotspots, which are small regions of the protein

interaction surface that contribute most significantly towards the binding energy. Despite some notable successes in targeting protein-protein interactions with small molecules, these instances remain the exception rather than the rule [11].
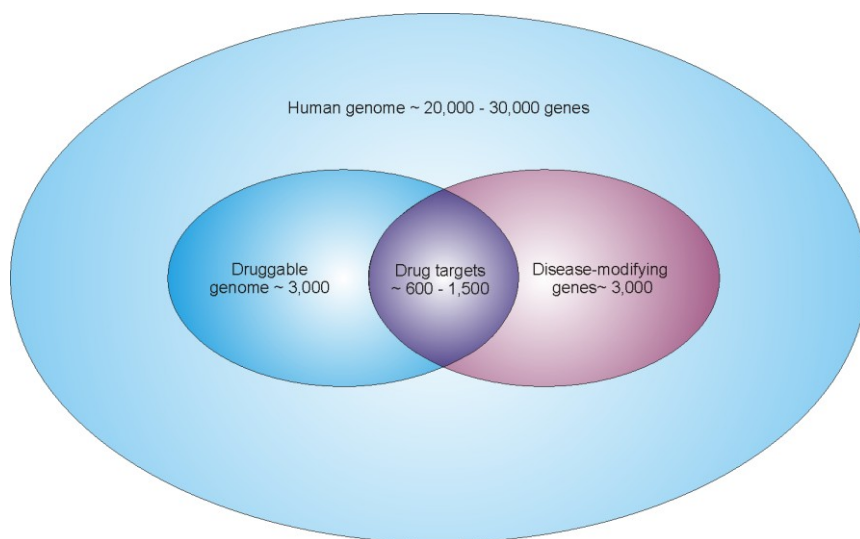
Figure 1.2. Schematic relationship between the human genome, the druggable genome for small molecule drugs, potential drug targets and the disease-modifying genes. Adapted from Hopkins and Groom with permission [10].

1.2   A growing need for drug delivery

Because of the downward trend in drug discovery, the classical drug discovery strategies and the development of protein therapeutics against extracellular targets are being complemented in several ways by novel drug development strategies. A prime category of strategies is the one that aims to develop biological molecules as medicines (biologics) against intracellular targets. An evident advantage of biologics against intracellular targets is that they can be directed towards a much larger pool of therapeutically relevant targets. Also important to note is that, in contrast to targeting undruggable proteins with small molecules, it is relatively simple to target these undruggable proteins in a highly specific manner with biologics.

  Biological molecules can target proteins either through direct binding, as in the case of peptides, antibodies and alternative protein scaffolds, or through modifying their splicing or

expression levels, as is the goal of most nucleotide-based strategies, of which siRNA is the most well-known example. Employing large biological molecules against intracellular therapeutic targets, however, means that attention has to be paid to their delivery, as these molecules are generally not able to reach their intracellular target *in vivo* in sufficient amounts in their naked and/or unmodified forms.

In this new way of designing therapeutic agents, the major bottleneck for the successful development of therapeutic strategies based on such biologicals is thus the adequate accumulation at the intracellular target site *in vivo,* where these molecules can accomplish their therapeutic task [12]. To achieve sufficient intracellular accumulation, several biological and/or synthetic hurdles must generally be overcome. Some of the issues, in particular those related to the biodistribution, are similar to those for extracellular protein therapeutics and have already been successfully addressed in various cases [7].

Biological hurdles include the first-pass effect, immune cell-mediated removal, aspecific cell- or tissue entry and the unduly recognition of specific blood vessel components [13]. Synthetic hurdles include the need to address poor solubility, poor stability and the tendency of proteins and/or nanosized drug delivery systems to aggregate *in vivo*. Naturally, the specific hurdles that are encountered depend on the choice of delivery route and the biomacromolecule in question. Even when sufficiently high concentrations can be reached at the target site, the minimization of side effects is also paramount to a successful development of a therapy. This usually depends not only strongly on the specificity of the delivery system, but also on the activity profile of the therapeutically active moiety.

So far, technologies for the intracellular delivery of biomacromolecules have been mainly applied as research tools to elucidate molecular mechanisms of disease *in cellulo*, but interest in these technologies as platforms for drugs that act inside the cell is on the rise [2, 13-16]. At present, numerous strategies for the development of intracellular next-generation medicines are being pursued, many of which are already in clinical trials [15, 17]. Some of these depend on carriers designed from scratch in the lab, such as polyplexes and liposomes for gene or siRNA delivery, whereas others are adapted designs of nature, such as viral vectors or bioengineered bacteria [16]. Other notable strategies for the development of next-generation intracellular therapeutics include the use of polymer-drug conjugates for improved small-molecule delivery [18], monoclonal antibodies for targeting of overexpressed receptors on cancer cells that lead to endocytic internalization [19] and gold nanoparticles for delivery of small molecules, genetic materials and/or proteins [20]. A special class of molecules, which has been used in combination with many of the

aforementioned constructs is the class of cell-penetrating peptides. These molecules, which have the capacity to efficiently induce the cellular uptake of cargo into the cell, are the central theme of this thesis and will now be introduced.

1.3   Cell-penetrating peptides

Approximately twenty years ago, remarkable observations were made for the homeodomain of Antennapedia from *Drosophila melanogaster* [21] and the Tat protein from the human immunodeficiency virus 1 [22]. Contrary to their expectations, the researchers found that, when added to cells externally, both proteins reached the cytosol by themselves. Later studies identified short peptide domains in these proteins that were responsible for this notable activity [23, 24]. These crucial observations turned out to be the birth of the research field of cell-penetrating peptides. As indicated, cell-penetrating peptides (CPPs) are now loosely defined as a class of peptides that have in common that they can induce the cellular uptake of membrane impermeable macromolecules, such as peptides, proteins, nucleic acids and nanoparticles. In general, CPPs are either cationic, amphipathic, or both [25]. Unlike receptor-targeting moieties such as transferrin, folate or antibodies, they do not require specific receptors for internalization that are typically only expressed in a subset of cell-types, making them capable of entering a wide variety of cell lines and primary cell types in a highly efficient manner. Given their capacity to facilitate cargo delivery, CPPs or CPP-like peptidomimetics have the potential to play an important role in the development of next-generation medicines with an intracellular activity. Their ability to do so is also reflected by the increasing number of CPP-based strategies that is in or heading towards clinical trials (for details see chapter 2).

### *1.1.1   Structural requirements of CPP for activity*

Several classes of CPPs can be distinguished, which have been extensively described elsewhere [25, 26]. Two of the most well-known classes of CPPs are the predominantly hydrophilic arginine-containing cell-penetrating peptides, of which Tat and penetratin are early members [23, 24], and the more membrane-active hydrophobic peptides, of which TP10 is the best investigated representative [27].

For the arginine-containing peptides, the CPP activity depends strongly on the presence of arginine residues, as replacing arginines by lysines, histidines or ornithines leads to far less efficient CPPs [28, 29]. These initial structure-activity relationship studies have also led to the identification of the highly efficient CPP nona-arginine. Currently, the

guanidinium moiety is considered to be of paramount importance for effective internalization, as attaching this group to various peptidomimetic, polymeric or carbohydrate-like structures results in efficient transporters [30]. For example, oligomers of β-amino acids exposing guanidinium groups via their side chains could be actively internalized [31, 32]. In addition, guanidinium groups have the ability to facilitate transport of dendritic polymers through liposomes and cellular membranes [33, 34]. Especially the combination of the delocalized positive charge and a bidentate hydrogen bond donor on the guanidinium group (Figure 1.3A-B) makes this chemical group ideally suited to interact with the negatively charged carboxylates, phosphates and sulfates that are present on many plasma membrane constituents including phospholipids, proteins and heparan sulfate proteoglycans [30]. Guanidinium groups are thought to promote uptake through direct interactions with these components, followed by an efficient partitioning into the lipophilic part of the bilayer.

Various research groups have also looked more closely at the conformational requirements of the backbone and to the attachment of guanidinium groups to the backbone for the CPP activity of these groups. It was found that linearity of the backbone is not a requirement for CPPs, as branched arginine-rich peptides are internalized even more efficiently [35], as are circularized peptides [36-39]. The improved internalization properties of several circularized arginine-rich CPPs has been ascribed to the spatial arrangement of their guanidinium groups [38]. According to this line of reasoning, restricting the conformational freedom increases the uptake efficiency. For the CPP hLF, derived from human lactoferrin, the effect of circularization is even more pronounced. Contrary to other CPPs that are active both in their linear and circular form, this CPP completely loses its activity when its ability to cyclize through formation of a disulfide bond is abolished [40]. Next to the effect of circularization, the conformational freedom of the guanidinium groups has also been investigated in different ways. For instance, Rothbard *et al.* increased backbone spacing via carbon spacers, thereby enhancing conformational freedom (Figure 1.3C) [41]. Remarkably, this enhancement also resulted in a considerably increased cellular uptake efficiency. These results are in contrast with the enhancing effects of circularized peptides, which are clearly restricted with respect to their conformational flexibility. A similar improvement of the efficiency was obtained when the conformational freedom of the guanidinium groups was increased by adding methylene in the side chains (Figure 1.3D) [42]. Given the contrary findings that so far have been obtained on the role of spatial positioning and/or conformational flexibility, this area of study will benefit from further investigations. Moreover, an increasing number of studies

now also show that the structure-activity relationship may be cell-type dependent to some degree, thereby even further increasing the complexity of the role of the guanidinium group in determining CPP-like properties (see also chapter 4).
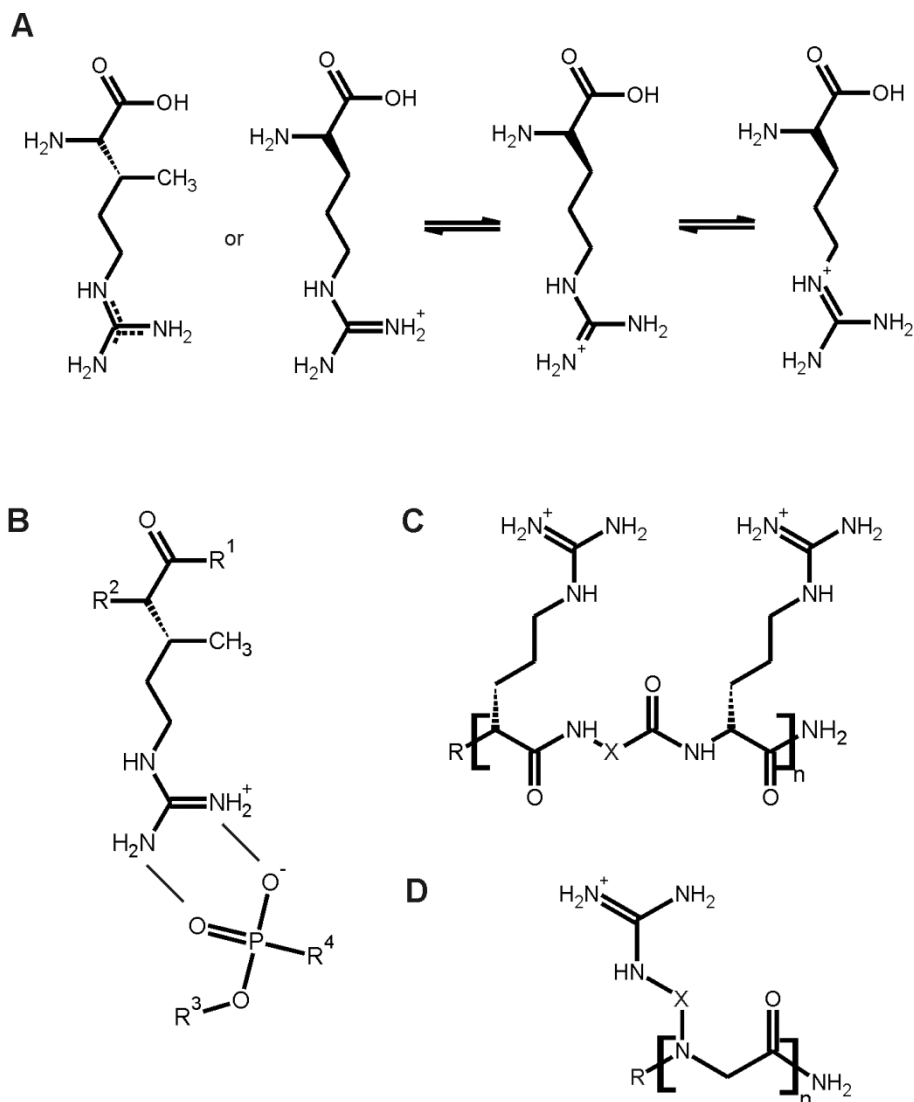
Figure 1.3. Relevant chemical structures and interactions. A) Illustration of delocalization of the charge of the arginine side-chain, which is important for efficient formation of bidentate hydrogen bonds. B) Example of a bidentate hydrogen bond between an arginine residue and a phosphate residue. C) Illustration of the increased backbone spacing in arginines used by Rothbard *et al.* [41]. D) Enhanced side chain spacing used by Wender *et al.*

in N-substituted peptides [38]. X indicates the position where carbon spacers of increasing chain length were introduced.

1.1.2   Interactions between cationic CPPs and glycosaminoglycans

The first interaction of a CPP when in contact with a mammalian cell is by necessity a physical interaction with a membrane-proximal structure. Candidate structures include carbohydrates, lipids and proteins, with which guanidinium groups can form bidentate hydrogen bonds (see previous section). The ability of cationic CPPs to interact with lipid headgroups and glycosaminoglycans (GAGs) has been detailed in many studies looking at the biophysics of such interactions (for a review, see ref [43]). Supporting evidence that cationic CPP have the ability to interact with GAGs also in biological systems has come from studies using HS or GAG-deficient CHO cells [44-46], from studies using heparinase treatments [40, 46, 47], from studies in which HS-carrying syndecans were overexpressed [45, 48] or from competition of CPP uptake through soluble GAGs [44, 49]. Interestingly, when comparing the affinities of cationic CPPs for lipid bilayers and glycosaminoglycans (GAGs), cationic CPPs had a much higher affinity for GAGs, making these molecules a much more likely candidate for the initial interaction with a biological membrane [50-52]. This idea is further supported by measurements of the apparent affinity of the CPP penetratin for membrane fragments of cells of WT and GAG-deficient CHO cells, which showed a greatly reduced affinity for the latter [53]. The interaction with GAGs on the plasma membrane is thought to be directly involved in the internalization. This means that it does not mediate a mere accumulation of peptide on the surface, which would passively increase the odds of an interaction with the real trigger for internalization. Instead, GAGs seem to actively respond to the presence of various well-known cationic CPPs, possibly through clustering [40, 51], which could facilitate the induction of uptake. For cationic CPPs, syndecans were recently shown to be directly involved in uptake [45, 48]. Interestingly, three cationic CPP, R8, Tat and penetratin, preferentially internalized via syndecan-4, which carries both heparan sulfate and chondroitin sulfate chains. It is at present unclear whether the preference is related to the glycosylation pattern or whether a direct interaction with a protein component on syndecan-4 is involved in this preference. A role for other GAGs besides HS is supported by a strong decrease in the internalization efficiency of several cationic CPP in GAG-deficient CHO cells as compared to HS-deficient CHO cells [45]. Although reports indicate that removal of HS chains reduces delivery of bioactive peptide nucleic acid [47], other reports dispute the existence of a productive GAG-dependent delivery route to the cytosol [54], indicating that cell or cargo-

type dependent differences may affect the productivity of GAG-dependent internalization. Peptide concentration may also affect their ability to exploit GAGs for improved cell entry, as GAG-dependency is reduced both at low [55] and at high peptide concentrations [39].

1.1.3 A three-step model for the cytosolic uptake of cationic CPPs

Under most conditions, cationic CPPs reach the cytosol via three sequential steps (Figure 1.4). First, they bind to heparan sulfates at the cell surface with low- or submicromolar affinity. Secondly, they trigger their own internalization into endosomes. It is not clear if the CPPs remain associated with HS chains, whether they must dissociate before entry, or whether both situations occur in parallel. Only in the third and final step do the peptides actually cross the membrane. In this translocation step, peptides leave the endosome and reach the cytosol in a process commonly referred to as endosomal escape. Endosomal escape is generally considered to be the rate-limiting step for cytosolic delivery. At present, it is unclear how arginine-rich peptides, which have a much higher affinity for HS chains compared to lipid membranes [43], manage to dissociate from HS chains before they can initiate the actual membrane translocation. The dissociation of CPPs from HS has indeed been implicated as a factor limiting their endosomal escape, as CPPs with an increased affinity for HS chains had a lower capacity to deliver splice-correcting steric-block oligonucleotides to the cytosol, which was independent of their ability to internalize via endocytosis [56]. An alternative hypothesis states that HS may be degraded in endosomal compartments, which would release CPPs in a manner that does not depend on the HS affinity [44]. Aside from endosomal escape, direct plasma membrane permeation has also been described both at high and at low concentrations for cationic CPPs [55, 57].

1.1.4 Endosomal escape of CPPs

Currently, the mechanisms of endosomal escape that distinct CPPs utilize are far from understood. Since CPPs with hydrophobic residues or hydrophobic cargo differ from exclusively arginine-rich peptides in their capacity to induce leakage and/or rupture of giant unilamellar vesicles [58], the existence of distinct escape mechanisms for different classes of CPPs is typically assumed. As indicated, the low affinity of arginine-rich peptides for lipid bilayers seems to be at odds with their ability to translocate these membranes [43]. Nevertheless, for both Tat and penetratin it has been shown that these peptides affect the membrane curvature and other properties of lipid bilayers in ways that support their capacity to directly translocate across such membranes [58-61]. The lipid

bis(monoacylglycero)phosphate, which is enriched in late endosomes, has been shown to enhance CPP-mediated membrane leakage, supporting the idea that specific lipids are required for efficient endosomal escape [62].

Interestingly, for Tat, its ability to translocate through membranes has been implicated in its ability to induce endocytosis. When conjugated to a macromolecular cargo, it has been proposed that Tat reaches through the plasma membrane to affect the properties of the cytoskeleton, mainly through inducing actin polymerization and bundle formation. This may then lead to a reduction of the number of actin-membrane contact points, which may in turn cause membrane rearrangements and endocytic processes that are reminiscent of macropinocytosis [57].

While there is thus supportive evidence for the ability of various CPPs to translocate through lipid bilayers, it is often unclear how large cargo is translocated across membranes. Most translocation mechanisms that have so far been hypothesized do not allow for large cargo to be transported across intact membranes. The well-described mechanisms that do allow for large cargo delivery, such as Pep-1 mediated protein delivery over the plasma membrane, typically involve CPPs with a high affinity for lipids and depend on local lipid bilayer pertubation for cargo delivery [63]. As such, the concentration range where these vectors are active but not damaging is expected to be small. The existence of temporary membrane-disturbances caused by CPPs is further underscored by the activation of the membrane repair response as described by Palm-Apergi *et al.* [64]. Nevertheless, numerous studies underscore the ability of CPPs to deliver large functional cargo into the cytosol with low toxicity, albeit with modest efficacy [14]. Therefore, one of the main open questions is how macromolecular cargo is translocated across membranes by these vectors and whether the translocation process leaves the endosomes intact or whether the membrane integrity has to be compromised for effective cytosolic delivery.
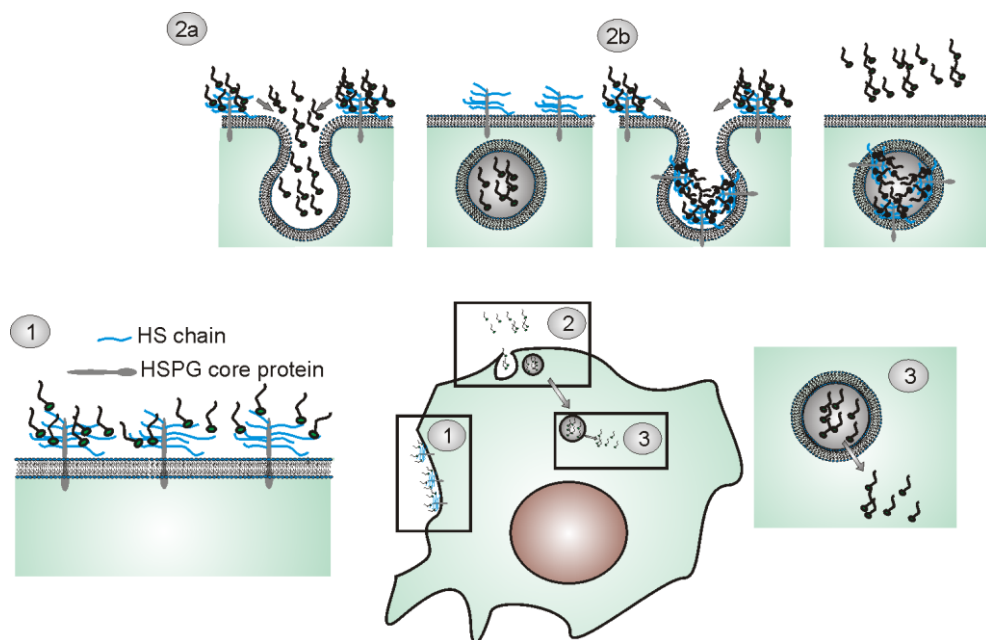
Figure 1.4. Three general steps in the internalization of cationic CPPs. 1) Cationic CPPs bind to HS chains. 2) Peptides trigger their internalization, either dissociating from the HS chains (a) or while remaining attached to them (b). It is not clear what the driving forces for dissociation are, though a very high affinity has been shown to negatively affect translocation [56]. 3) In the rate-limiting final step, peptides reach the cytosol after translocating through the endosomal membrane in a step called endosomal escape.

1.4   Outline of this thesis

The major aim of this thesis was to contribute to an in-depth understanding of the biology of CPPs. To this end, in **Chapter two,** the thesis starts by reviewing biological responses that are being elicited by biological drug delivery vehicles, with the emphasis on CPPs. The review summarizes the accumulating evidence that drug delivery vehicles are not simply Trojan horses until they reach a toxicity threshold. Instead, it is argued that many potential drug carriers affect cellular physiology in ways more subtle than large-scale membrane toxicity or massive oxidative stress resulting in necrosis and/or apoptosis. A prime example is the induction of ceramide formation by acid sphingomyelinase through CPPs (see also chapter 3).

Chapter three elucidates the molecular details of a previously described peptide translocation mechanism that occurs when peptide is present at concentrations of 10 μM or higher. As part of this uptake mechanism, local nucleation zones at the plasma membrane

arise at which peptide accumulates before it directly enters into the cytosol. A particular pharmacological profile of the import route led to the formulation of the hypothesis that this internalization depends on ceramide formation via acid sphingomyelinase. In this chapter, a set of experiments is presented that together strongly support this hypothesis.

In **chapter four**, differences in the internalization efficiency of CPPs composed of L- and/or D-amino acids are presented. Previously, no differences had been reported in the uptake of L- and D-CPPs, which had led to the paradigm that CPP internalization was independent of chirality. Here, it is shown that certain cell-types have a clear preference for L- over D-amino acid-containing peptides. In these cells, L-CPPs are internalized, whereas D-CPPs remain strongly membrane-bound, with D/L chimeric CPPs having a phenotype that depends on the number and position of the enantiomers in the peptide chain.

In **Chapter five**, the effect of epimerization of NMR labels at individual positions in the amphipathic CPP TP10 is investigated. The chapter shows that for this CPP, properties such as internalization efficiency, cytotoxicity and membrane binding depend strongly on whether there is an L- or a D-epimer introduced at a specific position. Remarkably, there is little correlation between the effect of these epimerizations on CPP properties and the effects on physicochemical characteristics of these peptides. Furthermore, despite the lack of a measurable affinity, heparan sulfate chains affect the binding of these peptides to the membrane and internalization.

Chapter six presents a protocol for the use of fluorescence correlation spectroscopy (FCS) to determine the intracellular stability of CPPs. The chapter not only presents a method for analyzing the intracellular stability using lysates of cells, but also provides a protocol for performing intracellular FCS to analyze the integrity of CPPs.

Chapter seven is the first chapter of this thesis that gives a concrete application of CPPs. The study deals with the delivery of artificial organelles, or polymersomes, by means of their conjugation with the CPP Tat. Specifically, this chapter illustrates how Tat-functionalized polymersomes loaded with enzymes are transported into various cell types through endocytosis. With horseradish peroxidase (HRP) as a model enzyme, enzymes remain active for much longer compared to what was previously observed for free enzymes. This indicates that polymersome-mediated enzyme delivery protects enzymes against intracellular degradation.

Chapter eight describes a modular leucine zipper-based strategy for cellular delivery of proteins. In this application, Tat and the reporter protein GFP are coupled to two complementary leucine zipper strands. Only in the presence of both modules, delivery of GFP into the cells is accomplished. The modular nature of this strategy indicates that this

system can easily be modified for the delivery of a wide range of other proteins or be used in conjunction with other CPPs and/or targeting agents.

1.5   References

[1] A.I. Graul, L. Revel, M. Tell, E. Rosa, E. Cruces, Overcoming the obstacles in the pharma/biotech industry: 2009 update, Drug News Perspect, 23 (2010) 48-63.

[2] M. Rask-Andersen, M.S. Almen, H.B. Schioth, Trends in the exploitation of novel drug targets, Nat Rev Drug Discov, 10 (2011) 579-590.

[3] J.W. Scannell, A. Blanckley, H. Boldon, B. Warrington, Diagnosing the decline in pharmaceutical R&D efficiency, Nat Rev Drug Discov, 11 (2012) 191-200.

[4] A. Mullard, 2011 FDA drug approvals, Nat Rev Drug Discov, 11 (2012) 91-94.

[5] R. Macarron, M.N. Banks, D. Bojanic, D.J. Burns, D.A. Cirovic, T. Garyantes, D.V. Green, R.P. Hertzberg, W.P. Janzen, J.W. Paslay, U. Schopfer, G.S. Sittampalam, Impact of high-throughput screening in biomedical research, Nat Rev Drug Discov, 10 (2011) 188-195.

[6] M.M. Hann, T.I. Oprea, Pursuing the leadlikeness concept in pharmaceutical research, Curr Opin Chem Biol, 8 (2004) 255-263.

[7] B. Leader, Q.J. Baca, D.E. Golan, Protein therapeutics: a summary and pharmacological classification, Nat Rev Drug Discov, 7 (2008) 21-39.

[8] M. Rohrbach, J.T. Clarke, Treatment of lysosomal storage disorders : progress with enzyme replacement therapy, Drugs, 67 (2007) 2697-2716.

[9] D.P. Williams, C.E. Snider, T.B. Strom, J.R. Murphy, Structure/function analysis of interleukin-2-toxin (DAB486-IL-2). Fragment B sequences required for the delivery of fragment A to the cytosol of target cells, J Biol Chem, 265 (1990) 11885-11889.

[10] A.L. Hopkins, C.R. Groom, The druggable genome, Nat Rev Drug Discov, 1 (2002) 727-730.

[11] A. Mullard, Protein-protein interaction inhibitors get into the groove, Nat Rev Drug Discov, 11 (2012) 173-175.

[12] R. Langer, Drug delivery. Drugs on target, Science, 293 (2001) 58-59.

[13] H. Hillaireau, P. Couvreur, Nanocarriers' entry into the cell: relevance to drug delivery, Cell Mol Life Sci, 66 (2009) 2873-2896.

[14] P. Jarver, I. Mager, U. Langel, In vivo biodistribution and efficacy of peptide mediated delivery, Trends Pharmacol Sci, 31 (2010) 528-535.

[15] S.T. Stern, J.B. Hall, L.L. Yu, L.J. Wood, G.F. Paciotti, L. Tamarkin, S.E. Long, S.E. McNeil, Translational considerations for cancer nanomedicine, J Control Release, 146 (2010) 164-174.

[16] J.W. Yoo, D.J. Irvine, D.E. Discher, S. Mitragotri, Bio-inspired, bioengineered and biomimetic drug delivery carriers, Nat Rev Drug Discov, 10 (2011) 521-535.

[17] T. Lammers, F. Kiessling, W.E. Hennink, G. Storm, Drug targeting to tumors: Principles, pitfalls and (pre-) clinical progress, J Control Release, (2011). In press

[18] R. Duncan, M.J. Vicent, Do HPMA copolymer conjugates have a future as clinically useful nanomedicines? A critical overview of current status and future opportunities, Adv Drug Deliv Rev, 62 (2010) 272-282.

[19] J. Majidi, J. Barar, B. Baradaran, J. Abdolalizadeh, Y. Omidi, Target therapy of cancer: implementation of monoclonal antibodies and nanobodies, Hum Antibodies, 18 (2009) 81-100.

[20] S. Rana, A. Bajaj, R. Mout, V.M. Rotello, Monolayer coated gold nanoparticles for delivery applications, Adv Drug Deliv Rev, (2011). In press

[21] A. Joliot, C. Pernelle, H. Deagostini-Bazin, A. Prochiantz, Antennapedia homeobox peptide regulates neural morphogenesis, Proc Natl Acad Sci U S A, 88 (1991) 1864-1868.

[22] A.D. Frankel, C.O. Pabo, Cellular uptake of the tat protein from human immunodeficiency virus, Cell, 55 (1988) 1189-1193.

[23] D. Derossi, A.H. Joliot, G. Chassaing, A. Prochiantz, The third helix of the Antennapedia homeodomain translocates through biological membranes, J Biol Chem, 269 (1994) 10444-10450.

[24] E. Vives, P. Brodin, B. Lebleu, A truncated HIV-1 Tat protein basic domain rapidly translocates through the plasma membrane and accumulates in the cell nucleus, J Biol Chem, 272 (1997) 16010-16017.

[25] R. Fischer, M. Fotin-Mleczek, H. Hufnagel, R. Brock, Break on through to the other side-biophysics and cell biology shed light on cell-penetrating peptides, Chembiochem, 6 (2005) 2126-2142.

[26] M. Magzoub, A. Graslund, Cell-penetrating peptides: [corrected] from inception to application, Q Rev Biophys, 37 (2004) 147-195.

[27] U. Soomets, M. Lindgren, X. Gallet, M. Hallbrink, A. Elmquist, L. Balaspiri, M. Zorko, M. Pooga, R. Brasseur, U. Langel, Deletion analogues of transportan, Biochim Biophys Acta, 1467 (2000) 165-176.

[28] H.L. Amand, K. Fant, B. Norden, E.K. Esbjorner, Stimulated endocytosis in penetratin uptake: effect of arginine and lysine, Biochem Biophys Res Commun, 371 (2008) 621-625.

[29] D.J. Mitchell, D.T. Kim, L. Steinman, C.G. Fathman, J.B. Rothbard, Polyarginine enters cells more efficiently than other polycationic homopolymers, J Pept Res, 56 (2000) 318-325.

[30] P.A. Wender, W.C. Galliher, E.A. Goun, L.R. Jones, T.H. Pillow, The design of guanidinium-rich transporters and their internalization mechanisms, Adv Drug Deliv Rev, 60 (2008) 452-472.

[31] N. Umezawa, M.A. Gelman, M.C. Haigis, R.T. Raines, S.H. Gellman, Translocation of a beta-peptide across cell membranes, J Am Chem Soc, 124 (2002) 368-369.

[32] T.B. Potocky, J. Silvius, A.K. Menon, S.H. Gellman, HeLa cell entry by guanidinium-rich beta-peptides: importance of specific cation-cell surface interactions, Chembiochem, 8 (2007) 917-926.

[33] A. Pantos, I. Tsogas, C.M. Paleos, Guanidinium group: a versatile moiety inducing transport and multicompartmentalization in complementary membranes, Biochim Biophys Acta, 1778 (2008) 811-823.

[34] T.A. Theodossiou, A. Pantos, I. Tsogas, C.M. Paleos, Guanidinylated dendritic molecular transporters: prospective drug delivery systems and application in cell transfection, ChemMedChem, 3 (2008) 1635-1643.

[35] S. Futaki, I. Nakase, T. Suzuki, Z. Youjun, Y. Sugiura, Translocation of branched-chain arginine peptides through cell membranes: flexibility in the spatial disposition of positive charges in membrane-permeable peptides, Biochemistry, 41 (2002) 7925-7930.

[36] S. Aubry, F. Burlina, E. Dupont, D. Delaroche, A. Joliot, S. Lavielle, G. Chassaing, S. Sagan, Cell-surface thiols affect cell entry of disulfide-conjugated peptides, FASEB J, 23 (2009) 2956-2967.

[37] L. Cascales, S.T. Henriques, M.C. Kerr, Y.H. Huang, M.J. Sweet, N.L. Daly, D.J. Craik, Identification and characterization of a new family of cell penetrating peptides: Cyclic cell penetrating peptides, J Biol Chem, 286 (2011) 36932-36943.

[38] G. Lattig-Tunnemann, M. Prinz, D. Hoffmann, J. Behlke, C. Palm-Apergi, I. Morano, H.D. Herce, M.C. Cardoso, Backbone rigidity and static presentation of guanidinium groups increases cellular uptake of arginine-rich cell-penetrating peptides, Nat Commun, 2 (2011) 453.

[39] D. Mandal, A. Nasrolahi Shirazi, K. Parang, Cell-penetrating homochiral cyclic peptides as nuclear-targeting molecular transporters, Angew Chem Int Ed Engl, 50 (2011) 9633-9637.

[40] F. Duchardt, I.R. Ruttekolk, W.P. Verdurmen, H. Lortat-Jacob, J. Burck, H. Hufnagel, R. Fischer, M. van den Heuvel, D.W. Lowik, G.W. Vuister, A. Ulrich, M. de Waard, R.

Brock, A cell-penetrating peptide derived from human lactoferrin with conformation-dependent uptake efficiency, J Biol Chem, 284 (2009) 36099-36108.

[41] J.B. Rothbard, E. Kreider, C.L. VanDeusen, L. Wright, B.L. Wylie, P.A. Wender, Arginine-rich molecular transporters for drug delivery: role of backbone spacing in cellular uptake, J Med Chem, 45 (2002) 3612-3618.

[42] P.A. Wender, D.J. Mitchell, K. Pattabiraman, E.T. Pelkey, L. Steinman, J.B. Rothbard, The design, synthesis, and evaluation of molecules that enable or enhance cellular uptake: peptoid molecular transporters, Proc Natl Acad Sci U S A, 97 (2000) 13003-13008.

[43] A. Ziegler, Thermodynamic studies and binding mechanisms of cell-penetrating peptides with lipids and glycosaminoglycans, Adv Drug Deliv Rev, 60 (2008) 580-597.

[44] S.M. Fuchs, R.T. Raines, Pathway for polyarginine entry into mammalian cells, Biochemistry, 43 (2004) 2438-2444.

[45] I. Nakase, A. Tadokoro, N. Kawabata, T. Takeuchi, H. Katoh, K. Hiramoto, M. Negishi, M. Nomizu, Y. Sugiura, S. Futaki, Interaction of arginine-rich peptides with membrane-associated proteoglycans is crucial for induction of actin organization and macropinocytosis, Biochemistry, 46 (2007) 492-501.

[46] J.P. Richard, K. Melikov, H. Brooks, P. Prevot, B. Lebleu, L.V. Chernomordik, Cellular uptake of unconjugated TAT peptide involves clathrin-dependent endocytosis and heparan sulfate receptors, J Biol Chem, 280 (2005) 15300-15306.

[47] P. Lundin, H. Johansson, P. Guterstam, T. Holm, M. Hansen, U. Langel, E.L.A. S, Distinct uptake routes of cell-penetrating peptide conjugates, Bioconjug Chem, 19 (2008) 2535-2542.

[48] T. Letoha, A. Keller-Pinter, E. Kusz, C. Kolozsi, Z. Bozso, G. Toth, C. Vizler, Z. Olah, L. Szilak, Cell-penetrating peptide exploited syndecans, Biochim Biophys Acta, 1798 (2010) 2258-2265.

[49] N. Ram, S. Aroui, E. Jaumain, H. Bichraoui, K. Mabrouk, M. Ronjat, H. Lortat-Jacob, M. De Waard, Direct peptide interaction with surface glycosaminoglycans contributes to the cell penetration of maurocalcine, J Biol Chem, 283 (2008) 24274-24284.

[50] E. Goncalves, E. Kitas, J. Seelig, Structural and thermodynamic aspects of the interaction between heparan sulfate and analogues of melittin, Biochemistry, 45 (2006) 3086-3094.

[51] A. Ziegler, X.L. Blatter, A. Seelig, J. Seelig, Protein transduction domains of HIV-1 and SIV TAT interact with charged lipid vesicles. Binding mechanism and thermodynamic analysis, Biochemistry, 42 (2003) 9185-9194.

[52] A. Ziegler, J. Seelig, Interaction of the protein transduction domain of HIV-1 TAT with heparan sulfate: binding mechanism and thermodynamic parameters, Biophys J, 86 (2004) 254-263.

[53] I.D. Alves, C. Bechara, A. Walrant, Y. Zaltsman, C.Y. Jiao, S. Sagan, Relationships between membrane binding, affinity and cell internalization efficacy of a cell-penetrating peptide: penetratin as a case study, PLoS One, 6 (2011) e24096.

[54] J.M. Gump, R.K. June, S.F. Dowdy, Revised role of glycosaminoglycans in TAT protein transduction domain-mediated cellular transduction, J Biol Chem, 285 (2010) 1500-1507.

[55] C.Y. Jiao, D. Delaroche, F. Burlina, I.D. Alves, G. Chassaing, S. Sagan, Translocation and endocytosis for cell-penetrating peptide internalization, J Biol Chem, 284 (2009) 33957-33965.

[56] S. Abes, H.M. Moulton, P. Clair, P. Prevot, D.S. Youngblood, R.P. Wu, P.L. Iversen, B. Lebleu, Vectorization of morpholino oligomers by the (R-Ahx-R)4 peptide allows efficient splicing correction in the absence of endosomolytic agents, J Control Release, 116 (2006) 304-313.

[57] F. Duchardt, M. Fotin-Mleczek, H. Schwarz, R. Fischer, R. Brock, A comprehensive model for the cellular uptake of cationic cell-penetrating peptides, Traffic, 8 (2007) 848-866.

[58] A. Mishra, V.D. Gordon, L. Yang, R. Coridan, G.C. Wong, HIV TAT forms pores in membranes by inducing saddle-splay curvature: potential role of bidentate hydrogen bonding, Angew Chem Int Ed Engl, 47 (2008) 2986-2989.

[59] A. Lamaziere, O. Maniti, C. Wolf, O. Lambert, G. Chassaing, G. Trugnan, J. Ayala-Sanmartin, Lipid domain separation, bilayer thickening and pearling induced by the cell penetrating peptide penetratin, Biochim Biophys Acta, 1798 (2010) 2223-2230.

[60] A. Lamaziere, C. Wolf, O. Lambert, G. Chassaing, G. Trugnan, J. Ayala-Sanmartin, The homeodomain derived peptide Penetratin induces curvature of fluid membrane domains, PLoS One, 3 (2008) e1938.

[61] A. Mishra, G.H. Lai, N.W. Schmidt, V.Z. Sun, A.R. Rodriguez, R. Tong, L. Tang, J. Cheng, T.J. Deming, D.T. Kamei, G.C. Wong, Translocation of HIV TAT peptide and analogues induced by multiplexed membrane and cytoskeletal interactions, Proc Natl Acad Sci U S A, 108 (2011) 16883-16888.

[62] S.T. Yang, E. Zaitseva, L.V. Chernomordik, K. Melikov, Cell-penetrating peptide induces leaky fusion of liposomes containing late endosome-specific anionic lipid, Biophys J, 99 (2010) 2525-2533.

[63] S.T. Henriques, M.A. Castanho, Translocation or membrane disintegration? Implication of peptide-membrane interactions in pep-1 activity, J Pept Sci, 14 (2008) 482-487.

[64] C. Palm-Apergi, A. Lorents, K. Padari, M. Pooga, M. Hallbrink, The membrane repair response masks membrane disturbances caused by cell-penetrating peptide uptake, FASEB J, 23 (2009) 214-223.

Biological responses to cationic peptides and drug carriers

Wouter P.R. Verdurmen and Roland Brock

2 Biological responses towards cationic peptides and drug carriers

Adapted from: **Trends in Pharmacological Sciences** 2011 **32**: 116-24

Wouter P.R. Verdurmen, Roland Brock

Department of Biochemistry, Nijmegen Centre for Molecular Life Sciences, Radboud University Nijmegen Medical Centre, The Netherlands

Abstract

In drug development, major resources are invested into the development of cellular delivery systems to increase the effectiveness of a large array of potential therapeutics, such as proteins and oligonucleotides. These carriers comprise cell-penetrating peptides, cationic lipids and cationic polymers. In recent years, evidence has been accumulating that these carriers do not only act as mere pharmacokinetic modifiers, but interfere with cellular processes in various ways. In this review we present an overview of the biological side effects associated with carrier systems. The focus will be on cell-penetrating peptides (CPPs), which have been explored for a diverse set of cargos. Reported activities range from an induction of receptor internalization to the generation of reactive oxygen species. Ultimately, cell-penetrating molecules with such biological side effects might evolve into new bioactive agents that combine delivery capacity and pharmacophore in a single molecular entity. First examples for such molecules will be presented.

2.1 Introduction

As research provides an ever greater understanding of disease at a molecular level, the number of potential therapeutic targets is increasing steadily. The challenge is to translate these targets into therapies [1]. Progress with classical, small-molecule based drug development has been slow. Underlying reasons include the need to target protein-protein interactions, reach targets inside cells and the difficulty to achieve specificity [2, 3].

Therefore, attention is shifting towards alternative approaches that enable a rapid rational design of active and specific molecules. Oligonucleotides, including siRNA, proteins and peptidomimetics are prominent examples [4-6]. However, for these molecules, a rapid and rational design is set off by poor bioavailability, which prevents them from

reaching their intended targets *in vivo*. The successful implementation of these molecules into new therapies therefore critically depends on delivery and targeting strategies [7], which generally involve the use of peptides, proteins, lipids, or polymers. Although the specific molecular design underlying these delivery strategies may vary in detail, the incorporation of positive charge is a common denominator [8-10]. The positive charge mediates the interaction with negatively charged sugar moieties and lipids on the outer leaflet of the plasma membrane which promotes cellular uptake.

Ideally, these carriers act exclusively as pharmacokinetic modifiers with no biological activity of their own. However, an increasing body of evidence indicates that these carriers may influence cellular activity in multiple ways [11-19]. Testing of carriers should therefore extend beyond mere cytotoxicity and delivery efficiency. In this review, we will therefore summarize recent results on biological responses towards cationic carriers. The focus will be on cationic cell-penetrating peptides (CPPs) and related transporters.

Research into the biological side effects of cationic and amphiphilic membrane-active peptides has a long tradition in the area of peptide toxins, with melittin and mastoparan being the paradigmatic examples. Extensive studies on structure-activity relationships have been conducted for induction of mast cell degranulation [20] and hemolysis [21]. Mast cell degranulation has been related to the interaction of the positive charges of the cationic peptides with sialic acids present on the plasma membrane and a G protein-coupled receptor (GPCR)-independent G-protein activation [20].

Many membrane-active peptides also have cell-penetrating activity. Therefore, it is difficult to make a clear distinction between both types of peptides [22]. CPPs might be considered membrane-active peptides with little toxicity. As a consequence, for CPPs research has focused on mechanisms of uptake and biomedical applications, rather than potential side effects. Especially because of the other activities that were reported to occur in the absence of acute toxicity, they may be very relevant in future clinical applications. In this review, we will present an overview of the *in vitro* and *in vivo* biological responses that have been reported for the interaction of cells and organisms with cationic carrier systems and especially cationic CPP. Frequently, these responses directly relate to uptake. Finally, we will provide examples of CPPs that have an intended intrinsic biological activity.

2.2   Cell-Penetrating Peptides: Promising Molecules For The Intracellular Delivery of Therapeutics

CPPs are characterized by their ability to promote the receptor-independent cellular uptake of membrane-impermeable macromolecules, such as peptides, proteins, nucleic acids and

nanoparticles [23]. CPP contain fewer than 30 amino acids and are mostly cationic, or cationic and amphipathic. Cationic and amphipathic CPP show some differences in their internalization mechanisms [24] which may be attributed to the ability of amphipathic CPP to more directly interact with membrane lipids [25]. Early CPP include the *Drosophilia melanogaster*-derived penetratin [26], the protein transduction domain from the tat protein [27] and the more hydrophobic CPP transportan, which is a chimeric molecule designed from parts of the neuropeptide galanin and the wasp venom mastoparan [28].

Cellular internalization is observed for virtually all cells, albeit with different efficiencies that depend on the CPP, the cargo and the cell type [29, 30]. Especially for large molecular weight complexes, internalization occurs mainly through endocytosis. Therefore, even though the ultimate target compartments typically are cytosol and nucleus, in many (if not most) cases the major part of the imported cargo is trafficked to the endolysosomal compartment [24]. Endocytic pathways that have been reported to contribute to CPP uptake include macropinocytosis and the clathrin-dependent and caveolae-dependent pathways [31]. It has been shown that a given CPP is not necessarily restricted to only one import pathway. Instead, CPPs might exploit multiple entry routes at the same time [32].

2.2.1   *Biological interactions involved in the internalization of cationic CPPs*

A CPP approaching a cell first encounters glycosaminoglycans (GAGs), negatively charged carbohydrate polymers on the surface of the plasma membrane. It is therefore no surprise that GAGs have been implicated in the cellular uptake of CPPs [33]. Affinity measurements typically show *Kd* values between 100 nM and 1 μM for the interaction of cationic peptides with GAGs, which provides evidence for their role as primary cellular interaction partner [34].

Conflicting evidence has been obtained on whether interaction with GAGs also triggers import or not. The role of GAGs as a direct trigger for uptake has been supported by a report from Letoha *et al*, who found that the proteoglycan syndecan-4 bound the cationic CPP tat, penetratin and octaarginine and facilitated their internalization in a PKC α-dependent manner [35]. Conversely, a role of GAGs in CPP import has been questioned entirely by research showing only minor differences in cellular delivery of a Tat-Cre recombinase into GAG-deficient or wild type cells [36].

In addition to studies addressing interactions with GAGs, research on lipid bilayer model systems has given ample indications for the potential of CPPs to interact with lipids,

though affinities are substantially lower [34]. It has been shown that cationic CPPs directly affect lipid bilayer organization in model systems. Disturbance of bilayer organization is a major requirement for uptake-related membrane processes such as fusion, fission or pore formation [37, 38]. In these processes, changes in membrane curvature are involved [37]. As an example, the CPP tat was found to induce negative curvature in artificial vesicles [39], which is a necessary condition for pore formation, dimple formation in caveolae-based endocytosis and for membrane protrusions in macropinocytosis [37]. Induction of vesicle fusion has also been observed for cationic CPP [40].

To this point structure-activity relationships of CPPs have been explored in rather simplistic model systems. Even though these systems have succeeded in identifying lipid composition, transbilayer potential and vesicle size as important determinants for peptide translocation, even the most complex of these models has failed to account for cellular responses that dynamically remodel the lipid composition.

2.3 Biological Activity of Cationic CPPs

Cationic CPPs were originally considered as 'Trojan Horse' delivery vehicles that enter cells without eliciting a cellular response [41]. However, CPPs can induce a wide range of side effects that may be more subtle than cell death. These side effects have been related to the uptake itself as well as to interactions inside the cell.

2.3.1 Effects of cationic CPPs on membrane integrity and cell viability

Cationic CPPs (for peptide sequences, see table 2.1) have a sound track record with respect to toxicity, both *in vitro* and *in vivo*. *In vitro*, the low toxicity holds for both acute membrane toxicity (as determined by a variety of membrane integrity assays) and for cell viability (as determined mainly by assays probing for mitochondrial activity) [32, 42, 43]. Tat and penetratin (with or without cargo) at concentrations of up to 50 μM had only minor effects on cell proliferation and membrane integrity [42]. By comparison, the more amphipathic CPPs MAP and TP10 affect proliferation at lower concentrations and show considerable membrane destabilization. For example, MAP and TP10 induce lactate dehydrogenase leakage at concentrations of 10 μM [42, 43].

At the high concentration of 50 μM, little hemolysis was observed for penetratin and none for tat, further supporting the lack of acute membrane toxicity for cationic CPPs [43]. Although amphipathic peptides were somewhat more hemolytic, none of the tested CPPs

had a hemolytic activity comparable to the one of membrane-active peptides such a mastoparan, which clearly distinguishes CPPs from other membrane-active peptides [43].

2.3.2 *Novel methods to detect subtle side effects of cationic CPP*

Now that cationic CPP are moving steadily towards preclinical and clinical development, the traditional toxicity analysis methods are being complemented with "-omics" assays that globally profile cell activities. These assays are more sensitive in profiling potential side effects of CPP-based therapeutics than the traditional assays. Consistent with results on membrane integrity and viability, a toxicity analysis based on metabolomic profiling also demonstrated that amphipathic peptides such as TP affect cellular metabolism at concentrations of 5 to 10 μM, whereas the cationic CPP penetratin, tat and nonaarginine had little effect at 10 μM [44]. No specific enzymes were identified as being directly affected by TP. Instead, reduced levels of GSH, glucose, purines, pyrimidines and related molecules led the authors to hypothesize that the cells countered oxidative stress caused by the peptide [44].

A transcriptome analysis for H1299 lung adenocarcinoma cells treated with a tat-conjugated dsRNA-binding domain (DRBD) indicated very few changes both after 12 h and 24 h [45]. None of the upregulated or downregulated genes clustered into a specific genetic pathway. Similarly, a transcriptome analysis in HeLa cells found that several unrelated genes were affected by penetratin, while for tat hardly any effects were observed [46].

To detect possible subtle side effects of CPPs on the immune system, Kuo et al. performed genome-wide profiling of gene expression with U-937 macrophages treated with octaarginine [47]. Although these researchers found an increase in the expression of several immune-related genes, this response did not result in cytokine release or reduced viability for concentrations of up to 40 μM. They did, however, find elevated superoxide levels 30 min after peptide addition, which normalized after 8 hours [47].

Table 2.1 Sequences of cationic peptides

Peptide	Sequence	Class	Origin	Reference
R9	RRRRRRRRR-NH$_2$	Cationic CPP	N/A	[48]
TAT	C-(acetamidomethyl) GRKKRRQRRRPPQQ	Cationic CPP	HIV TAT protein (48-60)	[27]
hLF	KCFQWQRNMRKVRGPP VSCIKR-NH$_2$	Cationic CPP	Human lactoferrin	[49]

(RXR)4	(R-Ahx[a]-R)4-PMO	Cationic CPP	N/A	[50]
Penetratin	RQIKIWFQNRRMKWKK	Cationic/ Amphipathic CPP	Antennapedia homeodomain	[26]
Transportan	GWTLNSAGYLLGKINLK ALAALAKKIL-NH$_2$	Amphipathic CPP	Galanin and mastoparan	[28]
TP10	AGYLLGKINLKALAALA KKIL-NH$_2$	Amphipathic CPP	Galanin and mastoparan	[51]
Maurocalcine	GDCLPHLKLCKENKDCC SKKCKRRGTNIEKRCR-COOH	Bioactive CPP	Scorpion venom	[52]
Vasostatin 1	MRSAAVLALLLCAGQV TALPVNSPMNKGDTEV MKCIVEVISDTLSKPSPM PVSQECFETLRGDERILSI LRHQNLL-COOH	Bioactive CPP	Vasostatin 1 (1-76)	[53]
p14ARF	MVRRFLVTLRIRRACGP PRVRV-NH$_2$	Bioactive CPP	p14ARF protein (1-22)	[54]
M511	FLGKKFKKYFLQLLK-NH$_2$	Bioactive CPP	Rodent angiotensin receptor	[55]
TBX2	GKMADWFRQTLLKKPK KRPNSPESTLQLRD ATPGGAIVS-NH$_2$	Bioactive CPP	Toll-receptor 4 adaptor protein (19-43)	[56]
Cyt c	GTKMIFVGIKKKEERAD LIAYLKKA-NH$_2$	Bioactive CPP	Human cytochrome C (77-101)	[57]
mPrP	MANLGYWLLALFVTM WTDVGLCKKRPKP-NH$_2$	Bioactive CPP	Mouse prion protein (1-28)	[58]
SAHB$_A$	EDIIRNIARHLAX[b]VGDX[b] N$_L$[c]DRSIW-NH$_2$	Chemically modified bioactive CPP	BID BH3	[59]
Lactoferricin B	FKCRRWQWRMKKLGAP SITCVRRAF[d]	Host defense peptide	Bovine lactoferrin (17-41)	[60]
Buforin IIb	TRSSRAGLQWPVGRVHR LLRK[d]	Host defense peptide	Histone H2A (Toad stomach)	[61]

a) Ahx stands for 6-aminohexanoic acid

b) X refers to the position of α,α-disubstituted non-natural amino acids containing olefin-bearing tethers. These amino acids were used for the formation of a hydrocarbon staple (cyclic alkene)

c) N$_L$ corresponds to the non-natural amino acid norleucine

d) No information was available regarding the amidation status

2.3.3   *Biological mechanisms of side effects of cationic CPPs*

Even though scientific understanding of the biological effects of CPP is far from complete, individual molecular mechanisms along the route of uptake and inside cells have been identified (Figure 2.1). At the first step of cellular entry, an interaction between heparan sulfate proteoglycans and the CPP tat has been found to affect the cell by reducing its responsiveness to exogenous polyamines via a competition for heparan sulfate binding sites [17].

Following their interaction with heparan sulfates, a principal effect of cationic CPPs is their ability to induce endocytosis of unconjugated constituents and transmembrane receptors, as detected by an increased uptake of fluorescently labeled dextran via fluid-phase endocytosis [15] and the internalization of TNF-receptors [14], respectively. Although the precise trigger has not yet been identified, this endocytosis induction can have profound effects on the capacity of a cell to respond to extracellular signals. Internalization of TNF-receptors occurred without receptor activation. As a consequence, the downregulation resulted in a reduced capacity to respond to TNF-α by up to 50 % [14]. Downregulation was also observed for epidermal growth factor receptor and was induced by penetratin, tat and nonaarginine [14].

Cationic CPP also evoke side effects by remodeling the plasma membrane. TAT-GFP fusion proteins were found to induce phosphatidylserine (PS) exposure, though without initiating apoptosis or necrosis. Recently, we confirmed and extended this observation by showing that cationic CPPs have the ability to not only alter the distribution of lipids in the bilayer, but also to induce changes in the lipid composition of the plasma membrane that depend on enzymatic activity [19]. The mechanism involves the induction of acid sphingomyelinase (ASMase), which converts sphingomyelin to ceramide at the outer leaflet of the plasma membrane. Because ceramide is a lipid with important second-messenger functions, this finding may have important implications for the interpretation and design of studies using CPP-based therapeutic strategies (Box 1). ASMase was identified as a key player in the plasma membrane repair response [62], which is known to be induced by several CPPs including TP10 and penetratin [63].

Box 1. The many faces of acid sphingomyelinase and ceramide

Acid sphingomyelinase (ASMase) and ceramide are subjects of intense research due to their recently discovered roles in the pathophysiology of common diseases [100] and the multifaceted roles of ceramide as a second messenger in several antiproliferative and/or apoptotic responses, in the arrangement of the cellular cytoskeleton and in motility. Currently, there is increasing interest in ceramide metabolism as a potential target for cancer therapy [101].

In lipid membranes, ceramide segregates into rigid domains and induces negative monolayer curvature [102], which has been associated with the internalization of several pathogens [103] and cationic CPP [19]. The initial trigger for ASMase translocation and ceramide formation is poorly understood, though reactive oxygen species have been implicated independently by various groups [104]. Although octaarginine also induced superoxide in U-937 macrophages [47], a direct link to ASMase activation has not been established.

The observation that cationic CPPs have the potential to influence ceramide metabolism may have important implications for cancer therapy. CPPs could serve to enhance the sensitivity of tumor cells to chemotherapeutic drugs. In fact, ceramide generation induced by cationic CPP might be part of the mechanism of enhanced toxicity of CPP-based chemotherapeutic approaches [105]. CPP-drug conjugates enhanced cytotoxicity and induced ceramide formation through acid sphingomyelinase, whereas the drugs by themselves did not. Although the mode of drug delivery was seen as the probable reason, the bioactivity of the cationic CPP could very well have contributed to the increased cytotoxicity.

Arginine-rich peptides also induce actin rearrangement in a proteoglycan-dependent manner [64]. Given the central role of the cytoskeleton in signaling processes, it remains to be determined to what extent this activity affects signaling cascades [65]. Very interestingly, differential effects on healthy and malignant fibroblasts were observed for several arginine (R9) and arginine/tryptophan-based (R/W)9 peptides [13]. Whereas these peptides restored a disrupted actin cytoskeleton in malignant fibroblasts, the peptides did not affect actin organization in untransformed fibroblasts. Furthermore, the CPPs reduced cell motility and wound healing. These activities were only observed with CPPs that had the ability to bind actin *in vitro* as determined by isothermal titration calorimetry [13]. The effects were not observed upon treatment with non-actin binding peptides, such as an

(R/W)9 peptide consisting of D-amino acids or penetratin, which both had a comparable capacity to enter the fibroblasts.

In addition to these activities, oligoarginines also act as protease inhibitors. Octaarginine reduced proteasome activity, leading to the accumulation of high-molecular-weight ubiquitin-conjugated proteins inside the cells as determined by analysis of whole cell lysates [16]. Oligoarginines more generally acted as furin inhibitors [11]. As again another mechanism-of-action, HIV replication was inhibited by tat, which is achieved through competition with the full HIV-1 tat protein for binding to the TAR element in the nucleus [18].

Given all these biological activities, cationic CPPs are thus far from true Trojan horses. Because arginine and tryptophan are residues enriched on protein interaction surfaces and because of the high energy contribution of these residues to protein-protein interactions [66], it should come as no surprise if next to the demonstrated interactions with actin and proteases, arginine- and trypophan-rich peptides had further proteinaceous interaction partners inside the cell. As we will detail more extensively below, many other specific intracellular interaction partners have been identified for particular bioactive cell-penetrating peptides.

2.3.4   *Toxicity and bioactivities of cationic drug delivery systems*

The scientific focus for other cationic carriers is also shifting from the application of standard toxicity assays towards a more complete understanding of the side effects through the analysis of specific biological interactions and global gene expression profiling [67, 68]. Selected examples that are pertinent to the discussion of cellular responses towards cationic carriers are presented. For the cationic polymer polyethyleneimine (PEI), two distinct phases in cytotoxicity were detected [68]. First, PEI induced lactate dehydrogenase leakage and PS externalization in a caspase-3 independent manner, which was then followed by the induction of caspase-3-dependent mitochondrial apoptosis, most likely caused by a direct interaction of PEI with the negatively charged mitochondrial membrane. A role for lysosomal destabilization could not be ruled out because PEI has been shown to disrupt lysosomes [69]. A similar caspase-3 independent PS externalization was observed for poly-L-lysine (PLL), which was also followed by a caspase-3 dependent apoptosis [70]. Another bioactivity that may be implicated in PLL-mediated apoptosis, but that has also been observed for poly-L-arginine, was the induction of phospholipase D through protein

kinase C [71]. Like PEI and PLL, chitosan and chitosan-derivates also induce apoptosis through caspase-3 [72].
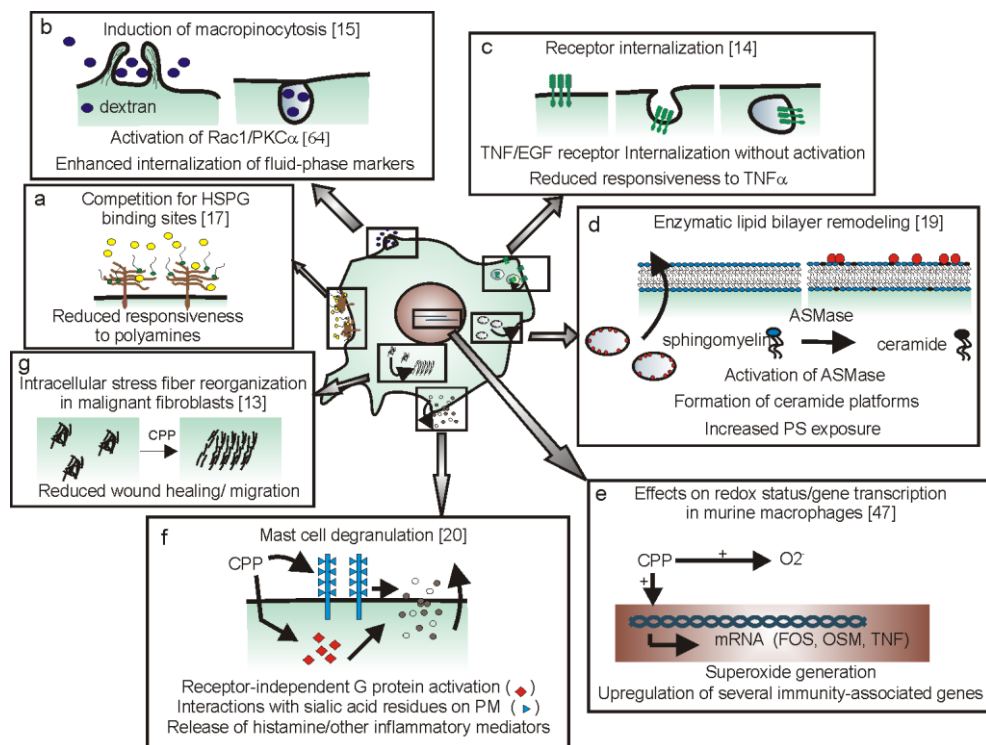
Figure 2.1. Common side effects elicited by multiple cationic CPPs. In recent years, multiple side effects of cationic CPPs have been described that can in some instances directly be related to their internalization mechanisms. The first step of internalization, the high-affinity interaction with heparan sulfates, is the primary reason for the reduced responsiveness to polyamines (a). The induction of internalization of fluid-phase markers and receptors are related to the ability of cationic CPPs to activate the endocytic machinery (b,c). The molecular triggers that lead to plasma membrane remodeling (d) or affect the redox status and/or gene transcription (e) have not yet been identified, whereas interactions with sialic acid residues and G proteins are thought to be responsible for mast cell degranulation (f). A direct interaction with intracellular actin has been proposed to underlie the ability to mediate stress fiber reorganization in malignant fibroblasts (g). HSPG, heparan sulfate proteoglycan; PM, plasma membrane.

Cholesterol-based cationic lipids, which are being investigated for gene delivery, have the potential to inhibit protein kinase C activity [73]. Factors that affect the inhibition are charge, the presence of steroid versus linear hydrocarbons and the presence of a quaternary ammonium cation versus a tertiary amine headgroup [73]. Reminiscent of the induction of receptor internalization by cationic CPPs, the transfection agent lipofectamin, which has

similarities with cationic lipids that are being developed into drug-delivery constructs, activates the insulin receptor at higher concentrations. This leads to a subsequent downregulation of insulin receptors and a lack of responsiveness to insulin in transfected cells [74].

2.3.5   *Toxicity and side effects of cationic CPP in vivo*

As very recently reviewed by Järver *et al.*, there is currently little information regarding the *in vivo* toxicology of cationic CPPs [75]. Despite numerous preclinical studies that indicate activity of CPP-based therapeutics (for examples, see below), few dedicated toxicity assessments of therapeutic CPP-constructs in preclinical or clinical development have been published. Nevertheless, the absence of obvious toxic effects in most of the studies assessing therapeutic effects is promising. Several notable constructs that are or have been in clinical development include: PsorBan, which is cyclosporin A coupled to heptaarginine via a pH-dependent linker [76]; KAI-9803, a tat-coupled peptide inhibitor of PKCδ [77]; (RXR)4 peptides coupled to anti-c-myc phosphorodiamidate morpholine oligomers (PMO) [78]; and XG-102, a tat-coupled c-Jun N-terminal kinase inhibitor [78-82]. In multiple studies with these compounds in rat, mouse and porcine models, but also in an exploratory study in humans (KAI-9803) [83], no apparent signs of acute or long-term toxicity were reported at therapeutic doses. Administration through various routes was well-tolerated, including: the   topical   administration   of   PsorBan   (Psorban; http://goliath.ecnext.com/coms2/gi_0199-2736134/CellGate-Announces-Phase-IIa-Study.html); the intracoronary administration of KAI-9803 [77, 83]; the intravenous administration of ((RXR)4-PMO) [78] and XG-102 [81]; and the intraperitoneal (IP) administration of XG-102 [80, 82]. Similarly, direct stereotactic delivery into the brain of tat coupled to a dsRNA-binding domain, a platform which is also being developed for clinical trials, seems to be well-tolerated at therapeutic levels in a glioblastoma mouse model [84].

   In line with the aforementioned findings, 14 subsequent days of IP injection of 20 nmol of a Tat-PKC peptide conjugate in rats did not result in organ toxicity, despite a widespread biodistribution [85]. Frequent IP injections of tat coupled to the enzyme purine nucleoside phosphorylase at a dose of 80 mg/kg body wt/wk in mice also did not result in any detectable toxicity, as determined by blood-based parameters of liver, kidney and hematological function [86]. By contrast, tat and penetratin were found to induce by themselves a reduction in the expression of the kinase p38 in a mouse lung delivery study

after intratracheal administration at 10 nmol [87], however, it was not investigated in more detail if the expression of other genes was affected as well. When coupled to siRNA, penetratin also activated innate immunity [87]. The mechanisms are not understood.

A recent report from Aguilera *et al*. described the *in vivo* distribution and toxicity of C-terminally amidated r9 (all D-amino acids) following intravenous administration in mice. The peptide was found to bind rapidly to the local vasculature and to redistribute within 30 min, with over 90 % localized to the liver [88]. These researchers observed that mice went into shock with dilated blood vessels and died of respiratory collapse within one minute after an injection of 100 nmol r9 (5 μmol/kg, which is ~7 mg/kg), though 4 out of 5 mice survived an injection of 50 nmol. The toxicity of r9 could be reduced by masking the arginine moieties in the bloodstream via a glutamic acid-based polyanion stretch coupled to the CPP via a protease-cleavable linker. A suspected reason for this adverse effect is massive mast cell degranulation, leading to a fatal vasodilation. These strong adverse effects of r9 in mice were in contrast to the results observed with peptide-PMO constructs in rats, where no adverse effects occurred at 15 mg/kg, and the LD_{50} lay between 210 and 250 mg/kg. Of note is that the total amount of positive charge at 15 mg/kg is about half of that for r9 at 7 mg/kg. The conjugate (RXR)4-PMO has one positive charge less than r9 and its molecular weight is about fourfold higher. Moreover, the charge density is substantially lower due to the insertion of four 6-aminohexanoic acid moieties in the octa-arginine sequence [78]. In the exploratory study in human volunteers with tat-PKCδ, corrected-for-weight quantities of the peptides were around 100-fold lower (~7 mg/kg in the mice study [88] vs. max. 70 μg/kg in the human study [83]). Other reasons that may contribute to the diverse biological responses include the different route of administration (intravenous vs. intracoronary), the difference in CPP and the conjugation to a peptide inhibitor (PKCδ**)**. Typically, the studies at therapeutic doses use far lower concentrations, which makes toxicity comparisons difficult, if not impossible.

Another consideration regarding the toxicity of CPPs *in vivo* is their lack of specificity. The implementation of targeting strategies to direct the CPP to the site of action may therefore help to avoid side effects in multiple tissues [75, 89]. So far, targeting strategies to improve specificity have focused on targeting CPP-conjugates to tumors. These strategies either exploited the tumor microenvironment [90, 91] or tumor-specific antigens [92, 93]. For instance, Whitney *et al*. increased specificity through a phage display-based selection of tumor-homing activatable CPPs, which incorporate a tumor protease-cleavable linker attached to an arginine-masking polyanion chain [91]. As indicated above, this strategy also decreases toxicity. The group of Torchilin made use of hydrazone-linked PEG

shells on liposomes, which shield the tat-moiety at physiological pH, but expose tat at lower pH values [90], which are normally encountered in the tumor microenvironment [94]. Myrberg *et al.* and Miyamoto *et al.* achieved enhanced specificity of CPPs through coupling to tumor-targeting peptides or antibodies, respectively [92, 93]. In the near future, cell-targeting peptides with an intrinsic cell-penetrating activity may expand the repertoire of strategies available to increase specificity [95].

2.4   CPPs with Intrinsic Bioactivity

In addition to the traditional cationic CPP that are applied as vectors for cargo-delivery, CPPs with intrinsic activities are rapidly gaining interest (Figure 2.2). This class of peptides demonstrates that cell entry and intracellular function can be combined effectively (for examples, see table 2.1).

One example of a bioactive cell-penetrating peptide is a seven arginine residue-containing CPP derived from the p14 ARF protein [54]. Internalization of this peptide is as efficient as uptake of the CPP TP10 and is associated with little membrane disturbance. Inside the cells, this peptide activates the apoptotic machinery by mimicking the function of the intact p14ARF protein, most likely by increasing p53 activity through inhibition of HMD2. In a similar vein, bioactive CPPs derived from cytochrome C were developed, which also combine efficient cellular internalization with the induction of tumor cell apoptosis. Another example is maurocalcine, which is a CPP derived from a scorpion venom that induces intracellular Ca(2+) release through activation of ryanodine receptors [52]. The peptide vasostatin 1 also shares multiple characteristics with cationic CPP, because it also binds to heparan sulfate proteoglycans (HSPGs) and is internalized via endocytosis. In addition, vasostatin 1 activates endothelial nitric oxide synthase (eNOS) phosphorylation in a PI3K- and proteoglycan-dependent manner, which stimulates caveolae-dependent endocytosis [53]. The increase in caveolae-dependent endocytosis is somewhat surprising, because PI3K is commonly associated with macropinocytosis [96]. A highly interesting finding has been presented for prion-derived peptides, which successfully entered cells and also caused a reduction of intracellular levels of the pathogenic prion isoform [58].

Furthermore, the G protein-binding parts of GPCRs have been employed as a source for CPP with an intrinsic bioactivity [55]. A CPP prediction algorithm was used to identify CPPs from various GPCRs. One of the peptides (M511) induced blood vessel contraction. This indicates that the peptide successfully mimicked the respective domain of its parent protein [55]. By contrast, a peptide derived from the Toll-receptor 4 (TLR-4) adaptor

protein blocked parent protein activity [56]. This peptide, TBX2, penetrated the plasma membrane and eliminated lipopolysaccharide-induced production of pro-inflammatory cytokines. Presumably it prevents TLR-4-mediated activation of downstream signaling events by competition for TLR-4 binding sites [56].

Walensky *et al.* followed a different route to confer cell-penetrating capacity to a cell-impermeable BID BH3 peptide, which is the conserved BH3 α-helical domain of the pro-apoptoic protein BID (a member of the Bcl-2 family). Unlike the aforementioned examples, cell-permeability of this peptide was not a function of its primary sequence, but instead the result of the inclusion of a cyclic alkene using α,α-disubstituted non-natural amino acids that constrains the molecule to assume an α-helical conformation. This chemical modification is referred to as stapling. The authors attributed the enhanced cell-penetrating capacity to the increased lipophilicity of the derivate. The stapled BID-BH3 peptide enters cells through macropinocytosis, localizes to mitochondria and binds to and activates Bcl-2-associated protein X (BAX), thereby initiating the apoptotic machinery [59]. *In vivo*, this peptide analog slows the growth of human leukemia xenografts.

2.4.1   Host defense peptides

A separate class of bioactive peptides that also comprises cell-penetrating members are the host defense peptides (see table 2.1). Although some of these peptides act by being preferentially membranolytic for cancer cells or bacteria, others have the ability to translocate into cells without major membrane disturbance. An example is the 7 arginine-residues-containing buforin IIb, a 22 amino acid peptide derive from histone H2A [61]. In studies, this peptide required cell surface gangliosides or sialic acids for efficient entry into cancer cells. Remarkably, buforin IIb did not enter healthy cells even at high concentrations, despite being very arginine-rich. After cell entry, buforin IIb causes mitochondria-dependent apoptosis through the activation of pro-caspase 9 and pro-caspase 3. It has not been established whether a direct interaction is involved. Mitochondria-dependent apoptosis has also been described for bovine lactoferricin B [60], a host defense peptide that also has the capacity to enter cells [97]. For bovine lactoferricin B, generation of reactive oxygen species has been implicated in the mechanism of apoptosis induction. Notably, the cyclic structure, while being essential for internalization of the human lactoferrin (hLF)-derived CPP (which is a part of human lactoferricin H), was not required for the cancer cell-selective induction of apoptosis of bovine lactoferricin B, emphasizing the distinct structure-activity relationship of these two peptides [49, 60].
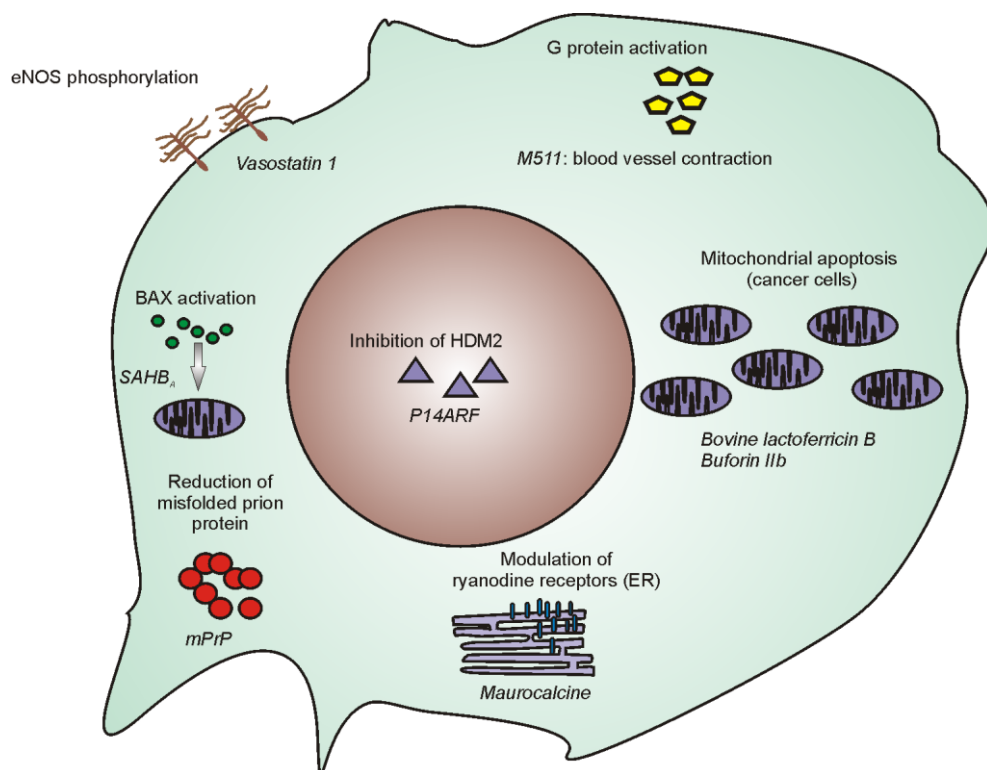
Figure 2.2. Examples of CPPs with intrinsic bioactivity. Cationic CPPs can have diverse effects on cellular physiology. At the plasma membrane, binding of vasostatin 1 to heparan sulfate proteoglycans is involved in eNOS phosphorylation [53]. In the cytosol, diverse activities have been described that include a reduction in the pathogenic isoform of the prion protein by prion-derived peptides [58] and blood vessel contraction through G proteins [55]. A cell-penetrating BH3 domain with a stabilized α-helical conformation acts by recruiting BAX to the mitochondria, where it is activated [59]. Several host defense peptides have been shown to cause mitochondrial apoptosis in cancer cells after having traversed the plasma membrane without major disturbances [60, 61]. Ryanodine receptors, located in the membrane of the ER, are modulated by a bioactive CPP derived from scorpion venom [52]. In the nucleus, a p14ARF-derived peptide is proposed to sequester HDM2 to the nucleolus, which leads to p53 activation and apoptosis [54]. ER, endoplasmic reticulum.

2.5 Concluding Remarks and Future Perspectives

The data reviewed in this article indicate that side effects of cationic delivery agents can be diverse and are not necessarily directly related to cellular uptake. Therefore, when screening for side effects, a comprehensive analysis of the interactions between the delivery agent and the biological system is required. Global gene expression profiling is the most straightforward screen. Ideally, such a screen should be complemented with a more

directed search for side effects based on available precedents. Testing procedures could encompass diverse assays for the detection of superoxide levels, receptor internalization, mast cell degranulation or the effect on lipid composition.

At present, it is difficult to foresee which side effects that were observed *in vitro* will be relevant *in vivo*. There are still very limited data to translate *in vitro* peptide concentrations into relevant *in vivo* concentrations. Nevertheless, we predict the start of an exciting new era in which it will be possible to use knowledge regarding molecular interactions of cell-entering peptides to design delivery agents that have themselves desired pharmacodynamic activity. Alternatively, the fundamental knowledge could be used to rationally engineer delivery agents without undesired side effects. A notable example is the (R/W)9 synthesized with either D- or L-amino acids, which have equal internalization efficiencies, but remarkably different molecular interactions and activities inside the cell [13]. A further example is the recent design of a pharmacologically inert D-maurocalcine, which, unlike its L-counterpart, does not affect calcium signaling inside the cell [98]. Another emerging trend is to identify cell-permeant proteomimetic peptides using quantitative structure-activity relationship-based algorithms [99], which has already provided several interesting new bioactive agents in which the delivery capacity and pharmacophore are present in the primary sequence in overlapping, but not identical, regions [55-57].

In conclusion, cationic peptides and cationic drug carriers show a large variety of side effects that might be related or unrelated to their internalization mechanisms. If bioactivities are associated with the internalization mechanisms of this type of carrier, then the choice of the class of delivery system should be compatible with or contribute to the therapeutic goal, such as for example the import of anti-cancer drugs with apoptosis-inducing peptides. Ultimately, the understanding of the structural determinants underlying these effects should allow us to rationally engineer new bioactive agents that only possess the properties that are deliberately introduced.

2.6   References

[1] U.A. Betz, R. Farquhar, K. Ziegelbauer, Genomics: success or failure to deliver drug targets?, Curr.Opin.Chem.Biol., 9 (2005) 387-391.

[2] J.P. Overington, B. Al-Lazikani, A.L. Hopkins, How many drug targets are there?, Nat.Rev.Drug Discov., 5 (2006) 993-996.

[3] G.L. Verdine, L.D. Walensky, The challenge of drugging undruggable targets in cancer: lessons learned from targeting BCL-2 family members, Clin.Cancer Res., 13 (2007) 7264-7270.

[4] L. Aagaard, J.J. Rossi, RNAi therapeutics: principles, prospects and challenges, Adv.Drug Deliv.Rev., 59 (2007) 75-86.

[5] A.K. Pavlou, J.M. Reichert, Recombinant protein therapeutics--success rates, market trends and values to 2010, Nat.Biotechnol., 22 (2004) 1513-1519.

[6] L.O. Sillerud, R.S. Larson, Design and structure of peptide and peptidomimetic antagonists of protein-protein interaction, Curr.Protein Pept.Sci., 6 (2005) 151-169.

[7] R. Langer, Drug delivery. Drugs on target, Science, 293 (2001) 58-59.

[8] E. Bilensoy, Cationic nanoparticles for cancer therapy, Expert.Opin.Drug Deliv., 7 (2010) 795-809.

[9] C.L. Murriel, S.F. Dowdy, Influence of protein transduction domains on intracellular delivery of macromolecules, Expert.Opin.Drug Deliv., 3 (2006) 739-746.

[10] L. Wasungu, D. Hoekstra, Cationic lipids, lipoplexes and intracellular delivery of genes, J.Control Release, 116 (2006) 255-264.

[11] A. Cameron, J. Appel, R.A. Houghten, I. Lindberg, Polyarginines are potent furin inhibitors, J.Biol.Chem., 275 (2000) 36741-36749.

[12] M.V. Del Gaizo, R.M. Payne, Transactivator of transcription fusion protein transduction causes membrane inversion, J.Biol.Chem., 279 (2004) 32541-32544.

[13] D. Delaroche, F.X. Cantrelle, F. Subra, H.C. Van, E. Guittet, C.Y. Jiao, L. Blanchoin, G. Chassaing, S. Lavielle, C. Auclair, S. Sagan, Cell-penetrating peptides with intracellular actin-remodeling activity in malignant fibroblasts, J.Biol.Chem., 285 (2010) 7712-7721.

[14] M. Fotin-Mleczek, S. Welte, O. Mader, F. Duchardt, R. Fischer, H. Hufnagel, P. Scheurich, R. Brock, Cationic cell-penetrating peptides interfere with TNF signalling by induction of TNF receptor internalization, J.Cell Sci., 118 (2005) 3339-3351.

[15] I.M. Kaplan, J.S. Wadia, S.F. Dowdy, Cationic TAT peptide transduction domain enters cells by macropinocytosis, J.Control Release, 102 (2005) 247-253.

[16] A. Kloss, P. Henklein, D. Siele, M. Schmolke, S. Apcher, L. Kuehn, P.W. Sheppard, B. Dahlmann, The cell-penetrating peptide octa-arginine is a potent inhibitor of proteasome activities, Eur.J.Pharm.Biopharm., 72 (2009) 219-225.

[17] K. Mani, S. Sandgren, J. Lilja, F. Cheng, K. Svensson, L. Persson, M. Belting, HIV-Tat protein transduction domain specifically attenuates growth of polyamine deprived tumor cells, Mol.Cancer Ther., 6 (2007) 782-788.

[18] D.M. Theisen, C. Pongratz, K. Wiegmann, F. Rivero, O. Krut, M. Kronke, Targeting of HIV-1 Tat traffic and function by transduction-competent single chain antibodies, Vaccine, 24 (2006) 3127-3136.

[19] W.P. Verdurmen, M. Thanos, I.R. Ruttekolk, E. Gulbins, R. Brock, Cationic cell-penetrating peptides induce ceramide formation via acid sphingomyelinase: Implications for uptake, J.Control Release, 147 (2010) 171-179.

[20] J. Oehlke, D. Lorenz, B. Wiesner, M. Bienert, Studies on the cellular uptake of substance P and lysine-rich, KLA-derived model peptides, J.Mol.Recognit., 18 (2005) 50-59.

[21] A.W. Bernheimer, B. Rudy, Interactions between membranes and cytolytic peptides, Biochim.Biophys.Acta, 864 (1986) 123-141.

[22] S.T. Henriques, M.N. Melo, M.A. Castanho, Cell-penetrating peptides and antimicrobial peptides: how different are they?, Biochem.J., 399 (2006) 1-7.

[23] M. Mae, U. Langel, Cell-penetrating peptides as vectors for peptide, protein and oligonucleotide delivery, Curr.Opin.Pharmacol., 6 (2006) 509-514.

[24] P. Lundin, H. Johansson, P. Guterstam, T. Holm, M. Hansen, U. Langel, A.S. El, Distinct uptake routes of cell-penetrating peptide conjugates, Bioconjug.Chem., 19 (2008) 2535-2542.

[25] E. Eiriksdottir, K. Konate, U. Langel, G. Divita, S. Deshayes, Secondary structure of cell-penetrating peptides controls membrane interaction and insertion, Biochim.Biophys.Acta, 1798 (2010) 1119-1128.

[26] D. Derossi, A.H. Joliot, G. Chassaing, A. Prochiantz, The third helix of the Antennapedia homeodomain translocates through biological membranes, J.Biol.Chem., 269 (1994) 10444-10450.

[27] E. Vives, P. Brodin, B. Lebleu, A truncated HIV-1 Tat protein basic domain rapidly translocates through the plasma membrane and accumulates in the cell nucleus, J.Biol.Chem., 272 (1997) 16010-16017.

[28] M. Pooga, M. Hällbrink, M. Zorko, Ü. Langel, Cell penetration by transportan, FASEB J., 12 (1998) 67-77.

[29] J.R. Maiolo, M. Ferrer, E.A. Ottinger, Effects of cargo molecules on the cellular uptake of arginine-rich cell-penetrating peptides, Biochim.Biophys.Acta, 1712 (2005) 161-172.

[30] J. Mueller, I. Kretzschmar, R. Volkmer, P. Boisguerin, Comparison of cellular uptake using 22 CPPs in 4 different cell lines, Bioconjug.Chem., 19 (2008) 2363-2374.

[31] H. Raagel, P. Saalik, M. Pooga, Peptide-mediated protein delivery-Which pathways are penetrable?, Biochim.Biophys.Acta, 1798 (2010) 2240-2248.

[32] F. Duchardt, M. Fotin-Mleczek, H. Schwarz, R. Fischer, R. Brock, A comprehensive model for the cellular uptake of cationic cell-penetrating peptides, Traffic., 8 (2007) 848-866.

[33] S.M. Fuchs, R.T. Raines, Pathway for polyarginine entry into mammalian cells, Biochemistry, 43 (2004) 2438-2444.

[34] A. Ziegler, Thermodynamic studies and binding mechanisms of cell-penetrating peptides with lipids and glycosaminoglycans, Adv.Drug Deliv.Rev., 60 (2008) 580-597.

[35] T. Letoha, A. Keller, E. Kusz, C. Kolozsi, Z. Bozso, G. Toth, C. Vizler, Z. Olah, L. Szilak, Cell-penetrating peptide exploited syndecans, Biochim.Biophys.Acta, 1798 (2010) 2258-2265.

[36] J.M. Gump, R.K. June, S.F. Dowdy, Revised role of glycosaminoglycans in TAT protein transduction domain-mediated cellular transduction, J.Biol.Chem., 285 (2010) 1500-1507.

[37] N. Schmidt, A. Mishra, G.H. Lai, G.C. Wong, Arginine-rich cell-penetrating peptides, FEBS Lett., 584 (2010) 1806-1813.

[38] G. van Meer, D.R. Voelker, G.W. Feigenson, Membrane lipids: where they are and how they behave, Nat.Rev.Mol.Cell Biol., 9 (2008) 112-124.

[39] A. Mishra, V.D. Gordon, L. Yang, R. Coridan, G.C. Wong, HIV TAT forms pores in membranes by inducing saddle-splay curvature: potential role of bidentate hydrogen bonding, Angew.Chem.Int.Ed Engl., 47 (2008) 2986-2989.

[40] P.E. Thoren, D. Persson, P. Lincoln, B. Norden, Membrane destabilizing properties of cell-penetrating peptides, Biophys.Chem., 114 (2005) 169-179.

[41] G.P. Dietz, M. Bahr, Delivery of bioactive molecules into the cell: the Trojan horse approach, Mol.Cell Neurosci., 27 (2004) 85-131.

[42] S. El-Andaloussi, P. Jarver, H.J. Johansson, U. Langel, Cargo-dependent cytotoxicity and delivery efficacy of cell-penetrating peptides: a comparative study, Biochem.J., 407 (2007) 285-292.

[43] K. Saar, M. Lindgren, M. Hansen, E. Eiriksdottir, Y. Jiang, K. Rosenthal-Aizman, M. Sassian, U. Langel, Cell-penetrating peptides: a comparative membrane toxicity study, Anal.Biochem., 345 (2005) 55-65.

[44] K. Kilk, R. Mahlapuu, U. Soomets, U. Langel, Analysis of in vitro toxicity of five cell-penetrating peptides by metabolic profiling, Toxicology, 265 (2009) 87-95.

[45] A. Eguchi, B.R. Meade, Y.C. Chang, C.T. Fredrickson, K. Willert, N. Puri, S.F. Dowdy, Efficient siRNA delivery into primary cells by a peptide transduction domain-dsRNA binding domain fusion protein, Nat.Biotechnol., 27 (2009) 567-571.

[46] W. Waldeck, R. Pipkorn, B. Korn, G. Mueller, M. Schick, K. Toth, M. Wiessler, B. Didinger, K. Braun, Transporter molecules influence the gene expression in HeLa cells, Int.J.Med.Sci., 6 (2009) 18-27.

[47] J.H. Kuo, M.S. Jan, Y.L. Lin, C. Lin, Interactions between octaarginine and U-937 human macrophages: global gene expression profiling, superoxide anion content, and cytokine production, J.Control Release, 139 (2009) 197-204.

[48] P.A. Wender, D.J. Mitchell, K. Pattabiraman, E.T. Pelkey, L. Steinman, J.B. Rothbard, The design, synthesis, and evaluation of molecules that enable or enhance cellular uptake: peptoid molecular transporters, Proc.Natl.Acad.Sci.U.S.A, 97 (2000) 13003-13008.

[49] F. Duchardt, I.R. Ruttekolk, W.P. Verdurmen, H. Lortat-Jacob, J. Burck, H. Hufnagel, R. Fischer, H.M. van den, D.W. Lowik, G.W. Vuister, A. Ulrich, W.M. de, R. Brock, A cell-penetrating peptide derived from human lactoferrin with conformation-dependent uptake efficiency, J.Biol.Chem., 284 (2009) 36099-36108.

[50] S. Abes, H.M. Moulton, P. Clair, P. Prevot, D.S. Youngblood, R.P. Wu, P.L. Iversen, B. Lebleu, Vectorization of morpholino oligomers by the (R-Ahx-R)4 peptide allows efficient splicing correction in the absence of endosomolytic agents, J.Control Release, 116 (2006) 304-313.

[51] U. Soomets, M. Lindgren, X. Gallet, M. Hallbrink, A. Elmquist, L. Balaspiri, M. Zorko, M. Pooga, R. Brasseur, U. Langel, Deletion analogues of transportan, Biochim.Biophys.Acta, 1467 (2000) 165-176.

[52] E. Esteve, K. Mabrouk, A. Dupuis, S. Smida-Rezgui, X. Altafaj, D. Grunwald, J.C. Platel, N. Andreotti, I. Marty, J.M. Sabatier, M. Ronjat, W.M. de, Transduction of the scorpion toxin maurocalcine into cells. Evidence that the toxin crosses the plasma membrane, J.Biol.Chem., 280 (2005) 12833-12839.

[53] R. Ramella, O. Boero, G. Alloatti, T. Angelone, R. Levi, M.P. Gallo, Vasostatin 1 activates eNOS in endothelial cells through a proteoglycan-dependent mechanism, J.Cell Biochem., 110 (2010) 70-79.

[54] H.J. Johansson, S. El-Andaloussi, T. Holm, M. Mae, J. Janes, T. Maimets, U. Langel, Characterization of a novel cytotoxic cell-penetrating peptide derived from p14ARF protein, Mol.Ther., 16 (2008) 115-123.

[55] P. Östlund, K. Kilk, M. Lindgren, M. Hallbrink, Y. Jiang, M. Budihna, K. Cerne, A. Bavec, C.G. Ostenson, M. Zorko, U. Langel, Cell-penetrating mimics of agonist-activated G-protein coupled receptors, International Journal of Peptide Research and Therapeutics, 11 (2005) 237-247.

[56] W. Low, A. Mortlock, L. Petrovska, T. Dottorini, G. Dougan, A. Crisanti, Functional cell permeable motifs within medically relevant proteins, J.Biotechnol., 129 (2007) 555-564.

[57] S. Jones, T. Holm, I. Mager, U. Langel, J. Howl, Characterization of Bioactive Cell Penetrating Peptides from Human Cytochrome c: Protein Mimicry and the Development of a Novel Apoptogenic Agent, Chem.Biol., 17 (2010) 735-744.

[58] K. Löfgren, A. Wahlström, P. Lundberg, Ü. Langel, A. Gräslund, K. Bedecs, Antiprion properties of prion protein-derived cell-penetrating peptides, FASEB J., 22 (2008) 2177-2184.

[59] L.D. Walensky, A.L. Kung, I. Escher, T.J. Malia, S. Barbuto, R.D. Wright, G. Wagner, G.L. Verdine, S.J. Korsmeyer, Activation of apoptosis in vivo by a hydrocarbon-stapled BH3 helix, Science, 305 (2004) 1466-1470.

[60] J.S. Mader, J. Salsman, D.M. Conrad, D.W. Hoskin, Bovine lactoferricin selectively induces apoptosis in human leukemia and carcinoma cell lines, Mol.Cancer Ther., 4 (2005) 612-624.

[61] H.S. Lee, C.B. Park, J.M. Kim, S.A. Jang, I.Y. Park, M.S. Kim, J.H. Cho, S.C. Kim, Mechanism of anticancer activity of buforin IIb, a histone H2A-derived peptide, Cancer Lett., 271 (2008) 47-55.

[62] C. Tam, V. Idone, C. Devlin, M.C. Fernandes, A. Flannery, X. He, E. Schuchman, I. Tabas, N.W. Andrews, Exocytosis of acid sphingomyelinase by wounded cells promotes endocytosis and plasma membrane repair, J.Cell Biol., 189 (2010) 1027-1038.

[63] C. Palm-Apergi, A. Lorents, K. Padari, M. Pooga, M. Hallbrink, The membrane repair response masks membrane disturbances caused by cell-penetrating peptide uptake, FASEB J., 23 (2009) 214-223.

[64] I. Nakase, A. Tadokoro, N. Kawabata, T. Takeuchi, H. Katoh, K. Hiramoto, M. Negishi, M. Nomizu, Y. Sugiura, S. Futaki, Interaction of arginine-rich peptides with membrane-associated proteoglycans is crucial for induction of actin organization and macropinocytosis, Biochemistry, 46 (2007) 492-501.

[65] G.J. Doherty, H.T. McMahon, Mediation, modulation, and consequences of membrane-cytoskeleton interactions, Annu.Rev.Biophys., 37 (2008) 65-95.

[66] A.A. Bogan, K.S. Thorn, Anatomy of hot spots in protein interfaces, J.Mol.Biol., 280 (1998) 1-9.

[67] A.C. Hunter, S.M. Moghimi, Cationic carriers of genetic material and cell death: A mitochondrial tale, Biochim.Biophys.Acta, 1797 (2010) 1203-1209.

[68] S.M. Moghimi, P. Symonds, J.C. Murray, A.C. Hunter, G. Debska, A. Szewczyk, A two-stage poly(ethylenimine)-mediated cytotoxicity: implications for gene transfer/therapy, Mol.Ther., 11 (2005) 990-995.

[69] A.R. Klemm, D. Young, J.B. Lloyd, Effects of polyethyleneimine on endocytosis and lysosome stability, Biochem.Pharmacol., 56 (1998) 41-46.

[70] P. Symonds, J.C. Murray, A.C. Hunter, G. Debska, A. Szewczyk, S.M. Moghimi, Low and high molecular weight poly(L-lysine)s/poly(L-lysine)-DNA complexes initiate mitochondrial-mediated apoptosis differently, FEBS Lett., 579 (2005) 6191-6198.

[71] S. Vepa, W.M. Scribner, V. Natarajan, Activation of endothelial cell phospholipase D by polycations, Am.J.Physiol, 272 (1997) L608-L613.

[72] M. Hasegawa, K. Yagi, S. Iwakawa, M. Hirai, Chitosan induces apoptosis via caspase-3 activation in bladder tumor cells, Jpn.J.Cancer Res., 92 (2001) 459-466.

[73] R. Bottega, R.M. Epand, Inhibition of protein kinase C by cationic amphiphiles, Biochemistry, 31 (1992) 9025-9030.

[74] C. Pramfalk, J. Lanner, M. Andersson, E. Danielsson, C. Kaiser, I.M. Renstrom, M. Warolen, S.R. James, Insulin receptor activation and down-regulation by cationic lipid transfection reagents, BMC.Cell Biol., 5 (2004) 7.

[75] P. Järver, I. Mäger, Ü. Langel, In vivo biodistribution and efficacy of peptide mediated delivery, Trends Pharmacol.Sci., 31 (2010) 528-535.

[76] J.B. Rothbard, S. Garlington, Q. Lin, T. Kirschberg, E. Kreider, P.L. McGrane, P.A. Wender, P.A. Khavari, Conjugation of arginine oligomers to cyclosporin A facilitates topical delivery and inhibition of inflammation, Nat.Med., 6 (2000) 1253-1257.

[77] K. Inagaki, L. Chen, F. Ikeno, F.H. Lee, K. Imahashi, D.M. Bouley, M. Rezaee, P.G. Yock, E. Murphy, D. Mochly-Rosen, Inhibition of delta-protein kinase C protects against reperfusion injury of the ischemic heart in vivo, Circulation, 108 (2003) 2304-2307.

[78] A. Amantana, H.M. Moulton, M.L. Cate, M.T. Reddy, T. Whitehead, J.N. Hassinger, D.S. Youngblood, P.L. Iversen, Pharmacokinetics, biodistribution, stability and toxicity of a cell-penetrating peptide-morpholino oligomer conjugate, Bioconjug.Chem., 18 (2007) 1325-1331.

[79] T. Borsello, C. Bonny, Use of cell-permeable peptides to prevent neuronal degeneration, Trends Mol.Med., 10 (2004) 239-244.

[80] J.R. Liu, Y. Zhao, A. Patzer, N. Staak, R. Boehm, G. Deuschl, J. Culman, C. Bonny, T. Herdegen, C. Eschenfelder, The c-Jun N-terminal kinase (JNK) inhibitor XG-102 enhances the neuroprotection of hyperbaric oxygen after cerebral ischaemia in adult rats, Neuropathol.Appl.Neurobiol., 36 (2010) 211-224.

[81] D. Michel-Monigadon, C. Bonny, L. Hirt, c-Jun N-terminal kinase pathway inhibition in intracerebral hemorrhage, Cerebrovasc.Dis., 29 (2010) 564-570.

[82] G. Milano, S. Morel, C. Bonny, M. Samaja, L.K. von Segesser, P. Nicod, G. Vassalli, A peptide inhibitor of c-Jun NH2-terminal kinase reduces myocardial ischemia-reperfusion injury and infarct size in vivo, Am.J.Physiol Heart Circ.Physiol, 292 (2007) H1828-H1835.

[83] E. Bates, C. Bode, M. Costa, C.M. Gibson, C. Granger, C. Green, K. Grimes, R. Harrington, K. Huber, N. Kleiman, D. Mochly-Rosen, M. Roe, Z. Sadowski, S. Solomon, P. Widimsky, Intracoronary KAI-9803 as an adjunct to primary percutaneous coronary intervention for acute ST-segment elevation myocardial infarction, Circulation, 117 (2008) 886-896.

[84] H. Michiue, A. Eguchi, M. Scadeng, S.F. Dowdy, Induction of in vivo synthetic lethal RNAi responses to treat glioblastoma, Cancer Biol.Ther., 8 (2009) 2306-2313.

[85] R. Begley, T. Liron, J. Baryza, D. Mochly-Rosen, Biodistribution of intracellularly acting peptides conjugated reversibly to Tat, Biochem.Biophys.Res.Commun., 318 (2004) 949-954.

[86] A. Toro, M. Paiva, C. Ackerley, E. Grunebaum, Intracellular delivery of purine nucleoside phosphorylase (PNP) fused to protein transduction domain corrects PNP deficiency in vitro, Cell Immunol., 240 (2006) 107-115.

[87] S.A. Moschos, S.W. Jones, M.M. Perry, A.E. Williams, J.S. Erjefalt, J.J. Turner, P.J. Barnes, B.S. Sproat, M.J. Gait, M.A. Lindsay, Lung delivery studies using siRNA conjugated to TAT(48-60) and penetratin reveal peptide induced reduction in gene expression and induction of innate immunity, Bioconjug.Chem., 18 (2007) 1450-1459.

[88] T.A. Aguilera, E.S. Olson, M.M. Timmers, T. Jiang, R.Y. Tsien, Systemic in vivo distribution of activatable cell penetrating peptides is superior to that of cell penetrating peptides, Integr.Biol.(Camb.), 1 (2009) 371-381.

[89] D. Sarko, B. Beijer, R.G. Boy, E.M. Nothelfer, K. Leotta, M. Eisenhut, A. Altmann, U. Haberkorn, W. Mier, The Pharmacokinetics of Cell-Penetrating Peptides, Mol.Pharm., 7 (2010) 2224-2231.

[90] R.M. Sawant, J.P. Hurley, S. Salmaso, A. Kale, E. Tolcheva, T.S. Levchenko, V.P. Torchilin, "SMART" drug delivery systems: double-targeted pH-responsive pharmaceutical nanocarriers, Bioconjug.Chem., 17 (2006) 943-949.

[91] M. Whitney, J.L. Crisp, E.S. Olson, T.A. Aguilera, L.A. Gross, L.G. Ellies, R.Y. Tsien, Parallel in vivo and in vitro selection using phage display identifies protease-dependent tumor-targeting peptides, J.Biol.Chem., 285 (2010) 22532-22541.

[92] R. Miyamoto, H. Akizawa, T. Nishikawa, T. Uehara, Y. Azuma, I. Nakase, S. Futaki, H. Hanaoka, Y. Iida, K. Endo, Y. Arano, Enhanced Target-Specific Accumulation of Radiolabeled Antibodies by Conjugating Arginine-Rich Peptides as Anchoring Molecules, Bioconjug.Chem., 21 (2010) 2031-2037.

[93] H. Myrberg, L. Zhang, M. Mae, U. Langel, Design of a tumor-homing cell-penetrating peptide, Bioconjug.Chem., 19 (2008) 70-75.

[94] F. Danhier, O. Feron, V. Preat, To exploit the tumor microenvironment: Passive and active tumor targeting of nanocarriers for anti-cancer drug delivery, J.Control Release, 148 (2010) 135-146.

[95] E. Vives, J. Schmidt, A. Pelegrin, Cell-penetrating and cell-targeting peptides in drug delivery, Biochim.Biophys.Acta, 1786 (2008) 126-138.

[96] G.J. Doherty, H.T. McMahon, Mechanisms of endocytosis, Annu.Rev.Biochem., 78 (2009) 857-902.

[97] H. Jenssen, K. Sandvik, J.H. Andersen, R.E. Hancock, T.J. Gutteberg, Inhibition of HSV cell-to-cell spread by lactoferrin and lactoferricin, Antiviral Res., 79 (2008) 192-198.

[98] C. Poillot, K. Dridi, H. Bichraoui, J. Pecher, S. Alphonse, B. Douzi, M. Ronjat, H. Darbon, W.M. de, D-maurocalcine, a pharmacologically-inert efficient cell penetrating peptide analogue, J.Biol.Chem., 285 (2010) 34168-34180.

[99] M. Hälbrink, K. Ilk, A. Elmquist, P. Lundberg, M. Lindgren, Y. Jiang, M. Pooga, U. Soomets, Ü. Langel, Prediction of Cell-Penetrating Peptides, International Journal of Peptide Research and Therapeutics, 11 (2005) 249-259.

[100] E.L. Smith, E.H. Schuchman, The unexpected role of acid sphingomyelinase in cell death and the pathophysiology of common diseases, FASEB J., 22 (2008) 3419-3431.

[101] S.A. Saddoughi, P. Song, B. Ogretmen, Roles of bioactive sphingolipids in cancer biology and therapeutics, Subcell.Biochem., 49 (2008) 413-440.

[102] L.R. Montes, M.B. Ruiz-Arguello, F.M. Goni, A. Alonso, Membrane restructuring via ceramide results in enhanced solute efflux, J.Biol.Chem., 277 (2002) 11788-11794.

[103] E. Gulbins, S. Dreschers, B. Wilker, H. Grassme, Ceramide, membrane rafts and infections, J.Mol.Med., 82 (2004) 357-363.

[104] C.A. Dumitru, Y. Zhang, X. Li, E. Gulbins, Ceramide: a novel player in reactive oxygen species-induced signaling?, Antioxid.Redox.Signal., 9 (2007) 1535-1540.

[105] S. Aroui, S. Brahim, J. Hamelin, W.M. de, J. Breard, A. Kenani, Conjugation of doxorubicin to cell penetrating peptides sensitizes human breast MDA-MB 231 cancer cells to endogenous TRAIL-induced apoptosis, Apoptosis., 14 (2009) 1352-1365.

Cationic cell-penetrating peptides induce ceramide formation via acid sphingomyelinase: implications for uptake

Wouter P.R. Verdurmen, Melissa Thanos, Ivo R. Ruttekolk, Erich Gulbins and Roland Brock

Chapter three

3 Cationic cell-penetrating peptides induce ceramide formation via acid sphingomyelinase: implications for uptake

Wouter P. R. Verdurmen[a], Melissa Thanos[b], Ivo R. Ruttekolk[a], Erich Gulbins[b], Roland Brock[a]

[a]Department of Biochemistry, Nijmegen Centre for Molecular Life Sciences, Radboud University Nijmegen Medical Centre, The Netherlands
[b]Department of Molecular Biology, University of Duisburg-Essen, Germany

Abstract

Cationic cell-penetrating peptides (CPP) are receiving increasing attention as molecular transporters of membrane-impermeable molecules. Import of cationic CPP occurs both via endocytosis and – at higher peptide concentrations – in an endocytosis-independent manner via localized regions of the plasma membrane. At present, this endocytosis-independent import of cationic CPP is not well understood, but has been shown to be sensitive to various pharmacological inhibitors, suggesting a role of an unidentified enzymatic activity. Here, we demonstrate that the direct translocation of cationic CPP depends on a CPP-induced translocation of acid sphingomyelinase (ASMase) to the outer leaflet of the plasma membrane and ceramide formation. The involvement of ASMase in uptake was confirmed by a pharmacological inhibition of ASMase by imipramine and a subsequent rescue of uptake through external addition of sphingomyelinase, and by using ASMase-deficient cells. We also found that the threshold for direct CPP translocation can be lowered through addition of sphingomyelinase and that sphingomyelinase enhances the translocation of R9 coupled to low-molecular weight cargos, but not high-molecular weight cargos. In conclusion, we show that a previously poorly understood mechanism of cationic CPP import depends on the ASMase-dependent formation of ceramide on the outer leaflet of the plasma membrane. To our knowledge, this is the first illustration that a class of delivery vectors operates through the induction of an enzymatic activity that changes the lipid composition of the plasma membrane.

3.1   Introduction

Interest in cell-penetrating peptides (CPP) as tools to deliver membrane-impermeable therapeutic molecules continues to increase. This development is illustrated by the increasing efforts of the scientific community to elucidate the chemical, physical and biological principles underlying the activity of CPP and CPP-based delivery systems [1-4] and the steep rise in the number of therapeutic strategies that are being pursued with these systems [5, 6]. It is becoming progressively clear that instead of a single mechanism that is valid for all CPP, multiple modes-of-action exist with respect to the route of internalization and intracellular trafficking, that depend on the cell line [7], the CPP [8], and the cargo [9, 10]. Although endocytosis is now considered the major internalization route of cationic CPP, [1, 11-14] direct translocation for cationic CPP has also been observed, mainly at high [8, 15-17], but also at low concentrations [18, 19].

For arginine-rich CPP the potential for direct translocation is thought be related to the ability of the guanidinium moieties of arginines to form bidentate hydrogen bonds with membrane lipids [20] and is underscored by the ability of the arginine-rich TAT peptide to induce pores in artificial membranes, as was observed by small angle X-ray scattering [21]. Moreover, molecular-dynamics simulations indicate the potential of arginine-rich peptides to form transient pores in plasma membranes in the presence of an electrochemical gradient and provide a mechanistic hypothesis for direct membrane translocation [22].

Nevertheless, biological details remain poorly understood and it is not clear to which degree *in vitro* models manage to reflect the complex molecular environment of a cell. At higher concentrations, direct cytoplasmic import of cationic CPP has been shown to depend on spatially confined nucleation zones. This rapid import is sensitive to the PKCδ inhibitor rottlerin and to chlorpromazine [8]. Available evidence indicates that the plasma membrane remains intact. In a search for a common denominator of the observed pharmacological profile, we discovered that both molecules act as inhibitors of acid sphingomyelinase (ASMase) activity [23-25]. This finding provided us with a rationale for investigating a possible involvement of ASMase in the CPP uptake via direct translocation.

Acid sphingomyelinase has traditionally been known in relation to Niemann-Pick disease, a lysosomal storage disorder [26]. More recently, an important role for this enzyme in ceramide-mediated signal transduction pathways has emerged, linking its activity to a variety of common diseases, among which are cancer, cardiovascular diseases and diabetes [27]. A major function of this enzyme is the hydrolysis of sphingomyelin to ceramide and phosphorylcholine following a trigger-initiated translocation from lysosomes to the outer leaflet of the plasma membrane. The details of the translocation mechanism are unknown at

present. Ceramide is a lipid with a well-established role in the induction of antiproliferative and apoptotic responses in a variety of cancer cells [28]. As a part of this role, ceramide greatly affects the structure and properties of cellular membranes. In the plasma membrane ceramide-enriched membrane domains modulate signaling [29, 30]. In the mitochondrial outer membrane ceramide increases permeability [31]. Here, we provide evidence for a role of ceramide formation by ASMase at the plasma membrane in the rapid cytoplasmic import of cationic CPP. This finding gives rise to the concept that cationic CPP enhance their own uptake by initiating a positive feed-back loop that involves an enzymatic alteration of the lipid composition of the plasma membrane.

3.2   Materials and methods

3.2.1   Materials

C-terminally amidated peptides were purchased from EMC microcollections (Tübingen, Germany). Fluorophore-labeled peptides were synthesized with an N-terminal carboxyfluorescein-label. Purity was evaluated by high-performance liquid chromatography (HPLC) and identity confirmed by mass spectrometry. If required, peptides were further purified to a purity of > 95 % using reversed-phase HPLC. The CPP hLF was oxidized before use as described previously [32]. Bovine serum albumin (BSA), glucose, imipramine, rottlerin and bacterial sphingomyelinase (from Bacillus Cereus, specific activity was 100 units/mg based on the Lowry protein assay) were from Sigma-Aldrich (Zwijndrecht, the Netherlands). Alexa-647 labeled annexin-V was from Invitrogen (Eugene, U.S.A.) and phenylmethylsulfonyl fluoride (PMSF) was from Research Organics (Cleveland, U.S.A). Standard chemicals were from Sigma-Aldrich and Merck (Darmstadt, Germany). HPMA-R9 conjugates were prepared as described previously [33].

3.2.2   Cell culture

HeLa cells were maintained in RPMI 1640 (PAN Biotech, Aidenbach, Germany) supplemented with 10 % fetal calf serum (FCS; PAN Biotech) and incubated at 37°C in a 5 % CO_2-containing, humidified incubator. Cells were passaged every 2 to 3 days. Primary mouse fibroblasts were obtained from lung or orbital tissue explants from wild-type (WT) and *Asm*$^{-/-}$ mice [34]. Mice were raised for 8-10 weeks before they were sacrificed. Primary fibroblasts were cultured in 6-cm dishes in minimum essential medium supplemented with 10 % FCS, penicillin and streptomycin, 1 % non-essential amino acid, 1 % sodium

pyruvate, 1 % 4-(2-hydroxyethyl)-1-piperazineethanesulfonic acid (HEPES) buffer, and 1 % L-glutamine (all from GIBCO, Invitrogen), at 37°C in a 10 % CO_2-containing humidified incubator and passaged every week. For experiments, passages 2 and 3 were used. For experiments with imipramine using primary cells, primary mouse feet fibroblasts were kindly provided by F. Valsecchi (Radboud University Nijmegen Medical Centre).

3.2.3 *Confocal laser scanning microscopy*

Confocal laser scanning microscopy was performed on a TCS SP5 confocal microscope (Leica Microsystems, Mannheim, Germany) equipped with an HCX PL APO 63 x N.A. 1.2 water immersion lens. Cells were maintained at 37°C on a temperature-controlled microscope stage. Images of ASMase-deficient cells were also taken with an HCX PL APO 63 x N.A. 1.4 oil immersion lens (Leica Microsystems) at room temperature (RT), as indicated. For all microscopy images, one confocal slice is shown.

3.2.4 *Peptide uptake*

For confocal microscopy, HeLa cells or primary mouse fibroblasts were seeded in 8-well microscopy chambers (Nunc, Wiesbaden, Germany) and grown to 75 % confluence. Cells were incubated with peptides in RPMI 1640 supplemented with 10 % FCS for durations and concentrations as indicated for the individual experiments. Imipramine pre-treatment to reduce ASMase activity was conducted by incubating cells for 30 min with 30 µM imipramine in RPMI 1640 without FCS. 30 µM imipramine and 10 % FCS were included during peptide incubations. In experiments with bacterial sphingomyelinase, imipramine was only present before, but not during the peptide incubations. Cells were washed twice after the incubation and living cells were analyzed immediately by confocal microscopy.

Modifications for uptake experiments by flow cytometry were the use of 24-well plates (Sarstedt, Numbrecht, Germany) and a trypsinization step, which was followed by centrifugation and resuspension in 200 µl HEPES-buffered saline (HBS; 10 mM HEPES, 135 mM NaCl, 5 mM KCl, 1 mM $MgCl_2$, 1.8 mM $CaCl_2$, pH 7.4). Cellular fluorescence of 10,000 cells, gated on the basis of forward and sideward scatter, was measured using a BD FACScan flow cytometer equipped with a 488 nm laser (BD Biosciences, Erembodegem, Belgium) and analyzed using Summit software (Fort Collins, USA).

3.2.5   Immunofluorescence

HeLa cells were seeded in 8-well microscopy chambers and grown to 75 % confluence. Cells were incubated with 20 µM R9 for 20 min at 37°C, washed twice with pre-warmed HBS containing 0.1 % (w/v) BSA and 5 mM glucose (HBS+) supplemented with 0.025 % Tween-20 and fixed for 15 min at RT with 3 % paraformaldehyde in HBS. Then, cells were washed twice with HBS+ supplemented with 0.025 % Tween-20 and blocked for 15 min at RT with the same buffer. Incubation with the primary antibody took place for 1 h at RT in 150 µl HBS containing 0.1 % (w/v) BSA (HBS/BSA) per well. The rabbit polyclonal IgG anti-ASMase antibody sc11352 (dilution 1:50, Santa Cruz Biotechnology, Santa Cruz, U.S.A.) was used for ASMase detection. A rabbit polyclonal IgG against NFκB was used as an isotype control (Santa Cruz Biotechnology). Ceramide was detected with a 1:50 dilution in HBS/BSA of a monoclonal mouse anti-ceramide IgM antibody 15B4 (Alexis biochemicals, Lausen, Switzerland). A b allotype, anti-KLH mouse IgM antibody (BD Pharmingen, San Diego, U.S.A.) was used as an isotype control for ceramide detection. After incubation with the primary antibody, cells were washed 2 x 5 min with HBS+ supplemented with 0.025 % Tween-20. Incubation with secondary antibodies was for 45 min in HBS/BSA, after which cells were washed twice. Confocal images were taken immediately. For detection of ASMase and isotype control, an Alexa-633-conjugated goat-anti-rabbit IgG (H+L) antibody (Invitrogen, 1:100 dilution) was used. For detection of ceramide and isotype, an Alexa-633-conjugated goat-anti mouse IgG (H+L) antibody (Invitrogen, 1:100 dilution) was used.

3.2.6   ASMase activity assay
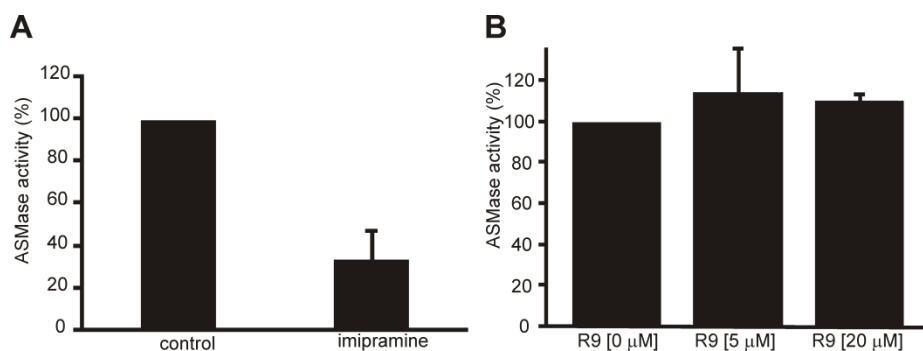
HeLa cells were seeded at a density of 80,000 cells in 24-well plates one day before the experiment. Cells were treated for 30 min with 30 µM imipramine or for 20 min with unlabeled R9 at 5 or 20 µM. Then, cells were lysed and scraped in cold distilled water containing 1 mM PMSF, followed by three freeze-thaw cycles using liquid nitrogen. The lysate was centrifuged for 10 min at 18,000 g and the ASMase activity in the supernatant was assayed using an ASMase activity kit (Echelon Biosciences, Salt Lake City, U.S.A.) according to the manufacturer's instructions.

3.3   Results

3.3.1   *Inhibition of direct translocation of nona-arginine (R9) after inhibition of ASMase*

Previously, we and others described the direct cytoplasmic import of cationic CPP through localized plasma membrane regions, which we termed nucleation zones [8, 15, 17]. This import has a particular pharmacological profile, being sensitive to rottlerin, and chlorpromazine. In a search for a common denominator of these findings, we found that both compounds have the potential to interfere with the activation of ASMase. Among other activities, rottlerin has been shown to directly prevent the activation of ASMase [25], whereas chlorpromazine accumulates in acidic compartments in living cells, leading to the displacement of ASMase from the membranes of acidic vesicles into the lumen, after which the enzyme is susceptible to proteolytic degradation by lysosomal proteases [23, 24]. Both compounds are no specific ASMase inhibitors. Nevertheless, given their shared effect on ASMase activity, we hypothesized that the rapid cytoplasmic import might depend on the activation and translocation of ASMase from an intracellular compartment to the extracellular leaflet of the plasma membrane, where it would change the plasma membrane composition by hydrolyzing sphingomyelin to ceramide [30]. To probe for the involvement of ASMase in the direct translocation of R9 in HeLa cells, we decided to first use imipramine as a pharmacological ASMase inhibitor. Like chlorpromazine, imipramine is a cationic amphiphile that accumulates in lysosomal compartments. With respect to ASMase inhibition, the mode of action of imipramine very likely corresponds to that of chlorpromazine [24]. We confirmed the inhibitory activity in our HeLa cells by probing for ASMase activity after treatment of cells with the compound (Figure 3.1A).

Figure 3.1. Effect of imipramine and unlabeled R9 on ASMase activity in HeLa cells. (A) HeLa cells were seeded at a density of 80,000 cells/well in a 24-well plate one day before the experiment. Cells were incubated with 30 μM imipramine in serum-free RPMI, detached by scraping in distilled water containing 1 mM PMSF and lysed by three freeze-thaw steps using liquid nitrogen. ASMase activity was determined using a commercially available ASMase activity kit according to the manufacturer's instructions and normalized to the ASMase activity of the control. Error bars denote the standard error of the mean of two independent experiments performed in triplicate. (B) HeLa cells were seeded at a density of 80,000 cells/well in 24-well plates, incubated with the indicated concentrations of unlabeled peptide for 20 min at 37°C in RPMI + 10 % FCS, washed and assayed for ASMase activity using a commercially available kit according to the manufacturer's instructions. Error bars denote the standard error of two independent experiments. In this assay, unlabeled R9 was employed in order to avoid interference with the fluorescence-based activity assay.

As predicted, imipramine greatly decreased the cytoplasmic uptake of the cationic CPP R9 to a similar degree as rottlerin (Figure 3.2A). By confocal microscopy no significant effects of both inhibitors were observed at a peptide concentration of 5 μM, suggesting that endocytosis was unaffected by these molecules. A quantitative analysis by flow cytometry confirmed that internalization of R9 was reduced by 64 % at 10 μM and even by 81 % at 20 μM R9 (Figure 3.2B-C). At 5 and 2.5 μM, the reduction of the median fluorescence was only 19 % and 22 %, respectively. The use of the human lactoferrin (hLF) peptide, a cationic CPP derived from human lactoferrin [32], demonstrated that imipramine-sensitivity of direct uptake was not restricted to R9. For hLF at 20 μM cytoplasmic fluorescence was also almost completely absent (Figure 3.2D). As for R9, hLF uptake via endocytosis at 5 μM was unaffected.
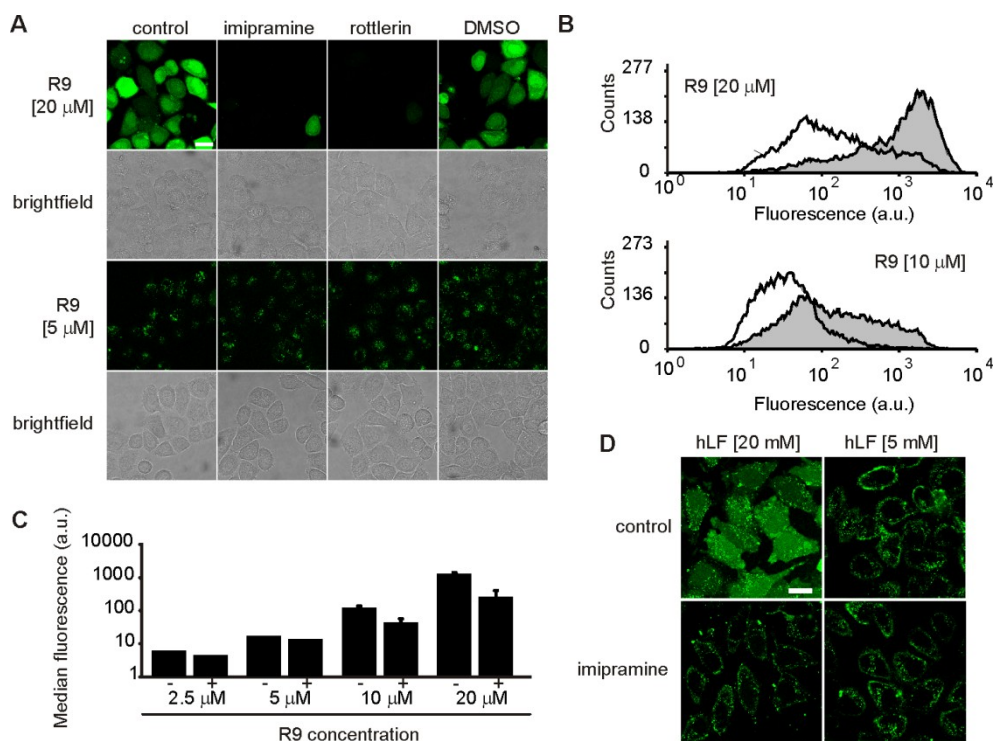
Figure 3.2. Uptake of cationic cell-penetrating peptides is sensitive to imipramine and rottlerin. (A) Effect of a pre-treatment with imipramine or rottlerin on the uptake of R9 in HeLa cells. HeLa cells were pre-treated for 30 min with imipramine or rottlerin and incubated for 20 min at 37°C with the indicated concentrations of R9 in the presence or absence of the inhibitors, washed and analyzed by confocal microscopy. 0.1 % Dimethyl sulfoxide (DMSO) was included as a vehicle control. Settings for image acquisition were optimized for the individual concentrations to avoid saturation or too poor detection (please note the logarithmic scale in panel C). Here, and for all other microscopy images, one confocal slice is shown. The scale bar corresponds to 20 μm. (B) Quantification of cellular fluorescence by flow cytometry. HeLa cells seeded in 24-wells plates were incubated with 20 or 10 µM R9 for 20 min at 37°C with (no fill) or without (grey) imipramine pre-treatment. (C) Median fluorescence intensity of uptake of R9 with (+) or without (-) imipramine as derived from flow cytometry performed as described in (B). Error bars indicate standard error of the mean of two independent experiments. (D) Effect of imipramine on the uptake of the cationic CPP hLF at 5 and 20 µM. Experimental conditions were similar as described in (A). The scale bar indicates 20 μm.

Our hypothesis implicated a role of ceramide formation at the plasma membrane following ASMase translocation in CPP uptake. Therefore, we reasoned that a direct translocation of cationic CPP after an imipramine pre-treatment may be rescued by addition of exogenous bSMase from *Bacillus cereus*, which is known to have a high specificity towards sphingomyelin [35]. Moreover, because the enzyme has a high specific activity

(100 units/mg), aspecific interactions between the enzyme and the peptide or plasma membrane are unlikely to influence peptide uptake. As can be seen in Figure 3.3A, the addition of bSMase rescued the cytoplasmic import of R9 in HeLa cells in a dose-dependent manner, providing more direct evidence for the notion that ceramide formation at the plasma membrane is required for the direct cytoplasmic import. This bSMase-dependent induction of uptake was not due to a compromise of membrane integrity. No uptake of propidium iodide (PI) was observed (Figure 3.3B). Only after addition of detergent, PI entered cells, while peptide rapidly leaked out. This result indicates that the capacity for rapid cytoplasmic uptake is a characteristic of R9, even if ceramide formation is induced by exogenously added enzyme.
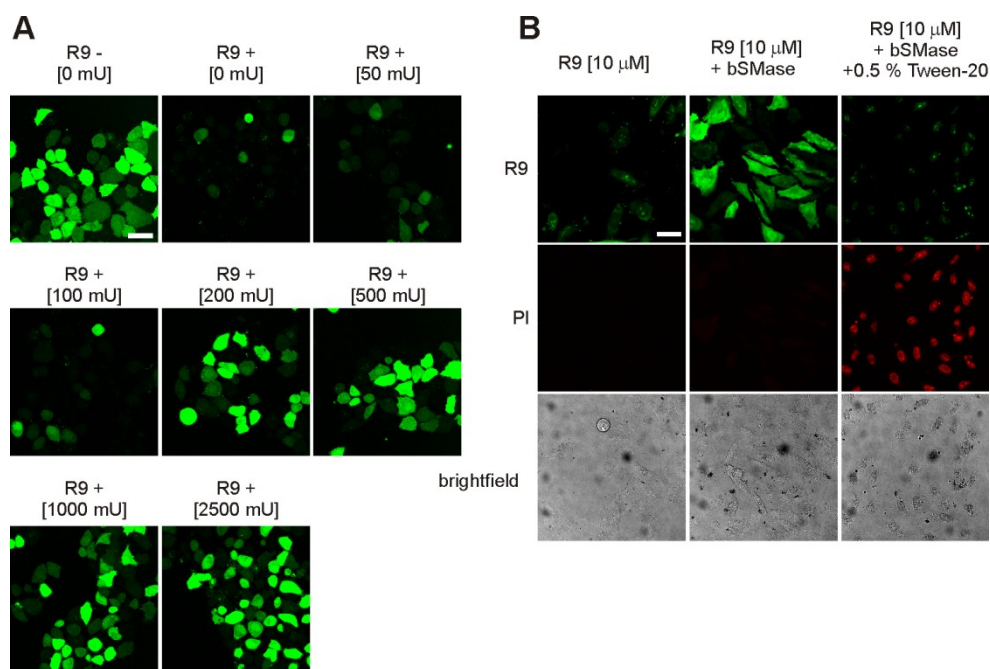
Figure 3.3. Reduced uptake of R9 in imipramine-treated HeLa cells can be rescued by external sphingomyelinase, while preserving membrane integrity. (A) HeLa cells were seeded in 8-well microscopy chambers and grown to 75 % confluence. Cells were pre-treated with 30 μM imipramine (+) for 30 min or left untreated (-). The effect of addition of the indicated concentrations (in mU) of bacterial sphingomyelinase (bSMase) on uptake of 20 μM R9 was evaluated by incubation of cells with peptide and bSMase for 20 min at 37°C, followed by a wash, and immediate analysis by confocal microscopy. (B) Bacterial sphingomyelinase (bSMase) treatment preserves membrane integrity. HeLa cells were seeded in 8-well chambered coverslips as described above and incubated with 10 μM R9 for 20 min at 37°C, in the presence of propidium iodide (PI, 5 μg/ml) and, bSMase (1000 mU) as indicated. Analysis by confocal microscopy was performed without a wash

step. As a positive control for PI uptake, Tween-20 was added to a concentration of 0.5 % in a sample treated with peptide and bSMase 20 min after the start of the incubation. This sample was analyzed 15 min later. The scale bars denote 40 µm.

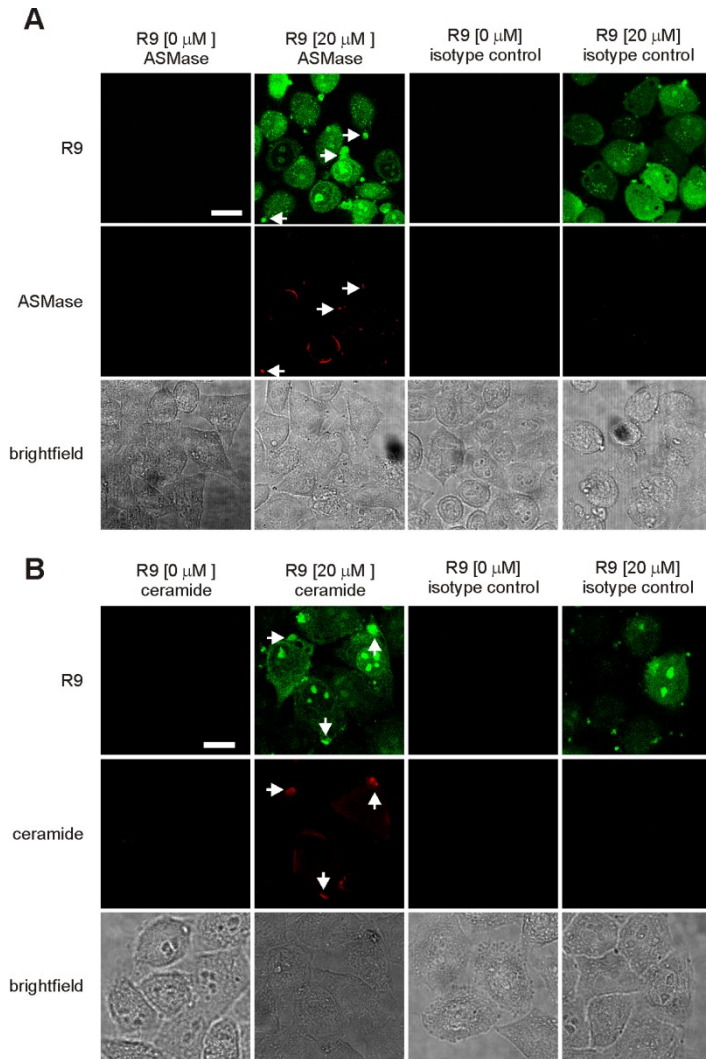### 3.3.2 Translocation of ASMase and the formation of ceramide-enriched membrane platforms

We then pursued the visualization of the translocation of ASMase to the extracellular leaflet of the plasma membrane. For this purpose, fixed but unpermeabilized HeLa cells that had been treated with 20 µM R9 or left untreated were probed for ASMase by immunofluorescence (Figure 3.4A). Translocated ASMase was detectable at the plasma membrane in confocal images of cells treated with R9 in some, but not all, cells. Although translocated ASMase is thought to be derived from intracellular vesicles, the enzyme was not only localized in punctate structures at the plasma membrane, but also across larger platforms, most likely due to rapid lipid raft clustering [36] (Figure 3.4A). In some locations, ASMase immunofluorescence colocalized with fixed nucleation zones (illustrated by arrows in Figure 3.4A), but this was not always evident. As fixation may lead to a redistribution of intracellular peptides, colocalization with fixed CPP should be interpreted with caution [37].

Translocated ASMase was only observed in cells that were brightly stained with fluorescein. To assess whether lower concentrations of R9 also induced ASMase activity, HeLa cells were assayed for total ASMase activity after a 20 min treatment with 5 or 20 µM unlabeled R9 at 37°C using a commercially available ASMase activity kit. However, using this kit, for both concentrations we could only observe a modest trend towards a slightly higher total ASMase activity at both concentrations (Figure 3.1B).

When the formation of ceramide-enriched membrane platforms was investigated by immunofluorescence (Figure 3.4B), we observed a more pronounced colocalization between fixed nucleation zones and ceramide-enriched membrane platforms. No ceramide platforms were identified on untreated cells. Because ceramide affects the membrane architecture in multiple ways, including facilitating the exposure of phosphatidylserine (PS) through transbilayer lipid flip-flop [38], we also probed for an enhanced PS-exposure following an R9 treatment, which was indeed found in a time-lapse experiment (Figure 3.5A).

3.3.3 *Reduced uptake in ASMase-deficient (Asm$^{-/-}$) primary fibroblasts*

To further validate that the reduced uptake after imipramine treatment was due to a reduction in ASMase activity, the cytoplasmic uptake of R9 was investigated in ASMase-deficient (*Asm$^{-/-}$*) primary mouse fibroblasts. Again, cytoplasmic fluorescence was strongly reduced for higher peptide concentrations (Figure 3.6A), thereby corroborating the role of ASMase for the direct cytoplasmic uptake of cationic CPP. At 10 μM peptide only little difference in ASM-deficient and wild-type cells was observed. In these fibroblasts cytoplasmic uptake led to a filamentous distribution of fluorescence, very likely reflecting binding to actin which has been reported for cationic peptides [39]. The effect of ASMase deficiency was similar to the effect of an imipramine treatment in primary mouse fibroblasts (Figure 3.5B), demonstrating that the decreased peptide uptake is due to a lack of ASMase activity and not due to compensatory changes in these cells. Consistently, for the ASM$^{-/-}$-cells, rapid uptake could also be rescued by addition of exogenous bSMase (Figure 3.6B).

Figure 3.4. R9 induces the translocation of ASMase and formation of ceramide platforms at the plasma membrane. HeLa cells were seeded in 8-well microscopy chambers and grown to 75 % confluence. Cells were treated with 20 µM R9 for 20 min at 37°C or left untreated. Immunofluorescence without permeabilization was performed using A) anti-ASMase (IgG) and B) anti-ceramide (IgM) antibodies, including isotype controls. Alexa-633 conjugated secondary antibodies were visualized by confocal microscopy. The scale bar corresponds to 15 (A) or 10 µm (B). The staining of nucleoli by R9 is typically observed upon fixation. Arrows indicate colocalization between nucleation zones and ASMase or ceramide.
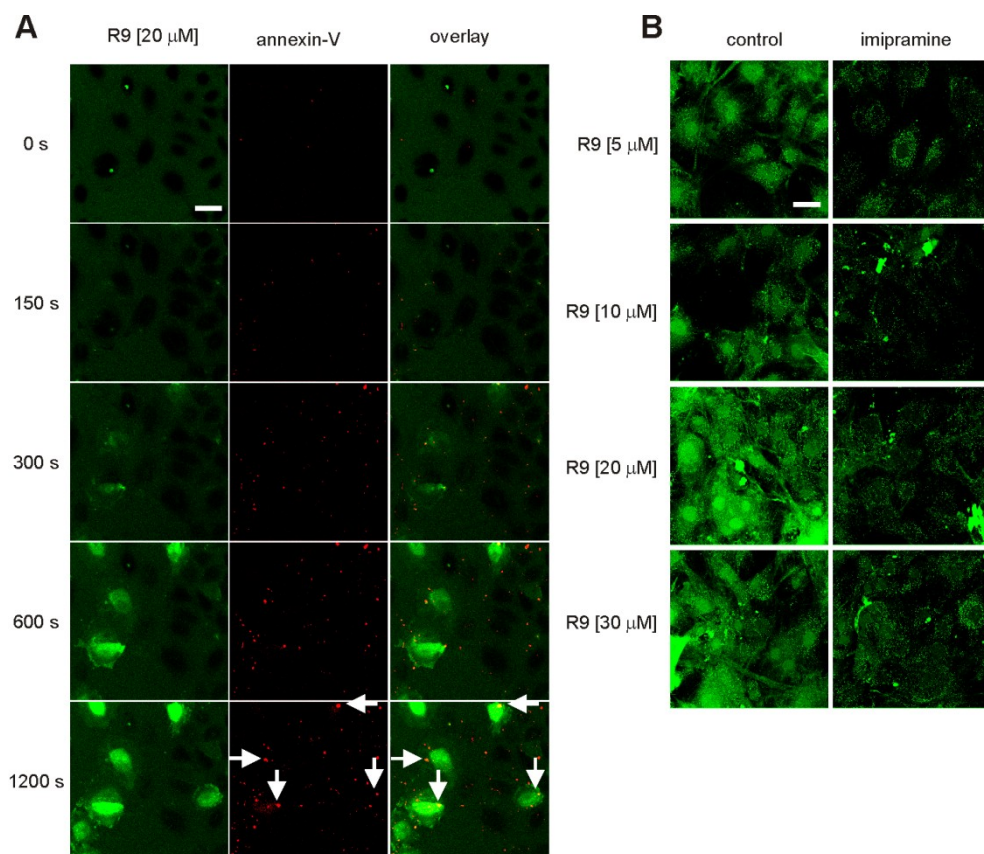
Figure 3.5. Time-lapse of R9-induced phosphatidylserine (PS) exposure and effect of a pre-treatment with imipramine on the uptake of R9 in primary mouse fibroblasts. (A) HeLa cells were seeded one day before the experiment at 40,000 cells/well in 8-well chambered coverslips. Cells were incubated with 20 μM R9 in the presence of Alexa-647 labeled annexin-V as a probe for PS (1:50 dilution) and images were acquired directly. A notable increase in punctate PS exposure following R9 treatment was observed, with all areas corresponding to nucleation zones showing overlap with PS exposure. Besides PS exposure at areas of nucleation zones, punctate PS exposure was also detected at many other areas. The scale bar indicates 20 μm. (B) Primary mouse feet fibroblasts were seeded one day before the experiment in 8-well chambered coverslips and grown to confluence in minimal essential medium supplemented with 10 % FCS. Fibroblasts were pre-treated for 30 min with 30 μM imipramine and incubated for 30 min at 37°C with the indicated concentrations of R9 in the presence (imipramine) or absence (control) of imipramine, washed and analyzed by confocal microscopy. The scale bar denotes 20 μm.

3.3.4 *Effect of exogenous SMase activity on the threshold for peptide uptake via direct translocation*

The results shown above suggested that high concentrations of peptide were required to induce sufficient ASMase activity to initiate rapid cytoplasmic import. We then investigated whether the concentration threshold for rapid cytoplasmic uptake could be lowered by treatment of HeLa cells with bSMase. Cells were incubated with 5 µM R9, a concentration at which direct translocation is not observed, in the presence of 1000 mU bSMase. This experiment would provide information on whether peptide concentration or the induction of sphingomyelinase activity is the limiting factor for uptake via direct translocation. As expected, in the untreated cell population rapid uptake of R9 was virtually absent. In contrast, many cells with intense cytoplasmic and nuclear fluorescence were detected in the sphingomyelinase-treated cell population (Figure 3.7A). Similar observations were made in mouse fibrosarcoma MC57 cells (data not shown).

To assess the size limit for this sphingomyelinase-induced uptake of direct translocation, HeLa cells were incubated with R9 coupled to differently sized cargos. In the presence of sphingomyelinase, we found an increased direct translocation of R9 conjugated to a short 7 amino acids apoptosis-enhancing smac-derived peptide derived from the proapoptotic smac protein [40-42] though only at higher peptide concentrations than for R9 (Figure 3.7A). For R9 coupled to 28 kDa N-(2-hydroxylpropyl) methyl acrylamide (HPMA) polymers [33] no direct translocation was observed at concentrations up to 20 µM of the HPMA polymer, indicating that the sphingomyelinase-mediated uptake was restricted to low-molecular weight molecules.

Previously, we had established that rapid uptake at high R9 concentrations occurred through spatially confined nucleation zones [8]. We were now interested to learn whether external addition of bSMase led to a similar internalization mechanism via localized plasma membrane domains or whether uptake occurred homogeneously distributed over the plasma membrane because of the ubiquitous presence of bSMase. Therefore, a time-lapse experiment was conducted. Peptide uptake was followed in real-time at low concentrations in the presence or absence of bSMase, and at high concentrations in the absence of bSMAse (Figure 3.7B). Also for the externally added bSMase entry was restricted to confined zones at the plasma membrane. Uptake occurred minutes after the start of the incubation and had the same morphological characteristics as the uptake observed for 20 µM R9 in the absence of bSMase. Without bSMase, no rapid cytoplasmic uptake was observed at 5 µM.
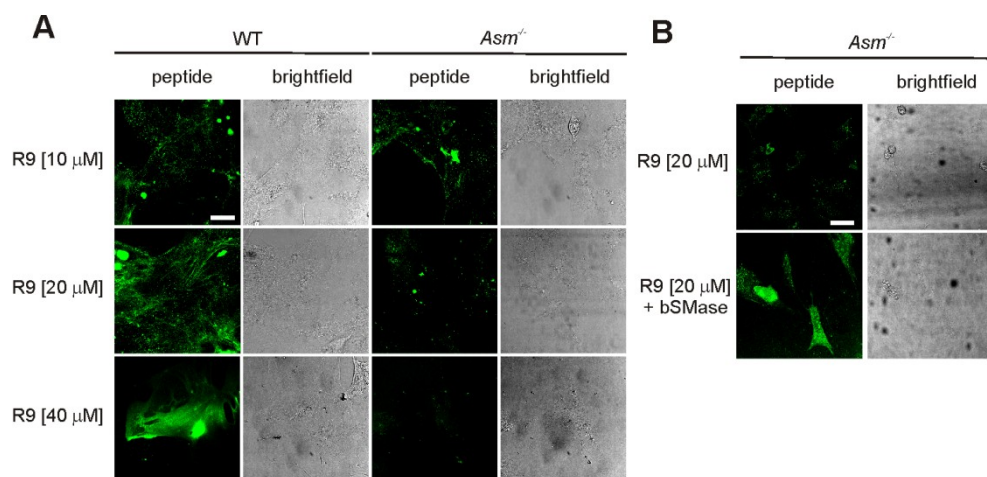
Figure 3.6. Cytoplasmic import of R9 is inhibited in ASMase-deficient primary fibroblasts. Primary mouse fibroblasts were seeded one day before the experiment in 8-well microscopy chambers. (A) R9 was added to wild-type (WT) and ASMase-deficient primary mouse fibroblasts at the indicated concentrations and incubated for 30 min at 37°C in serum-containing medium. Cells were then washed twice and analyzed immediately by confocal microscopy. Image acquisition parameters were optimized for the individual peptide concentrations. (B) ASMase-deficient fibroblasts were incubated with 20 µM R9 for 30 min at 37°C in the presence or absence of 1000 mU bSMase, washed and analyzed immediately by confocal microscopy. Scale bars correspond to 40 µm.
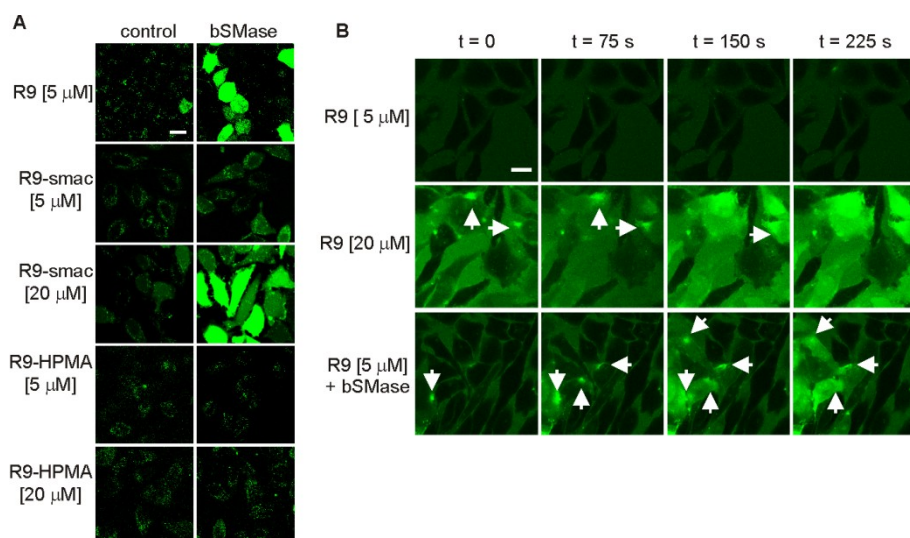
Figure 3.7. Effects of bacterial sphingomyelinase (bSMase) on the uptake of R9 and R9-conjugates. (A) HeLa cells were seeded in 8-well microscopy chambers and grown to 75 % confluence. Cells were incubated for 30 min with the indicated concentrations of R9 or R9-conjugates +/- 1000 mU bSMase, washed and analyzed by confocal microscopy. Settings were optimized for the individual samples. The scale bar corresponds to 20 µm. (B)

Time-lapse experiment of uptake of R9 after bSMase treatment. HeLa cells were seeded in 8-well microscopy chambers, grown to confluence and incubated with the indicated peptide concentrations and bSMase (1000 mU) as indicated. Uptake was followed in real-time by confocal microscopy at 37 °C on a temperature-controlled stage. The timepoint t = 0 corresponds to the first image acquired, which was taken as soon as possible after peptide addition. The scale bar indicates 20 μm.

3.4 Discussion

CPP hold a great potential for the delivery of membrane-impermeable molecules. To exploit this potential to the fullest, it is imperative that the import mechanisms and the associated effects on the cells are well understood. Despite various reports of direct translocation of arginine-rich CPP [8, 15-17, 20], and biophysical [21] and molecular dynamics [22] studies supporting this ability, the biology behind these observations has proven elusive. Here, we demonstrate that the previously poorly understood mechanism of rapid cytoplasmic entry of cationic CPP via nucleation zones strongly depends on the induction of translocation of ASMase to the plasma membrane and ceramide formation.

We verified the involvement of ASMase activity in the rapid import mechanism a) by a pharmacological inhibition of ASMase using imipramine, b) by a rescue of the cytoplasmic CPP uptake via exogenous addition of bSMase, c) by showing a reduced cytoplasmic import in ASMase-deficient primary mouse fibroblasts and d) the corresponding rescue of efficient uptake by exogenously added bSMase. The cellular events involved in the process, a translocation of ASMase to the outer leaflet of the plasma membrane and the formation of ceramide-enriched membrane platforms, were visualized by immunofluorescence microscopy. While phosphatidylserine exposure is only indirect evidence for ceramide formation, our time-lapse experiments nevertheless provide further evidence for an impact of the peptides on membrane architecture [43].

We also showed that the threshold for direct translocation can be lowered by co-incubation of R9 with bSMase. Finally, by real-time confocal microscopy, we demonstrated that the uptake mechanism of R9 at 20 μM is similar to the uptake of 5 μM R9 in the presence of bSMase: both lead to rapid cytoplasmic entry of peptide through spatially confined nucleation zones. To our knowledge, this is the first demonstration of a CPP-mediated induction of enzymatic activity that changes the lipid composition of the plasma membrane, which then stimulates CPP uptake. A schematic representation of the proposed import mechanism is presented in Figure 3.8. Our data suggests the presence of a positive feed-back mechanism: an initial induction of ASMase translocation, followed by a remodeling of the plasma membrane and subsequent cytoplasmic entry. Peptide concentration is limiting for the first step, but not for rapid entry, as demonstrated by

cytoplasmic entry at low peptide concentrations in the presence of exogenously added bSMase. It is interesting to note, that even in the presence of exogenously added bSMase entry is confined to nucleation zones. At this point, we can only speculate that this localized entry reflects the tendency of ceramide-rich microdomains to coalesce to larger structures referred to as ceramide-enriched membrane platforms [44]. Nevertheless, despite these clear indications for a direct role of ceramide in enhancing peptide translocation, the involvement of ceramide-dependent signaling pathways or ceramide-derived metabolites in peptide uptake cannot be excluded.
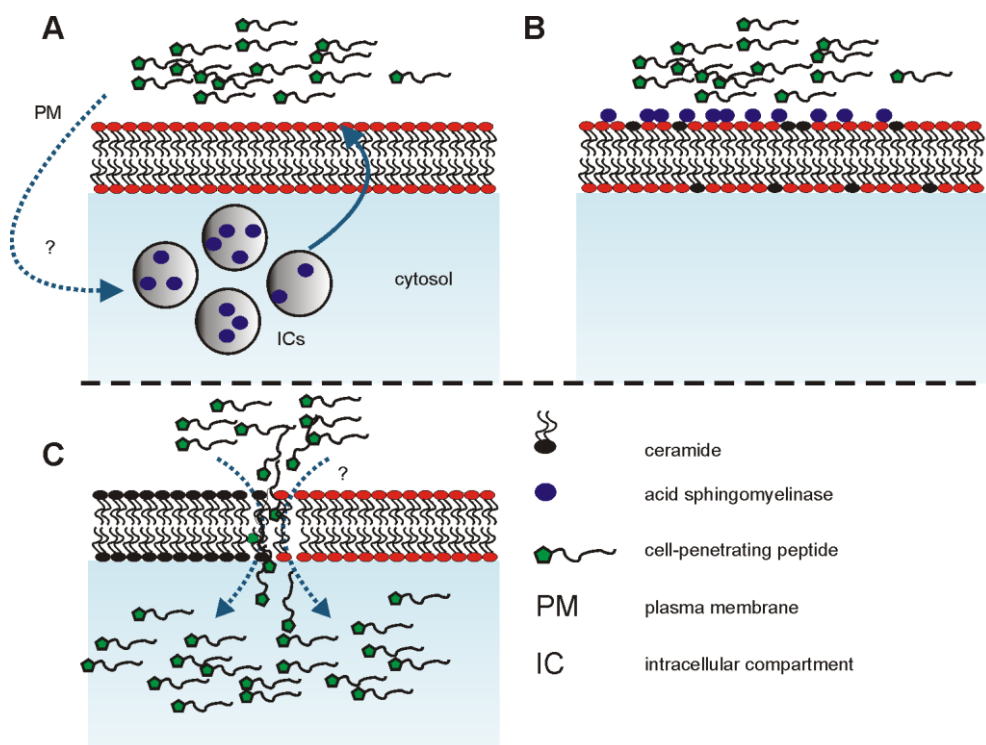
Figure 3.8. Schematic overview depicting the proposed import mechanism of cationic CPP via direct translocation through nucleation zones. (A) First, CPP induce the translocation of ASMase from intracellular compartments to the outer leaflet of the plasma membrane via an unknown mechanism. (B) Second, ASMase hydrolyzes sphingomyelin, resulting in the formation of ceramide-enriched microdomains that may fuse to form larger platforms. (C) Third, cationic CPP enter the cytosol directly across the plasma membrane, most likely at the border region of segregated gel-like ceramide-rich domains and more fluid domains, as this border region is expected to be the most permeable part of the plasma membrane [45]. In their combination, these steps constitute a positive feed-back loop.

It still remains to be resolved by which mechanism the cationic CPP activate ASMase. It is known that, next to apoptosis-inducing growth factors, ASMase is activated by a variety of stressors [25, 46], with a possible role for reactive oxygen species [47-49]. Of note is that superoxide formation induced by octa-arginine was recently described in macrophages [50], although it is currently unclear whether there is a relationship with our present findings. It is also attractive to speculate that CPP-induced exocytosis-dependent membrane repair mechanisms, through release or translocation of lysosomal enzymes [51] lead to an enhanced sphingomyelinase activity at the plasma membrane. However, one should note, that the molecular mechanism underlying the cellular translocation of ASMase is poorly understood in general [52].

Our results are not the first to implicate ceramide in membrane permeability. Even though such effects have been mainly described in model systems [53], an effect of ceramide on the release of pro-apoptotic proteins with a size of up to 57 kDa from mitochondria has also been described [54]. More recently, increases of ceramide concentration in the mitochondrial outer membrane were found to correlate directly with cytochrome C (12 kDa) release [31]. Nevertheless, our data did not support a general increase in membrane permeability as the source of the ASMase-induced rapid peptide uptake. An increased uptake was confined to small molecules directly conjugated to a CPP. No increased uptake was observed if the small molecule was applied by co-administration.

In mammalian cells, many other lipids influence plasma membrane properties. Of special interest in the relationship between cholesterol and ceramide. Cholesterol prevents both ceramide-induced membrane changes through a competition with ceramide for association with lipid rafts [55, 56] and inhibits ASMase activity directly [56], which might explain our previous finding that methyl-β-cyclodextrin enhances peptide uptake [8].

It has been demonstrated that at 4°C direct membrane translocation may be induced in suspension cells, although the mechanism does not involve nucleation zones [15, 19]. It is tempting to speculate that lowering of temperature may affect membrane fluidity or microdomain organisation in a similar way as does ceramide formation, which could create a common denominator for these observations.

Our findings show that cationic CPP do not function as inert delivery vectors, but have significant biological effects instead. Besides its effects on membrane physical properties, ceramide and ASMase are also a major players in widely differing pathological conditions, ranging from Niemann-Pick disease [26] to heart disease and cancer [27]. Given their effect on ceramide and ASMase, the pharmacodynamic properties of cationic CPP should evidently be taken into account when designing CPP-based therapeutic strategies and

evaluating their outcomes. For instance, multiple cationic CPP-drug conjugates were shown to induce ceramide, whereas the drugs did not do so by themselves [57]. This activity was attributed to the mode of drug delivery rather than the vector itself. Our results indicate that the bioactive properties of the cationic CPP may have contributed to the enhanced cytotoxicity. Nevertheless, it should be pointed out that the CPP by themselves were well tolerated, also at concentrations at which nucleation zone-dependent entry was observed [8, 32]. In future studies, it will be highly interesting to investigate whether cationic CPP preferentially induce ceramide in tumor cells, which might be useful for enhancing cytotoxic effects of chemotherapeutic drugs [58]. Noteworthy is also that ASMase activation is not just required for apoptosis initiation or sphingomyelin turnover. Being at the center of sphingolipid catabolism, ASMase is, through its impact on ceramide generation, implicated in numerous other physiological processes [52, 59]. The exact effect of generated ceramide depends on the cellular context and is affected by multiple factors including the presence of ceramidases and effector proteins such as ceramide-activated protein phosphatases. The activation of the ASMase/ceramide pathway is also associated with other pathophysiologically relevant phenomena, as is illustrated by recent findings showing that measles virus-induced membrane ceramide accumulation targets specific processes in T cell activation and function [29]. To what degree there is a physiological mechanism coupling membrane-active peptides to ceramide formation is unknown, although pathological amyloid peptides were found to be able to induce apoptosis in an ASMase-dependent manner [60].

By shedding light on a biological mechanism involved in membrane translocation, our findings regarding membrane remodeling will also be relevant for the choice of a model system for biophysical studies. Ideally, such model systems should have a capacity to reflect the effect ceramide has on the membrane properties in order to be an accurate model system. It will therefore be highly interesting to include ceramide in such experiments or perform experiments with sphingomyelin-containing model membranes in the presence of bSMase.

In conclusion, we show that the previously poorly understood direct cytoplasmic uptake of the cationic CPP depends on a specifically induced enzymatic alteration of the composition of the plasma membrane, namely sphingomyelin hydrolysis to ceramide by ASMase. To our knowledge, no earlier studies have shown that delivery vectors can operate through actively changing the composition of the plasma membrane via an induced enzymatic activity. The finding that cationic CPP by themselves induce ASMase is a further example of the notion that cationic CPP do not act as true Trojan horses, i.e. purely

pharmacokinetic modifiers, but have their own pharmacodynamic activity. Together with the induction of receptor internalization [41], the activation of ASMase is another important factor that requires scrutiny in the application of CPP.

Acknowledgements

Competing interests
The authors declare no competing financial interests.

3.5 References

[1] R. Fischer, M. Fotin-Mleczek, H. Hufnagel, R. Brock, Break on through to the other side-biophysics and cell biology shed light on cell-penetrating peptides, Chembiochem., 6 (2005) 2126-2142.

[2] M. Magzoub, A. Graslund, Cell-penetrating peptides: [corrected] from inception to application, Q.Rev.Biophys., 37 (2004) 147-195.

[3] M.C. Morris, S. Deshayes, F. Heitz, G. Divita, Cell-penetrating peptides: from molecular mechanisms to therapeutics, Biol.Cell, 100 (2008) 201-217.

[4] L.N. Patel, J.L. Zaro, W.C. Shen, Cell penetrating peptides: intracellular pathways and pharmaceutical perspectives, Pharm.Res., 24 (2007) 1977-1992.

[5] C. Foerg, H.P. Merkle, On the biomedical promise of cell penetrating peptides: limits versus prospects, J.Pharm.Sci., 97 (2008) 144-162.

[6] K.M. Stewart, K.L. Horton, S.O. Kelley, Cell-penetrating peptides as delivery vehicles for biology and medicine, Org.Biomol.Chem., 6 (2008) 2242-2255.

[7] J. Mueller, I. Kretzschmar, R. Volkmer, P. Boisguerin, Comparison of cellular uptake using 22 CPPs in 4 different cell lines, Bioconjug.Chem., 19 (2008) 2363-2374.

[8] F. Duchardt, M. Fotin-Mleczek, H. Schwarz, R. Fischer, R. Brock, A comprehensive model for the cellular uptake of cationic cell-penetrating peptides, Traffic., 8 (2007) 848-866.

[9] P. Lundin, H. Johansson, P. Guterstam, T. Holm, M. Hansen, U. Langel, A.S. El, Distinct Uptake Routes of Cell-Penetrating Peptide Conjugates, Bioconjug.Chem., 19 (2008) 2535-2542.

[10] G. Tünnemann, R.M. Martin, S. Haupt, C. Patsch, F. Edenhofer, M.C. Cardoso, Cargo-dependent mode of uptake and bioavailability of TAT-containing proteins and peptides in living cells, FASEB J., 20 (2006) 1775-1784.

[11] I.M. Kaplan, J.S. Wadia, S.F. Dowdy, Cationic TAT peptide transduction domain enters cells by macropinocytosis, J.Control Release, 102 (2005) 247-253.

[12] I. Nakase, M. Niwa, T. Takeuchi, K. Sonomura, N. Kawabata, Y. Koike, M. Takehashi, S. Tanaka, K. Ueda, J.C. Simpson, A.T. Jones, Y. Sugiura, S. Futaki, Cellular uptake of arginine-rich peptides: roles for macropinocytosis and actin rearrangement, Mol.Ther., 10 (2004) 1011-1022.

[13] J.P. Richard, K. Melikov, H. Brooks, P. Prevot, B. Lebleu, L.V. Chernomordik, Cellular uptake of unconjugated TAT peptide involves clathrin-dependent endocytosis and heparan sulfate receptors, Journal of Biological Chemistry, 280 (2005) 15300-15306.

[14] J.S. Wadia, R.V. Stan, S.F. Dowdy, Transducible TAT-HA fusogenic peptide enhances escape of TAT-fusion proteins after lipid raft macropinocytosis, Nature Medicine, 10 (2004) 310-315.

[15] M.M. Fretz, N.A. Penning, S. Al-Taei, S. Futaki, T. Takeuchi, I. Nakase, G. Storm, A.T. Jones, Temperature-, concentration- and cholesterol-dependent translocation of L- and D-octa-arginine across the plasma and nuclear membrane of CD34+ leukaemia cells, Biochem.J., 403 (2007) 335-342.

[16] G. Ter-Avetisyan, G. Tunnemann, D. Nowak, M. Nitschke, A. Herrmann, M. Drab, M.C. Cardoso, Cell entry of arginine-rich peptides is independent of endocytosis, J.Biol.Chem., 284 (2009) 3370-3378.

[17] G. Tünnemann, G. Ter Avetisyan, R.M. Martin, M. Stoockl, A. Herrmann, C. Cardoso, Live-cell analysis of cell penetration ability and toxicity of oligo-arginines, Journal of Peptide Science, 14 (2008) 469-476.

[18] C.Y. Jiao, D. Delaroche, F. Burlina, I.D. Alves, G. Chassaing, S. Sagan, Translocation and endocytosis for cell-penetrating peptides (CPP) internalization, J.Biol.Chem., (2009).

[19] C.L. Watkins, D. Schmaljohann, S. Futaki, A.T. Jones, Low concentration thresholds of plasma membranes for rapid energy-independent translocation of a cell-penetrating peptide, Biochem.J., 420 (2009) 179-189.

[20] J.B. Rothbard, T.C. Jessop, R.S. Lewis, B.A. Murray, P.A. Wender, Role of membrane potential and hydrogen bonding in the mechanism of translocation of guanidinium-rich peptides into cells, J.Am.Chem.Soc., 126 (2004) 9506-9507.

[21] A. Mishra, V.D. Gordon, L. Yang, R. Coridan, G.C. Wong, HIV TAT forms pores in membranes by inducing saddle-splay curvature: potential role of bidentate hydrogen bonding, Angew.Chem.Int.Ed Engl., 47 (2008) 2986-2989.

[22] H.D. Herce, A.E. Garcia, J. Litt, R.S. Kane, P. Martin, N. Enrique, A. Rebolledo, V. Milesi, Arginine-rich peptides destabilize the plasma membrane, consistent with a pore formation translocation mechanism of cell-penetrating peptides, Biophys.J., 97 (2009) 1917-1925.

[23] M. Kolzer, N. Werth, K. Sandhoff, Interactions of acid sphingomyelinase and lipid bilayers in the presence of the tricyclic antidepressant desipramine, FEBS Lett., 559 (2004) 96-98.

[24] J. Kornhuber, P. Tripal, M. Reichel, L. Terfloth, S. Bleich, J. Wiltfang, E. Gulbins, Identification of new functional inhibitors of acid sphingomyelinase using a structure-property-activity relation model, J.Med.Chem., 51 (2008) 219-237.

[25] Y.H. Zeidan, Y.A. Hannun, Activation of acid sphingomyelinase by protein kinase Cdelta-mediated phosphorylation, J.Biol.Chem., 282 (2007) 11549-11561.

[26] R.O. Brady, J.N. Kanfer, M.B. Mock, D.S. Fredrickson, The metabolism of sphingomyelin. II. Evidence of an enzymatic deficiency in Niemann-Pick diseae, Proc.Natl.Acad.Sci.U.S.A, 55 (1966) 366-369.

[27] E.L. Smith, E.H. Schuchman, The unexpected role of acid sphingomyelinase in cell death and the pathophysiology of common diseases, FASEB J., 22 (2008) 3419-3431.

[28] B. Ogretmen, Y.A. Hannun, Biologically active sphingolipids in cancer pathogenesis and treatment, Nat.Rev.Cancer, 4 (2004) 604-616.

[29] E. Gassert, E. Avota, H. Harms, G. Krohne, E. Gulbins, S. Schneider-Schaulies, Induction of membrane ceramides: a novel strategy to interfere with T lymphocyte cytoskeletal reorganisation in viral immunosuppression, PLoS.Pathog., 5 (2009) e1000623.

[30] H. Grassme, A. Jekle, A. Riehle, H. Schwarz, J. Berger, K. Sandhoff, R. Kolesnick, E. Gulbins, CD95 signaling via ceramide-rich membrane rafts, J.Biol.Chem., 276 (2001) 20589-20596.

[31] L.J. Siskind, R.N. Kolesnick, M. Colombini, Ceramide forms channels in mitochondrial outer membranes at physiologically relevant concentrations, Mitochondrion., 6 (2006) 118-125.

[32] F. Duchardt, I.R. Ruttekolk, W. Verdurmen, H. Lortat-Jacob, J. Burck, H. Hufnagel, R. Fischer, H.M. van den, D.W. Lowik, G.W. Vuister, A. Ulrich, W.M. De, R. Brock, A cell-penetrating peptide derived from human lactoferrin with conformation-dependent uptake efficiency, J.Biol.Chem., 248 (2009) 36099-36108.

[33] I.R. Ruttekolk, F. Duchardt, R. Fischer, K.H. Wiesmuller, J. Rademann, R. Brock, HPMA as a scaffold for the modular assembly of functional peptide polymers by native chemical ligation, Bioconjug.Chem., 19 (2008) 2081-2087.

[34] H. Grassme, V. Jendrossek, A. Riehle, K.G. von, J. Berger, H. Schwarz, M. Weller, R. Kolesnick, E. Gulbins, Host defense against Pseudomonas aeruginosa requires ceramide-rich membrane rafts, Nat.Med., 9 (2003) 322-330.

[35] H. Ikezawa, M. Mori, T. Ohyabu, R. Taguchi, Studies on sphingomyelinase of Bacillus cereus. I. Purification and properties, Biochim.Biophys.Acta, 528 (1978) 247-256.

[36] J.X. Bao, M. Xia, J.L. Poklis, W.Q. Han, C. Brimson, P.L. Li, Triggering Role of Acid Sphingomyelinase in Endothelial Lysosome-Membrane Fusion and Dysfunction in Coronary Arteries, Am.J.Physiol Heart Circ.Physiol, 298 (2010) H992-H1002.

[37] J.P. Richard, K. Melikov, E. Vives, C. Ramos, B. Verbeure, M.J. Gait, L.V. Chernomordik, B. Lebleu, Cell-penetrating peptides. A reevaluation of the mechanism of cellular uptake, J.Biol.Chem., 278 (2003) 585-590.

[38] F.X. Contreras, A.V. Villar, A. Alonso, F.M. Goni, Ceramide-induced transbilayer (flip-flop) lipid movement in membranes, Methods Mol.Biol., 462 (2009) 155-165.

[39] D. Delaroche, F.X. Cantrelle, F. Subra, H.C. Van, E. Guittet, C.Y. Jiao, L. Blanchoin, G. Chassaing, S. Lavielle, C. Auclair, S. Sagan, Cell-penetrating peptides with intracellular actin-remodeling activity in malignant fibroblasts, J.Biol.Chem., 285 (2010) 7712-7721.

[40] C. Du, M. Fang, Y. Li, L. Li, X. Wang, Smac, a mitochondrial protein that promotes cytochrome c-dependent caspase activation by eliminating IAP inhibition, Cell, 102 (2000) 33-42.

[41] M. Fotin-Mleczek, S. Welte, O. Mader, F. Duchardt, R. Fischer, H. Hufnagel, P. Scheurich, R. Brock, Cationic cell-penetrating peptides interfere with TNF signalling by induction of TNF receptor internalization, J.Cell Sci., 118 (2005) 3339-3351.

[42] G. Wu, J. Chai, T.L. Suber, J.W. Wu, C. Du, X. Wang, Y. Shi, Structural basis of IAP recognition by Smac/DIABLO, Nature, 408 (2000) 1008-1012.

[43] M.V. Del Gaizo, R.M. Payne, Transactivator of transcription fusion protein transduction causes membrane inversion, J.Biol.Chem., 279 (2004) 32541-32544.

[44] H. Grassme, A. Riehle, B. Wilker, E. Gulbins, Rhinoviruses infect human epithelial cells via ceramide-enriched membrane platforms, J.Biol.Chem., 280 (2005) 26256-26262.

[45] F.M. Goni, A. Alonso, Sphingomyelinases: enzymology and membrane activity, FEBS Lett., 531 (2002) 38-46.

[46] J.A. Rotolo, J. Zhang, M. Donepudi, H. Lee, Z. Fuks, R. Kolesnick, Caspase-dependent and -independent activation of acid sphingomyelinase signaling, J.Biol.Chem., 280 (2005) 26425-26434.

[47] C.A. Dumitru, E. Gulbins, TRAIL activates acid sphingomyelinase via a redox mechanism and releases ceramide to trigger apoptosis, Oncogene, 25 (2006) 5612-5625.

[48] P.A. Lang, M. Schenck, J.P. Nicolay, J.U. Becker, D.S. Kempe, A. Lupescu, S. Koka, K. Eisele, B.A. Klarl, H. Rubben, K.W. Schmid, K. Mann, S. Hildenbrand, H. Hefter, S.M. Huber, T. Wieder, A. Erhardt, D. Haussinger, E. Gulbins, F. Lang, Liver cell death and anemia in Wilson disease involve acid sphingomyelinase and ceramide, Nat.Med., 13 (2007) 164-170.

[49] H. Qiu, T. Edmunds, J. Baker-Malcolm, K.P. Karey, S. Estes, C. Schwarz, H. Hughes, S.M. Van Patten, Activation of human acid sphingomyelinase through modification or deletion of C-terminal cysteine, J.Biol.Chem., 278 (2003) 32744-32752.

[50] J.H. Kuo, M.S. Jan, Y.L. Lin, C. Lin, Interactions between octaarginine and U-937 human macrophages: Global gene expression profiling, superoxide anion content, and cytokine production, J.Control Release, 139 (2009) 197-204.

[51] C. Palm-Apergi, A. Lorents, K. Padari, M. Pooga, M. Hallbrink, The membrane repair response masks membrane disturbances caused by cell-penetrating peptide uptake, FASEB J., 23 (2009) 214-223.

[52] Y.H. Zeidan, Y.A. Hannun, The Acid Sphingomyelinase/Ceramide Pathway: Biomedical Significance and Mechanisms of Regulation, Curr.Mol.Med., 10 (2009) 454-466.

[53] M.B. Ruiz-Arguello, G. Basanez, F.M. Goni, A. Alonso, Different effects of enzyme-generated ceramides and diacylglycerols in phospholipid membrane fusion and leakage, J.Biol.Chem., 271 (1996) 26616-26621.

[54] D.R. Green, J.C. Reed, Mitochondria and apoptosis, Science, 281 (1998) 1309-1312.

[55] Megha, E. London, Ceramide selectively displaces cholesterol from ordered lipid domains (rafts): implications for lipid raft structure and function, J.Biol.Chem., 279 (2004) 9997-10004.

[56] L.C. Silva, A.H. Futerman, M. Prieto, Lipid raft composition modulates sphingomyelinase activity and ceramide-induced membrane physical alterations, Biophys.J., 96 (2009) 3210-3222.

[57] S. Aroui, S. Brahim, J. Hamelin, W.M. De, J. Breard, A. Kenani, Conjugation of doxorubicin to cell penetrating peptides sensitizes human breast MDA-MB 231 cancer cells to endogenous TRAIL-induced apoptosis, Apoptosis., 14 (2009) 1352-1365.

[58] S.A. Saddoughi, P. Song, B. Ogretmen, Roles of bioactive sphingolipids in cancer biology and therapeutics, Subcell.Biochem., 49 (2008) 413-440.

[59] R.W. Jenkins, D. Canals, Y.A. Hannun, Roles and regulation of secretory and lysosomal acid sphingomyelinase, Cell Signal., 21 (2009) 836-846.

[60] N.T. Xuan, E. Shumilina, D.S. Kempe, E. Gulbins, F. Lang, Sphingomyelinase dependent apoptosis of dendritic cells following treatment with amyloid peptides, J.Neuroimmunol., 219 (2010) 81-89.

Preferential uptake of L- versus D-amino acid cell-penetrating peptides in a cell-type dependent manner

Wouter P.R. Verdurmen, Petra Bovee-Geurts, Parvesh Wadhwani, Anne S. Ulrich, Mattias Hällbrink, Toin H. van Kuppevelt and Roland Brock

4 Preferential uptake of L- versus D-amino acid cell-penetrating peptides in a cell type-dependent manner

Wouter P.R. Verdurmen[a], Petra Bovee-Geurts[a], Parvesh Wadhwani[b], Anne S. Ulrich[b], Mattias Hällbrink[c], Toin H. van Kuppevelt[a] and Roland Brock[a]

[a] Department of Biochemistry, Nijmegen Centre for Molecular Life Sciences, Radboud University Nijmegen Medical Centre, Nijmegen, 6525 GA, The Netherlands
[b] Karlsruhe Institute of Technology, Institute for Biological Interfaces (IBG-2), Institute of Organic Chemistry and CFN, Karlsruhe, Germany.
[c] Department of Neurochemistry, Stockholm University, S-10691, Stockholm, Sweden

Abstract

The use of protease-resistant D-peptides is a prominent strategy to overcome proteolytic sensitivity in the use of cell-penetrating peptides (CPPs) as delivery vectors. So far, no major differences have been reported for the uptake of L- and D-peptides. Here, we report that cationic L-CPPs are taken up more efficiently than their D-counterparts in MC57 fibrosarcoma and HeLa cells, but not in Jurkat T leukemia cells. Reduced uptake of D-peptides co-occurred with persistent binding to heparan sulfates (HS) at the plasma membrane. *In vitro* binding studies of L- and D-peptides with heparan sulfate indicated similar binding affinities. Our results identify two key events in the uptake of CPPs: binding to HS chains and the initiation of internalization. Only the second event depends on the chirality of the CPP. This knowledge may be exploited for a stereochemistry-dependent preferential targeting of cells.

4.1 Introduction

The use of cell-penetrating peptides (CPPs) such as nona-arginine (R9), TAT or penetratin as delivery vectors for molecules that otherwise do not cross the plasma membrane is gaining significance in biomedicine [1]. Although different strategies are pursued for the optimization of CPP-based delivery, premature degradation of CPPs before they reach their target *in vivo* remains a common concern for therapeutic applications [2]. The relevance of this concern is exemplified by the rapid degradation of CPPs when they are in contact with

various cell lines [2-4] or when they are exposed to serum [5, 6]. A common strategy to combat this issue is to employ CPPs consisting of D-amino acids (D-CPPs). The altered stereochemistry of peptides containing D-amino acids renders D-CPPs much more protease resistant than their L-amino acid counterparts [5-7].

The increased stability in serum is not limited to peptides composed entirely of D-amino acids, but was also observed for partial D-amino acid substitutions at the termini in small peptides [8] and for CPPs conjugated to morpholino-nucleotide oligomers [7].

For penetratin uptake was observed for the reverse L-amino acids sequence, the D-peptide and a retro-inverso analog, suggesting that backbone chirality is not important for uptake of this CPP [9, 10]. Since uptake was also observed at 4°C, the authors suggested that internalization occurred via a receptor-independent mechanism, most likely involving direct interactions with membrane phospholipids [10]. Later studies corroborated this hypothesis for inverso and retro-inverso analogs of poly-arginines and the arginine-rich TAT peptide [11, 12], which together have led to the prevailing paradigm that cellular uptake of CPPs is a chirality-independent process. Studies using these and other CPPs, including pVEC and sweet arrow peptide provided additional support for this current paradigm [5, 13, 14]. A higher uptake efficiency of D-TAT and D-poly-arginines in the presence of serum [12] was attributed to an increased proteolytic stability [15].

While the available studies thus appear to sketch a uniform picture, one should acknowledge that these studies were conducted with a rather limited number of cell-types. It is well established, however, that different mechanisms for CPP uptake are operating in different cell types [16]. Moreover, some of the earlier studies did not distinguish between membrane-bound and internalized peptides. Nowadays, the distinction between internalized and membrane-associated peptide is considered a vital aspect for the quantification of CPP uptake [17-19] and is generally accomplished by a specific modification of the membrane-bound fraction [17, 18] or by a trypsin and/or heparin treatment of cells. Since trypsin does not degrade D-peptides, in studies comparing the uptake of D- and L-CPP an incubation of cells with heparin is the appropriate treatment for removal of membrane-bound peptides.

Recent advances in the quantification of internalization, and the introduction of protocols to study CPP uptake using live cell confocal microscopy warrant a new analysis of L- and D-CPP uptake. Therefore, the goal of the present study was to study in detail possible differences in the cellular uptake of arginine-rich as well as cationic amphiphilic all-L-CPPs and their all-D counterparts, using a panel of cell types for which we had previously noted differences in the intracellular distribution of CPPs. The CPPs used were nona-arginine (R9), which is considered to be conformationally unstructured, and the

amphiphilic CPP penetratin, which adopts different conformations depending on the local environment and also contains several arginine residues. Furthermore, the human lactoferrin-derived peptide hLF(38-59) was included [20]. Being entirely composed of D-amino acids, the inverso peptide D-nona-arginine (r9) is at the same time also the retro-inverso analog of R9, and as such it is topologically essentially equivalent to R9 with respect to the absolute side-chain orientation. For hLF, uptake efficiency is conformation-dependent. Presence of a disulfide bridge is required for activity [20].

Surprisingly, we found significant differences in the uptake of all-L- and all-D CPPs in HeLa and MC57 cells, but not in Jurkat cells. In cells with reduced uptake of D-peptides, a persistent binding to heparan sulfates (HS) was observed. These differences in uptake were restricted to uptake via endocytosis. In contrast, rapid cytoplasmic uptake by nucleation zones, which occurs for R9 and hLF at higher concentrations [21], was even more effective for r9. Detailed binding studies by surface plasmon resonance (SPR) and isothermal titration calorimetry (ITC) indicated that D- and L-peptides bound to HS with similar affinities, indicating that they also bind cellular heparan sulfates with similar propensity, but differ in their capacity to trigger their endocytic uptake. Results obtained for a series of peptides with partial D-amino acid substitutions suggest that a consecutive stretch of L-amino acids is required to trigger uptake. The cell type dependence of the L versus D preference suggests that the stereochemistry of cationic CPPs may be exploited as a new principle for a cell type selective targeting.

4.2 Results

4.2.1 Cellular uptake of R9 and r9

To address potential differences in the cellular uptake and intracellular trafficking of CPP (for peptide sequences, see table 4.1), we analyzed the uptake and intracellular distribution of R9 and r9 by confocal microscopy in MC57 fibrosarcoma [22], HeLa, and Jurkat cells. The selection of cell lines was motivated by previously observed differences in cytoplasmic fluorescence at low peptide concentrations, at which uptake via endocytosis occurs. In MC57 fibrosarcoma cells, fluorescence was to a larger extent cytoplasmic, while in HeLa cells fluorescence was more restricted to vesicular structures [23]. At low concentrations, fluorescence was also strongly cytoplasmic in Jurkat cells and other leukocytes [13]. Uptake and intracellular distribution were compared after a 45-min incubation with the peptides at a concentration of 5 μM (Figure 4.1A-C).

Table 4.1 Peptide sequences

	Sequence	MW	Ref
R9	[1]Fluo-RRRRRRRRR-NH$_2$[2]	1781	[12]
r9	Fluo-rrrrrrrrr-NH$_2$	1781	[12]
r9-fluo	Ac-rrrrrrrrrk-fluo	1955	n/a
R9 (1,9)	Fluo-rRRRRRRRr-NH$_2$	1781	n/a
R9 (1,3,5,7,9)	Fluo-rRrRrRrRr-NH$_2$	1781	n/a
L-penetratin	Fluo- RQIKIWFQNRRMKWKK-NH$_2$	2605	[10]
D-penetratin	Fluo-rqikiwfqnrrmkwkk-NH$_2$	2605	[10]
L-hLF	Fluo-KCFQWQRNMRKVRGPPVSCIKR-NH$_2$	3076	[20]
D-hLF	Fluo-kcfqwqrnmrkvrgppvscikr-NH$_2$	3076	n/a

[1] Fluo = fluorescein; [2] NH$_2$ indicates C-terminal amide

Unexpectedly, major differences were observed in the uptake of r9 and R9 in both HeLa and MC57 cells (Figure 4.1A-B). Punctate vesicular structures inside cells were more numerous and brighter for R9 compared to r9. Next to this punctate staining, a cytosolic fluorescence was observed for R9 but not for r9 in MC57 and, to a lesser extent, also in HeLa cells for R9. In contrast, for r9 there was a more intense staining of the plasma membrane (Figure 4.1A-B). This staining was more pronounced for MC57 than for HeLa cells. For Jurkat cells, no membrane staining was observed (Figure 4.1C). Instead, only differences in the intracellular localization of R9 and r9 were observed. The distribution of r9 differed from the one of R9 in that the former strongly stained the nucleoli, in accordance with previous observations [13].
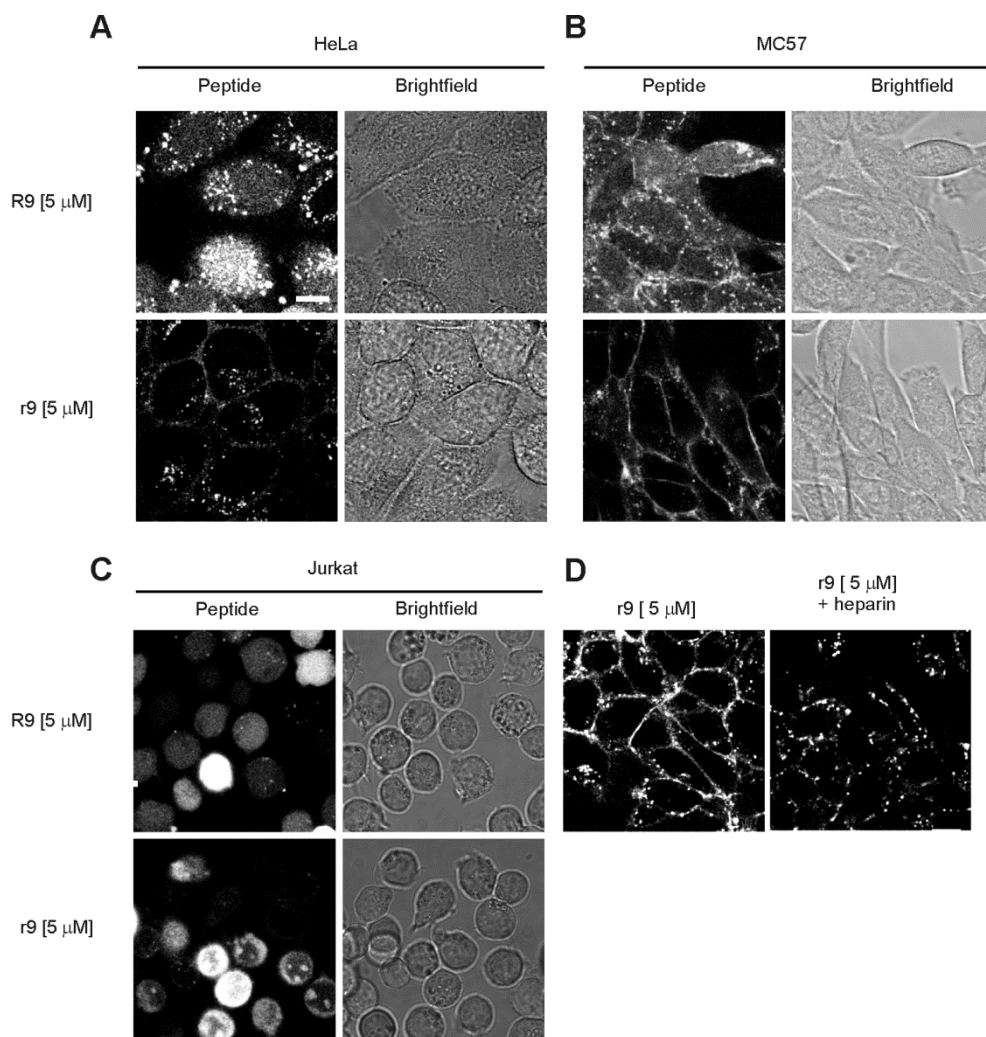
Figure 4.1. Cellular distribution and uptake of R9 and r9 in HeLa (A), MC57 (B), and Jurkat cells (C). HeLa and MC57 cells were seeded in 8-well microscopy chambers, grown to 75 % confluence and incubated with 5 μM of the peptides for 45 min. Jurkat cells were similarly incubated with peptide for 45 min, washed, and then transferred into the microscopy chambers. All cells were washed after incubation with heparin. Confocal images were acquired immediately. (D) Illustration of the heparin-induced removal of cell-associated fluorescence of r9 in living MC57 cells. Following peptide uptake, cells were incubated 2 x 5 min with 100 μg/ml heparin. The scale bar represents 10 μm.

We and others had previously described that at higher peptide concentrations, an alternative internalization mechanism occurs that rapidly leads to cytoplasmic fluorescence [13, 21, 24, 25]. Entry occurs through restricted membrane areas by an acid sphingomyelinase-dependent mechanism [25]. The population of cells that shows peptide entry via this mechanism can be clearly distinguished as cells with high intensity by flow cytometry. Direct cytoplasmic entry was reported to be higher for r9 compared to R9 in various cell types, including HeLa cells [15]. Here, we also observed a much larger proportion of HeLa cells with high total fluorescence after being treated with r9 versus R9 at 20 µM (Figure 4.2). On the other hand, for r9, flow cytometry histograms showed the presence of cells with lower fluorescence than was observed for R9, in agreement with the microscopy data (Figure 4.1). These differences indicate that r9 enters more efficiently by direct cytoplasmic entry and less efficiently via endocytosis. It should be noted, however, that a quantitative determination of peptide uptake by flow cytometry may be hampered by quenching of fluorescence of fluorophores bound to cellular structures or present in acidic vesicular compartments.
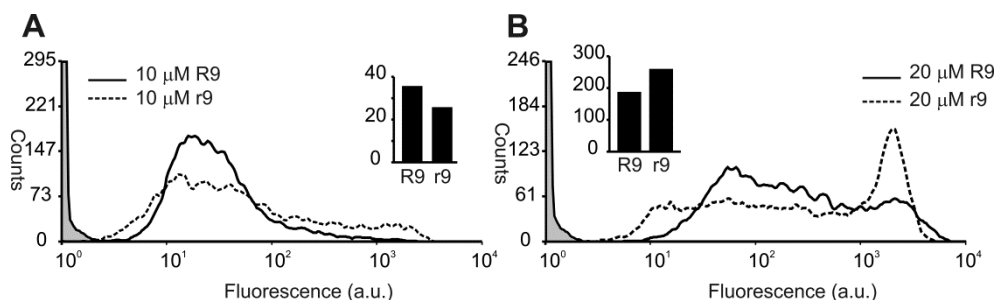
Figure 4.2. Uptake of R9 and r9 measured by flow cytometry. HeLa cells were seeded in 24-wells plates and grown to ~ 75 % confluence. Cells were incubated with 10 (A) or 20 µM (B) R9 or r9 for 20 min at 37°C, washed twice with heparin, trypsinized and resuspended in HBS. Peptide internalization in resuspended cells was then analyzed by flow cytometry. Insets represent median fluorescence intensity of 10,000 gated living cells.

4.2.2   Quantification of uptake

Confocal microscopy showed a more pronounced punctate staining for R9 in comparison to r9 in MC57 and HeLa cells at a peptide concentration of 5 µM, indicative of a more efficient endocytic uptake. To quantitatively confirm these differences, a quantification method was developed based on fluorescence correlation spectroscopy (FCS) in cell lysates, in order to overcome difficulties potentially associated with fluorophore-based assays. Before lysis, cell-associated fluorescence was removed by incubation of cells with

heparin [26], which proved highly efficient in the removal of surface-bound fluorescence (Figure 4.1D). However, even after washing off all membrane-bound peptides, the fluorescence intensity could be influenced by a variety of factors that may differ between R9 and r9. For instance, instead of detecting a genuine difference in peptide uptake, it was also conceivable that differences in fluorescence intensity for R9- and r9-treated MC57 cells may arise due to a higher brightness of the fluorophore when attached to R9. Moreover, quenching of fluorescence in potential peptide aggregates could affect peptide quantification. Furthermore, a fluorescein-labeled degradation product of R9 might be more strongly fluorescent than r9, for which no degradation is expected. Lastly, differential binding to poly-anions, such as oligonucleotides or protein aggregates, could lead to the removal of intact peptides during centrifugation steps which are frequently applied in quantification protocols.

To address all of the above points, we exploited the capacity of FCS to provide information on the total fluorescence, the particle number, the fluorescence per molecule, and the presence of aggregates [27]. Nucleic acids were degraded with benzonuclease, followed by complete degradation of all proteinaceous components by proteinase K (Figure 4.3).

When we quantified the intracellular fluorescence of R9 and r9 with the above-described protocol, the uptake of r9 was only 21 % of that of R9. Even when we corrected for detection efficiency (see legend of Figure 4.3), the uptake of r9 was still only 36 % compared to uptake of R9, supporting the observation that peptide uptake is indeed more efficient for R9. Notably, also the interaction with HS chains that will also be present in lysates did not significantly alter the fluorescence of R9 and r9 (Figure 4.4).
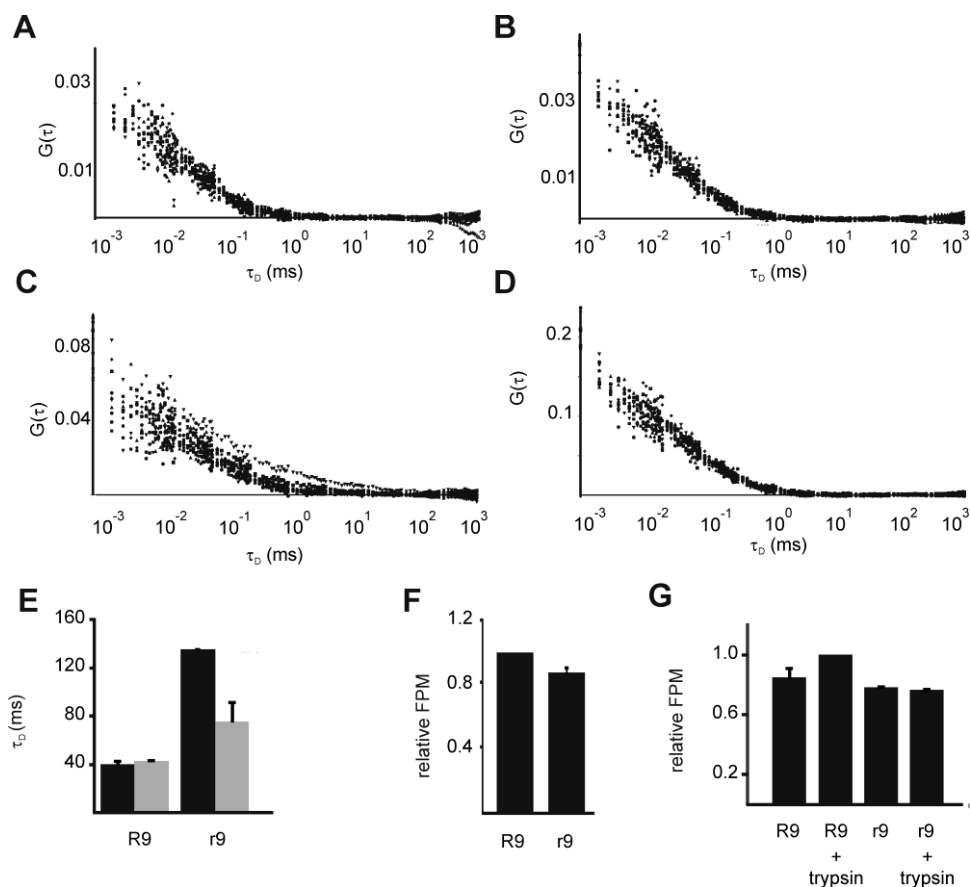
Figure 4.3. Quantification and analysis of fluorescence of internalized fluorophores from R9 and r9 by fluorescence correlation spectroscopy. (A-D) Autocorrelation functions acquired from MC57 cells incubated with R9 (A,B) or r9 (C,D). Measurements were obtained directly after lysis (A,C) or after a treatment of the lysate with benzonuclease and proteinase K (B,D). (E) Diffusional autocorrelation times τ_D of R9 and r9 in MC57 cell lysates directly after lysis (black bars) or after being treated with benzonuclease and proteinase K (grey bars). The diffusion constant of R9 in lysates was unaltered by this treatment, suggesting that most of the fluorescence present in cell lysates represents degradation products also before proteinase K treatment. On the other hand, r9-treated lysates showed shorter diffusion times (τ_D) upon enzyme treatment, i.e. a higher diffusion constant, which is attributed to a reduced association with digested cellular proteins and nucleic acids. Consistent with the expected degradation of R9, the diffusion of fluorophores in R9-treated samples was faster than that of r9 (43 vs 76 µs). After digestion, no aggregates were observed that could have compromised the acquisition of autocorrelation functions. Therefore, the fluorophore concentrations could be determined directly in cell lysates without any centrifugation steps that might have precipitated and thereby removed intact peptides. Notably, even after benzonuclease and proteinase K treatment, τ_D values of intact r9 were longer compared to typical τ_D values of r9 in buffer (40 to 50 µs). This difference is most likely due to the increased viscosity of the lysate. The average number of fluorescent particles in the detection volume is inversely related to the amplitude of the autocorrelation

function. On this basis, besides the total fluorescence intensity, FCS provides information on molecule numbers that is not affected by potential differences in molecular brightness. Furthermore, the ratio of the total fluorescence divided by the number of molecules yields the fluorescence per molecule (FPM) (F,G). (F) FPM of R9 and r9 in lysates treated with benzonuclease and proteinase K. (G) FPM of R9 and r9 in PBS incubated for 3 h at 37 °C with or without trypsin, as indicated. It was found that the fluorescence per molecule differed only marginally between r9 and intact or degraded R9, with similar effects of degradation in buffer (F) and in lysates (G). To be able to compare the uptake of R9 and r9, it was also needed to examine the detection efficiency. Since r9 cannot be degraded by proteinase K, it is still possible that the detection of fluorescently labeled r9 and arginine-coupled fluorophore, the ultimate degradation product of R9, does not occur with equal efficiency. To address this possible source of inaccuracy, a control experiment was carried out in which detection efficiency was analyzed for 10 or 50 nM R9 or r9 added to lysates, which were then treated with benzonuclease and proteinase K. 50 and 10 nM were chosen because this resulted in a similar peptide concentration in the lysate as compared to cellular uptake experiments, ensuring its relevance. It was found that fluorophores attached to intact r9 were indeed less efficiently detected than fluorophores derived from protease-degraded R9 (42 +/- 6 % less efficiently; data not shown). In HBS, both peptides were detected with a comparable efficiency (r9 was detected 4 +/- 13 % less efficiently; data not shown). The data represent the mean +/- SEM.
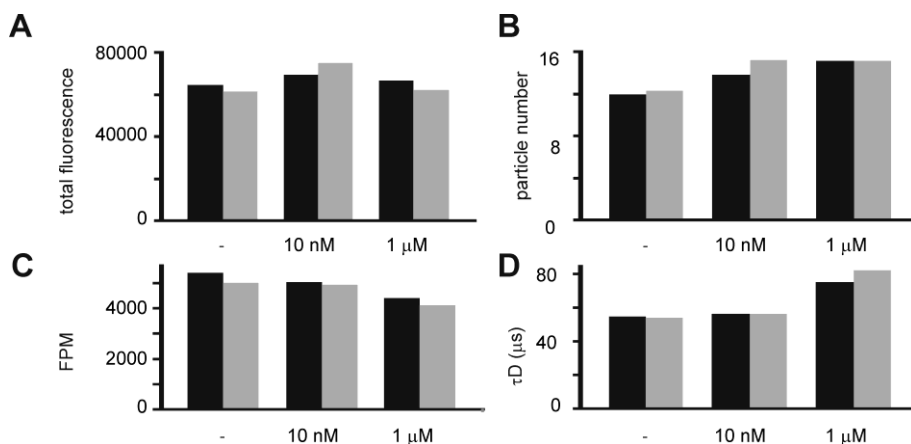
Figure 4.4. Effect of heparan sulfate on fluorescence of nona-arginine. 80 nM of R9 or r9 was incubated with no, 10 nM or 1 μM HS and autocorrelation measurements were acquired by FCS. In panel A, the data show that concentrations of HS of up to 1 μM do not affect the fluorescence significantly. Panel B shows the particle number, which reflects the relative peptide concentration, and panel C the fluorescence per molecule. In panel D, the diffusional autocorrelation times (τD) are represented, which indicate that diffusion of R9/r9 is slower in the presence of a high concentration of heparan sulfate (1 μM). This indicates some interaction of the peptides with HS. However, the increase in τD is too small to relate to large clusters. HS concentrations are indicated at the X-axis. Black and grey bars indicate R9 and r9, respectively.

Due to the complexity of the FCS-based method, we also used a simpler fluorimetry method to assess peptide internalization. With this method, we found that uptake of r9 was

46 +/- 2 % of that of R9 in MC57 cells, and comparable observations were made for HeLa cells (53 +/- 1 %), whereas no significant differences were observed in Jurkat cells (91 +/- 8 % of r9 compared to R9).

Another factor possibly contributing to the observed differences in cellular uptake was the structural environment of the fluorophore. Since r9 corresponds to a retro-inverso R9, coupling of the fluorophore to the C-terminus of r9 should even more closely mimic R9. However, very similar cellular distributions of fluorescence were found for (i) N-terminally carboxyfluorescein-labeled and C-terminally amidated r9, and an (ii) N-terminally acetylated and C-terminally amidated r9, for which the carboxyfluorescein moiety was attached to the C-terminus [28] (Figure 4.5A), demonstrating that the position of the fluorophore does not explain the differences in distribution and uptake between r9 and R9.

4.2.3   *Peptide export*

Another factor that may lead to a different distribution and amount of cell-associated fluorescence is the rate of export of either the CPP or its degradation products. To investigate whether R9 or its degradation products were retained more efficiently in HeLa or MC57 cells over the 1-h time course of the experiments, these cells were electroporated with a 5 μM solution of either R9 or r9 (Figure 4.5B,C). Electroporation delivers a pulse of peptides directly into the cytosol. Therefore, this method is well suited to follow the release kinetics of molecules. Both, the images *per se* and the image-based quantification of the mean intracellular fluorescence illustrate that no relevant differences could be detected in the export of R9 and r9 after 30 min and 1 h, both in MC57 and in HeLa cells. This result indicates that a differential export is also not a likely reason for the observed differences.
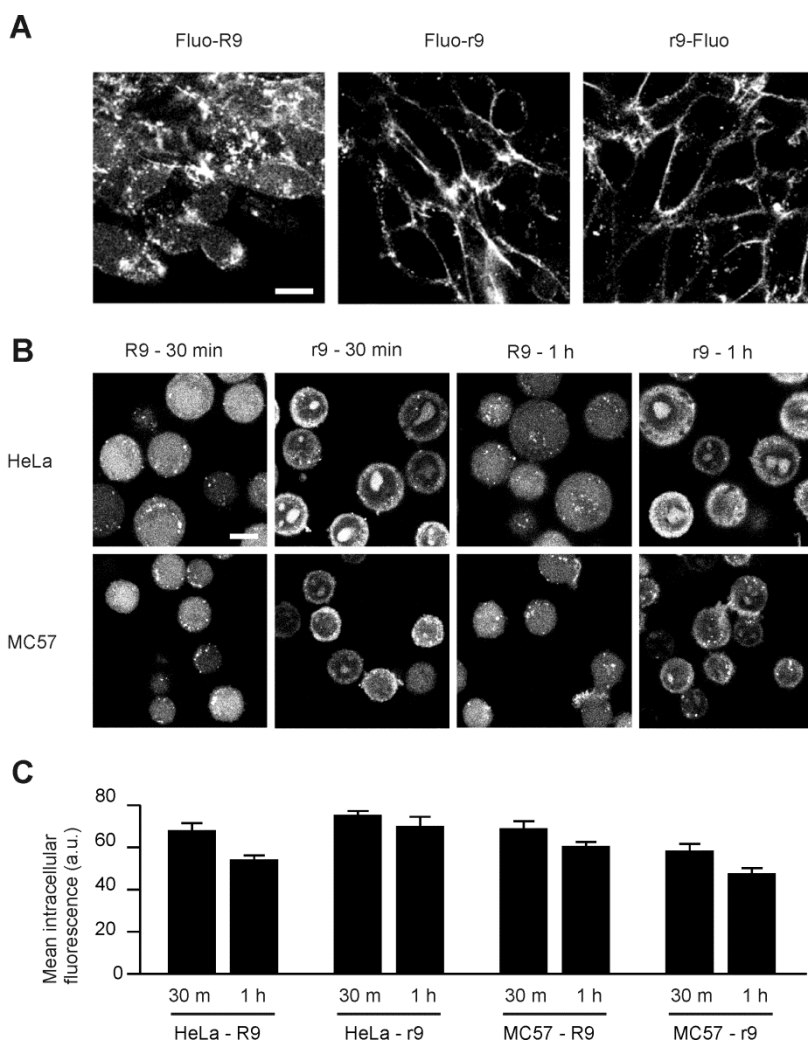
Figure 4.5. Effect of fluorophore position and the rate of export on peptide uptake and/or retention in HeLa and MC57 cells. (A) Cellular uptake and distribution of R9, r9-Fluo and Fluo-r9 after a 45-min incubation in MC57 cells. Cells were seeded in 8-well microscopy chambers, grown to 75 % confluence and incubated with 5 µM of each peptide at 37°C. Cells were washed twice and confocal images were taken immediately. The scale bar represents 20 µm. (B,C) Pulse-chase experiment of R9 and r9 in HeLa and MC57 cells. (B) Cells were electroporated with 5 µM peptide, washed with medium and seeded in 8-well microscopy chambers. Confocal images were taken 30 min and 1 h after electroporation. Cells are round as they had to be detached from the surface before electroporation. The scale bar represents 10 µm. (C) Quantification of mean intracellular fluorescence. The data represent the mean +/- SEM. For each condition, over 40 cells were analyzed.

4.2.4   Difference in uptake of other cationic L- and D-CPPs in HeLa and MC57 cells

To investigate whether the differences in uptake were restricted to the poly-arginines R9 and its all-D counterpart or were also valid for other types of cell-penetrating peptides, we compared the uptake of the L- and D-forms of the CPPs penetratin, and hLF, corresponding to amino acids 38 to 59 of human lactoferrin [20], in HeLa and MC57 cells (Figure 4.6A-B). For both of these L-peptides and their D-counterparts, the D-peptides remained much more membrane-bound than the L-counterparts in MC57 cells, in agreement with the observations for the nona-arginine peptides. For hLF, membrane-bound fluorescence was observed for both stereoisomers, but endocytosis of D-hLF was clearly reduced, as quantitatively confirmed by measuring the intracellular fluorescence in cell lysates (see below and Figure 4.8).
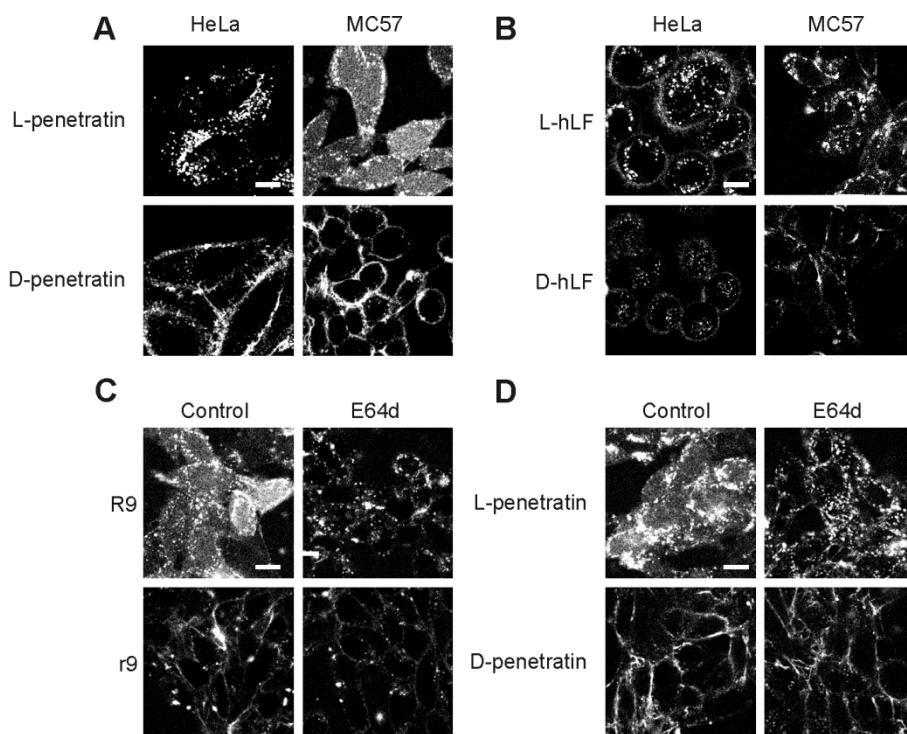
Figure 4.6. Differences in uptake are observed for various different CPPs, and are not explained by stability of D-peptides against cysteine proteases. For all experiments, cells were seeded in 8-well microscopy chambers, grown to 75 % confluence and incubated with 5 µM of each peptide. Cells were washed twice, and confocal images were taken immediately. HeLa and MC57 cells were incubated for 45 min with L- or D-penetratin (A) or for 30 min with L- or D-hLF (B). (C,D) MC57 cells were pre-incubated with 40 µM E64d before a 45-min CPP

incubation in the presence or absence of E64d with R9 or r9 (C), or with L- or D-penetratin (D). The scale bars represent 10 μm.

4.2.5   Effects of intracellular stability on peptide localization

Previously, we reported that under conditions where endocytosis was the dominant route of uptake the cytoplasmic fluorescence, but not the vesicular fluorescence of L-penetratin in MC57 cells was reduced by the broad-range cysteine protease inhibitor E64d [29]. Cysteine proteases of the cathepsin family are a major part of proteolytic activity in the endolysosomal compartment. Therefore, the result indicated that fluorescein-bearing proteolytic fragments escape the endosome more efficiently than intact peptides. We thus reasoned that the differences in distribution of intracellular fluorescence of D- and L-peptides observed by confocal microscopy might be related to the intracellular stability of the peptides. To investigate this possibility, MC57 cells were incubated with E64d and treated with either R9 or r9. Similar to our previous results, we observed that cytoplasmic fluorescence upon R9 and L-penetratin treatment was completely abolished by E64d (Figure 4.6C,D). However, vesicular fluorescence was unaffected. Moreover, no effect on the distribution of either CPP was apparent. These results indicate that the cytoplasmic fluorescence but not the differences in vesicular fluorescence are related to intracellular CPP stability.

4.2.6   Stimulation of uptake of fluorescein-labeled r9 by unlabeled R9/r9

We and others had demonstrated that CPPs can actively induce endocytosis [30, 31]. We therefore tested whether endocytosis of r9 could be increased by co-incubation with unlabeled R9. However, no increased internalization of r9 could be observed (Figure 4.7).
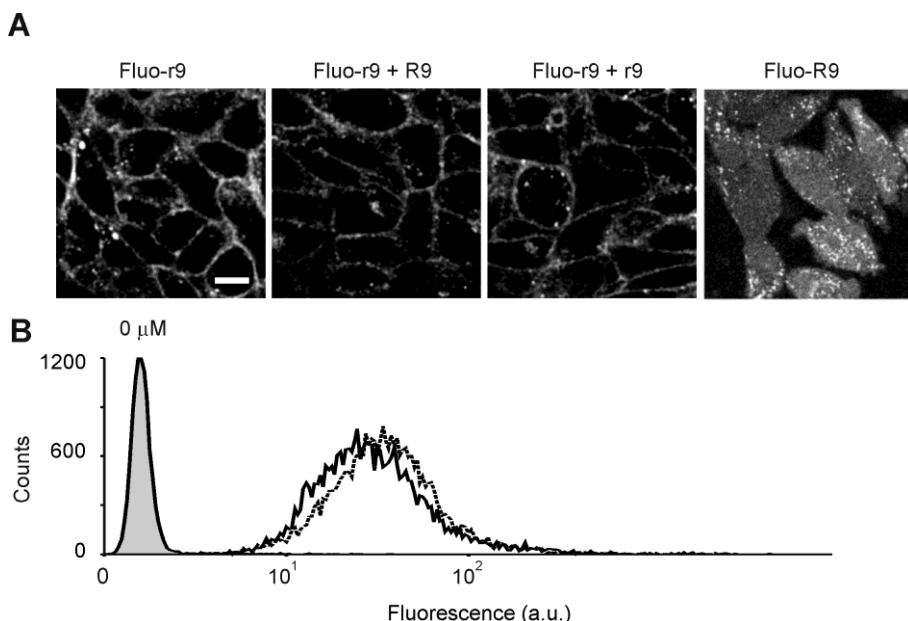
Figure 4.7. Effect of potential endocytosis triggers on uptake of L- and D-CPPs. (A) Uptake of fluo-R9 in MC57 cells in the presence or absence of unlabeled R9 or r9. MC57 cells were seeded in 8-well microscopy chambers and grown to confluence. Cells were incubated with 5 μM fluo-r9 in the presence or absence of 5 μM of unlabeled R9 or r9 for 45 min at 37°C. As a comparison, cells were also incubated with fluo-R9. After incubation, cells were washed and immediately analyzed by confocal microscopy. The scale bar represents 10 μm. (B) Uptake of R9 in HeLa cells treated with the nitric oxide synthase inhibitor L-NAME. HeLa cells were seeded in 24-well plates and grown to confluence. Cells were pre-incubated with 200 μM L-NAME or control medium for 30 min in the absence of serum and then for 30 min in RPMI containing 0 or 200 μM L-NAME, 5 μM R9 and 10 % fetal calf serum. Cell were washed, treated with trypsin, spun down, resuspended in HBS and analyzed by flow cytometry. Continuous lines indicate untreated control (R9) or no peptide (filled with grey). Dashed lines indicate R9 in the presence of 200 μM L-NAME. Results from one representative experiment are shown.

4.2.7 Role of HS chains in membrane binding and cellular uptake of L- versus D-CPPs

Heparan sulfate chains have been shown to interact with arginine-rich cell-penetrating peptides [32, 33] and to play a role in the uptake of CPPs [34, 35]. We therefore hypothesized that binding of peptides to HS chains might contribute to the different uptake of L- and D-peptides. If this was the case, one consequence would be that Jurkat cells, for which no differences in uptake were observed, should expose fewer HS chains on their surface than MC57 and HeLa cells. Furthermore, removal of HS chains by heparinase should reduce the absolute difference in peptide uptake.

In order to test these predictions, first, the presence of HS chains on three cell types was investigated by immunofluorescence. Immunofluorescence staining of all three cell lines was conducted both separately (Figure 4.8A) and, in order to ensure maximum comparability of signal intensities, also in one sample (Figure 4.8B). In accordance with our prediction, there was a clear correlation between the presence of HS and the preference for internalization of R9 over r9. HS chains were present on MC57 cells and on HeLa cells, but were undetectable on Jurkat cells.

To further investigate whether the membrane staining of the D-CPP observed for MC57 and HeLa cells represented peptides binding to HS, MC57 cells were treated with heparinases to remove HS chains from the cell surface (Figure 4.8C). For r9, the heparinase pre-treatment of cells abolished the membrane-bound fluorescence. Only little punctate fluorescence inside the cells was still observed. For R9, heparinase treatment had very little effect on the distribution of fluorescence. Instead, there was a reduction in the intensity of the cytoplasmic fluorescence, demonstrating a reduction of uptake. In order to quantitatively investigate these differences cellular peptide uptake in all three cell lines was quantitated by fluorimetry after removal of membrane-bound peptides (Figure 4.8D-F). Consistent with the microscopy data, after heparinase treatment a clear trend was visible showing a greater absolute decrease of R9 than for r9 in HS-rich MC57 and HeLa cells, and for L-hLF compared to D-hLF in HeLa cells. A combined statistical analysis of the HS-rich HeLa and MC57 cells demonstrated that the absolute decrease of R9 after heparinase treatment was greater than for r9 ($p < 0.01$). When data for L- and D-hLF were also included in this analysis, the different effects of heparinase treatment on the uptake of L- and D-peptides were even more significant ($p < 0.001$), arguing that the absolute decrease of uptake of L-CPPs was significantly more affected by a heparinase treatment in HS-rich cells. In line with these findings, the effect of HS chain removal on r9 internalization was non-significant.
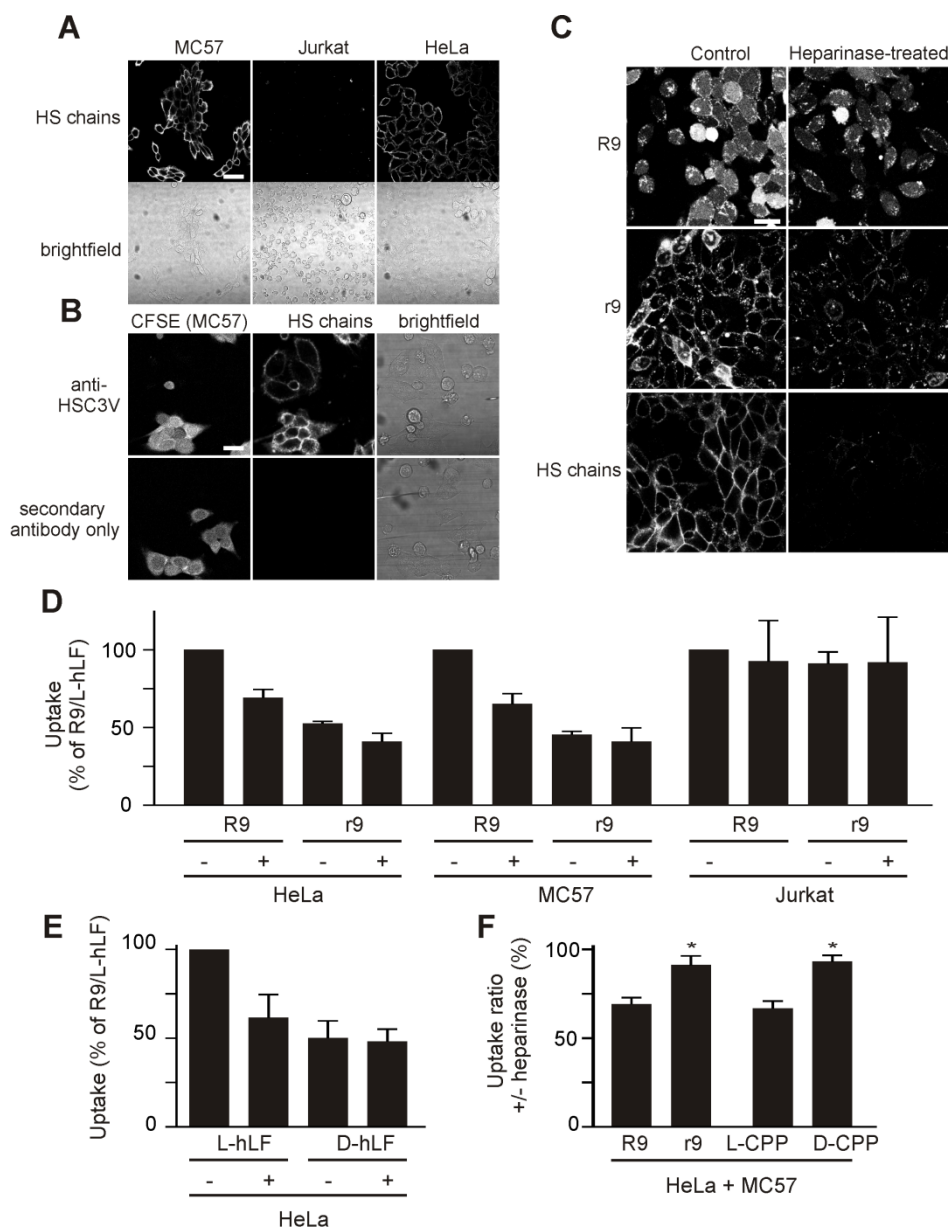
Figure 4.8. Role of HS chains in CPP binding and uptake. (A) Detection of HS on HeLa, MC57 and Jurkat cells. MC57 cells and HeLa cells were seeded in 8-well microscopy chambers, and Jurkat cells were obtained from a culture flask at the start of the experiment. All three cell lines were probed for HS chains by indirect immunofluorescence of living cells. The scale bar represents 40 µm. (B) Parallel detection of HS on HeLa, MC57 and Jurkat cells. MC57 cells were distinguished by CFSE labeling and seeded together with HeLa cells in an 8-well microscopy chamber. Jurkat cells were stained according to the same procedure in parallel and seeded in the

wells after the final washing steps. Jurkat cells could be detected based on their size and morphology. In the control, only the secondary antibody was applied. The scale bar represents 10 μm. (C) Effect of HS chain removal on the uptake and distribution of R9 and r9 in MC57 cells. MC57 cells were pre-treated with heparinases for 1 h or left untreated. Cells were washed and incubated with 5 μM of the indicated peptide for 45 min. HS chains were labeled by indirect immunofluorescence of living cells. The scale bar represents 20 μm. (D-F) Quantification of the impact of HS chain removal on peptide uptake. HeLa, MC57 and Jurkat cells were pre-treated with heparinases (+) for 1 h to remove HS chains or left untreated (-), washed, and incubated for 45 min with 5 μM of the indicated peptide. Subsequently, cells were washed with heparin to remove membrane-bound peptides, lysed and centrifuged. Fluorescence in the supernatant was measured using a microplate reader. The fluorescence of R9 (D) and L-hLF (E) in untreated cells was set at 100 % to aid comparison with the treated peptides or analogs. In (F), the effect of a heparinase treatment on uptake of R9 and r9 (left bars), and other L-CPPs and D-CPPs (right bars, analysis includes L/D-penetratin and L/D-hLF) is depicted as the ratio of uptake before and after a heparinase treatment in cells expressing heparan sulfates. Error bars indicate the mean +/- SEM. * indicates p < 0.05.

4.2.8   Heparan sulfate binding

Having shown that heparan sulfates contribute to the effectiveness of peptide entry, especially of L-peptides, it was still unclear at this point whether heparan sulfates serve as mere attachment factors, or as true receptors with an active role in the induction of internalization. The major reason for the inability to directly distinguish between these roles is that both mechanisms would contribute to the effectiveness of peptide entry. Similar practical problems are encountered when trying to distinguish between attachment factors and receptors in elucidating the entry mechanisms of viruses [36].

To probe for differences in the interaction between heparan sulfates and L- and D-CPPs, we first conducted SPR spectroscopy with immobilized heparan sulfate. With SPR, a slightly higher affinity of r9 for HS chains was observed compared to R9, whereas affinites for L- and D-penetratin were very similar (Figure 4.9A-D and table 4.2). With ITC, too, similar K_D values were obtained for both peptide pairs, although these values differed somewhat from those obtained with SPR (Figure 4.9E-H and table 4.2). Notably, the stoichiometry, enthalpy (ΔH) and entropy (ΔS), but not the K_D, were changed slightly for r9 compared to R9, indicative of a somewhat different mode of binding. In contrast, for L- and D-penetratin the contributions of enthalpy and entropy, as well as the stoichiometry and binding affinity, were all very similar. Therefore, it is very unlikely that the slight differences in HS-binding observed for R9 and r9 underlie the pronounced differences in behavior of these peptides at the plasma membrane in HeLa and MC57 cells.
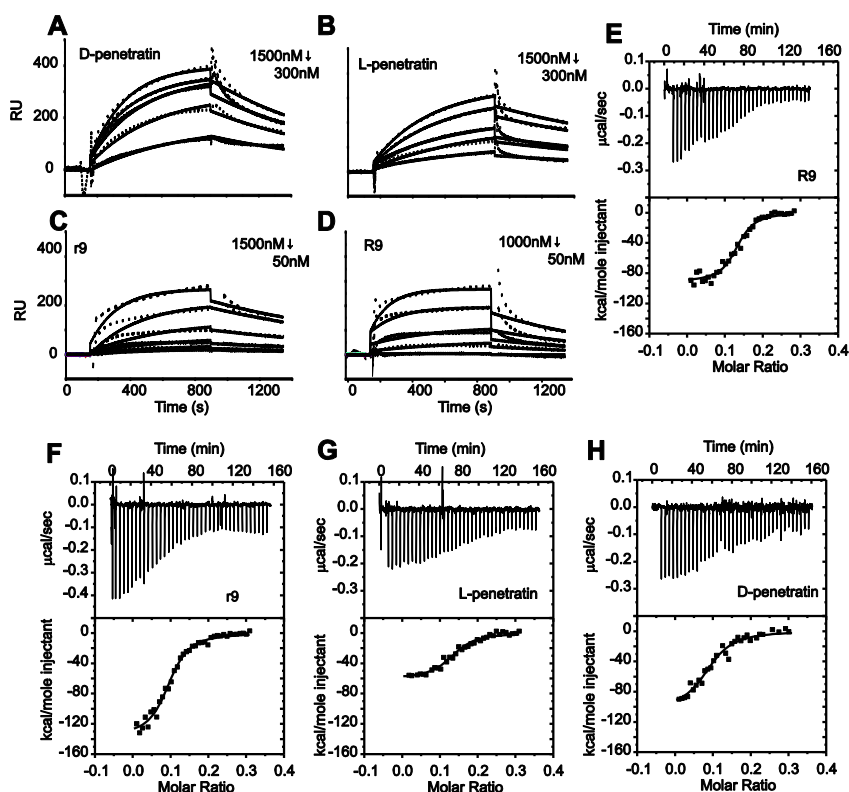
Figure 4.9. Interaction between HS and L- and D- CPPs as determined by SPR and ITC. (A-D) SPR diagrams of D- and L-peptides binding to immobilized HS. Peptides and concentration ranges are indicated in the figures. (E-H) ITC of the interaction between HS and L- and D-CPPs. The raw ITC graphs show the reference power as a function of time over the course of a single representative experiment, where 1 µl injections of 30 µM HS were added to 200 µl of 20 µM R9 or r9 in the sample cell. The ITC graphs in the lower panels show the integrated heats per HS injection, expressed as heat per injected mole of HS, as a function of the molar ratio of HS and peptide in the cell.

Table 4.2. Results of SPR and ITC binding studies between HS and L- and D-CPPs

|	SPR	ITC			
Peptide	K_d (µM)	K_d (µM)	Stoichio-metry	ΔH (kcal/mole)	ΔS (kcal/mole) degrees
R9	0.30 ± 0.13	0.14 ± 0.04	8 ± 1	-99 ± 4	-0.32 ± 0.01
r9	0.19 ± 0.06	0.16 ± 0.01	11 ± 1	-129 ± 7	-0.43 ± 0.03
L-penetratin	0.53 ± 0.15	0.15 ± 0.02	10 ± 3	-78 ± 11	-0.25 ± 0.05
D-penetratin	0.48 ± 0.02	0.16 ± 0.03	10 ± 3	-89 ± 9	-0.29 ± 0.03

4.2.9   Nitric oxide and uptake

As a further potential molecular mechanism to explain the differences in the uptake of arginine-containing L- and D-peptides, we examined an involvement of nitric oxide formation. L-arginine released from the L-peptides through proteolysis may serve as a substrate for nitric oxide generation by nitric oxide synthase. Nitric oxide is a free radical that can lead to cellular stress and the activation of stress-induced p38, which could in turn stimulate endocytosis [37]. Cells were incubated with the nitric oxide synthase inhibitor L-NAME. The differences in uptake efficiency that were observed for R9 and r9 were very minor (Figure 4.7B), indicating the absence of a pivotal role for nitric oxide generation in the differences in uptake of R9 and r9.

4.2.10   Uptake of L/D- chimaeras of nona-arginine in MC57 cells

Having strong indications that L- and D-CPPs differ with respect to triggering their uptake, we were interested to learn more about the structure-activity relationship of this trigger. Therefore, internalization of L/D-chimaeras of nona-arginine was assessed in MC57 cells (Figure 4.10). When only the C- and N-terminal L-amino acids were exchanged for D-amino acids, endocytic internalization still occurred, but cytoplasmic fluorescence was abolished. In contrast, when multiple L-amino acids were mutated to D-amino acids, a persistent membrane-binding was observed, resembling the phenotype of r9. These data suggest that a consecutive stretch of L-amino acids is required to trigger efficient endocytic uptake.
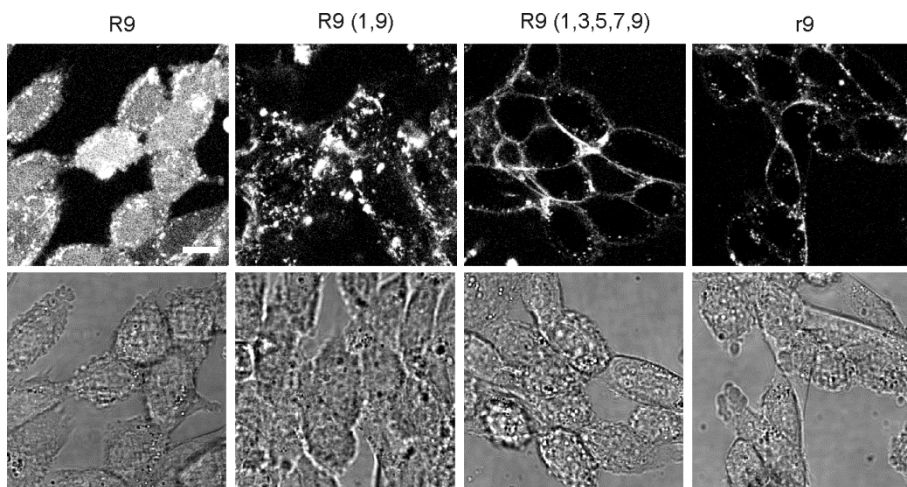
Figure 4.10. Uptake of R9, r9, and of nona-arginine chimaeras composed of L- and D-amino acids in MC57 cells. Cells were seeded in 8-well microscopy chambers, grown to 75 % confluence and incubated with 5 µM of the indicated peptides for 45 min. Cells were washed twice and confocal images were taken immediately. The scale bar represents 10 µm.

4.3   Discussion

According to the paradigm, chirality does not play a role in the uptake of CPPs. However, here we demonstrate a clear chirality-dependence in the uptake of the arginine-containing CPPs nona-arginine, hLF and penetratin. Differences in internalization were observed in MC57 and HeLa cells in a concentration range for which endocytosis dominates the uptake of arginine-containing CPPs [21]. No differences were observed in Jurkat cells, in agreement with previous observations [12].

The preference for L-peptides was only observed in cells containing significant amounts of heparan sulfate on the plasma membrane. On these cells, D-CPPs of nona-arginine, penetratin and hLF remained strongly membrane-associated, whereas no such prominent association was observed in HeLa cells for the corresponding L-CPPs, except for L-hLF. Also, only in these HS-positive cell types was the internalization of L-CPPs higher compared to D-CPPs. The importance of the chirality of the amino acids was further underscored by the use of two nona-arginine chimaeras composed of D- and L-amino acids that showed different phenotypes of internalization, depending on the position and numbers of D-amino acids. For nona-arginine, HS was identified as an important interaction partner in MC57 cells, as its removal reduced the membrane-binding of r9. Additionally, HS chain

removal had a greater absolute effect on the internalization of all-L-CPPs in comparison to all-D-CPPs in MC57 and HeLa cells.

Heparan sulfates have recently been proposed as receptors for arginine-rich peptides [34, 35]. This view is based on the observation that arginine-rich CPPs, upon their interaction with HS proteoglycans, induce actin rearrangements typical for macropinocytosis [34]. In our study, SPR and ITC binding assays indicated marginal differences in the binding of the various arginine-containing L- and D-CPPs to HS, supporting the notion that HS serve primarily as attachments factors instead of true receptors in MC57 and HeLa cells. As a consequence, the recognition event at the plasma membrane, which is responsible for the more efficient internalization of L-CPPs *versus* D-CPPs, remains unknown at present. Since the internalization of L- and D-CPPs was much more similar after removal of HS chains, it is reasonable to speculate that the presence of HS chains strongly facilitates this unknown interaction. One prominent possibility is the presence of a protein receptor that carries HS chains, such as the recently proposed syndecan-4 [38]. An involvement of a protein factor associated with internalization of CPPs is supported by studies in CHO cells, where the selective removal of glycosaminoglycans only partially reduced internalization, whereas trypsin treatment almost completely abolished internalization via endocytosis [39]. A distinction between binding and internalization has also recently been observed for HS chain-directed single chain variable domain antibody fragments (scFv). Only one scFv of several tested was efficiently internalized, whereas others remained membrane-bound [40]. Remarkably, we were not able to stimulate uptake of labeled r9 by the addition of unlabeled R9, even though it had been previously shown that CPP can actively induce endocytosis [30, 31]. These data indicate that both isomers behave as distinct molecular entities at the plasma membrane. Interestingly, similar results were reported for the induction of nucleation zone-dependent uptake [15].

Intracellular degradation [23, 29, 41] and re-export [18] have been shown to affect the cellular distribution and intracellular retention time of CPPs. Moreover, the sensitivity of the fluorescence of the fluorescein moiety to the chemical environment, e.g. pH or hydrophobicity, and to collision quenching with neighboring groups is well known. In addition, careful preparation of lysates is an important factor when comparing numbers of fluorophores from intact D- and (partially) degraded L-peptides. In our experiments, we could exclude all of these factors as a source of the observed differences. However, the cytoplasmic fluorescence observed after treatment of cells with L-peptides under conditions where endocytosis is the dominant route of uptake, very likely relates to their proteolytic

sensitivity, as R9 or L-penetratin-incubated cells were devoid of cytoplasmic fluorescence after pre-treatment with the endolysosomal protease inhibitor E64d (Figure 4.6). We had previously reported the same observation for L-penetratin [29]. Quite remarkably, the internalization pattern of an R9-analog with terminal D-amino acids reflected the same pattern observed with R9 after pre-treatment with E64d. We thus conclude that the terminal D-amino acids were sufficient to inhibit proteolysis in endocytic vesicles, while the central stretch of seven consecutive L-amino acids was sufficient to induce endocytosis effectively.

Extracellular peptide degradation is also a very unlikely cause of differences in the internalization as shorter oligo-arginine fragments (< R9) are taken up with a considerably lower efficiency [12]. Regarding the heparin treatment we used, it may not have removed membrane-bound peptides completely, but this would only have led to an overestimation of the internalization of D-peptides.

The reason for the higher proportion of HeLa cells showing internalization of r9 via direct translocation is not necessarily a consequence of a greater stability towards proteolytic activity. Instead, the reduction of internalization via endocytosis might accelerate accumulation of peptide at the plasma membrane, which might trigger direct translocation more rapidly. Consistent with this hypothesis, the concentration threshold at which the direct translocation occurs could be lowered by incubation of cells with endocytosis inhibitors [21].

Even though our results clearly refute the earlier paradigm of a chirality-independent uptake of CPPs, our results do not contradict earlier findings. Instead, prior experiments had been designed in such a way that they missed these differences. In accordance with previous findings, we did not detect a difference in the uptake of R9 and r9 in Jurkat cells [12]. When Tünnemann *et al.* compared the uptake of R9 and r9, they only focused on the number of cells that showed rapid translocation across the membrane [15].

It should also be pointed out that differences were previously reported for molecular complexes containing L- and D-CPPs. Mason *et al*. found a reduced transfection efficiency for DNA-complexes containing the amphipathic peptide D-LAH4 compared to L-LAH3 [42], and Abes *et al.* found a reduced biological activity of morpholino oligomer-peptide complexes with partial D-amino acid substitutions [43]. Remarkably, retro-inverso CPPs were much more toxic to cells, demonstrating that in spite of very similar side chain orientations, these peptides also induced very different biological responses [44]. Although these studies indicate a different behavior for peptides containing D-amino acids, none of these studies had explicitly addressed the impact of chirality on internalization efficiency.

Taken together, our findings indicate that cell surface binding and the induction of internalization are distinct mechanisms with individual structure-activity relationships. For the CPPs nona-arginine, penetratin and the hLF peptide, our data indicate that binding to heparan sulfates is chirality-independent, whereas the efficiency of internalization is related to chirality. We envision that these findings will have important consequences for the use of L- or D- amino acids in drug delivery strategies in general.

The cell line-dependence of our results also suggests a potential to employ the HS-dependent discrimination of CPPs for tissue-selective targeting. The preferential uptake of arginine-containing L-CPPs by cells expressing HS may be exploited for a preferential targeting of these cells. Conversely, targeting to cells not expressing HS can be more easily accomplished with CPPs synthesized with D-amino acids.

4.4 Significance

Cell-penetrating peptides (CPPs) represent a class of short, usually cationic peptides that are able to efficiently induce cellular uptake of membrane-impermeable macromolecules. However, an important factor limiting the pharmacological potential of CPPs is their proteolytic instability, which can be overcome through incorporation of D-amino acids which renders the peptides protease resistant. Contrary to the current paradigm, our results show clear differences in the uptake efficiency of the L- and D-form of three arginine-containing CPPs. These differences can be understood in terms of a two-step internalization process of CPPs at low concentrations: first, the peptides bind to heparan sulfates on the plasma membrane. Second, the peptides are internalized by endocytosis. Our data indicates that in the presence of HS chains only the second step occurs less efficiently for D-CPPs and can therefore be considered chirality-dependent. Data supporting this hypothesis include (i) the correlation of a more efficient internalization of L-CPPs with the expression of HS, and (ii) the pronounced membrane fluorescence of D-CPPs, but not L-CPPs, in HS-expressing cells, which can be eliminated by a heparinase treatment. Moreover, HS removal affects mainly the internalization of L-CPPs in cell lines with high levels of HS. We could exclude alternative interpretations of the observed differences through a comprehensive set of control experiments. Even though our results disagree with the current paradigm of an equal efficiency of L- and D-CPPs, our results do not contradict any published findings, as these previous results addressed differences for only a limited set of conditions. For *in vivo* applications, the balance of *in vivo* proteolytic stability, cellular internalization efficiency and intracellular trafficking may ultimately be decisive. Results

obtained for chimaeric L/D-peptides revealed an interesting structure-activity relationship. It will be highly interesting to explore to which degree such peptides containing only few D-amino acids may combine the high stability of all-D-CPPs with the higher uptake of arginine-containing all-L-CPPs.

4.5   Experimental procedures

4.5.1   Materials

All-L and all-D peptides were purchased from EMC microcollections (Tübingen, Germany). Chimaeric peptides (R9 (1,9) and R9(1,3,5,7,9)) were synthesized using standard Fmoc/OtBu-solid phase peptide synthesis protocols on a rink amide resin. Each amino acid was coupled using HOBt/HBTU in the presence of DIPEA as a base. Peptides were cleaved from the resin using TFA/TIS/H_2O (92.5:5:2.5, v/v/v) and the crude peptides were purified on C18 reversed-phase high-performance liquid chromatography (HPLC) columns using water/acetonitrile gradients. N-terminal fluorophore labeling was performed using 5(6) -carboxyfluorescein as previously described [28]. Peptides were synthesized C-terminally amidated and N-terminally fluorescein-labeled, unless stated otherwise. Purity was evaluated by analytical HPLC and identity confirmed by mass spectrometry. hLF peptides were oxidized by purging oxygen through the peptide solution for 5 min, followed by a 2-h incubation at 37°C. The oxidation leads to cyclization by disulfide bridge formation.

The Zenon mouse IgG1 labelling kit was from Invitrogen (Karlsruhe, Germany), bovine serum albumin (BSA), octyl β-D-glucopyranoside, heparin and glucose were from Sigma-Aldrich (Zwijndrecht, The Netherlands). Heparan sulfate (average MW 15 kDa) was from Celsus (Cincinnati, USA). Heparinases I-III were purchased from IBEX (Montreal, Canada). The anti-HS VSV-tagged single chain Fv fragment HS4C3V was described previously [45] and the mouse anti-VSV (clone P5D4) antibody was from Boehringer Mannheim (Mannheim, Germany). E64d was from Bachem (Heidelberg, Germany). Standard chemicals were from Sigma-Aldrich and Merck (Darmstadt, Germany).

4.5.2   Cell culture

All cell lines were maintained in RPMI 1640 (PAN Biotech, Aidenbach, Germany) supplemented with 10 % heat-inactivated fetal calf serum (PAN Biotech) and passaged every 2 to 3 days. Cells were incubated at 37°C in a 5 % CO_2, humidified incubator.

4.5.3 Confocal laser scanning microscopy and fluorescence-correlation spectroscopy (FCS)

Confocal laser scanning microscopy and FCS were performed on a TCS SP5 confocal microscope (Leica Microsystems, Mannheim, Germany) equipped with an HCX PL APO 63 x N.A. 1.2 water immersion lens and a dual channel FCS unit. Fluorescein fluorescence was excited with the 488 nm line of an argon ion laser. Detection took place with a 500-550 nm filter-block for FCS measurements and with a 500-550 nm detection range for confocal microscopy. Cells were maintained at 37°C on a temperature-controlled microscope stage.

4.5.4 Peptide uptake

MC57 and HeLa cells were seeded in 8-well microscopy chambers (Nunc, Wiesbaden, Germany) and grown to 75 % confluence. Jurkat cells were transferred from the tissue culture flask immediately before the experiment. Cells were incubated at 37˚C with 5 μM of the peptides in RPMI 1640 supplemented with 10 % fetal calf serum. The duration of incubations is indicated for each experiment, separately. Cells were washed twice with medium after the incubation with peptides and living cells were analyzed immediately or after settling for about 15 min in the microscopy chambers (Jurkat cells) by confocal microscopy. Removal of HS chains from the cell surface was accomplished by a 1-h incubation at 37°C with RPMI 1640, supplemented with 1 % fetal calf serum and 33 mIU/ml of heparinase I, 8 mIU/ml of heparinase II and 5 mIU/ml of heparinase III.

4.5.5 Quantification of cellular uptake

After incubation with the peptides, cells were washed with pre-warmed HEPES-buffered saline (HBS)/BSA/glucose (10 mM HEPES, 135 mM NaCl, 5 mM KCl, 1 mM MgCl$_2$, 1.8 mM CaCl$_2$, pH 7.4, containing 0.1 % (w/v) BSA and 5 mM glucose), treated twice for 5 min at 37°C with 100 μg/ml heparin in HBS/BSA/glucose and washed again with HBS/BSA/glucose. Cells were then lysed in 150 μl lysis buffer (10 mM Bis-Tris propane, 50 mM octyl β-D-glucopyranoside, 1 mM EDTA and 150 mM NaCl, pH 7.2) for 15 min on ice, the lysate was centrifuged for 10 min at 18,000 x *g* and the fluorescence in 120 μl of the supernatant was measured using a Synergy 2 microplate reader (Biotek, Winooski, USA) by excitation at 488 ± 10 nm and detection at 528 ± 10 nm in a flat-bottom 96-well plate (Nunc). Values were corrected for total protein content on the basis of results from the Bio-Rad protein assay in microtiter plates with the dye reagent from Bio-Rad (München,

Germany). For quantification by FCS, 150 μl of lysate were treated with 2 μl of benzonuclease (2U; Novagen, Merck, Darmstadt, Germany) for 30 min at 37°C, followed by a 3-h incubation with 3.3 mg/ml proteinase K (diluted from a 20 mg/ml stock; Roche, Mannheim, Germany) at 37°C.

4.5.6   Fluorescence correlation spectroscopy (FCS)

Autocorrelation measurements of intact and degraded peptides in PBS and in lysates were performed at 37°C in a 384-well plate (175 μm, low-base design, MMI, Eching, Germany). Proteolytic degradation of peptides in buffer was accomplished by a 3-h incubation at 37°C in PBS containing 400 μg/ml trypsin and 40 μg/ml EDTA (trypsin/EDTA solution purchased from PAN Biotech). Lysate preparation is described in the section 'quantification of cellular uptake' in the main article. Autocorrelation functions were analyzed using the ISS VISTA software (ISS, inc., Illinois, USA). Fitting was performed according to a 3D-Gaussian model containing a triplet component. Diffusional autocorrelation times τ_D which were used to assess degradation and the presence of aggregates were obtained from the fitting procedure. The particle number obtained from the fit was corrected for uncorrelated background (Koppel,1974) (eq. 1).

$$G(0) = 1 + 1/N_{app} = 1 + (1\text{-}CPS_b/CPS_t)^2/N_{corr} \text{ (eq. 1)}$$

Where CPS_t is the total signal (counts-per-second) and CPS_b the background signal, N_{app} the apparent particle number obtained from the fit to the autocorrelation function and N_{corr} the corrected particle number. The fluorescence per molecule (FPM) was then determined according to (eq. 2).

$$FPM = (CPS_t - CPS_b)/N_{corr} \text{ (eq. 2)}$$

4.5.7   Immunofluorescence

Cells were washed with ice-cold HBS/BSA/glucose and incubated with 125 μl of a periplasmic fraction containing the anti-HS single chain Fv fragment HS4C3V for 1 h on ice in 8-well microscopy chambers (MC57 and HeLa cells) or in the same volume in Eppendorf tubes (800,000 Jurkat cells). After incubation, cells were washed again with ice-cold HBS/BSA/glucose and incubated for 1 h with an anti-VSV antibody (P5D4)/Zenon IgG1-Alexa Fluor 647 conjugate on ice. The antibody staining was analyzed by confocal

microscopy. When co-seeding MC57, HeLa and Jurkat cells, MC57 cells were distinguished from HeLa cells using the Celltrace CFSE proliferation kit (Molecular Probes, Invitrogen, Carlsbad, USA) according to the manufacturer's instructions.

4.5.8   Pulse-chase experiment

MC57 and HeLa cells were detached by trypsinization for 5 min and incubated with pre-warmed RPMI 1640, supplemented with 10 % fetal calf serum. One million cells were mixed with 5 µM of the indicated peptide and immediately electroporated using the Amaxa nucleofector kit R (Lonza, Basel, Switzerland), according to the manufacturer's instructions. After electroporation, cells were washed twice with medium and 125,000 cells per well were seeded in 8-well microscopy chambers. Confocal images were taken 30 min and 1 h after electroporation. Mean intracellular fluorescence was quantitated using the Image J software package (Rasband, W.S., ImageJ, U. S. National Institutes of Health, Bethesda, Maryland, USA, http://rsb.info.nih.gov/ij/).

4.5.9   Flow cytometry

HeLa cells were seeded in 24-well plates (Sarstedt, Numbrecht, Germany) at a density of 40,000 cells/well two days prior to the experiment. For experiments probing for an involvement of NO synthase in uptake differences, cells were incubated for 30 min with or without 200 µM N (G)-nitro-L-arginine methyl ester (L-NAME) in RPMI 1640 without serum followed by a 30-min incubation with 5 or 10 µM R9 in the presence or absence of 200 µM L-NAME in serum-containing RPMI. Subsequently, cells were washed, detached by trypsinization for 5 min, spun down, re-suspended in 200 µl HBS and cellular fluorescence was measured using a BD FACScan flow cytometer equipped with a 488 nm laser (BD Biosciences, Erembodegem, Belgium). The analysis was performed using Summit software (Fort Collins, USA). Results were based on 10,000 gated cells.

4.5.10   Surface plasmon resonance (SPR)

 SPR was performed on a Biacore 2000 (GE Healthcare, Diegem, Belgium). Streptavidin-coupled chips (Sensor Chip SA, GE Healthcare, Uppsala Sweden) were first functionalized with biotinylated HS (working solution: 10 µg/ml), leading to an immobilization level of approximately 100 and 200 RU. The peptides were injected at concentrations between 50 and 1500 nM in HBS-P buffer (GE Healthcare). Peptide association and dissociation took

place for 12.5 and 10 min, respectively. All measurements were conducted at 25°C at a flow rate of 20 µl/min. To calculate K_D values for the peptides, the binding curves of each peptide concentration were fitted using the 1:1 Langmuir binding model of the Biacore software. RU_{max} was fitted locally to take the differences in maximum binding level (RU_{max}) of the different peptide concentrations into account. At least two replicates were conducted for each peptide.

4.5.11 Isothermal titration calorimetry (ITC)

ITC experiments were performed with an ITC_{200} Microcal (MicroCal LLC, Wolverton Mill UK) at 5°C. Peptide and HS solutions were diluted in HBS to 30 µM and 50 µM, respectively. All solutions were degassed before use. The sample cell was filled with the peptide solution and 39 times 1 µl of the HS solution was injected into the sample cell. To correct for dilution effects, the heat effects of the last five measurements of each run (in which no decrease of binding-specific heat effects was observed) were averaged and subtracted from the generated heat during experiments with HS and peptides. Data was analyzed using the ITC_{200} Microcal software. Fitting was accomplished using a one-site binding model.

4.5.12 Statistical procedures

Quantitative data represent mean +/- standard error of the mean. The threshold for significance was set at $p < 0.05$, based on a two-tailed paired Student's *t*-test.

4.6 Acknowledgements

4.7 References

[1] P. Järver, I. Mager, U. Langel, In vivo biodistribution and efficacy of peptide mediated delivery, Trends Pharmacol Sci, 31 (2010) 528-535.

[2] L.N. Patel, J.L. Zaro, W.C. Shen, Cell penetrating peptides: intracellular pathways and pharmaceutical perspectives, Pharm Res, 24 (2007) 1977-1992.

[3] M.E. Lindgren, M.M. Hallbrink, A.M. Elmquist, U. Langel, Passage of cell-penetrating peptides across a human epithelial cell layer in vitro, Biochem J, 377 (2004) 69-76.

[4] R. Trehin, H.M. Nielsen, H.G. Jahnke, U. Krauss, A.G. Beck-Sickinger, H.P. Merkle, Metabolic cleavage of cell-penetrating peptides in contact with epithelial models: human calcitonin (hCT)-derived peptides, Tat(47-57) and penetratin(43-58), Biochem J, 382 (2004) 945-956.

[5] A. Elmquist, U. Langel, In vitro uptake and stability study of pVEC and its all-D analog, Biol Chem, 384 (2003) 387-393.

[6] S. Pujals, E. Sabido, T. Tarrago, E. Giralt, all-D proline-rich cell-penetrating peptides: a preliminary in vivo internalization study, Biochem Soc Trans, 35 (2007) 794-796.

[7] D.S. Youngblood, S.A. Hatlevig, J.N. Hassinger, P.L. Iversen, H.M. Moulton, Stability of cell-penetrating peptide-morpholino oligomer conjugates in human serum and in cells, Bioconjug Chem, 18 (2007) 50-60.

[8] R. Tugyi, K. Uray, D. Ivan, E. Fellinger, A. Perkins, F. Hudecz, Partial D-amino acid substitution: Improved enzymatic stability and preserved Ab recognition of a MUC2 epitope peptide, Proc Natl Acad Sci U S A, 102 (2005) 413-418.

[9] J. Brugidou, C. Legrand, J. Mery, A. Rabie, The retro-inverso form of a homeobox-derived short peptide is rapidly internalised by cultured neurones: a new basis for an efficient intracellular delivery system, Biochem Biophys Res Commun, 214 (1995) 685-693.

[10] D. Derossi, S. Calvet, A. Trembleau, A. Brunissen, G. Chassaing, A. Prochiantz, Cell internalization of the third helix of the Antennapedia homeodomain is receptor-independent, J Biol Chem, 271 (1996) 18188-18193.

[11] D.J. Mitchell, D.T. Kim, L. Steinman, C.G. Fathman, J.B. Rothbard, Polyarginine enters cells more efficiently than other polycationic homopolymers, J Pept Res, 56 (2000) 318-325.

[12] P.A. Wender, D.J. Mitchell, K. Pattabiraman, E.T. Pelkey, L. Steinman, J.B. Rothbard, The design, synthesis, and evaluation of molecules that enable or enhance cellular uptake: peptoid molecular transporters, Proc Natl Acad Sci U S A, 97 (2000) 13003-13008.

[13] M.M. Fretz, N.A. Penning, S. Al-Taei, S. Futaki, T. Takeuchi, I. Nakase, G. Storm, A.T. Jones, Temperature-, concentration- and cholesterol-dependent translocation of L- and D-octa-arginine across the plasma and nuclear membrane of CD34+ leukaemia cells, Biochem J, 403 (2007) 335-342.

[14] S. Pujals, J. Fernandez-Carneado, M.D. Ludevid, E. Giralt, D-SAP: a new, noncytotoxic, and fully protease resistant cell-penetrating peptide, ChemMedChem, 3 (2008) 296-301.

[15] G. Tünnemann, G. Ter-Avetisyan, R.M. Martin, M. Stockl, A. Herrmann, M.C. Cardoso, Live-cell analysis of cell penetration ability and toxicity of oligo-arginines, J Pept Sci, 14 (2008) 469-476.

[16] J. Mueller, I. Kretzschmar, R. Volkmer, P. Boisguerin, Comparison of cellular uptake using 22 CPPs in 4 different cell lines, Bioconjug Chem, 19 (2008) 2363-2374.

[17] F. Burlina, S. Sagan, G. Bolbach, G. Chassaing, Quantification of the cellular uptake of cell-penetrating peptides by MALDI-TOF mass spectrometry, Angew Chem Int Ed Engl, 44 (2005) 4244-4247.

[18] J. Oehlke, A. Scheller, B. Wiesner, E. Krause, M. Beyermann, E. Klauschenz, M. Melzig, M. Bienert, Cellular uptake of an alpha-helical amphipathic model peptide with the potential to deliver polar compounds into the cell interior non-endocytically, Biochim Biophys Acta, 1414 (1998) 127-139.

[19] J.P. Richard, K. Melikov, E. Vives, C. Ramos, B. Verbeure, M.J. Gait, L.V. Chernomordik, B. Lebleu, Cell-penetrating peptides. A reevaluation of the mechanism of cellular uptake, J Biol Chem, 278 (2003) 585-590.

[20] F. Duchardt, I.R. Ruttekolk, W.P. Verdurmen, H. Lortat-Jacob, J. Burck, H. Hufnagel, R. Fischer, M. van den Heuvel, D.W. Lowik, G.W. Vuister, A. Ulrich, M. de Waard, R. Brock, A cell-penetrating peptide derived from human lactoferrin with conformation-dependent uptake efficiency, J Biol Chem, 284 (2009) 36099-36108.

[21] F. Duchardt, M. Fotin-Mleczek, H. Schwarz, R. Fischer, R. Brock, A comprehensive model for the cellular uptake of cationic cell-penetrating peptides, Traffic, 8 (2007) 848-866.

[22] Y. Hosaka, Y. Yasuda, O. Seriburi, M.G. Moran, K. Fukai, In vitro secondary generation of cytotoxic T lymphocytes in mice with mumps virus and their mumps-specific cytotoxicity among paramyxoviruses, J Virol, 57 (1986) 1113-1118.

[23] R. Fischer, K. Kohler, M. Fotin-Mleczek, R. Brock, A stepwise dissection of the intracellular fate of cationic cell-penetrating peptides, J Biol Chem, 279 (2004) 12625-12635.

[24] M. Kosuge, T. Takeuchi, I. Nakase, A.T. Jones, S. Futaki, Cellular internalization and distribution of arginine-rich peptides as a function of extracellular peptide concentration, serum, and plasma membrane associated proteoglycans, Bioconjug Chem, 19 (2008) 656-664.

[25] W.P. Verdurmen, M. Thanos, I.R. Ruttekolk, E. Gulbins, R. Brock, Cationic cell-penetrating peptides induce ceramide formation via acid sphingomyelinase: implications for uptake, J Control Release, 147 (2010) 171-179.

[26] S. Al-Taei, N.A. Penning, J.C. Simpson, S. Futaki, T. Takeuchi, I. Nakase, A.T. Jones, Intracellular traffic and fate of protein transduction domains HIV-1 TAT peptide and octaarginine. Implications for their utilization as drug delivery vectors, Bioconjug Chem, 17 (2006) 90-100.

[27] I.R. Ruttekolk, W.P. Verdurmen, Y.D. Chung, R. Brock, Measurements of the intracellular stability of CPPs, Methods Mol Biol, 683 (2011) 69-80.

[28] R. Fischer, O. Mader, G. Jung, R. Brock, Extending the applicability of carboxyfluorescein in solid-phase synthesis, Bioconjug Chem, 14 (2003) 653-660.

[29] R. Fischer, H. Hufnagel, R. Brock, A doubly labeled penetratin analogue as a ratiometric sensor for intracellular proteolytic stability, Bioconjug Chem, 21 (2010) 64-73.

[30] M. Fotin-Mleczek, S. Welte, O. Mader, F. Duchardt, R. Fischer, H. Hufnagel, P. Scheurich, R. Brock, Cationic cell-penetrating peptides interfere with TNF signalling by induction of TNF receptor internalization, J Cell Sci, 118 (2005) 3339-3351.

[31] I.M. Kaplan, J.S. Wadia, S.F. Dowdy, Cationic TAT peptide transduction domain enters cells by macropinocytosis, J Control Release, 102 (2005) 247-253.

[32] E. Goncalves, E. Kitas, J. Seelig, Binding of oligoarginine to membrane lipids and heparan sulfate: structural and thermodynamic characterization of a cell-penetrating peptide, Biochemistry, 44 (2005) 2692-2702.

[33] A. Ziegler, J. Seelig, Interaction of the protein transduction domain of HIV-1 TAT with heparan sulfate: binding mechanism and thermodynamic parameters, Biophys J, 86 (2004) 254-263.

[34] I. Nakase, M. Niwa, T. Takeuchi, K. Sonomura, N. Kawabata, Y. Koike, M. Takehashi, S. Tanaka, K. Ueda, J.C. Simpson, A.T. Jones, Y. Sugiura, S. Futaki, Cellular uptake of arginine-rich peptides: roles for macropinocytosis and actin rearrangement, Mol Ther, 10 (2004) 1011-1022.

[35] J.P. Richard, K. Melikov, H. Brooks, P. Prevot, B. Lebleu, L.V. Chernomordik, Cellular uptake of unconjugated TAT peptide involves clathrin-dependent endocytosis and heparan sulfate receptors, J Biol Chem, 280 (2005) 15300-15306.

[36] J. Mercer, M. Schelhaas, A. Helenius, Virus entry by endocytosis, Annu Rev Biochem, 79 (2010) 803-833.

[37] A. Sorkin, M. von Zastrow, Endocytosis and signalling: intertwining molecular networks, Nat Rev Mol Cell Biol, 10 (2009) 609-622.

[38] T. Letoha, A. Keller-Pinter, E. Kusz, C. Kolozsi, Z. Bozso, G. Toth, C. Vizler, Z. Olah, L. Szilak, Cell-penetrating peptide exploited syndecans, Biochim Biophys Acta, 1798 (2010) 2258-2265.

[39] J.M. Gump, R.K. June, S.F. Dowdy, Revised role of glycosaminoglycans in TAT protein transduction domain-mediated cellular transduction, J Biol Chem, 285 (2010) 1500-1507.

[40] A. Wittrup, S.H. Zhang, G.B. ten Dam, T.H. van Kuppevelt, P. Bengtson, M. Johansson, J. Welch, M. Morgelin, M. Belting, ScFv antibody-induced translocation of cell-surface heparan sulfate proteoglycan to endocytic vesicles: evidence for heparan sulfate epitope specificity and role of both syndecan and glypican, J Biol Chem, 284 (2009) 32959-32967.

[41] M. Hällbrink, J. Oehlke, G. Papsdorf, M. Bienert, Uptake of cell-penetrating peptides is dependent on peptide-to-cell ratio rather than on peptide concentration, Biochim Biophys Acta, 1667 (2004) 222-228.

[42] A.J. Mason, C. Leborgne, G. Moulay, A. Martinez, O. Danos, B. Bechinger, A. Kichler, Optimising histidine rich peptides for efficient DNA delivery in the presence of serum, J Control Release, 118 (2007) 95-104.

[43] R. Abes, H.M. Moulton, P. Clair, S.T. Yang, S. Abes, K. Melikov, P. Prevot, D.S. Youngblood, P.L. Iversen, L.V. Chernomordik, B. Lebleu, Delivery of steric block morpholino oligomers by (R-X-R)4 peptides: structure-activity studies, Nucleic Acids Res, 36 (2008) 6343-6354.

[44] T. Holm, H. Raagel, S.E. Andaloussi, M. Hein, M. Mae, M. Pooga, U. Langel, Retro-inversion of certain cell-penetrating peptides causes severe cellular toxicity, Biochim Biophys Acta, 1808 (2011) 1544-1551.

[45] T.H. van Kuppevelt, M.A. Dennissen, W.J. van Venrooij, R.M. Hoet, J.H. Veerkamp, Generation and application of type-specific anti-heparan sulfate antibodies using phage display technology. Further evidence for heparan sulfate heterogeneity in the kidney, J Biol Chem, 273 (1998) 12960-12966.

Effects of the stereochemistry of amino acid replacements in transportan-10 on cellular interactions

Wouter P.R. Verdurmen, Parvesh Wadhwani,
Susanne Fanghänel, Anne S. Ulrich and
Roland Brock

Chapter five

5 Effects of the stereochemistry of amino acid replacements in transportan-10 on cellular interactions

Manuscript in preparation

Wouter P. R. Verdurmen[a], Parvesh Wadhwani[b], Susanne Fanghänel[b], Anne S. Ulrich[b,c], Roland Brock[a]

[a]Department of Biochemistry, Nijmegen Centre for Molecular Life Sciences, Radboud University Nijmegen Medical Centre, Nijmegen, The Netherlands
[b]Karlsruhe Institute of Technology (KIT), Institute for Organic Chemistry and CFN, Karlsruhe, Germany
[c]DFG-Center for Functional Nanostructures (TP E1.2)

Abstract

Cell-penetrating peptides (CPPs) are a class of short peptides that induce the cellular uptake of a variety of cargo molecules. So far, relatively little attention has been paid to the relevance of the stereochemistry of individual amino acids on activity, despite recent findings that stereochemistry is important for arginine-rich peptides. The aim of this study was to address the role of the stereochemistry of individual amino acid replacements on biological properties of the amphipathic CPP transportan 10 (TP10). To this end, a set of eighteen TP10 analogs was prepared containing an L- or D-epimer of an NMR label at nine distinct positions in the TP10 sequence. Similar to arginine-rich peptides, major effects of the chirality of individual amino acids were found on cellular uptake, membrane binding and cytotoxicity. Surprisingly, there were no clear correlations between the secondary structure or the aggregation behavior in model systems and their behavior in a cellular environment. In addition, remarkable similarities in the dependency on heparan sulfate (HS) chains for membrane binding were observed, despite a lack of a measurable affinity of TP10 (analogs) for HS. In contrast, phosphatidylserine exposure was induced to a much greater degree by TP10 compared to R9. In suspension Jurkat cells, our results suggest that only some TP10 analogs have the capacity to directly translocate across the membrane at the concentration of 2 μM. In conclusion, our results establish an important role of the stereochemistry of individual amino acid replacements of TP10 with regard to a variety of properties that are important for their use as CPPs.

5.1   Introduction

Cell-penetrating peptides (CPPs) are a promising class of compounds that are being applied to shuttle membrane-impermeable cargo into the cell. To date, applications typically focus on biomedical research. Ultimately, the goal will be to apply these molecules for therapeutic purposes. After almost twenty years of research into CPPs, there is now a considerable understanding of the entry routes that CPPs may exploit to enter the cell [1, 2]. There is widespread agreement that the route depends on multiple factors, including the type and concentration of the CPP, the cell type and the cargo, and that multiple pathways may be exploited simultaneously [1, 3, 4]. Many studies have been performed to relate uptake efficiency and route of uptake to the physicochemical characteristics of various subclasses of CPPs, typically in the presence of lipid vesicles or glycosaminoglycans [5-8]. Interestingly, until recently little attention had been paid to the stereochemistry of the peptides. This is partially due to the original concept of a stereochemistry-independent uptake mechanism for CPPs [9]. However, this initial concept has been refuted by us and others [10]. For the arginine-rich CPP nona-arginine (R9), for the amphipathic cationic CPP penetratin and for the cyclization-dependent CPP hLF, the uptake efficiency of all D-peptides was lower than the uptake of all L-peptides in certain cell types. The molecular basis underlying these observations is currently not clear. However, we have obtained evidence that L- and D-peptides differ in their capacity to trigger endocytosis. In contrast, for uptake at higher concentrations via sphingomyelinase-dependent nucleation zones [11], also referred to as transduction [12], nona-arginine composed of D-arginines showed a slightly more efficient uptake compared to L-R9, which could be due to reduced proteolytic degradation or an increased accumulation at the plasma membrane [10, 12].

Interestingly, for the CPP mastoparan, uptake and toxicity also depended on the stereochemistry [13]. This CPP is quite different from the aforementioned CPP in that it lacks arginines and is more membrane toxic than the arginine-containing CPP. The membrane toxicity is presumably related to the ability of mastoparan to induce pores into lipid membranes through which even polar molecules can pass [14-16]. Associated with this activity is the strong propensity of the C-terminal part of mastoparan to form an α helix, even in solution [17, 18]. Therefore, the question arises to which degree the uptake efficiency of these membrane-active CPPs depends on stereochemistry and whether this can be related to secondary structure and aggregation behavior on the plasma membrane.

In a related study using solid state NMR, we observed that epimerization of an NMR label at individual positions of TP10 influenced the secondary structure and the aggregation behavior of this peptide (manuscript in preparation; thesis of Susanne Fanghänel). To

provide a better insight into a possible correlation of peptide conformation and uptake, we synthesized a set of fluorescein labeled analogs of these TP10 epimers. These analogs contained either the D- or L-variant of the 19F-NMR label CF3-bicyclopentylglycine (CF3-BPG). Cellular uptake and intracellular distribution were investigated for both an adherent and a suspension model cell line. For the TP10 analogs, we find that activity as a CPP is strongly dependent on the chirality of single amino acid substitutions. Moreover, the behavior in cellular systems does not correlate with the behavior in artificial systems. In addition, the cellular activities of these subtly different peptides proved to be highly cell-type dependent and unexpected with regard to the requirement of heparan sulfate chains. Together, the findings further stress the importance of stereochemistry as a determinant in CPP activity. In addition, the results emphasize the need to take into account the complex biological environment that CPPs encounter during the process of cellular entry in order to obtain useful knowledge for their use as drug delivery vehicles.

5.2 Results

5.2.1 Structural effects of fluorescein conjugation to TP10 analogs

Solid-state 19F-NMR analyses revealed a major impact of the epimerization of individual amino acid positions on TP10 conformation and aggregation. Peptides with a D-epimer replacement in the C-terminal part had a disturbed helix formation when in contact with a lipid bilayer. This led to aggregation as β-sheets via the intrinsically unstructured N-terminal part in the presence of lipid vesicles. In order to explore to which degree this differential behavior affected uptake and would eventually permit a correlation of structural characteristics with cellular uptake, a collection of fluorescein-labeled analogs was synthesized. In the first step, we addressed whether for these peptides epimerization affected the conformation and/or aggregation behavior in a similar way as for the non-fluorescent peptides. Although most peptides behaved similarly in the presence or absence of CF in oriented CD and ^{19}F-NMR studies, some notable differences were observed (table 5.1). The main difference was a reduced tendency to aggregate in the presence of the CF label, which is reflected by fewer CF-labeled TP10 analogs showing either β-sheet formation and/or immobilization with oriented CD and solid state NMR, respectively.

Table 5.1. The secondary structure of CF-labeled TP10 analogs as measured by oriented CD and their immobilization as determined by ^{19}F-NMR

Epimerized position	Oriented Circular Dichroism[a]		Solid State NMR[b]	
	L-CF$_3$-Bpg	*D*-CF$_3$-Bpg	*L*-CF$_3$-Bpg	*D*-CF$_3$-Bpg
Gly2	α-helical	α-helical	immobilized	not immobilized
Leu4	α-helical	α-helical	not immobilized	not immobilized
Leu5	α-helical	α-helical	not immobilized	not immobilized
Ile8	α-helical	α-helical	not immobilized	not immobilized
Leu10	α-helical[c]	α-helical	not immobilized	not immobilized
Leu13	α-helical[c]	β-sheet	not immobilized	not immobilized
Leu16	α-helical[c]	β-sheet	not immobilized	not immobilized[d]
Ile 20	α-helical	α-helical[c]	not immobilized	not immobilized
Leu 21	α-helical	α-helical[c]	not immobilized	not immobilized

a: after five days of incubation under a fully hydrated atmosphere (peptide/lipid ratio of 1:50)

b: peptide/lipid ratio of 1:200

c: was beta sheet without CF label

d: was immobilized without CF label

5.2.2 *Uptake and membrane binding of TP10 analogs depends on the stereochemistry of the introduced 19F-NMR label*

The two TP10 analogs Gly2→*L*-CF$_3$-Bpg and Leu4→*L*-CF$_3$-Bpg showed a pronounced membrane staining that was stronger than the one observed for the wild-type peptide (manuscript in preparation). In contrast to this very similar cellular staining, these two CF-labeled TP10 analogs exhibited different characteristics in solid-state ^{19}F-NMR measurements. While the CF-labeled analog Gly2→*L*-CF$_3$-Bpg was immobilized at a peptide/lipid ratio of 1:200, which is strongly indicative of aggregation, this was not the case for Leu4→*L*-CF$_3$-Bpg. The observed membrane staining was analogous to what we had observed with arginine-rich peptides that are composed completely or mostly of *D*-amino acids [10]. To assess a role of amino acid chirality in this binding pattern, we compared cell binding and uptake in HeLa cells of two TP10 analogs that showed a pronounced membrane binding when an *L*-CF$_3$-BPG was introduced, with the TP10 analogs that had a D-CF$_3$-BPG substituted at the same position (Figure 5.1). In addition, the pair of peptides with the *L*- or *D*-variant of the 19F-NMR label at position 16 was

included, for which the *D*-variant showed a high tendency to form β-sheets. Remarkably, changing the stereochemistry of the introduced NMR label had a major effect on the membrane staining. Membrane-bound fluorescence was markedly reduced or even absent for those peptides that had a *D*-CF$_3$-BPG substitution in the sequence. In contrast, endocytosis was much less or not affected, as both TP10 Gly2→*D*-CF$_3$, Leu4→*D*-CF$_3$-Bpg and TP10 showed a similar punctate staining compared to the *L*-epimers. The peptide with a *D*-epimer substitution in position 16, TP10 Leu16→*D*-CF$_3$, was an exception in that it did not show any cell binding and/or endocytosis at all.
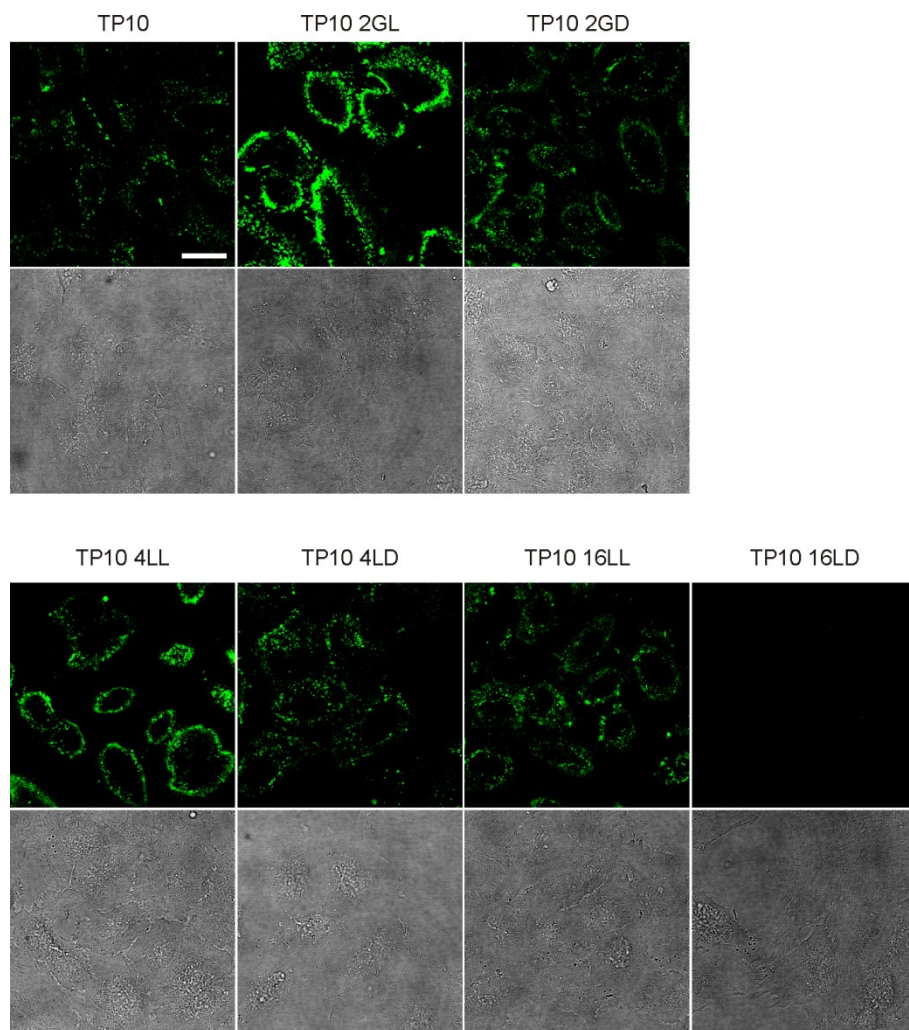
Figure 5.1. Cellular association of TP10 and TP10 analogs with D- or L-CF3-BPG amino acid replacements in HeLa cells. HeLa cells were incubated with 5 µM of the respective peptides for 30 min at 37°C, washed and imaged immediately by confocal microscopy. The scale bar corresponds to 20 µm.

5.2.3   Heparan sulfates and membrane binding

For D-amino acid-containing arginine-rich peptides, we showed that the enzymatic removal of HS chains strongly reduced the membrane staining. Furthermore, isothermal titration calorimetry (ITC) measurements of the interaction of these peptides with heparan sulfates gave binding constants in the submicromolar range [10], suggesting that membrane staining

was due to binding to heparan sulfates at the cell surface. Since TP10 lacks arginine residues and has a strong propensity to form an amphipathic α-helix [17, 18], we reasoned that enrichment at the plasma membrane would likely be independent of interactions with heparan sulfates.

To experimentally address this hypothesis, we cleaved off the HS chains from the cell surface with the enzyme heparinase III (Figure 5.2A). To make sure that heparinase did not modify the overall structure of the plasma membrane, the plasma membrane stain CellMask was included as a control after a heparinase treatment. The distribution and intensity for CellMask was not altered after the treatment. However, in contrast to our expectations, the heparinase treatment effectively reduced the intensity of the membrane staining of TP10 Gly2$\rightarrow$*L*-CF$_3$-Bpg. Also, TP10 Gly2$\rightarrow$*D*-CF$_3$-Bpg, for which no prominent membrane staining was observed, showed a reduction of punctate intracellular structures, supporting a role for HS chains for the productive internalization of this CPP. Since this result suggested a direct interaction between HS chains and TP10 analogs, we set out to measure the affinity of TP10 WT and the analog TP10 Gly2$\rightarrow$*L*-CF$_3$-Bpg for HS chains by ITC. Using similar conditions that gave submicromolar affinities for D/L-R9 and D/L-penetratin [10], we could not observe any binding enthalpy (Figure 5.2B). Since these results argued for an indirect binding to the HS layer, we furthermore considered the possibility that binding to the HS layer on the cell was enabled through some component in the fetal calf serum (FCS) that was included in all cellular experiments. To test this possibility, we performed the experiment in the presence or absence of FCS. A lower peptide concentration was used (2 μM), because leaving out FCS in the experiment was expected to result in higher effective peptide concentrations [19]. Moreover, we investigated the ability of externally added HS chains to compete with plasma membrane binding. Very interestingly, externally added HS chains inhibited membrane binding of TP10 Gly2$\rightarrow$*L*-CF$_3$-Bpg. No dependence on FCS components for membrane binding was detected.
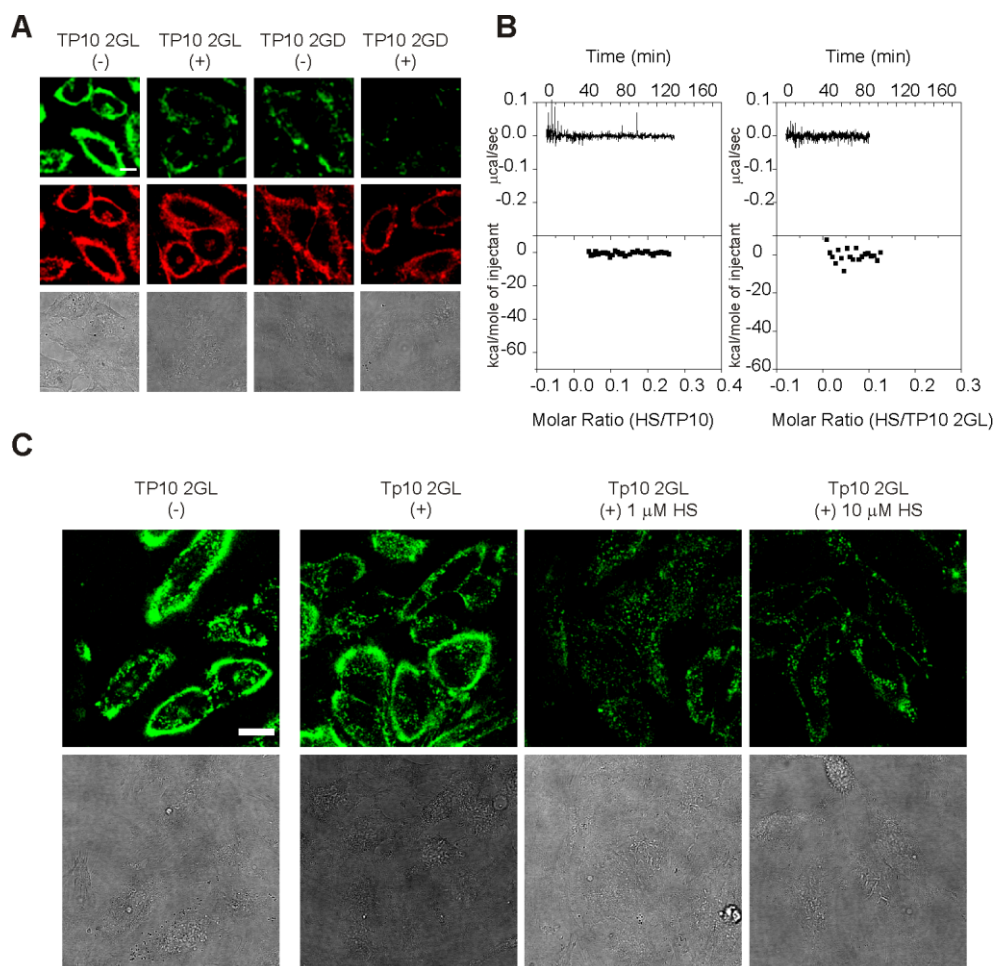
Figure 5.2. Role of heparan sulfates in cell association. A) Effect of heparinase treatment on membrane staining of the TP10 analogs Gly2→*L*-CF$_3$-Bpg and Gly2→*D*-CF$_3$-Bpg. B) Isothermal titration calorimetry with HS titrated into a sample cell containing either TP10 or the TP10 analog Gly2→*L*-CF$_3$-Bpg. C) Effect of omitting serum or competition with externally added HS chains on TP10 Gly2→*L*-CF$_3$-Bpg membrane binding. 2 μM of the indicated peptides were incubated for 30 min at 37°C in the presence (+) or absence (-) of fetal calf serum and in the presence of increasing amounts of HS. After the incubation, cells were washed twice and imaged immediately by confocal microscopy. The scale bar corresponds to 10 μm (A) and 20 μm (C).

5.2.4   Induction of phosphatidylserine exposure by TP10 and R9

In spite of the effect of heparan sulfate removal, which is difficult to interpret at present, the differences in HS binding argue for a different binding mechanism of these peptides to

the plasma membrane. To provide more insight into the way TP10 and its analogs affect the organization of the plasma membrane, we tested the ability of TP10 to induce phosphatidylserine (PS) exposure. Typically, PS is confined to the inner leaflet of the plasma membrane. Exposure of this phospholipid therefore indicates a disturbance of the lipid bilayer. In this case a concentration of 25 μM was selected. For arginine-rich peptides at this concentration lipid remodeling through induction of sphingomyelinase activation occurs. However, the integrity of the plasma membrane barrier function remains preserved [11]. Already after four minutes a marked difference in PS exposure was observed, which co-occurred with massive internalization of peptides into the cytoplasm. R9 only induced punctate exposure of PS (Figure 5.3). Although most regions where nucleation zones occurred also showed PS staining, as was shown before [11], nucleation zones were not observed at all regions where PS was exposed. In contrast to the findings with R9, the incubation with TP10 resulted in PS exposure all over the cell, supporting the hypothesis that the activity of TP10 is much more directed towards the lipid bilayer as compared to R9.
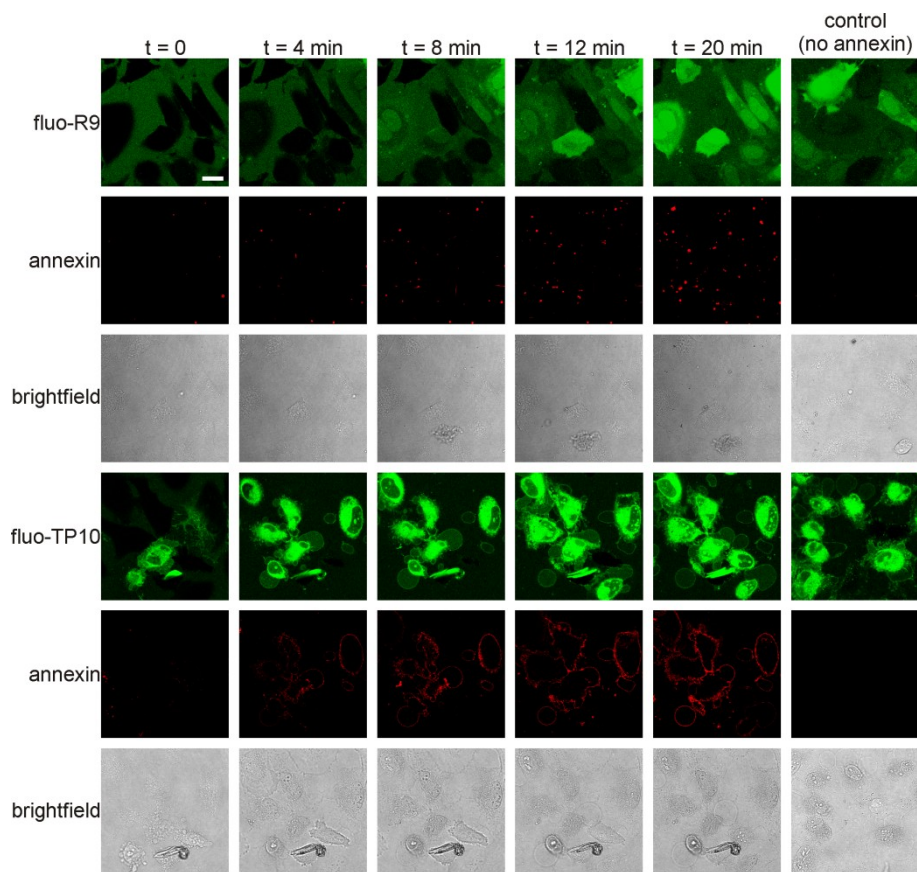
Figure 5.3. Induction of PS exposure by R9 and TP10. HeLa cells were co-incubated with 25 μM of the indicated peptides and AnnexinV-Alexa Fluor 647. Peptide internalization and PS exposure were followed from the first image acquired (t=0) up to 20 minutes. The scale bar corresponds to 20 μm.

5.2.5   Cytosolic uptake in suspension Jurkat cells

Since all previous experiments in this study were performed in HeLa cells and differences in the uptake of CPPs have been observed for different cell types, uptake in the suspension Jurkat E6.1 cells was investigated as well. This cell line is particularly interesting for a comparison, because this cell line has been shown by us to expose little or no HS chains and because it shows comparable uptake for *D*- and *L*-arginine-rich peptides, unlike HeLa cells [10]. Given the apparent role of HS chains in enriching peptide at the membrane, one might wonder whether the TP10 analogs Gly2→*L*-CF$_3$-Bpg and Leu4→*L*-CF$_3$-Bpg would be less enriched at the membrane in these cells. In order to investigate this, the TP10

analogs Gly2→*L*-CF$_3$-Bpg and Leu4→*L*-CF$_3$-Bpg, and the corresponding *D*-epimer-substituted analogs, were incubated with Jurkat cells (Figure 5.4). Indeed, no membrane binding was evident under these conditions. Instead, rather than showing a more pronounced membrane staining compared to the D-epimers, the L-epimers showed a more intense cytoplasmic fluorescence.

Previously, we have established that cytoplasmic fluorescence of arginine-rich L-peptides at a low peptide concentration (5 µM) in adherent cell lines mostly reflects degraded peptide fragments. Upon incubation with the cysteine protease inhibitor E64d, the cytoplasmic fluorescence was abolished and fluorescence was confined to endocytic vesicles. Moreover, after E64d treatment, the diffusion speed of fluorescent particles was decreased, as measured in lysates from cells incubated with peptides. Together, these findings indicate that an E64d treatment results in a greater fraction of intact peptides that ineffectively escape from the endosome to the cytosol [7, 11]. Furthermore, in adherent cell lines *D*-amino acid CPPs are internalized via endocytosis as well, albeit to a lesser degree than *L*-peptides, but show no cytoplasmic fluorescence observable by confocal microscopy [10]. Because *D*-amino CPPs differ from *L*-amino acid CPPs in that they cannot give rise to degraded fragments, the absence of cytoplasmic fluorescence might relate to the inability of *D*-CPPs to be cleaved into peptide fragments that may escape to the cytosol.

Initially, we assessed whether cytoplasmic fluorescence of R9 at 2 µM was also eliminated by the protease inhibitor E64d in suspension Jurkat cells. The low concentration of 2 µM was chosen because at this concentration R9 and r9 show clear differences in cytoplasmic fluorescence (Figure 5.4B), reminiscent of the E64d-sensitive differences that were observed in HeLa and MC57 cells at 5 µM [10]. At 5 µM in Jurkat cells, both R9 and r9 already show a pronounced cytoplasmic staining [10]. Most likely, Jurkat cells have a lower threshold for the rapid cytoplasmic uptake mechanism that is observed in MC57 and HeLa cells at concentrations starting from ~ 10 µM.

When we co-incubated the protease inhibitor E64d with the peptides at 2 µM, the cytoplasmic fluorescence of R9 was practically abolished and the uptake phenotype of R9 was converted to the uptake phenotype of r9 (Figure 5.4B). The reduction of cytoplasmic fluorescence after an E64d treatment is analogous to what was observed for R9 in MC57 cells. However, both R9 and r9 were present inside the Jurkat cells with the same intensity. In this respect, these observations for Jurkat cells clearly differ from the observations made for MC57. In the latter, in the presence of E64d, r9 was much less efficiently endocytosed and remained much more membrane-bound [10]. Strikingly, at 2 µM a weak plasma membrane staining also became evident in Jurkat cells, which was previously not observed

at higher concentrations [10]. Probably, this membrane staining is also present at higher concentration but was made visible due to the much greater laser intensity and/or digital amplification of the signal that was required to visualize the peptides at this low concentration. Since Jurkat cells have no or little heparan sulfates [10], this indicates that the peptides may either bind to other membrane sugars such as chondroitin sulfates [20] and/or negatively charged lipids or proteins of the plasma membrane. In contrast to the effect on R9, the protease inhibitor E64d did not affect the cytoplasmic fluorescence of the TP10 analogs at all, indicating that these peptides follow an alternative route towards the cytosol that does not involve passage via an E64d-sensitive compartment (Figure 5.4C).

5.2.6   *Membrane binding in Jurkat cells*

Since no membrane staining was observed for the TP10 analogs at 2 μM, an uptake experiment was also performed at 10 μM. Since at this concentration TP10 analogs may potentially damage the plasma membrane, the marker propidium iodide (PI) was included, which only enters cells that have a comprised membrane integrity (Figure 5.4D). Of all four peptides tested, only one peptide, TP10 Gly2→L-CF$_3$-Bpg, was not overtly toxic at this peptide concentration, as reflected by the absence of an intracellular PI staining. Of note is that the PI staining was non-typical in that it did not clearly accumulate in the nuclei. Since the control without PI did not show any signal in the PI channel and the brightfield images showed very obvious toxic effects, this non-typical PI staining is most likely due to the phase of cell disintegration and/or the cell type in question. Remarkably, instead of a membrane-wide staining as observed in HeLa cells, the staining pattern for TP10 Gly2→L-CF$_3$-Bpg in Jurkat cells was restricted to parts of the membrane, indicating that this peptide has an increased affinity for specific membrane domains with an altered lipid microenvironment. Isolated instances of the staining of such membrane patches were also observed for the other peptides, albeit at a far lower frequency (data not shown). In addition, cytoplasmic fluorescence was detected at a similar level as at 2 μM (Figure 5.4E).
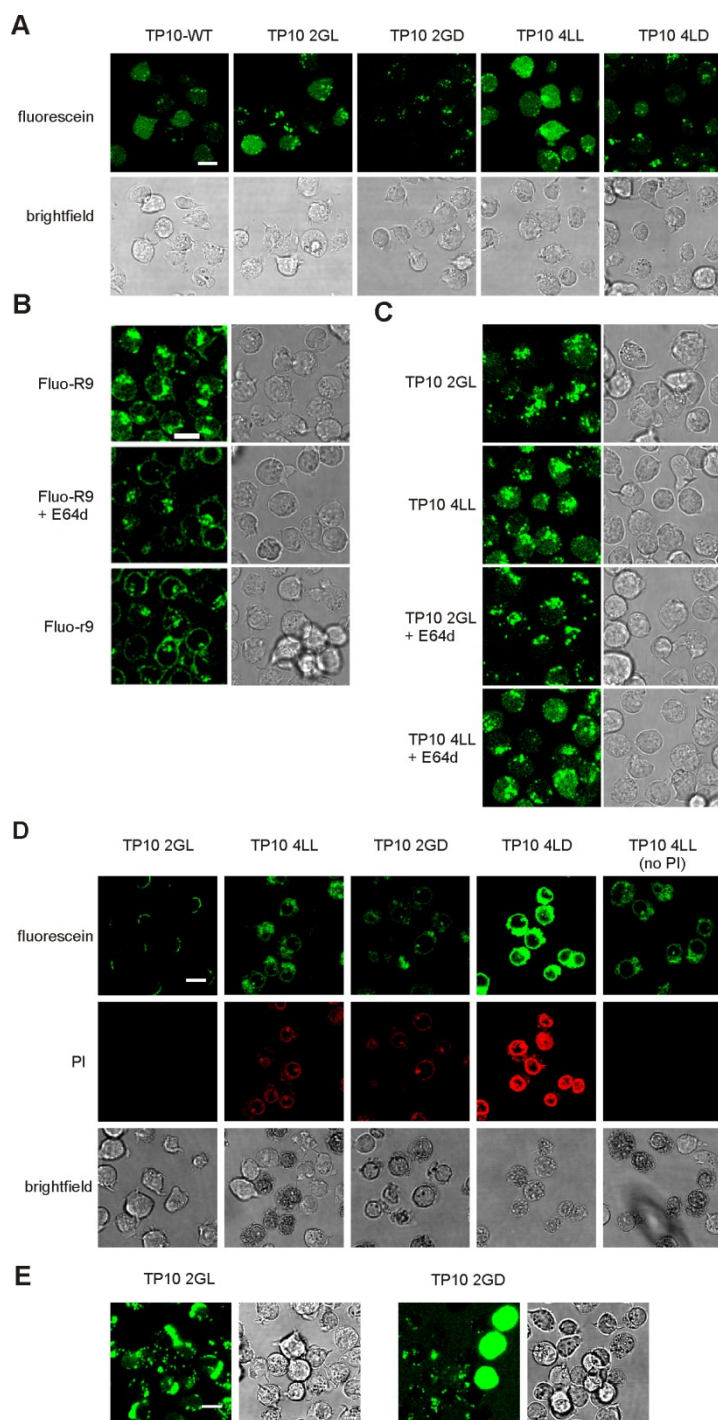
Figure 5.4. A) Uptake of TP10 and analogs in Jurkat cells. Cells were incubated with 5 μM of the respective peptide for 30 min at 37°C, washed twice by centrifugation, resuspended and allowed to settle in 8-well microscopy chambers. Analysis by confocal microscopy was performed as soon as cells had settled. B-C) Uptake of peptides in the presence or absence of the cysteine protease inhibitor E64d. Jurkat E6.1 cells were pre-incubated for 30 min with 100 μM E64d or left untreated. Cells were washed, incubated in the presence or absence of 100 μM E64d for 30 min at 37°C and 2 μM of the indicated peptides, washed and analyzed immediately by confocal microscopy. D-E) Jurkat cells were incubated for 30 min at 37°C with the indicated peptides at 10 μM, washed and analyzed by confocal microscopy. In D, 5 μg/ml propidium iodide (PI) was added after the incubation to distinguish intact cells from those with a compromised plasma membrane. The scale bars represent 10 μm.

5.3   Discussion

Despite the field of CPPs moving ever closer to clinical applications, there is still relatively little known about the intermolecular interactions of CPPs in a cellular context. Given recent findings from our laboratory on all-*D*, all-L and *D*/*L* chimeric peptides, in particular the role of stereochemistry in CPP functionality requires further attention. Against this background, we investigated the molecular interactions between two model cell lines and various TP10 analogs containing the *D*- and *L*-variant of the NMR label CF$_3$-Bpg. Comparisons were made with the prototypic arginine-rich CPP R9, which was used as a representative peptide from the subclass of arginine-rich CPPs [11, 12]. TP10 is generally considered as a much more membrane-active peptide because it causes membrane leakage at a much lower concentration compared to arginine-rich peptides [21, 22]. A main reason is its much higher tendency, compared to R9, to spontaneously insert into lipid membranes, where it undergoes conformational rearrangements [23].

Internalization efficiency, binding to the plasma membrane and cytotoxicity were strongly dependent on the stereochemistry of the amino acid that was introduced at distinct positions in the CPP sequence in a manner that was not evident from the conformation and/or aggregation behavior of the peptide. An exception was the lack of CPP activity of TP10 Leu16→*D*-CF$_3$-Bpg, which is most likely due its very high tendency to aggregate via β-sheets.

Very prominently, TP10 Gly2→*L*-CF$_3$-Bpg and Leu4→*L*-CF$_3$-Bpg showed a pronounced membrane binding, which is reminiscent of our previous results for r9 and *D*-penetratin [10]. Since the TP10 analogs do not contain any arginines, we were surprised to see that this membrane staining could be reduced either by a heparinase pre-treatment or by co-incubating the peptides with HS chains, even though ITC measurements showed no measurable affinity. In stark contrast, the arginine-rich CPPs R9 and penetratin showed submicromolar affinities for HS chains [10]. Nevertheless, the ITC values are in

accordance with previous studies, which showed that changing lysines to arginines on one side of a helical heparin-binding peptide improved heparin affinity from 640 nM to 3 nM [24]. The reason underlying the improved affinity is thought to be the 2.5 times higher enthalpic contribution of the binding of arginines to heparin in comparison to the binding of lysines [25]. The presence of fetal calf serum did not affect membrane binding of TP10 Gly2→L-CF$_3$-Bpg, ruling out the possibility that components in fetal calf serum mediate the binding between HS and TP10 Gly2→L-CF$_3$-Bpg on cells. In HS-poor Jurkat, no membrane staining was evident for the TP10 analogs at low concentrations, providing further support for the idea that the presence of HS affects the membrane binding of TP10 to the membrane. Although our results with a heparinase treatment were unexpected, previous studies have already shown that removal of HS chains by heparinase can lead to a reduced ability of TP10 to carry a PNA-cargo into the cytosol [26].

Given the observation that TP10 does not directly bind to HS chains, the effects HS chains have on membrane binding and uptake might be influenced indirectly through changes in the properties of the plasma membrane, in particular the surface charge. One might argue that negatively charged membrane-bound HS chains might enrich ions or other molecules close to the membrane in a manner that might facilitate the interaction of the plasma membrane with TP10 analogs or, alternatively, affect the lipid composition of the external leaflet of the plasma membrane. According to this hypothesis, removal of HS chains would then indirectly decrease the ability of TP10 analogs to bind to the membrane. This ability could in principle also be abolished through the external addition of an access of HS chains, which would prevent the cell-surface HS chains from exerting this particular function required for TP10 analog binding and uptake. The details of such a potential mechanism are unclear at present. If the ability of HS to affect plasma membrane properties would indeed be required, then a similar external addition of HS chains would have no effect on TP10/TP10 analog uptake in Jurkat cells, which have low amounts or no HS chains on their surface.

Regarding the membrane behavior of TP10 in comparison to arginine-rich peptides, previous studies have indicated that TP10 already causes membrane disturbances and/or effects on cell proliferation at much lower concentrations compared to arginine-rich peptides such as Tat or penetratin in both adherent and suspension cell lines [21, 22]. Our study further supports the differences in the membrane behavior of arginine-rich CPPs and TP10 through the comparison of R9 and TP10 with respect to their ability to induce PS exposure, a classical marker of membrane disturbance. Whereas R9 only caused local

exposure of PS, in accordance with previous observations [11], TP10 caused a rapid plasma membrane-wide presence of PS in a matter of minutes.

Of further interest is that we exclusively observed intracellular staining, and thus no membrane staining, of the TP10 analog Gly2→*L*-CF$_3$-Bpg at 2 μM, whereas at 10 μM the peptide stained membrane patches at the Jurkat cell membrane. Membrane patches were not as evident for the other three peptides tested in Jurkat cells. Interestingly, this specific TP10 analog also showed immobilization during the solid state NMR studies (table 5.1). This is a second example of a correlation between peptide behavior in an artificial system and in cells, next to the loss of CPP activity of Leu16→*D*-CF$_3$-Bpg. To what extent the segregation of the peptide on the plasma membrane also occurs in other cell lines remains to be investigated. No such membrane patches were observed in HeLa cells. However, only concentrations of up to 5 μM were tested in this cell line. The threshold for cytotoxicity also proved to be dependent on the enantiomer. In contrast to Gly2→*L*-CF$_3$-Bpg the *D*-epimer TP10 Gly2→*D*-CF$_3$-Bpg showed massive membrane toxicity at 10 μM in Jurkat cells (Figure 5.4D).

Very remarkably, in Jurkat cells some, but not all, TP10 analogs also stained the cytosol at the low concentration of 2 μM. Fluorescence staining of the cytosol was insensitive to E64d, which is indicative of intact peptide reaching the cytosol in an endocytosis-independent fashion. The inhibitor E64d abolishes the cytoplasmic fluorescence of the proteolytically labile *L*-CPPs nona-arginine and penetratin in adherent MC57 cells [10]. For R9, the dependency on proteolytic breakdown for cytoplasmic fluorescence in Jurkat cells at 2 μM was confirmed in this study (Figure 5.4B).

In conclusion, for the TP10 analogs our results clearly show that various CPP properties depend on the stereochemistry of individual amino acids. Epimerization of a single amino acid has large effects on internalization efficiency, membrane binding and cytotoxicity. These characteristics had only a very limited correlation with the secondary structure and aggregation characteristics of these peptides as determined by solid-state NMR and oriented CD, demonstrating that such *in vitro* experiments still fail to recapitulate key molecular events associated with the interaction of these peptides with cells.

5.4   Experimental procedures

5.4.1   Cell culture

HeLa and Jurkat E6.1 cells were maintained in DMEM and RPMI 1640 (Gibco, Invitrogen, Eugene, U.S.A.), respectively, supplemented with 10 % fetal calf serum (FCS; PAN Biotech). All cells were incubated at 37°C in a 5 % CO_2-containing, humidified incubator. Cells were passaged every 2 to 3 days.

5.4.2   Solid-phase peptide synthesis (SPPS)

All peptides were synthesized on an automated Syro II multiple peptide synthesizer (MultiSynTech, Witten, Germany) with standard Fmoc SPPS protocols and HOBt/HBTU as coupling reagents. The 19F-labeled amino acid CF_3-Bpg was coupled for 2 h. Peptides were N-terminally labeled with CF before cleaving off the resin and side chain deprotection. For labeling, diisopropylcarbodiimide (DIC), HOBt and 5,6-CF were dissolved in dimethylformamide (DMF) in a molar ratio of 1:1:1, mixed with the peptide on the resin in a molar ratio of 5:1 and coupled for 12 h. After washing with DMF, dichlormethane (DCM), methanol (MeOH) and diethyl ether, piperidine (20% v/v in DMF) was added for 30 min. Afterwards the resin was washed with DMF, DCM and MeOH, dried under reduced pressure and the peptide cleaved off the resin and side chain deprotected using a mixture of trifluoroacetic acid (TFA) (93.5%), triisopropanyl (TIS) (4%) and H_2O (2.5%), precipitated with diethyl ether and lyophilized. The crude peptides were purified by high-performance liquid chromatography (HPLC) on a preparative C18 column (22x250 mm) (Vydac, Hesperia, CA, USA) using acetonitril water gradients supplemented with 5 mM HCl. The identity of all peptides was confirmed by mass spectrometry. The purity of the peptides was found to be over 95%. The concentration of fluorescein-labeled peptides was determined by measuring A_{492} in Tris-HCl buffer (pH 8.8), assuming a molar extinction coefficient of 75,000 M^{-1} cm^{-1}.

5.4.3   Imaging of peptide uptake by confocal microscopy

HeLa cells were seeded one (40,000 cells/well) to three (10,000 cells/well) days before the experiment in 8-well microscopy chambers (Nunc, Wiesbaden, Germany, or 8-well Ibidi chambers (Martinsried, Germany), and grown to 75 % confluence. Cells were incubated with the indicated concentrations of TP10 or TP10 analogs for 30 min at 37°C. Cells were

washed twice after incubation and living cells were analyzed immediately by confocal microscopy using a TCS SP5 confocal microscope (Leica Microsystems, Mannheim, Germany) equipped with an HCX PL APO 63 x N.A. 1.2 water immersion lens. Cells were maintained at 37°C on a temperature-controlled microscope stage. AnnexinV-Alexa Fluor 647 was used at a dilution of 1:50 (Invitrogen). E64d (Bachem, Bubendorf, Switzerland) was used at a concentration of 100 μM for pre- and co-incubations. For heparinase treatments, HeLa cells were pre-incubated with 750 μIU of heparinase III (Ibex, Quebec, Canada) in DMEM containing 1 % FCS for 1 h at 37°C.

5.4.4   ITC

ITC experiments were performed with an ITC$_{200}$ Microcal instrument (MicroCal LLC, Wolverton Mill UK) at 25°C, using comparable conditions as were used for arginine-rich peptides before [10]. Briefly, peptide and HS solutions were diluted in HBS to 60 μM and 75 μM, respectively. All solutions were degassed before use. The sample cell was filled with the peptide solution and 39 times 1 μl of the HS solution was injected into the sample cell. Data were analyzed using the ITC$_{200}$ Microcal software.

5.4.5   Oriented circular dichroism spectroscopy (OCD)

OCD experiments were performed on a J-810 spectropolarimeter (Jasco, Tokyo, Japan) with an in-house set-up for the OCD-cell. Lipids were dissolved in chloroform and peptides in MeOH, appropriate amounts mixed and spread on a 12 mm diameter quartz glass plate. After drying under reduced pressure, the samples were hydrated over night at 40°C in 97 % relative humidity. The spectra were recorded in the range of 260 to 180 nm using a scan rate of 20 nm/min, 8-s response time, 1-nm bandwidth, at eight different rotations of the cell and referenced by subtracting the background signal that was recorded with a sample containing the same amount of lipids without peptides.

5.4.6   Solid-state NMR spectroscopy

All experiments were performed on a Bruker Avance 500 MHz NMR spectrometer (Bruker BioSpin, Rheinstetten, Germany) at 313 K. 31P-NMR was performed at a frequency of 202.5 MHz using a Hahn echo sequence [27] with a 90° pulse of 5 μs, 30 μs echo time, a sweep width of 200 kHz, 4096 data points and proton decoupling using tppm [28]. Usually 128 scans were recorded. 19F-NMR was performed at a frequency of 470.6 MHz using an

anti-ringing sequence with a 90° pulse of 3.25 μs, a sweep width of 500 kHz, 4096 data points and proton decoupling using tppm. For preparing the oriented samples, a DMPC/DMPG mixture in a molar ratio of 3:1 was dissolved in chloroform and peptide was dissolved in MeOH. Both solutions were thoroughly mixed and equally distributed on 18 glass plates (15 mm x 7.5 mm x 0.08 mm) (Marienfeld Laboratory Glassware, Lauda-Königshofen, Germany). The glass plates were stacked and hydrated at 48°C in 96% relative humidity for 24 h after drying under reduced pressure for at least 3 h. The hydrated samples were wrapped in parafilm and plastic foil before the NMR experiments.

5.5   References

[1] F. Duchardt, M. Fotin-Mleczek, H. Schwarz, R. Fischer, R. Brock, A comprehensive model for the cellular uptake of cationic cell-penetrating peptides, Traffic, 8 (2007) 848-866.

[2] F. Madani, S. Lindberg, U. Langel, S. Futaki, A. Graslund, Mechanisms of cellular uptake of cell-penetrating peptides, J Biophys, 2011 (2011) 414729.

[3] J. Mueller, I. Kretzschmar, R. Volkmer, P. Boisguerin, Comparison of cellular uptake using 22 CPPs in 4 different cell lines, Bioconjug Chem, 19 (2008) 2363-2374.

[4] G. Tunnemann, R.M. Martin, S. Haupt, C. Patsch, F. Edenhofer, M.C. Cardoso, Cargo-dependent mode of uptake and bioavailability of TAT-containing proteins and peptides in living cells, FASEB J, 20 (2006) 1775-1784.

[5] I.D. Alves, N. Goasdoue, I. Correia, S. Aubry, C. Galanth, S. Sagan, S. Lavielle, G. Chassaing, Membrane interaction and perturbation mechanisms induced by two cationic cell penetrating peptides with distinct charge distribution, Biochim Biophys Acta, 1780 (2008) 948-959.

[6] E. Goncalves, E. Kitas, J. Seelig, Binding of oligoarginine to membrane lipids and heparan sulfate: structural and thermodynamic characterization of a cell-penetrating peptide, Biochemistry, 44 (2005) 2692-2702.

[7] M. Magzoub, A. Pramanik, A. Graslund, Modeling the endosomal escape of cell-penetrating peptides: transmembrane pH gradient driven translocation across phospholipid bilayers, Biochemistry, 44 (2005) 14890-14897.

[8] Y. Su, T. Doherty, A.J. Waring, P. Ruchala, M. Hong, Roles of arginine and lysine residues in the translocation of a cell-penetrating peptide from (13)C, (31)P, and (19)F solid-state NMR, Biochemistry, 48 (2009) 4587-4595.

[9] P.A. Wender, D.J. Mitchell, K. Pattabiraman, E.T. Pelkey, L. Steinman, J.B. Rothbard, The design, synthesis, and evaluation of molecules that enable or enhance cellular uptake: peptoid molecular transporters, Proc Natl Acad Sci U S A, 97 (2000) 13003-13008.

[10] W.P. Verdurmen, P.H. Bovee-Geurts, P. Wadhwani, A.S. Ulrich, M. Hallbrink, T.H. van Kuppevelt, R. Brock, Preferential uptake of L- versus D-amino acid cell-penetrating peptides in a cell type-dependent manner, Chem Biol, 18 (2011) 1000-1010.

[11] W.P. Verdurmen, M. Thanos, I.R. Ruttekolk, E. Gulbins, R. Brock, Cationic cell-penetrating peptides induce ceramide formation via acid sphingomyelinase: implications for uptake, J Control Release, 147 (2010) 171-179.

[12] G. Tunnemann, G. Ter-Avetisyan, R.M. Martin, M. Stockl, A. Herrmann, M.C. Cardoso, Live-cell analysis of cell penetration ability and toxicity of oligo-arginines, J Pept Sci, 14 (2008) 469-476.

[13] S. Jones, J. Howl, Enantiomer-specific bioactivities of peptidomimetic analogues of mastoparan and mitoparan: characterization of inverso mastoparan as a highly efficient cell penetrating Peptide, Bioconjug Chem, 23 (2012) 47-56.

[14] A. Arbuzova, G. Schwarz, Pore-forming action of mastoparan peptides on liposomes: a quantitative analysis, Biochim Biophys Acta, 1420 (1999) 139-152.

[15] T. Katsu, M. Kuroko, T. Morikawa, K. Sanchika, H. Yamanaka, S. Shinoda, Y. Fujita, Interaction of wasp venom mastoparan with biomembranes, Biochim Biophys Acta, 1027 (1990) 185-190.

[16] I.R. Mellor, M.S. Sansom, Ion-channel properties of mastoparan, a 14-residue peptide from wasp venom, and of MP3, a 12-residue analogue, Proc R Soc Lond B Biol Sci, 239 (1990) 383-400.

[17] E. Barany-Wallje, A. Andersson, A. Graslund, L. Maler, NMR solution structure and position of transportan in neutral phospholipid bicelles, FEBS Lett, 567 (2004) 265-269.

[18] M. Lindberg, J. Jarvet, U. Langel, A. Graslund, Secondary structure and position of the cell-penetrating peptide transportan in SDS micelles as determined by NMR, Biochemistry, 40 (2001) 3141-3149.

[19] M. Kosuge, T. Takeuchi, I. Nakase, A.T. Jones, S. Futaki, Cellular internalization and distribution of arginine-rich peptides as a function of extracellular peptide concentration, serum, and plasma membrane associated proteoglycans, Bioconjug Chem, 19 (2008) 656-664.

[20] I. Nakase, A. Tadokoro, N. Kawabata, T. Takeuchi, H. Katoh, K. Hiramoto, M. Negishi, M. Nomizu, Y. Sugiura, S. Futaki, Interaction of arginine-rich peptides with

membrane-associated proteoglycans is crucial for induction of actin organization and macropinocytosis, Biochemistry, 46 (2007) 492-501.

[21] S. El-Andaloussi, P. Jarver, H.J. Johansson, U. Langel, Cargo-dependent cytotoxicity and delivery efficacy of cell-penetrating peptides: a comparative study, Biochem J, 407 (2007) 285-292.

[22] K. Saar, M. Lindgren, M. Hansen, E. Eiriksdottir, Y. Jiang, K. Rosenthal-Aizman, M. Sassian, U. Langel, Cell-penetrating peptides: a comparative membrane toxicity study, Anal Biochem, 345 (2005) 55-65.

[23] E. Eiriksdottir, K. Konate, U. Langel, G. Divita, S. Deshayes, Secondary structure of cell-penetrating peptides controls membrane interaction and insertion, Biochim Biophys Acta, 1798 (2010) 1119-1128.

[24] A. Rullo, M. Nitz, Importance of the spatial display of charged residues in heparin-peptide interactions, Biopolymers, 93 (2010) 290-298.

[25] J.R. Fromm, R.E. Hileman, E.E. Caldwell, J.M. Weiler, R.J. Linhardt, Differences in the interaction of heparin with arginine and lysine and the importance of these basic amino acids in the binding of heparin to acidic fibroblast growth factor, Arch Biochem Biophys, 323 (1995) 279-287.

[26] P. Lundin, H. Johansson, P. Guterstam, T. Holm, M. Hansen, U. Langel, E.L.A. S, Distinct uptake routes of cell-penetrating peptide conjugates, Bioconjug Chem, 19 (2008) 2535-2542.

[27] M. Rance, R.A. Byrd, Obtaining High-Fidelity Spin-1/2 Powder Spectra in Anisotropic Media - Phase-Cycled Hahn Echo Spectroscopy, J Magn Reson, 52 (1983) 221-240.

[28] A.E. Bennett, C.M. Rienstra, M. Auger, K.V. Lakshmi, R.G. Griffin, Heteronuclear Decoupling in Rotating Solids, J Chem Phys, 103 (1995) 6951-6958.

Measurements of the intracellular stability of CPPs

Ivo R. Ruttekolk[+], Wouter P. R. Verdurmen[+],
Yi-Da Chung and Roland Brock

6   Measurements of the intracellular stability of CPPs

Ivo R. Ruttekolk[+], Wouter P. R. Verdurmen[+], Yi-Da Chung, Roland Brock

[+]these authors contributed equally

Department of Biochemistry, Nijmegen Centre for Molecular Life Sciences, Radboud University Nijmegen Medical Centre, Nijmegen, The Netherlands

Abstract

Nowadays, the analysis of the uptake and intracellular distribution of cell-penetrating peptides mostly relies on fluorescence microscopy, using fluorescently labeled CPP analogs. However, fluorescence microscopy does not reveal to which degree fluorescence reflects the intact peptide or only breakdown products. We here introduce fluorescence correlation spectroscopy (FCS) as a powerful method to address peptide stability in cells and in cell lysates. Measurements in lysates of cells incubated with peptide yield information on degradation of the total cellular peptide content. In combination with protease inhibitors such measurements enable conclusions on trafficking pathways. Intracellular FCS measurements provide direct information on peptide degradation and association with cellular structures in intact cells.

6.1   Introduction

Conjugation to fluorophores has become the method of choice for analyzing the uptake of cell-penetrating peptides. Using confocal microscopy the uptake and subcellular distribution can be followed in real time [1-5]. Moreover, fluorescence enables a straight-forward quantitative comparison of uptake efficiencies using flow cytometry. Nevertheless, most techniques that rely on fluorescence are not able to distinguish between intact, fluorescently labeled molecules and their degradation products, which can complicate the interpretation of results obtained with these techniques. In particular with respect to the subcellular localization it is not clear, to which degree the distribution of fluorescence reflects the characteristics of the intact peptide. Moreover, given that proteolytic stability,

both extracellular and intracellular, is of major importance for determining the uptake efficiency of a CPP, it is evident that there is an unmet need to follow the stability of CPPs during the course of experiments [6-9]. This requirement is furthermore illustrated by the fact that different CPPs and cargo constructs use distinct intracellular endocytotic pathways that differ strongly in proteolytic activity [1, 10-12].

One technique that enables a direct detection of intact CPPs and CPP-cargo constructs and their digestion products without fluorescent labels is mass spectrometry [6, 13, 14]. Using stable isotopes as an internal standard this method can moreover provide information on absolute quantities. However, fully degraded peptides will not be amenable to detection by MS-based techniques. Another way of assessing delivery of intact molecules is through biological assays. The luciferase-based splice correction assay that detects the delivery of CPP-coupled oligonucleotides [15, 16] is a prominent example for these techniques. Nevertheless, in spite of the advancements that both types of techniques have brought to the detection of intact peptide reaching the cytosol, both types of methods fail to provide quantitative information on the sequestration and degradation of peptides in the endolysosomal compartment.

Fluorescence correlation spectroscopy (FCS) is a technique that has the potential to complement these other techniques for providing information on peptide degradation in cell lysates and intact cells. FCS extracts information on the concentration and mobility of fluorescently labeled molecules from temporal fluctuations of the fluorescence intensity in a confocal detection volume the size of an *E. coli* [17]. In biological samples, mobility is a function of the size and molecular interactions of a molecule. When combined with imaging, such information can also be obtained for molecules in intact cells [18, 19]. This chapter provides protocols for FCS measurements of CPP integrity in cell lysates and in intact cells. For obtaining overall information on intracellular peptide break-down, a protocol for performing FCS experiments in lysates of human cervical carcinoma (HeLa) cells that were incubated with a CPP before lysis is described (see also Figure 6.1A-E). Lysosomal protease inhibitors are employed to assess the influence of various classes of lysosomal proteases in the intracellular breakdown of CPPs in endolysosomal compartments. The second protocol describes the measurement of the stability of CPPs composed of D- and L-amino acids in single living Jurkat E6.1 T cell leukemia cells.
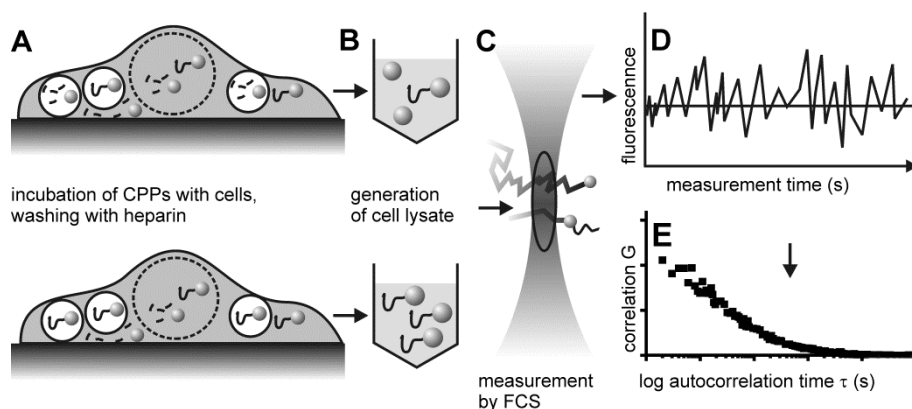
Figure 6.1. Schematic overview illustrating sequential steps for the execution of an FCS experiment using cell lysates.

6.2   Materials

All cell lines are in principle amenable to analysis by fluorescence correlation spectroscopy. For measurements in cell lysates, interactions of peptides with cellular components such as DNA and cellular membranes can complicate especially the quantification of the fraction of intact peptides. Our own experience shows that these molecules are more prone to such interactions than proteolytic fragments. For intracellular FCS measurements, the feasibility and quality of the measurements is influenced to a significant degree by cellular characteristics such as size, morphology and mobility of cells.

6.2.1   *Preparation of lysates of HeLa cells treated with lysosomal protease inhibitors*

1. HeLa cells from the American-Type Culture Collection (ATCC, Manassas, USA); maintained in RPMI 1640 (Pan Biotech, Aidenbach, Germany) supplemented with 10 % fetal calf serum (Pan Biotech).
2. 24-well culture plates (Sarstedt, Nümbrecht, Germany).
3. Lysosomal protease inhibitors: Pepstatin A (Sigma-Aldrich, Steinheim, Germany), which can be dissolved at 3 mM in DMSO, and E64d (Bachem, Heidelberg, Germany) which can be dissolved in DMSO in concentrations up to 50 mM. Inhibitors can be stored at -20°C for months.

4. Lysis buffer: PBS containing 1 % (v/v) Triton-X-100 (Sigma-Aldrich). This solution is stable at room temperature (RT) for months. For each experiment, add a fresh protease inhibitor cocktail from a frozen or dry stock (Roche Diagnostics, Mannheim, Germany).

5. Fluorescein-labeled nona-arginine (R9) (EMC microcollection, Tübingen, Germany). All peptides are dissolved in a minimal amount of DMSO (peptide concentration ~ 10 mM). Concentration is determined by measuring A_{492} in Tris-HCl buffer (pH 8.8) assuming a molar extinction coefficient of 75,000 M^{-1} cm^{-1}. Peptides dissolved in DMSO can be stored for extended periods at 4°C.

6. Heparin (Sigma-Aldrich): Dissolve at 2 mg/ml in H_2O and freeze aliquots at -20°C. Aliquots are stable for months. Do not re-use thawed aliquots.

6.2.2   *FCS measurements in HeLa cell lysates*

1. Trypsin/EDTA solution. PBS containing 400 μg/ml trypsin and 40 μg/ml EDTA. Trypsin/EDTA mix was purchased from PAN Biotech.

2. 384-well plate (175 μm, low-base design, MMI, Eching, Germany)

3. Tris buffer: 100 mM Tris-HCl, pH 8.8.

4. Bovine serum albumin (BSA; Sigma-Aldrich): 5 % (w/v) BSA stocks can be prepared by adding BSA to water, which will dissolve by itself without mixing. When dissolved, aliquot and freeze at -20°C, where it will be stable for months. Aliquots can be thawed and refrozen several times.

5. TCS SP5 confocal microscope (Leica Microsystems, Mannheim, Germany) equipped with an HCX PL APO 63 x N.A. 1.2 water immersion lens and an FCS detection unit fitted with a 500-550 nm filter cube (Leica Microsystems, Mannheim, Germany). The carboxyfluorescein moieties were excited by the 488 nm line of an argon ion laser.

6. ISS VISTA software (ISS, inc. Illinois, USA).

6.2.3   *Preparation of live cells treated with nona-arginine composed of D- and L-amino acids*

1. Jurkat E6.1 T cell leukemia cells (ATCC) maintained in RPMI 1640 supplemented with 10 % fetal calf serum (both Pan Biotech).

2. Fluorescein-labeled nona-arginine composed of L- (R9) or D- (R9) amino acids (EMC microcollections).

6.2.4   Intracellular FCS measurements in living Jurkat cells

1-4. As for 6.2.2.

5. The microscope was fully encapsulated in an air-heated incubator with humidity control, in order to maintain cell viability during the measurement procedure.

6. Globals for Spectroscopy software (Laboratory for Fluorescence Dynamics, Irvine, CA, USA).

6.3   Methods

6.3.1   Preparation of lysates of HeLa cells treated with lysosomal protease inhibitors

1. Seed HeLa cells at a density of 80,000 cells/well in a 24-well plate in 800 μlRPMI + 10 % fetal calf serum.

2. 24 h later, wash cells and pre-incubate for 30 min with 10 μM pepstatin A to inhibit aspartic proteases [20] or with 40 μM E64d to inhibit cysteine proteases [21]. Include two untreated controls[1] and a control for the vehicle of pepstatin A (0.33 % DMSO).

3. Remove medium containing lysosomal protease inhibitors or control vehicle. Incubate for 60 min at 37°C with 5 μM R9 in the presence of the inhibitors or control vehicle at the same concentration as during the pre-incubation.

4. Wash cells twice with RPMI supplemented with 10 % fetal calf serum and incubate them twice for 5 min at 37°C with 100 μg/ml heparin in RPMI containing 10 % fetal calf serum to remove surface-bound peptides [2].

5. Add 500 μl of freshly prepared lysis buffer[3] to the cells and incubate samples for 60 min on ice for complete lysis.

6. Agitate the lysate by pipetting and centrifuge the lysate for 20 min at 20,000 *g* at 4°C to remove any remaining membrane debris[4]. Freeze lysates at -20°C until further use[5].

---

[1] To lysates of untreated controls, intact and degraded R9 will be added. These measurements will serve as references for the analysis of the degree of degradation. The background signal of untreated controls will be applied for correcting particle numbers estimated by the analysis software.

[2] In our hands, a heparin treatment at the indicated concentration performs as well as trypsin to remove surface-bound nona-arginine, but is a milder treatment for the cells.

[3] The application of a minimal amount of lysis buffer reduces the likelihood of any interferences of the lysis buffer in the FCS measurements due to changes in refractive index.

[4] It is expected that some remaining debris-bound peptides will be removed by centrifugation. The amount will depend on the interactions of the peptide with lysate components. Free fluorophores that result from the

6.3.2   FCS measurements in HeLa cell lysates

1. For obtaining a reference of digested peptide, digest R9 with PBS containing trypsin (400 µg/ml) and EDTA (40 µg/ml) 16 h at 37°C.

2. Coat the wells of a 384-well plate with a 0.1 % BSA solution in PBS for 30 min at RT to reduce adsorption of peptides to the walls of the wells. Afterwards wash twice with PBS.

3. Dilute cell lysates 5x in Tris buffer (pH 8.8)[6] and keep lysates on ice until the measurement.

4. Include a well containing 10 nM fluorescein in PBS as a standard and a well containing pure PBS[7]. Also include wells for trypsin-degraded R9 and intact R9 in a similar cell lysate/buffer composition as the samples treated with lysosomal protease inhibitors.

5. Determine the laser power that maximizes the signal-to-ratio of the signal[8]. Use the FCS wizard of the Leica SP5 software to control the laser power and the ISS vista software package for the acquisition of the FCS data.

6. Determine the structure parameter and the triplet time using fluorescein[9].

7. Perform autocorrelation measurements of intact and trypsin-degraded R9 added to 20% cell lysate/80% TRIS-buffer[10].

---

degradation of labeled peptides are less prone to removal by centrifugation due to less association with lysate components.

[5] Of course, FCS experiments can also be conducted without the freezing step. However, for practical reasons, it is often desirable to freeze the lysates on the day that the cellular experiment was conducted. We recommend to store lysates no longer than a few days at -20°C to avoid unwanted storage effects.

[6] A buffer with a pH of 8.8 is used because in this pH range, the brightness of the fluorescein moiety attached to the peptides is optimal, which yields a better signal-to-noise ratio in the FCS measurements. In a similar manner, buffering conditions for other fluorophores should be optimized for obtaining optimum fluorescence brightness as well.

[7] As FCS measurements provide optimum signal-to-noise ratios for concentrations of fluorophores between 1-100 nM, samples should be diluted accordingly. The inclusion of a PBS control for background fluorescence enables the adjustment of the laser intensity to the optimal signal-to-noise ratio [22].

[8] Above a certain laser power, the specific fluorescence signal will not increase anymore because of saturation of the fluorophores. Instead, only the background signal will further increase. The optimum laser power yields an optimum ratio of specific signal over background. Especially for more photosensitive dyes such as fluorescein, bleaching of fluorophores at higher laser powers may impose a further constraint.

[9] A too large structure parameter is either an indication of a misaligned pinhole or incorrect adjustment of the correction ring for the thickness of the coverslip, or of the presence of several molecular species with similar diffusion autocorrelation times. A structure parameter between 4 and 8 should be obtained.

[10] In 384-well plates, a volume 50 µl is standard in our laboratory, although volumes as low 20 µl are also sufficient.

8. Add the cell lysates to BSA-coated wells of the 384-well plate and perform autocorrelation measurements of 5 x 10 s per sample.

6.3.3   Analysis of lysate FCS measurements using the ISS software package

1. Choose a 3D Gaussian model assuming a triplet term and one diffusive component and fix the structure parameter and the triplet term to the values determined for the fluorescein standard.

2. Determine the diffusion autocorrelation time of trypsin-degraded R9, using a 3D Gaussian model assuming one diffusing species. For samples containing different fractions of degraded peptide, which will be fitted with a two-component model, the diffusion autocorrelation time of the fast component will be fixed to this value (representing fully degraded R9). Remaining variables are allowed to vary.

3. Fit the intact R9 using a two-species model. Fix the fast component at the diffusion time of the fully degraded R9. Intact R9, in the presence of lysate, bears two components: (a) a slow component, reflecting peptide interacting with high-molecular weight molecules from the lysate, and (b) a fast component, reflecting peptide molecules that do not interact with molecules from the lysate. Therefore, fitting intact R9 with a two component fit where the fast component is fixed at the diffusion time of the degraded peptide will also result in a small percentage of fast component (13 % in the present experiment). The fraction intact R9 in the lysates from HeLa cells treated with lysosomal protease inhibitors can be calculated by a normalization of the fraction slow component, taking into account the fraction of fast component that is observed for the completely intact R9, according to the following formula:

fraction intact R9$_{sample\ in\ lysate}$ = fraction slow component $_{sample\ in\ lysate}$/(1- fraction fast component $_{intact\ R9\ in\ lysate}$)   (1)

4. Proceed with the fitting procedure for all other measurements using a 3D Gaussian model assuming two diffusing species and a fixed fast component, representing degraded R9 as well as intact R9 not interacting with lysate components. Calculate relative quantities of intact R9 according to formula 1.

6.3.4   Interpretation of result

Examples of raw autocorrelation curves from an experiment using lysosomal protease inhibitors can be found in Figure 6.2A,B. An overlay of representative curves from

different treatments illustrates that the autocorrelation curves are unaffected by a treatment with DMSO or pepstatin A, but a clear shift to the right, representing a slower diffusion, is observed for the lysate obtained from HeLa cells treated with E64d (Figure 6.2C). The shift to the right indicates the presence of more intact R9.The slower diffusion time is not just a reflection of the higher molecular weight, but indicates the association with other cellular components present in the lysate, which is not observed for degraded R9. This is illustrated by the differences in diffusion time between degraded and intact R9 in buffer and in the buffer lysate-mixture. In buffer, degraded R9 shows a diffusion time of about 30 μs, compared to about 47 μs for intact R9 (the actual values will differ between days and between set-ups). The differences are much larger in the lysate-buffer mix, where degraded R9 has an average diffusion time of 74 μs compared to 900 μs for intact R9. Relative quantities of intact R9 after the incubation in the presence or absence of lysosomal protease inhibitors were calculated. In cells incubated with E64d, 60 % of R9 had remained intact, whereas all other conditions led to a percentage of intact R9 lower than 20 % (Figure 6.2D). This result therefore demonstrates that in HeLa cells, R9 is mainly degraded by cysteine proteases and that this degradation can be inhibited by the cysteine protease inhibitor E64d. Besides information on the average diffusion time through the confocal volume, FCS measurements also provide information on the concentration, represented as the average background-corrected fluorescent molecule number in the confocal volume at any given time, which can be calculated as follows:

$$G_{tot}(0) = 1 + 1/N_{app} = 1 + (1-CPS_b/CPS_t)^2/N_{corr} \text{ [22]}$$

A comparison of the lysate peptide concentrations from the samples above showed that in the samples treated with E64d, the concentration, as reflected by the average molecule number N, was substantially lower (N= 0.29 vs. 1.17-1.38) than for the other three samples. Since we previously established that E64d does not affect uptake as witnessed by confocal microscopy in live cells (data not shown), we assume that this observation reflects an increased removal of debris-bound peptide during the centrifugation step included to obtain a homogeneous solution. This furthermore underscores the differences in intracellular association of R9 in cells treated with E64d compared to other treatments or no treatment.[11]

---

[11]This interpretation assumes equal initial cell numbers and an equal lysis efficiency. An additional control where absolute protein concentrations are determined could be included as further proof.
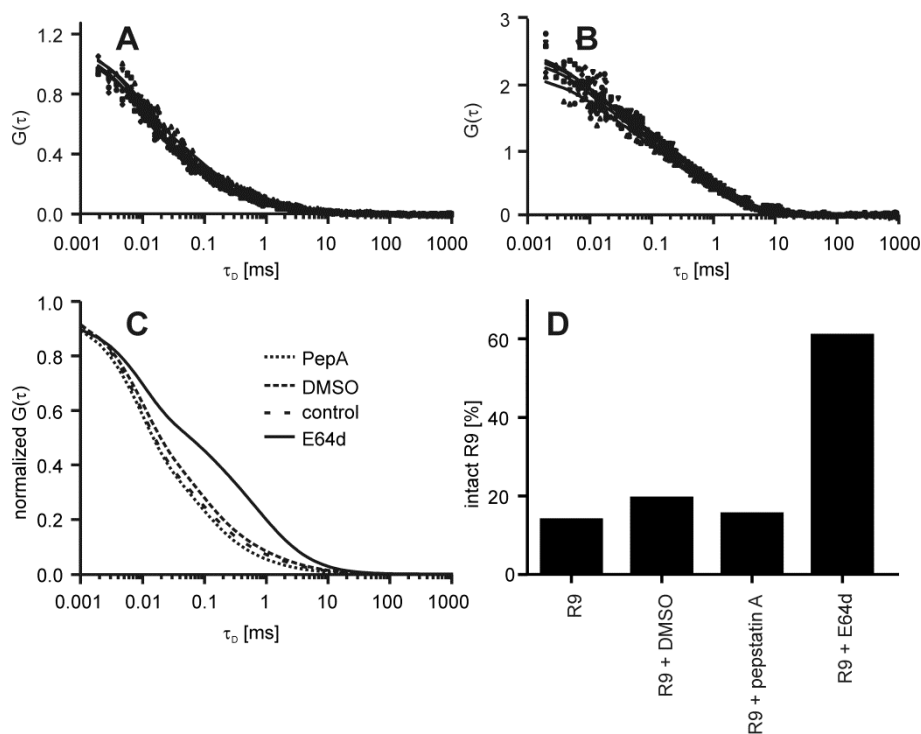
Figure 6.2. Fluorescence correlation spectroscopy for the analysis of the stability of R9 in HeLa cells treated with lysosomal protease inhibitors. (A,B) Autocorrelation functions of lysates from HeLa cells incubated with 5 µM R9 for 1 h at 37°C without inhibitor (A) or with 40 µM E64d (B). Lysates were prepared after the incubation in the presence of protease inhibitors. (C) Comparison of representative fits for autocorrelation curves obtained from HeLa cell lysates obtained as described above. Included are the control treated with peptide only, cells treated with DMSO as a vehicle control, 10 µM pepstatin A and 40 µM E64d. All lines indicate fits that were obtained using a 3D Gaussian model assuming a triplet state and the presence of a slow-diffusing and a fast-diffusing molecular species. (D) Quantification of intact R9 in HeLa cells treated with lysosomal protease inhibitors. Relative quantities of intact R9 were determined using a two-species 3D Gaussian triplet model with intact and degraded R9 as references.

6.3.5 Preparation of live cells treated with nona-arginine composed of D- and L-amino acids

1. Spin down 300,000 Jurkat E6.1 leukemia cells and resuspend in 200 µl RPMI + 10 % fetal calf serum containing 500 nM R9 or r9.

2. Incubate for 30 min at 37°C. Wash with RPMI supplemented with 10 % fetal calf serum, spin down for 5 min and resuspend in fresh medium. Seed cells in 8-well microscopy chamber (Nunc, Wiesbaden, Germany) and allow them to settle.

6.3.6   Intracellular FCS measurements in living Jurkat cells

1. Determine and fix the structure parameter and the triplet time using fluorescein as described above.

2. 1 h after the wash step, single cells are identified by confocal microscopy[12] and the confocal detection volume is positioned in the nucleus.

3. Autocorrelation measurements are acquired in each cell for 5 x 10 s using the ISS vista software. Repeat the procedure in at least 3 or 4 cells and in the background of the same incubation chamber.

6.3.7   Analysis of intracellular FCS measurements using Globals for spectroscopy software

1. Define a 3D Gaussian diffusion model assuming a triplet term and two diffusive components with offset.

2. Determine the triplet time (τ_T), the lateral radius of the detection volume (ω_{xy}) and the structure parameter (ratio of ω_z / ω_{xy}) by fitting the autocorrelation function acquired for the fluorescein standard. Fix these values in the fit for the peptide samples. Allow other variables to vary.

3. Perform global curve fitting. Results for living Jurkat cells are shown in Figure 6.3.

6.3.8   Interpretation of result

Unlike measurements in cell lysates, intracellular FCS measurements do not give consecutive measurements (10 s each) that can be easily combined, because the calculated autocorrelation functions can differ quite substantially (Figure 6.3). In contrast, curves should be inspected individually. Cells were incubated with 500 nM peptide. This concentration is considerably lower than concentrations typically used for following the uptake of peptides by confocal imaging. As a consequence, no fluorescence could be seen inside the cells. The positioning of the confocal detection volume was therefore based on transmission images (Figure 6.3A,D).

   In all cases, measurements showed a rapid bleaching at the beginning of the acquisition of autocorrelation functions, indicating the presence of a substantial amount of immobile peptides in the cell. Because no diffusion occurs for this population of peptides, no reliable estimates of the quantity can be made. In addition, we observed that during some 10-s

---

[12] Make sure to identify the cells with a low laser power in order to minimize photobleaching.

measurement intervals of Jurkat cells treated with R9, species with a high mobility were dominant (Figure 6.3E, left curve), reminiscent of free fluorescein. The average molecule number N corresponded to a concentration of free fluorophores of less than 50 nM. During other measurement intervals, a slower diffusive component was more dominant, reflecting intact R9 interacting with cellular components (Figure 6.3E, right curve). The slower diffusing component was also observed for r9 (Figure 6.3C), in addition to measurement intervals where no signal above the background was present (Figure 6.3B). In contrast, no rapidly diffusing molecular species was observed in cells treated with r9, confirming the assumption that the rapidly diffusing species indicates the presence of breakdown products of R9. Moreover, bleaching was more dominant for r9, furthermore indicating a larger immobile fraction of r9.
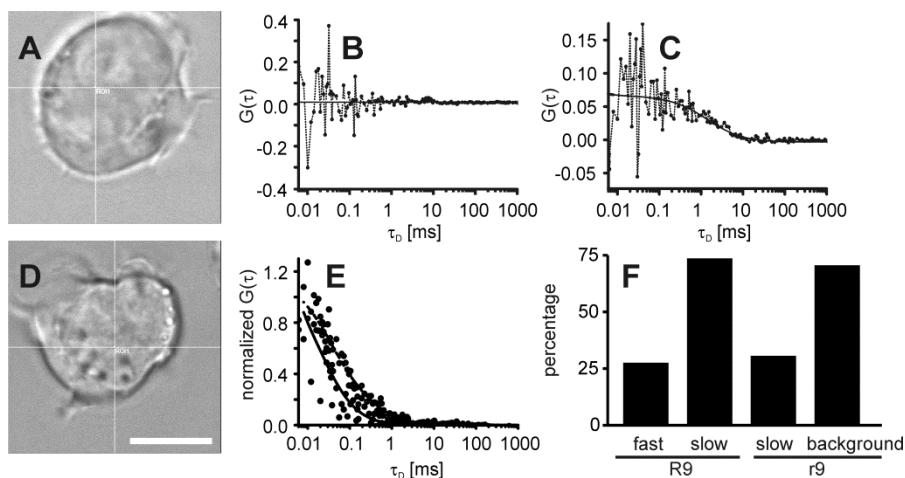
Figure 6.3. Intracellular FCS of R9 and r9 in Jurkat cells. Jurkat cells were treated with 500 nM R9 or r9 for 30 min, spun down and washed, and seeded in 8-well microscopy chambers. After 1 h, the detection volume for FCS measurements was placed into the nuclei of living cells identified by transmission microscopy, as indicated in panel A (for r9) and D (for R9). The cross-hair cursor indicates the position of the detection volume in the optical plane. The scale bar indicates 5 μm. Representative measurements for r9 (B and C) and R9 (E) are indicated. In panel F, the relative frequencies of autocorrelation functions with a dominating fast or slow component (R9) or slow component and background signal (r9) are indicated. The result in F reflects the average ratio of measurements from 3 (R9) and 4 (r9) different cells. The left autocorrelation function in E shows an example in which the fast component was dominant, whereas the dominance of the slow component can be seen in C and the right curve in E. B shows an uncorrelated background signal from the nucleus of r9-treated cells.

6.4 References

[1] F. Duchardt, M. Fotin-Mleczek, H. Schwarz, R. Fischer, R. Brock, A comprehensive model for the cellular uptake of cationic cell-penetrating peptides, Traffic., 8 (2007) 848-866.

[2] M. Fotin-Mleczek, S. Welte, O. Mader, F. Duchardt, R. Fischer, H. Hufnagel, P. Scheurich, R. Brock, Cationic cell-penetrating peptides interfere with TNF signalling by induction of TNF receptor internalization, J Cell Sci, 118 (2005) 3339-3351.

[3] S.T. Henriques, M.N. Melo, M.A. Castanho, How to address CPP and AMP translocation? Methods to detect and quantify peptide internalization in vitro and in vivo (Review), Mol Membr Biol, 24 (2007) 173-184.

[4] M.E. Herbig, K.M. Weller, H.P. Merkle, Reviewing biophysical and cell biological methodologies in cell-penetrating peptide (CPP) research, Crit Rev Ther Drug Carrier Syst, 24 (2007) 203-255.

[5] E. Vives, J.P. Richard, C. Rispal, B. Lebleu, TAT peptide internalization: seeking the mechanism of entry, Curr Protein Pept Sci, 4 (2003) 125-132.

[6] A. Elmquist, U. Langel, In vitro uptake and stability study of pVEC and its all-D analog, Biol Chem, 384 (2003) 387-393.

[7] R. Fischer, D. Bachle, M. Fotin-Mleczek, G. Jung, H. Kalbacher, R. Brock, A targeted protease substrate for a quantitative determination of protease activities in the endolysosomal pathway, Chembiochem., 7 (2006) 1428-1434.

[8] C. Palm, M. Jayamanne, M. Kjellander, M. Hallbrink, Peptide degradation is a critical determinant for cell-penetrating peptide uptake, Biochim Biophys Acta, 1768 (2007) 1769-1776.

[9] R. Trehin, H.M. Nielsen, H.G. Jahnke, U. Krauss, A.G. Beck-Sickinger, H.P. Merkle, Metabolic cleavage of cell-penetrating peptides in contact with epithelial models: human calcitonin (hCT)-derived peptides, Tat(47-57) and penetratin(43-58), Biochem J, 382 (2004) 945-956.

[10] C.S. Pillay, E. Elliott, C. Dennison, Endolysosomal proteolysis and its regulation, Biochem J, 363 (2002) 417-429.

[11] H. Raagel, P. Saalik, M. Hansen, U. Langel, M. Pooga, CPP-protein constructs induce a population of non-acidic vesicles during trafficking through endo-lysosomal pathway, J Control Release, 139 (2009) 108-117.

[12] G. Tunnemann, R.M. Martin, S. Haupt, C. Patsch, F. Edenhofer, M.C. Cardoso, Cargo-dependent mode of uptake and bioavailability of TAT-containing proteins and peptides in living cells, FASEB J, 20 (2006) 1775-1784.

[13] F. Burlina, S. Sagan, G. Bolbach, G. Chassaing, Quantification of the cellular uptake of cell-penetrating peptides by MALDI-TOF mass spectrometry, Angew Chem Int Ed Engl, 44 (2005) 4244-4247.

[14] F. Burlina, S. Sagan, G. Bolbach, G. Chassaing, A direct approach to quantification of the cellular uptake of cell-penetrating peptides using MALDI-TOF mass spectrometry, Nat Protoc, 1 (2006) 200-205.

[15] S. El Andaloussi, P. Guterstam, U. Langel, Assessing the delivery efficacy and internalization route of cell-penetrating peptides, Nat Protoc, 2 (2007) 2043-2047.

[16] S.H. Kang, M.J. Cho, R. Kole, Up-regulation of luciferase gene expression with antisense oligonucleotides: implications and applications in functional assay development, Biochemistry, 37 (1998) 6235-6239.

[17] R. Rigler, U. Mets, J. Widengren, P. Kask, Fluorescence Correlation Spectroscopy with High Count Rate and Low-Background - Analysis of Translational Diffusion, European Biophysics Journal with Biophysics Letters, 22 (1993) 169-175.

[18] K. Bacia, P. Schwille, Fluorescence correlation spectroscopy, Methods Mol Biol, 398 (2007) 73-84.

[19] T. Waizenegger, R. Fischer, R. Brock, Intracellular concentration measurements in adherent cells: a comparison of import efficiencies of cell-permeable peptides, Biol.Chem., 383 (2002) 291-299.

[20] D.H. Rich, M.S. Bernatowicz, N.S. Agarwal, M. Kawai, F.G. Salituro, P.G. Schmidt, Inhibition of aspartic proteases by pepstatin and 3-methylstatine derivatives of pepstatin. Evidence for collected-substrate enzyme inhibition, Biochemistry, 24 (1985) 3165-3173.

[21] M. Tamai, K. Matsumoto, S. Omura, I. Koyama, Y. Ozawa, K. Hanada, In vitro and in vivo inhibition of cysteine proteinases by EST, a new analog of E-64, J Pharmacobiodyn, 9 (1986) 672-677.

[22] D.E. Koppel, Statistical Accuracy in Fluorescence Correlation Spectroscopy, Physical Review A, 10 (1974) 1938-1945.

Cellular integration of an enzyme-loaded polymersome nanoreactor

Wouter P.R. Verdurmen[+], Stijn F.M. van Dongen[+],
Ruud J.R.W. Peters, Roeland J.M. Nolte,
Roland Brock and Jan C.M. van Hest

7 Cellular integration of an enzyme-loaded polymersome nanoreactor

Wouter P.R. Verdurmen[+a], Stijn F.M. van Dongen[+b], Ruud J.R.W. Peters[b], Roeland J.M. Nolte[b], Roland Brock[a], Jan C.M. van Hest[b]

[+] These authors contributed equally to this work
[a]Department of Biochemistry, Nijmegen Centre for Molecular Life Sciences, Radboud University Nijmegen Medical Centre, The Netherlands
[b]Institute for Molecules and Materials, Department of Organic Chemistry, Radboud University Nijmegen, The Netherlands

7.1 Introduction

Protein therapy aims to use *in vitro* produced proteins to intracellularly replace or complement faulty ones [1, 2], making it a promising strategy to fight protein deficiency diseases [3, 4]. Unfortunately, the hurdles a protein must take to reach its therapeutic effect have hampered clinical applications. Many proteins suffer from poor *in vivo* stability, and cellular uptake and directed intracellular trafficking are hard to achieve [5]. Due to these issues, the success of protein therapy is limited to a small set of lysosomal diseases [3, 4], for which delivery efficiency is still low, costs are high, and long-term efficiency has not yet been established.

A way to overcome some of these limitations is to couple therapeutic proteins to cell penetrating peptides (CPPs) which promote the cellular uptake of their linked cargoes [6, 7]. It has become clear, however, that most CPP-mediated uptake of proteins occurs via endocytosis. Poor release from the endosome and proteolytic breakdown have been identified as major factors limiting the biological activity of delivered molecules [3, 4]. Protection may be achieved by encapsulation of unmodified proteins inside delivery vehicles such as liposomes that display CPPs [8, 9]. Once inside the cell, the enzyme is released. However, inside the cytoplasm, the lifetime of an enzyme may be limited by denaturation or degradation.

Cells often use compartmentalization to organize, isolate, or protect enzymes, which provides optimal conditions for specific cellular reactions. In compartments, e.g.

organelles, reactants are exchanged by diffusion, channels, or transporter molecules. Therefore, it stands to reason that the introduction of new protein functionality to a cell may be best achieved by delivering the biomacromolecule encapsulated in a porous shell [10], mimicking an organelle. To be suited for protein therapy, this artificial compartment should be stable in the bloodstream and capable of cellular uptake. Furthermore, it should offer protection against proteases but be permeable to the substrates and products of its cargo.

Here, we describe the preparation and cellular uptake of enzyme-loaded polymersome capsules, and we report on the intracellular routing and activity of these nano-objects in mammalian cells. Cellular internalization of the capsules is mediated by the CPP tat linked to their surfaces [11].

7.2   Results and discussion

Polymersomes are self-assembled vesicles made from block copolymers and may be regarded as stable alternatives to liposomes [2, 12]. They have dimensions in the nanometer range, a size considered to be suitable for *in vivo* applications [13]. Their properties can be engineered by changing their constituent polymers. As illustrated in , we present here a polymersome with a semi-porous membrane based on polystyrene$_{40}$-*block*-poly[L-isocyanoalanine(2-thiophen-3-yl-ethyl)amide]$_{50}$ (PS-PIAT, **1**) [14]. Enzyme-filled PS-PIAT polymersomes have been reported as efficient nanoreactors [15-17], capable of protecting their contents from proteolytic degradation [18]. To promote the cellular uptake of such a nanoreactor, an azide-containing version of tat was covalently linked to a polystyrene-*block*-poly(ethylene glycol)-oxanorbornadiene (PS-PEG-crDA, **2**) using a Cu-free tandem cycloaddition-retro-Diels-Alder (crDA) 'click' reaction [19]. Coassembly of 10 wt.-% PS-PEG-tat (**3**) with PS-PIAT thus constructed a tat-presenting nano-capsule, hereinafter referred to as a tat-polymersome (Figure 7.1).
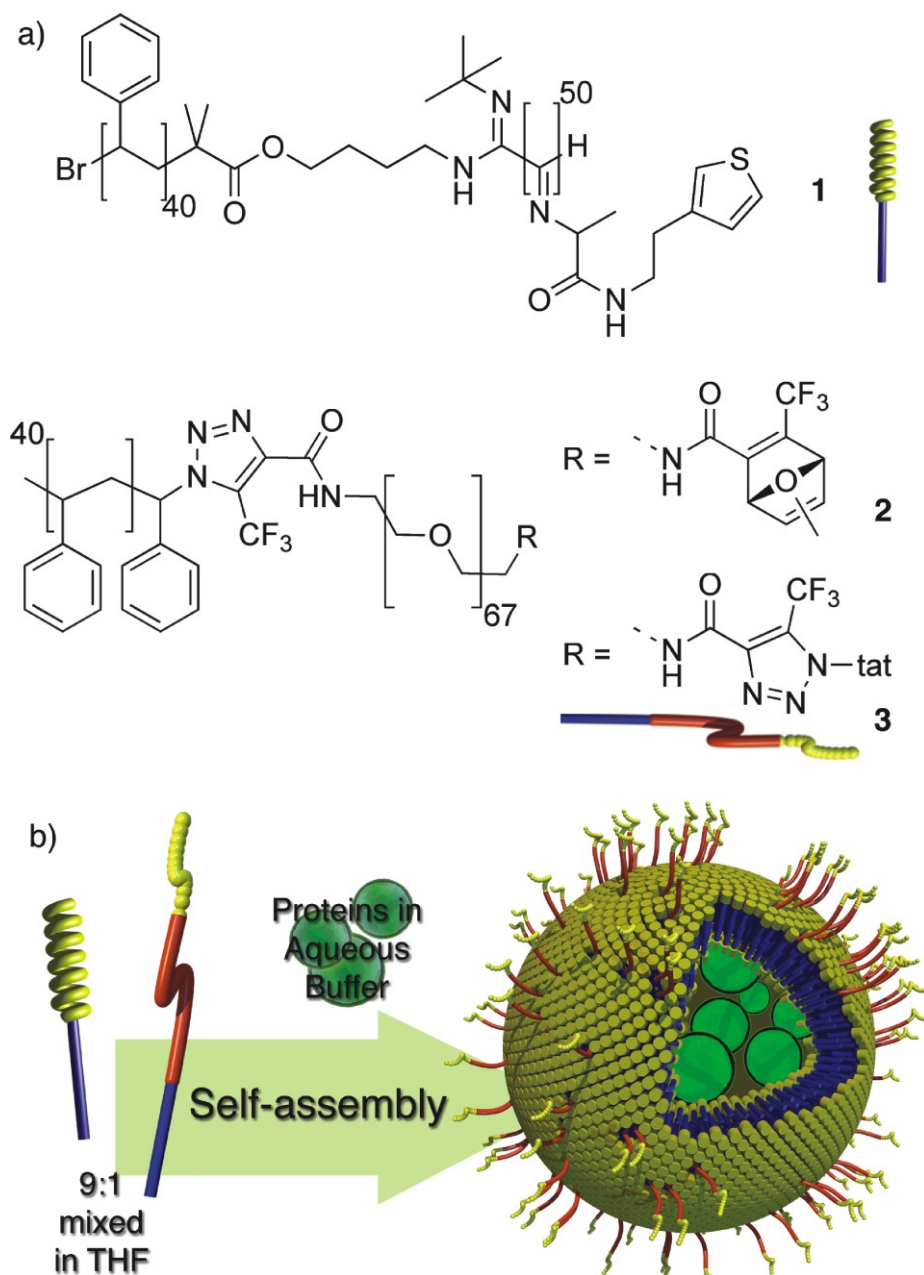
Figure 7.1. a) Structures and cartoon representations of the used polymers; b) In our strategy, 10 wt.-% of **3** was mixed with **1** to produce porous tat-functionalized polymersomes loaded with protein.

Figure 7.2 shows transmission electron microscopy (TEM) images of polymersomes prepared in hepes-buffered saline (HBS) containing either green fluorescent protein (GFP, a) or horseradish peroxidase (HRP, 1b, c). Neither the handling, the aggregation behavior, nor the spherical morphology of the polymersomes was influenced by the admixture of **3**, which is in line with previous results for PS-PEG-enzyme conjugates [20]. The tat-polymersomes had an average diameter of 114 +/- 28 nm, with no obvious size variation between the polymersomes with different protein contents. This demonstrates that the tat-polymersomes provide a modular platform for protein and enzyme encapsulation.
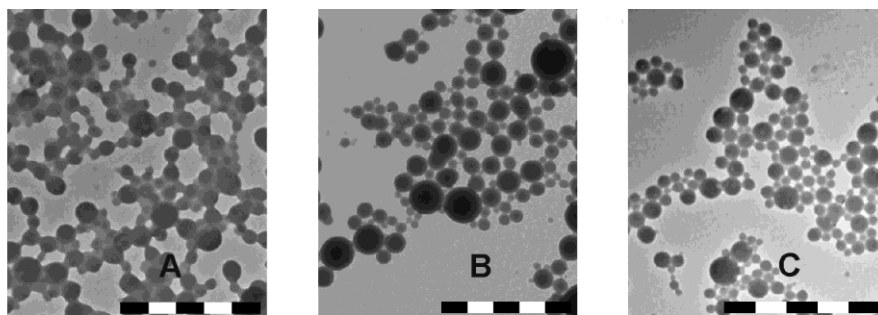
Figure 7.2. Transmission electron micrographs of PS–PIAT polymersomes prepared in HBS. a) GFP-loaded, with 10 wt.-% 3; b) HRP-loaded; c) HRP-loaded, with 10 wt.-% 3. Scale bars: 1 μm.

To investigate whether tat would induce efficient cellular uptake, unmodified polymersomes and tat-polymersomes, both loaded with GFP, were incubated with a variety of cell lines (HeLa, Jurkat and HEK 293). To this point, directed cellular uptake of polymersomes was restricted to cells with high phagocytic activity, i. e. the intrinsic ability to engulf large particles [21-23]. As shown in Figure 7.3, tat-polymersomes were taken up by all three cell types. No internalization of unmodified polymersomes was detected. Residual fluorescence could be attributed to extracellular polymersomes that had not been washed away. Having established their efficient internalization, we set out to investigate the route of uptake.
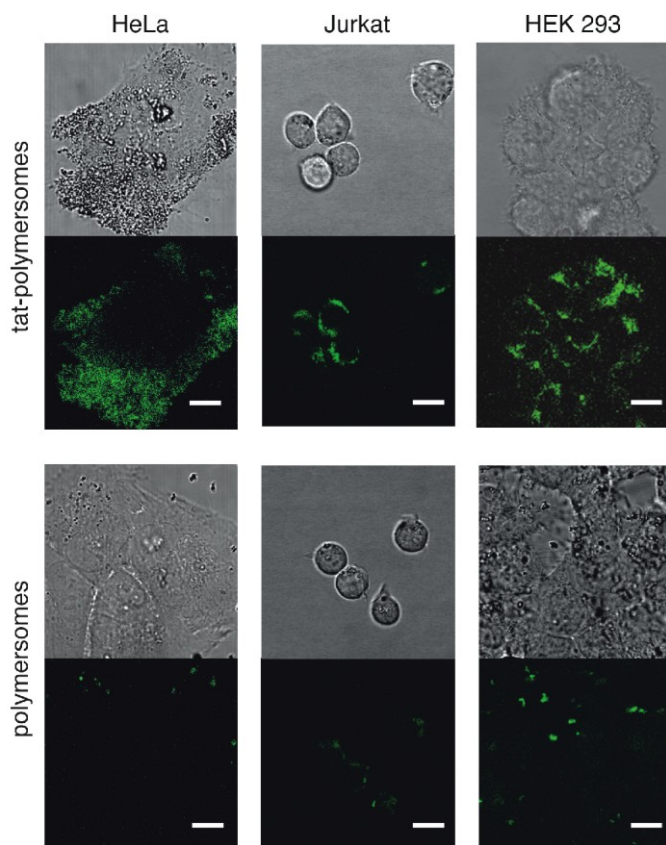
Figure 7.3. Confocal micrographs of different cell types incubated with GFP-loaded polymersomes with or without tat. Scale bars: 10 μm

Arginine-rich peptides like tat are a class of CPPs for which endocytosis is known to be important, and macropinocytosis is the endocytic pathway that has been most regularly associated with their cellular uptake [24, 25]. Also, given the average size of the present polymersomes (114 nm), macropinocytosis can be expected to be the most prominent mechanism for their uptake, as size-restrictions are typically ascribed to other pathways [26].

To address the involvement of macropinocytosis in uptake, HeLa cells were incubated with GFP-loaded polymersomes and fluorescently labeled dextran, a polysaccharide that is a marker for macropinocytosis. Incubation was limited to 25 minutes to prevent endosomal mixing and ensure that colocalization did indeed result from endocytosis along a shared uptake route. Cells co-incubated with both GFP-loaded tat-polymersomes and Texas Red-labeled dextran (70 kDa) showed a prominent Texas Red fluorescence. The GFP signal that

was detected was low, but colocalized with the dextran signal (Figure 7.4). Next to the colocalization, uptake through a common route was supported by two further observations. First, with tat-free polymersomes, Texas Red fluorescence was greatly reduced, indicating that tat-polymersomes induced the uptake of dextran (Figure 7.4c). Second, dextran inhibited the uptake of polymersomes, as can be concluded by comparison of GFP fluorescence in Figure 7.4a,b.
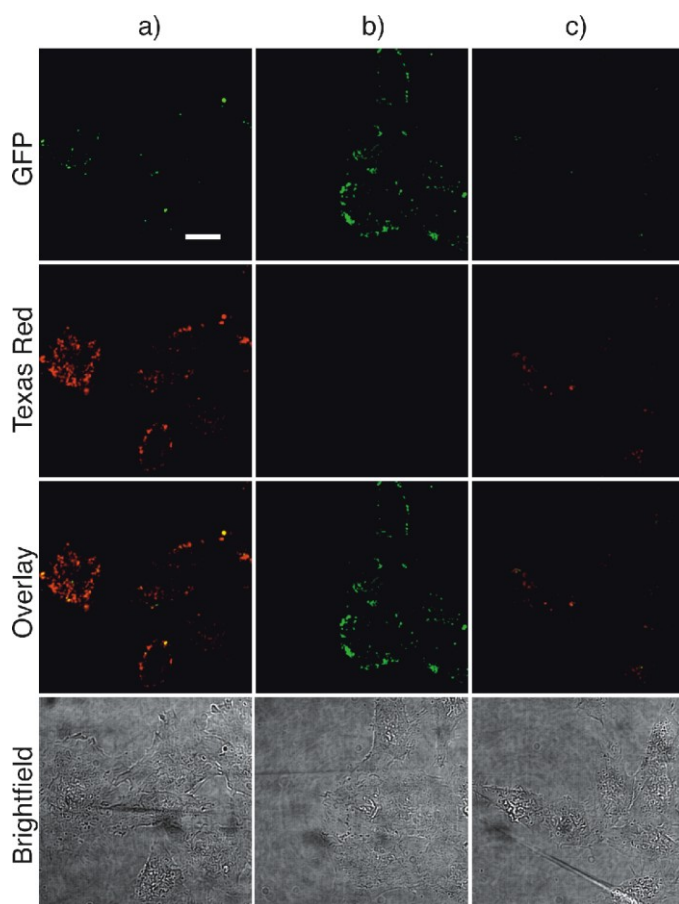
Figure 7.4. Confocal micrographs of HeLa cells incubated. a) GFP-loaded tat-polymersomes and Texas Red-labeled dextran (70kDa); b) GFP-loaded tat-polymersomes; c) GFP-loaded polymersomes and Texas Red-labeled dextran (70kDa). Scale bar: 20 μm.

Next, we investigated the fate of tat-polymersomes after their uptake into cells. A frequently observed trafficking route for cell-penetrating peptides leads to late endosomes and lysosomes [27]. These compartments have an acidic pH and can be labeled by

Lysotracker Red. After incubation of HeLa cells with tat-polymersomes for four hours, a considerable fraction of the GFP signal colocalized with acidic vesicles (Figure 7.5). An almost equally large population of GFP-containing punctuate structures retained a neutral pH, indicated by the lack of Lysotracker staining. It is unclear whether this indicates that polymersomes were retained in non-acidic vesicles, as reported for tat-cargo constructs [28], or whether the absence of colocalization indicates cytosolic delivery. Both options would be advantageous for the use of polymersomes in protein therapy, as they avoid acidification.
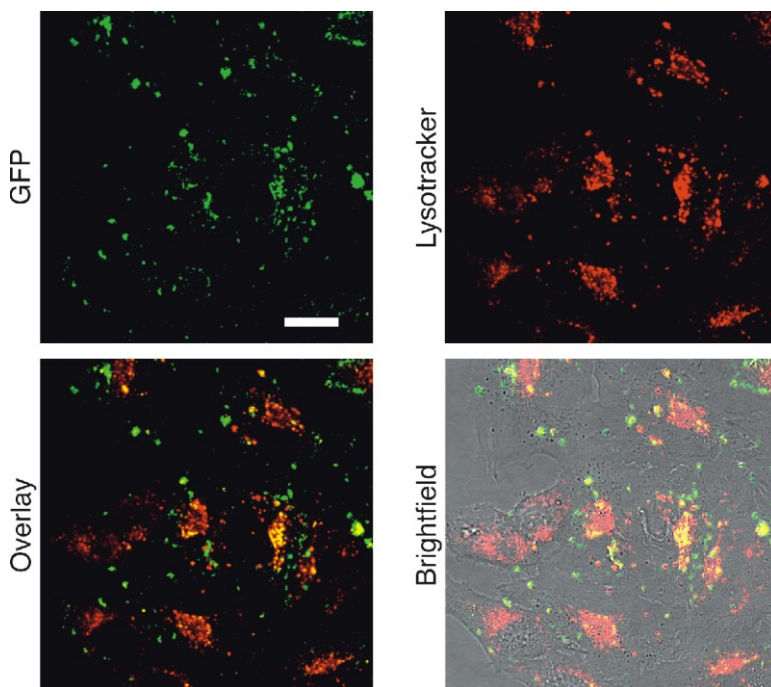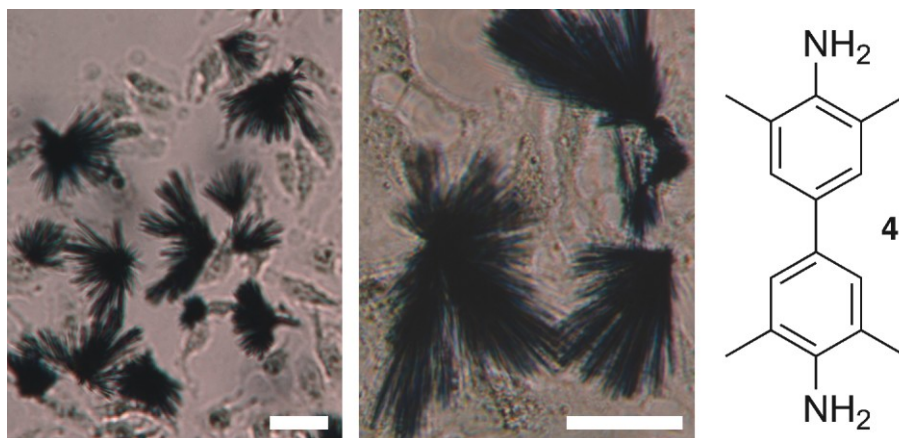

Figure 7.5. Confocal micrographs of HeLa cells incubated with GFP-loaded tat-polymersomes and Lysotracker Red. Scale bar: 20 μm.

The efficient uptake of tat-polymersomes through pinocytosis and their merely partial colocalization with acidic vesicles are promising starting points for the introduction of enzyme-loaded nanoreactors into cells. We previously reported a variety of nanoreactors containing different enzymes, one of which was horseradish peroxidase (HRP) [18, 29]. A substrate that is neutral under physiological conditions both prior to and after oxidation by HRP is 3,3',5,5'-tetramethylbenzidine (TMB, **4**) [30]. It can diffuse through most lipid-

based membranes, making TMB in the culture medium intracellularly available. The oxidation product of TMB is easily detected by measuring its absorbance ($\lambda = 370$ nm).

To assess the ability of polymersome nanoreactors to function inside cells, we incubated HeLa cells with HRP-loaded tat-polymersomes for four hours to allow their internalization. The cells were then washed and incubated with TMB (120 μg/ml) and H_2O_2 (250 μM). Visual inspection of the samples revealed the intracellular activity of HRP by the appearance of a blue color. Microscopy showed that the stain emanated from the cells, leading to the formation of precipitates (Figure 7.6). The rate at which TMB was converted was linearly dependent on the administered dosage of polymersomes (Figure 7.9).


Figure 7.6. Representative transmission micrographs of HeLa cells containing HRP-loaded tat-polymersomes after 30 min. of TMB conversion. The scale bars approximate 30 μm; 4 is TMB.

This demonstrated that the assay provided the possibility to quantitatively assess cellular HRP activity. Therefore, we next investigated how long intracellular activity of HRP-loaded tat-polymersomes persisted over time. Four hours after internalization, 75% of the original activity was still present. After 16 hours, 42% of the original activity was preserved (Figure 7.7a). These results show that the polymersome-based approach maintained activity to a much higher degree than what was reported for free HRP trafficked to lysosomes, which achieved a lysosomal half-life of ~1 hour [31]. The half-life of HRP encapsulated in PS-PIAT polymersomes in buffer is 15 days [18]. To identify why the HRP activity decreased over time, we tested the effects of chloroquine and nordihydroguaiaretic acid (NDGA) on our system. Both compounds can induce the release of endosomal contents into the cytoplasm [27, 32]. If the observed decrease was due to degradation of the

enzyme molecules in an acidic environment or endosomal recycling and cellular release, then these compounds should increase HRP activity. However, none of them exhibited a pronounced effect (Figure 7.7b). The reason for the decrease in HRP activity is therefore unknown at present.

In summary, we have designed a polymersome nanoreactor that is capable of entering cells, where it can induce intracellular catalysis. To this point, the cellular delivery of polymersomes was restricted to cells with an intrinsically high phagocytic activity. The catalytic activity conferred to the cells was maintained at levels that were significantly higher than those reported for soluble enzymes. The results therefore represent a significant step towards a functional artificial organelle.
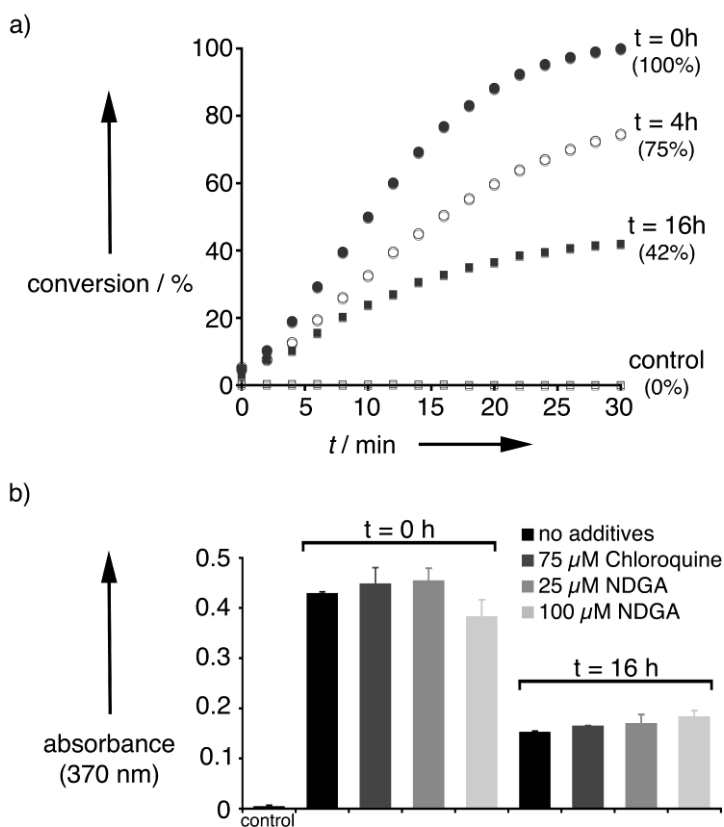
Figure 7.7. Activity of intracellular HRP-loaded tat-polymersomes over time ("control" denotes HRP-loaded polymersomes without **3**). a) TMB conversion at various points of time after cell uptake; b) The effect of chloroquine and NDGA; cells were pulsed with chloroquine or NDGA during the final hour of incubation.

7.3   Materials and methods

7.3.1   Synthetic procedures

Polystyrene40-block-poly[L-isocyanoalanine(2-thiophen-3-yl-ethyl)amide]50 (PS-PIAT, **1**) was a gift of Hans-Peter M. de Hoog and prepared as previously described [33]. Azido-tat was a kind donation by Morten Borre Hansen and synthesized using standard solid phase peptide synthesis protocols (sequence: N3-YGRKKRRQRRRGC(acm)-NH2). The azide moiety was introduced through diazo transfer to the N-terminus while the peptide was still on the resin. Other chemicals, methods and instrumentation were previously reported [17]. GFP was expressed as previously reported [34].

7.3.2   *3-Trifluoromethyl-7-oxa-bicyclo[2.2.1]hepta-2,5-diene-2-carboxylic acid ethyl ester (S1)*

Ethyl 2-fluorobut-2-ynoate (0.9101 gr, 5.47 mmol) was added to a Schlenk tube and fitted with a stopper, evacuated and backfilled with N2. 3-Methylfuran (1.2 equiv., 514 µL, 6.57 mmol) was added to the reaction vessel, which was then heated to 40°C and left to stir for 4 days. The resulting mixture was purified by column chromatography (ether/pentane, 1:4 v/v, Rf-values: 0.56 (S1), 0.14 (methylfuran)). After evaporation of the solvent and drying in vacuo, **S1** was obtained as a yellow oil, all of which was used to subsequently prepare S2. 1H NMR (400 MHz, CDCl3): δ = 1.32 (m, 3H), 2.00 (d, 3H), 4.29 (m, 2H), 5.31 (d, 1H), 5.57 (d, 1H), 6.58 (d, 1H); HRMS (EI+) *m/z* calcd for C10H10F3O3 [M+H]+ 234.0506, found 234.050.

7.3.3   *3-Trifluoromethyl-7-oxa-bicyclo[2.2.]hepta-2,5-diene-2-carboxylic acid (S2)*

All product resulting from the synthesis of **S1** was dissolved in THF (30 mL) and kept at 0°C. Aqueous NaOH (13 mL, 1 M) was dripped to the solution over a period of 30 min, after which the reaction mixture was allowed to warm to room temperature and stirred for another 2 hrs. It was then washed with EtOAc (3X) and dried (MgSO4). The resulting mixture was co-evaporated with CH2Cl2 twice and dried in vacuo, yielding **S2** as an off-white wax (0.4575 g, 38% over two steps) 1H NMR (400 MHz, CDCl3): δ = 2.00 (d, 3H), 5.34 (d, 1H), 5.59 (d, 1H), 6.59 (d, 1H); HRMS (EI+) *m/z* calcd for C8H6F3O3 [M+H]+ 206.0191, found 206.019.

7.3.4   α-ω-Poly(ethylene glycol)65-diazide (S3)

Dihydroxy-PEG65 (10.2 g, 3.4 mmol) was dissolved in CH2Cl2 (30 mL) and Et3N (10 equiv., 4.74 mL, 34 mmol) was added under stirring. After one min., mesonyl chloride (MeSO2Cl, 10 eq, 2.62 mL, 34 mmol) was dripped to the solution and it was left to stir for 16 hrs. The reaction was quenched by addition of CH2Cl2 (40 mL), after which it was washed with brine (6X) and evaporated to dryness. The product was dissolved in DMF (60 mL) and sodium azide (NaN3, 6 equiv., 1.35 g, 20.4 mmol) was added. This mixture was left to stir for 16 hrs at room temperature, concentrated in vacuo, dissolved in CH2Cl2 and washed with brine (3X). Afterwards, the product was isolated by precipitation in hexane and dried in vacuo to obtain **S3** as a white powder (5.0 g, 49%) GPC: Mn: 2.9 kg mol-1, Mw: 3.0 kg mol-1, Mw/Mn: 1.04; 1H NMR (400 MHz, CDCl3): δ = 3.31 (t, 4H), 3.4-3.9 (b, ~260H); FTIR-ATR: 3550, 2859, 2098 (v N3), 1636 cm-1.

7.3.5   α-ω-Poly(ethylene glycol)65-diamine (S4)

S3 (5.372 g, 1.79 mmol) was dissolved in THF (40 mL), to which PPh3 (10 equiv., 4.70 g, 17.9 mmol) was added. After 16 hrs, the reaction was quenched with ultrapure water and the solvent was evaporated in vacuo. The residue was suspended in ultrapure water and filtered through a hyfloplug. After repeated suspension and filtration, lyophilisation yielded **S4** (2.808 g (52.3%) with 2% PPh3O) as a white powder. 1H NMR (400 MHz, CDCl3): δ = 2.86 (t, 4H), 3.50 (t, 4H) 3.4-3.9 (b, ~256H); FTIR-ATR: 3550, 2859, 2127, 1636, 1470, 1440 cm-1.

7.3.6   α-ω-Poly(ethylene glycol)65-dioxanorbornadiene (S5)

S4 (0.68 g, 0.23 mmol) and **S2** (1.1 equiv., 0.11 g, 0.5 mmol) were dissolved in CH2Cl2 (5 mL). DMAP (2.2 equiv., 0.125 g, 1 mmol) was added, and the mixture was cooled to 0°C. EDC (1.1 equiv., 0.1 g, 0.5 mmol) was added to the solution, which was left to stir for 1h. It was then allowed to return to room temperature and stirred for an additional 16 hrs. The mixture was washed with aqueous HCl (1M, 2X) and with brine (2X). The combined HCl layers were washed with CH2Cl2, after which the combined organic layers were concentrated in vacuo. The residue was dissolved in CH2Cl2 and washed with an aqueous NaHCO3 solution (5%, 1X) to remove traces of acid. The product was then lyophilized from ultrapure water to obtain **S5** as a white solid (0.504 g, 65%). 1H NMR (400 MHz,

CDCl3): δ = 1.98 and 2.16 (s, 3H), 2.88 and 2.95 (d, 2H), 3.4-3.9 (b, ~256H), 5.35 (d, 1H), 5.52 (d, 1H).

7.3.7 α-Bromo-ω-methyl-polystyrene38 (S6)

CuBr (141.7 mg, 1 mmol) was added to a Schlenk tube, which was evacuated and backfilled with argon three times. A solution of distilled styrene (80 equiv., 8994 μl, 80 mmol), anisole (4 equiv., 426.6 μl, 4 mmol), PMDETA (1 equiv., 205.1 μl,1 mmol) and α-methylbenzyl bromide (initiator, 1 equiv., 135.4 μl,1 mmol) was added to the Schlenk tube and stirred. The mixture was allowed to react at 90°C until the conversion was 50% (monitored by NMR and GPC analysis). The reaction was quenched by rapid cooling and the product was precipitated in methanol. The resulting solid was dissolved in toluene and precipitated in methanol twice and subsequently dried in vacuo. **S6** was obtained as a white powder (4.262 g, 97%). 1H NMR (400 MHz, CDCl3): δ = 1.04 (b, 3H), 1.2-2.3 (b, ~114H), 4.45 (b, 1H), 6.3-7.3 (b, ~190H); FTIR-ATR: 3026, 2919, 2845, 2358, 2243, 1942, 1872, 1802, 1600 cm-1; GPC: Mn: 3510, Mw: 3803, PDI: 1.05.

7.3.8 α-Azido-ω-methyl-PS38 (S7)

S6 (2.118 g, 0.54 mmol) was dissolved in DMF (40 mL) and heated to 80°C. NaN3 (10 equiv., 375.1 mg, 5.4 mmol) was added to the solution, which was left to react overnight. The solvent was evaporated and the residue was redissolved in CH2Cl2 and filtered using a paper filter. The volume of the mixture was reduced in vacuo and the product was precipitated in methanol. The resulting N3- PS39-Me (**7**) was obtained as a white powder (1.93 g, 91%). 1H NMR (400 MHz, CDCl3): δ = 1.04 (b, 3H), 1.2-2.3 (b, ~114H), 3.95 (b, 1H), 6.3-7.3 (b, ~190H); FTIR-ATR: 3028, 2915, 2363, 2103 (ν N3), 1714, 1597, 1489, 1464, 1066, 1018, 754, 698 cm-1; GPC: Mn: 3934, Mw: 4278, PDI: 1.08.

7.3.9 Me-polystyrene50-block-poly(ethylene glycol)65-oxanorbornadiene (2)

PS **S7** (268 mg, 0.0536 mmol) and PEG **S5** (1.6 equiv., 293 mg, 0.085 mmol) were dissolved in distilled THF (10 mL) and stirred for 10 days at 40ºC. After evaporation of the solvent the crude reaction mixture was separated by silica column chromatography (eluents CH2Cl2 and MeOH, from 1:0 to 4:1 v/v). Repeated precipitation in ultrapure water yielded **2** as a white powder (22.6 mg, 5.1%). 1H NMR (400 MHz, CDCl3): δ = 1.2-2.3 (b,

~114H), 3.4-3.9 (b, ~256H), 5.12 and 5.34 (s, 2H, oxanorbornadiene bridging protons), 6.3-7.3 (b, ~190H); GPC: Mn: 5203, Mw: 5720, PDI: 1.09.

7.3.10   Me-polystyrene50-block-poly(ethylene glycol)65-block-tat (3)

Azido-tat (1.12 equiv., 4.95 mg, 3.18 μmol) and **2** (22.6 mg, 2.83 μmol) were dissolved in DMF (2 mL) and stirred for 30 days at 40ºC. The crude reaction mixture was concentrated in vacuo and purified by size exclusion chromatography (Biobeads column in DMF). After concentration in vacuo and lyophilisation from dioxane, **3** was obtained as a white solid (18.8 mg, 69.5%). 1H NMR (400 MHz, CDCl3): δ = 1.2-2.3 (b, ~114H), 3.4-3.9 (b, ~256H), 6.3-7.3 (b, ~190H) (numerous small peaks for tat are visible. The bridging protons of oxanorbornadiene from **2** had disappeared, indicating full conversion); GPC: Mn: 6807, Mw: 7174, PDI: 1.04. Staining on TLC plates with chlorine-TDM was positive for amines.

7.3.11   tBuO-polystyrene50-block-poly(ethylene glycol)65-block-tat using Cu(II)-catalysis (S8)

Azido-tat (5.18 mg, 3.33 μmol), PS50-PEG65-acetylene (1.6 equiv., 41.6 mg, 5.2 μmol, for synthesis, see ref [4]), CuBr (6 equiv., 6.76 mg, 0.047 mmol) and PMDETA (6 equiv., 10.13 μL, 0.047 mmol) were dissolved in THF/H2O (2:1 v/v, 3 mL) and stirred for 4 days. After 2 days, sodium ascorbate was added (6 equiv., 4 mg, 0.02 mmol). After 3 days the reaction mixture was evaporated and the crude product was purified by silica column chromatography CH2Cl2/MeOH, 3:1 v/v). Lyophilisation yielded a mixture of **S8** (33%) and unreacted PS-PEG as an off-white solid (22.5 mg, 72%). 1H NMR (400 MHz, CDCl3): δ = 1.2-2.3 (b, ~150H), 3.4-3.9 (b, ~260H), 6.3-7.3 (b, ~250H) (numerous small peaks for tat are visible); FTIR-ATR: 3442, 3018, 2915, 2867, 1942, 1869, 1774, 1722, 1644, 1597, 1489, 1445, 1346, 1290, 1247,1100, 1026, 940, 845, 750, 698, 538 cm-1; GPC: Mn: 9432, Mw: 9616, PDI: 1.02; Staining on TLC plates with chlorine-TDM was positive for amines.

7.3.12   Analysis of Cu-levels in PS-PEG-tat

Inductively coupled plasma - mass spectrometry (ICP-MS) analysis was used to assay Cu-levels in PS-PEG-tat block copolymers. PS-PEG-tat was prepared through either the Cu-catalyzed azidealkyne cycloaddition (CuAAC, synthesis vide supra) or the tandem cycloaddition-retro-Diels-Alder reaction between an azide and an oxanorbornadiene (crDA, compound **3**). The indicated amount of polymer was destructed in concentrated nitric acid

(0.5 mL) at 80°C for 3 hours. The samples were cooled to room temperature and silver acetate (AgOAc) was added as an internal standard (2 mg mL-1 in ultrapure water, 1.25 mL). The total volume of each sample was then brought to 5.0 mL using ultrapure water prior to measurement. Resulting ppm values for Cu were standardized on values for the internal standard Ag to enable expression of Cu per milligram. The ratio between CuAAC and crDA Cu-levels was $(71.84/9.08 \cdot 10\text{-}2) = 791.20$.

7.3.13   HEPES-Buffered Saline Solution

HEPES-buffered saline (HBS) used in this report was prepared from a 10X-stock solution. Diluted 1X buffer contained 4-(2-hydroxyethyl)-1-piperazineethanesulfonic acid (HEPES, 10 mM), NaCl (135 mM), KCl (5 mM), $CaCl_2$ (1.8 mM), $MgCl_2$ (1 mM), pH = 7.4.

7.3.14   General Procedure for Polymersome Formation

A solution of PS40-PIAT50 (admixed with 10 wt.-% of **3**, when applicable) in THF (0.5 mL, 1.0 g·L^{-1}) was manually injected into HBS (2.5 mL) using a pipette. For HRP-filled polymersomes, prior to THF addition, 200μL of HBS was replaced by 200μL of HRP solution (2.5 g·L^{-1}, (Sigma, type XII) in ultrapure water). For GFP-filled polymersomes, 96μL of HBS was replaced by 96μL of GFP solution (3.75 g·L^{-1} in HBS). After equilibration for 30 minutes the suspension was transferred to a Spectra/Por (Breda, The Netherlands) Biotech Cellulose Ester Dialysis Membrane tube (MWCO: 300kDa). The dispersion was dialyzed against HBS for 36 hours, with regular changes of the dialysis bath to fresh HBS. The resulting vesicles were analyzed with TEM and stored in a glass vial. To attenuate incidental concentration differences between tat- and non-tat batches of GFP polymersomes used in the same fluorescence-based experiments, their concentrations were standardized based on adsorption at 490 nm of their GFP cargo through dilution with HBS.

7.3.15   Cell Culture

HeLa and Jurkat E6.1 cells were maintained in RPMI 1640 and HEK 293 cells in DMEM (Both PAN Biotech, Aidenbach, Germany), each supplemented with 10% fetal calf serum (FCS; PAN Biotech). All cell lines were incubated at 37°C in a 5% CO2-containing, humidified incubator.

7.3.16 Confocal Laser Scanning Microscopy

Confocal laser scanning microscopy was performed on a TCS SP5 confocal microscope (Leica Microsystems, Mannheim, Germany) equipped with an HCX PL APO 63 x N.A. 1.2 water immersion lens. Live cells were maintained at 37°C on a temperature-controlled microscope stage. GFP, lysotracker and Texas Red were excited using a 488 nm argon ion laser, a HeNe 561 nm laser and a HeNe 594 nm laser, respectively. Emission was detected between 500 and 550 nm for GFP, between 575 and 670 nm for lysotracker and between 610 and 700 nm for Texas Red.

7.3.17 Cellular Uptake and Colocalization Studies

HeLa cells or HEK cells were seeded at a density of 30,000 cells per well one day before the experiment in 8-well microscopy chambers (Nunc, Wiesbaden, Germany). Jurkat cells were counted at the day of the experiment and 300,000 cells were incubated with polymersomes in each well. For uptake studies, GFP and tat-GFP polymersomes were added to a final concentration of 50 μg/mL (polymer / medium). Cells were incubated with polymersomes in fresh medium containing 10% FCS at 37°C for four hours. For colocalization experiments using lysotracker red (Invitrogen, Eugene, USA), the polymersome concentration was 16.7 μg/mL (polymer / medium) and during the last 60 min 100 nM lysotracker was added. Cells were washed twice with fresh medium and imaged immediately using confocal microscopy. For colocalization studies with dextran, polymersomes at a concentration of 16.7 μg/mL were incubated with 0.2 mg/mL Texas Red-labeled dextran (MW = 10,000; Invitrogen) for 25 min, after which they were washed and imaged immediately as described above.

7.3.18 Quantification of Polymersome Uptake by Flow Cytometry

Adherent HeLa or HEK 293 cells were seeded in 24-well plates (Sarstedt, Nümbrecht, Germany) at a density of 80,000 cells per well one day before the experiment. At the day of the experiment, 600,000 Jurkat E6.1 suspension cells were used per condition. For uptake studies, polymersomes were diluted in RPMI supplemented with 10% FCS to the concentrations 16.7 and 50 μg/mL (polymer / medium). Cells were incubated with the polymersomes for 4 h at 37°C, washed twice with HBS, trypsinated for 5 min at 37°C to dissociate cells (HeLa and HEK 293 cells) or to enhance removal of membrane-bound polymersomes (Jurkat E6.1 cells) and washed again by centrifugation using fresh medium

containing FCS. For the dextran inhibition assay, HeLa cells were treated with polymersomes at the concentrations of 16.7 or 50 µg/mL (polymer / medium) for 25 min at 37°C in the presence or absence of 0.2 or 0.4 mg/mL Texas red-labeled dextran (MW = 10,000). For all conditions, cellular fluorescence of 10,000 cells, gated on the basis of forward and sideward scatter, was measured using a BD FACScan flow cytometer equipped with a 488 nm laser (BD Biosciences, Erembodegem, Belgium). Data were analyzed using Summit software (Fort Collins, USA). Represented data, shown in Figure 7.8, have been corrected for background fluorescence and were normalized on the basis of the uptake of tat-modified polymersomes at the highest measured concentration for each experiment and/or cell line.
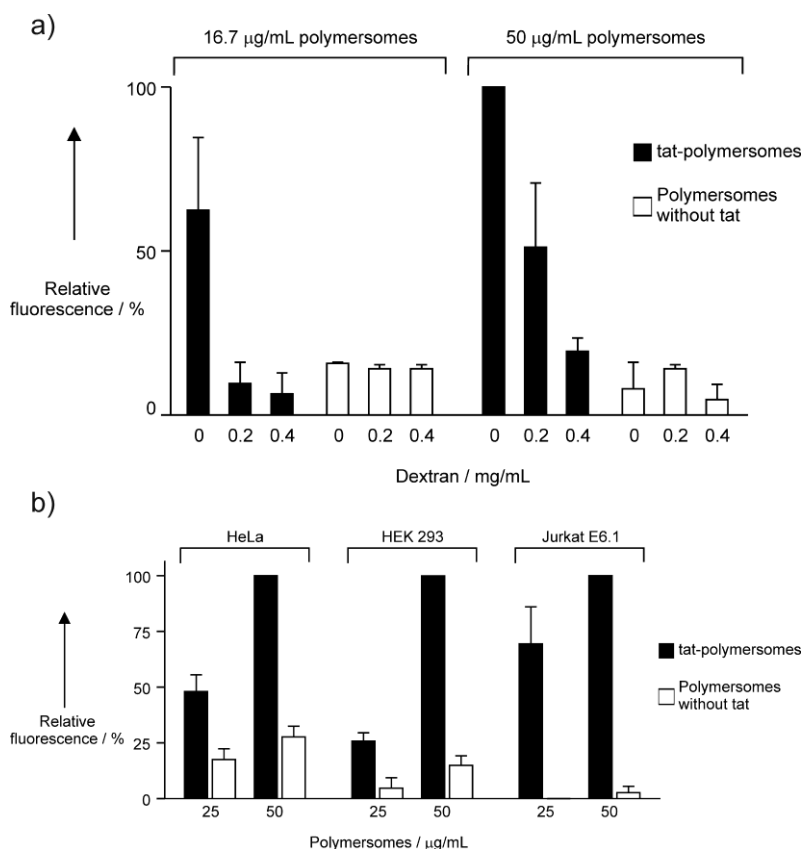

Figure 7.8. Flow cytometric quantification of the cellular uptake of tat-polymersomes. a) The uptake of tat-polymersomes by different cell lines at different concentrations after 4h incubation at 37°C. b) The effect of increasing concentrations of dextran on the uptake of tat-polymersomes after 25 min incubation at 37°C.

7.3.19 Horseradish Peroxidase (HRP) Assay

HeLa cells were seeded at a density of 6,000 cells per well one day before the experiment in 96-well plates (Sarstedt, Nümbrecht, Germany) and grown to 75% confluence. Incubation with the indicated concentrations of HRP-polymersome [100% reflects 167 µg/mL (polymer / medium)] took place in HBS containing 5 mM glucose and 0.1% bovine serum albumin (BSA, all Sigma-Aldrich, Zwijndrecht, the Netherlands) (HBS+). If indicated, cells were pulsed with 75 µM chloroquine (Sigma-Aldrich) or 25 µM or 100 µM nordihydroguaiaretic acid (NDGA; Sigma-Aldrich) during the final hour of the incubation. After the four hour incubation, cells were washed and grown in RPMI + 10% FCS with 1% of a standard penicillin-streptomycin preparation (Gibco) for the indicated periods. To assay the intracellular HRP activity, cells were washed and incubated with 60 µg/mL of the membrane-permeable HRP substrate 3,3',5,5'-tetramethylbenzidine (TMB; Sigma-Aldrich) in the presence of 250 µM H_2O_2 (Malinckrodt Baker, Deventer, the Netherlands) for 30 min at 37°C. The conversion of the product was measured each two minutes via the absorption at 370 nm (A370). Represented values have been corrected for the A370 of cells that did not receive the substrate. All conditions have been tested at least in duplicate during single experiments.

7.3.20 Dose Dependence of HRP Activity on Polymersome Concentration

The rate at which TMB was converted was linearly dependent on the administered dosage of polymersomes. Dilution with HBS of the original 167 µg / mL (polymer / medium) dispersion to 50% or 25% of its original polymersome content resulted in a corresponding decrease in HRP activity (Figure 7.9).
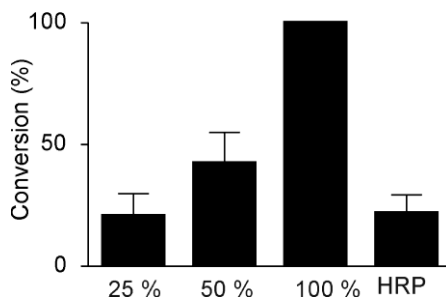
Figure 7.9. Dose-dependence of the rate of TMB conversion by polymersome-loaded cells on the concentration of the tat-polymersome dispersion that was used to load the cells. [100% polymersomes reflects 167 µg/mL (polymer / medium)] Conversion was measured after 30 minutes and standardized to 100% for 100% polymersomes; "Free HRP" denotes cells treated with HRP that was not encapsulated in tat-polymersomes.

7.4 References

[1] C. De Duve, R. Wattiaux, Functions of lysosomes, Annu Rev Physiol, 28 (1966) 435-492.

[2] B.M. Discher, Y.Y. Won, D.S. Ege, J.C. Lee, F.S. Bates, D.E. Discher, D.A. Hammer, Polymersomes: tough vesicles made from diblock copolymers, Science, 284 (1999) 1143-1146.

[3] N.W. Barton, R.O. Brady, J.M. Dambrosia, A.M. Dibisceglie, S.H. Doppelt, S.C. Hill, H.J. Mankin, G.J. Murray, R.I. Parker, C.E. Argoff, R.P. Grewal, K.T. Yu, Replacement Therapy for Inherited Enzyme Deficiency - Macrophage-Targeted Glucocerebrosidase for Gauchers-Disease, New Engl J Med, 324 (1991) 1464-1470.

[4] M. Rohrbach, J.T.R. Clarke, Treatment of lysosomal storage disorders - Progress with enzyme replacement therapy, Drugs, 67 (2007) 2697-2716.

[5] C.O. Fagain, Understanding and increasing protein stability, Biochim Biophys Acta, 1252 (1995) 1-14.

[6] B. Gupta, T.S. Levchenko, V.P. Torchilin, Intracellular delivery of large molecules and small particles by cell-penetrating proteins and peptides, Adv Drug Deliv Rev, 57 (2005) 637-651.

[7] F. Heitz, M.C. Morris, G. Divita, Twenty years of cell-penetrating peptides: from molecular mechanisms to therapeutics, Br J Pharmacol, 157 (2009) 195-206.

[8] T. Kaasgaard, T.L. Andresen, Liposomal cancer therapy: exploiting tumor characteristics, Expert Opin Drug Deliv, 7 (2010) 225-243.

[9] Y.L. Tseng, J.J. Liu, R.L. Hong, Translocation of liposomes into cancer cells by cell-penetrating peptides penetratin and tat: a kinetic and efficacy study, Mol Pharmacol, 62 (2002) 864-872.

[10] M. Yan, J. Du, Z. Gu, M. Liang, Y. Hu, W. Zhang, S. Priceman, L. Wu, Z.H. Zhou, Z. Liu, T. Segura, Y. Tang, Y. Lu, A novel intracellular protein delivery platform based on single-protein nanocapsules, Nat Nanotechnol, 5 (2010) 48-53.

[11] P.A. Wender, D.J. Mitchell, K. Pattabiraman, E.T. Pelkey, L. Steinman, J.B. Rothbard, The design, synthesis, and evaluation of molecules that enable or enhance cellular uptake: peptoid molecular transporters, Proc Natl Acad Sci U S A, 97 (2000) 13003-13008.

[12] S.F.M. van Dongen, H.P.M. de Hoog, R.J.R.W. Peters, M. Nallani, R.J.M. Nolte, J.C.M. van Hest, Biohybrid Polymer Capsules, Chem Rev, 109 (2009) 6212-6274.

[13] H. Hillaireau, P. Couvreur, Nanocarriers' entry into the cell: relevance to drug delivery, Cell Mol Life Sci, 66 (2009) 2873-2896.

[14] D.M. Vriezema, J. Hoogboom, K. Velonia, K. Takazawa, P.C.M. Christianen, J.C. Maan, A.E. Rowan, R.J.M. Nolte, Vesicles and polymerized vesicles from thiophene-containing rod-coil block copolymers, Angew Chem Int Edit, 42 (2003) 772-776.

[15] J.J.L.M. Cornelissen, H.M. de Hoog, M. Nallani, A.E. Rowan, R.J.M. Nolte, I.W.C.E. Arends, Biocatalytic oxidation by chloroperoxidase from Caldariomyces fumago in polymersome nanoreactors, Org Biomol Chem, 7 (2009) 4604-4610.

[16] M. Nallani, R. Woestenenk, H.P.M. de Hoog, S.F.M. van Dongen, J. Boezeman, J.J.L.M. Cornelissen, R.J.M. Nolte, J.C.M. van Hest, Sorting Catalytically Active Polymersome Nanoreactors by Flow Cytometry, Small, 5 (2009) 1138-1143.

[17] S.F.M. van Dongen, M. Nallani, J.L.L.M. Cornelissen, R.J.M. Nolte, J.C.M. van Hest, A Three-Enzyme Cascade Reaction through Positional Assembly of Enzymes in a Polymersome Nanoreactor, Chem-Eur J, 15 (2009) 1107-1114.

[18] S.M. Kuiper, M. Nallani, D.M. Vriezema, J.J.L.M. Cornelissen, J.C.M. van Hest, R.J.M. Nolte, A.E. Rowan, Enzymes containing porous polymersomes as nano reaction vessels for cascade reactions, Org Biomol Chem, 6 (2008) 4315-4318.

[19] S.S. van Berkel, A.T.J. Dirks, M.F. Debets, F.L. van Delft, J.J.L.M. Cornelissen, R.J.M. Nolte, F.P.J.T. Rutjes, Metal-free triazole formation as a tool for bioconjugation, Chembiochem, 8 (2007) 1504-1508.

[20] S.F.M. van Dongen, M. Nallani, S. Schoffelen, J.J.L.M. Cornelissen, R.J.M. Nolte, J.C.M. van Hest, A block copolymer for functionalisation of polymersome surfaces, Macromol Rapid Comm, 29 (2008) 321-325.

[21] N. Ben-Haim, P. Broz, S. Marsch, W. Meier, P. Hunziker, Cell-specific integration of artificial organelles based on functionalized polymer vesicles, Nano Lett, 8 (2008) 1368-1373.

[22] N.A. Christian, M.C. Milone, S.S. Ranka, G. Li, P.R. Frail, K.P. Davis, F.S. Bates, M.J. Therien, P.P. Ghoroghchian, C.H. June, D.A. Hammer, Tat-functionalized near-infrared emissive polymersomes for dendritic cell labeling, Bioconjug Chem, 18 (2007) 31-40.

[23] Y. Kim, M. Tewari, J.D. Pajerowski, S. Cai, S. Sen, J.H. Williams, S.R. Sirsi, G.J. Lutz, D.E. Discher, Polymersome delivery of siRNA and antisense oligonucleotides, J Control Release, 134 (2009) 132-140.

[24] I. Nakase, A. Tadokoro, N. Kawabata, T. Takeuchi, H. Katoh, K. Hiramoto, M. Negishi, M. Nomizu, Y. Sugiura, S. Futaki, Interaction of arginine-rich peptides with membrane-associated proteoglycans is crucial for induction of actin organization and macropinocytosis, Biochemistry, 46 (2007) 492-501.

[25] J.S. Wadia, R.V. Stan, S.F. Dowdy, Transducible TAT-HA fusogenic peptide enhances escape of TAT-fusion proteins after lipid raft macropinocytosis, Nat Med, 10 (2004) 310-315.

[26] J. Rejman, V. Oberle, I.S. Zuhorn, D. Hoekstra, Size-dependent internalization of particles via the pathways of clathrin- and caveolae-mediated endocytosis, Biochem J, 377 (2004) 159-169.

[27] R. Fischer, K. Kohler, M. Fotin-Mleczek, R. Brock, A stepwise dissection of the intracellular fate of cationic cell-penetrating peptides, J Biol Chem, 279 (2004) 12625-12635.

[28] H. Raagel, P. Saalik, M. Hansen, U. Langel, M. Pooga, CPP-protein constructs induce a population of non-acidic vesicles during trafficking through endo-lysosomal pathway, J Control Release, 139 (2009) 108-117.

[29] S.F.M. van Dongen, R.L.M. Teeuwen, M. Nallani, S.S. van Berkel, J.J.L.M. Cornelissen, R.J.M. Nolte, J.C.M. van Hest, Single-Step Azide Introduction in Proteins via an Aqueous Diazo Transfer, Bioconjugate Chem, 20 (2009) 20-23.

[30] M.M. Mesulam, Tetramethyl benzidine for horseradish peroxidase neurohistochemistry: a non-carcinogenic blue reaction product with superior sensitivity for visualizing neural afferents and efferents, J Histochem Cytochem, 26 (1978) 106-117.

[31] S. Mumtaz, B.K. Bachhawat, Enhanced intracellular stability of dextran-horse radish peroxidase conjugate: an approach to enzyme replacement therapy, Biochim Biophys Acta, 1117 (1992) 174-178.

[32] C. de Duve, T. de Barsy, B. Poole, A. Trouet, P. Tulkens, F. Van Hoof, Commentary. Lysosomotropic agents, Biochem Pharmacol, 23 (1974) 2495-2531.

[33] H.P.M. de Hoog, D.M. Vriezema, M. Nallani, S. Kuiper, J.J.L.M. Cornelissen, A.E. Rowan, R.J.M. Nolte, Tuning the properties of PS-PIAT block copolymers and their assembly into polymersomes, Soft Matter, 4 (2008) 1003-1010.

[34] I.J. Minten, L.J.A. Hendriks, R.J.M. Nolte, J.J.L.M. Cornelissen, Controlled Encapsulation of Multiple Proteins in Virus Capsids, J Am Chem Soc, 131 (2009) 17771-17773.

A modular and non-covalent transduction system for leucine zipper-tagged proteins

Morten B. Hansen, Wouter P.R. Verdurmen,
Elizabeth H.P. Leunissen, Inge Minten, Jan C.M.
van Hest, Roland Brock and Dennis W.P.M. Löwik

Chapter eight

8   A modular and non-covalent transduction system for leucine zipper-tagged proteins

Morten B. Hansen[b], Wouter P.R. Verdurmen[a], Elizabeth H.P. Leunissen[b], Inge Minten[b], Jan C.M. van Hest[b], Roland Brock[a] and Dennis W.P.M. Löwik[b]

[a] Department of Biochemistry, Nijmegen Centre for Molecular Life Sciences, Radboud University Nijmegen Medical Centre, Nijmegen, 6525 GA, The Netherlands
[b] Institute for Molecules and Materials, Department of Organic Chemistry, Radboud University Nijmegen, The Netherlands

8.1   Introduction

Cell-penetrating peptides (CPPs) have attracted much interest in recent years as they have the ability to induce cellular uptake of almost any kind of cargo to which they have been attached [1-8]. CPPs are typically 8-30 residues long; in nearly all cases conjugation to the cargo of choice is based on covalent attachment, or association *via* uncontrolled charge-based interactions [9-12]. Covalent attachment can be achieved chemically or, if the cargo is a protein, *via* genetic fusion. Chemical coupling often involves conditions which may compromise sensitive cargos like proteins. In addition, coupling reactions are often rather unselective, which may lead to linking of (multiple) CPP(s) to essential functional amino acid residues in proteins. Moreover, it may also lead to impairment of the cargo [13, 14]. Genetic fusion, albeit selective, may result in low expression levels [15] and is a strategy that is inherently labor-intensive in case a variety of CPPs is to be examined.

Non-covalent association systems, of which the streptavidin-biotin system is the paradigmatic example, have been of enormous benefit for the biomolecular sciences [16]. These non-covalent association systems have also been implemented in delivery systems to develop a methodology that separates the synthesis of cargo and CPP, after which a supramolecular interaction brings both elements together in a non-covalent delivery vehicle [17-20]. However, the few non-covalent delivery systems available to date have their shortcomings: streptavidin [17, 19] is of considerable size and also requires the covalent modification of one interactor with biotin. Another system which has been employed is the interaction of oligohistidine tags with oligovalent nitrilotriacetic acid (NTA) tags, facilitated by metal ions [21-24]. In this system, some selectivity can be achieved by

adjusting the oligovalency of NTA and histidine [25]. However, the presence of metal-ions may lead to binding and inactivation of protein cargos, besides the issue of their inherent cytotoxicity [18, 20, 26, 27].

In this respect, coiled-coil forming peptides form an interesting alternative, as strong and specific binding can be achieved by two short, complementary interaction partners [28, 29]. The leucine zipper motif, found in many transcription factors, belongs to this class of peptides [30-32]. These peptides consist of a heptad repeat, **abcdefg**, in which residues **a** and **d** are hydrophobic, packing together with **a**' and **d**' from the second peptide in a *knobs-into-holes manner* [33]. Residues **e** and **g** are often charged residues responsible for key *i* to *i*'+5 electrostatic interactions ensuring heterodimerization and providing directionality of the peptide pair (parallel vs. anti-parallel) [34, 35]. Very recently, such leucine zippers were used to link a small fluorescent molecule to a polymer non-covalently and transport the entire complex into cells [36]. However, like the streptavidin-biotin system, this approach also suffers from being fairly sizable.

Here we present a novel, low-molecular weight, non-covalent and modular transduction system based on the strong and specific binding of two complementary leucine zippers (Figure 8.1) [29]. Our delivery system consists of three modules: a CPP (module 1), which can be conjugated *via* copper-catalyzed azide/alkyne 'click chemistry' to a leucine zipper peptide (module 2). Subsequently, this CPP-leucine zipper peptide can bind specifically to its complementary leucine zipper fused to a proteinaceous cargo (module 3).

The advantages of this modular design over covalent systems and genetic fusion-protein approaches are multiple: (*i*) The modular assembly allows easy variation of the CPP (module 1). This feature could be of great interest to the field of targeted delivery using homing peptides to target specific organs/tumours as different organs are targeted by different peptides [37, 38]. (*ii*) The CPP can be synthesized independently of the cargo and independently of the leucine zipper. This fragment synthesis strategy confers a synthetic freedom enabling the otherwise laborious and complicated synthesis of longer CPPs and leucine zippers. (*iii*) It is possible to use non-natural amino acids such as D-amino acids. (*iv*) Functionalities *e.g.* labels can be introduced on the leucine zipper (module 2) without affecting the cargo.

To evaluate the effectiveness of this association system in a cell biological context we conjugated an enhanced green fluorescent protein non-covalently to a TAT peptide, a CPP derived from an HIV transcription factor [39, 40].
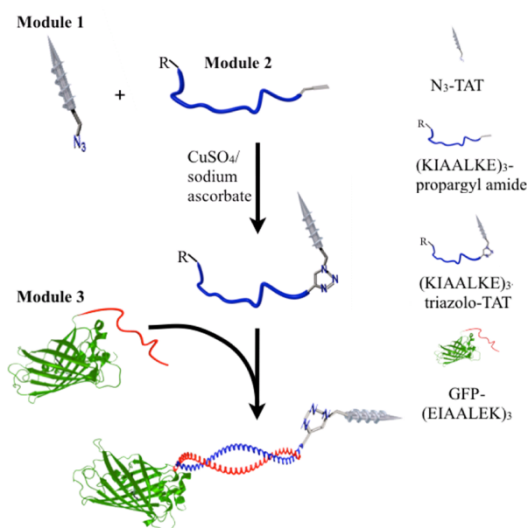
Figure 8.1. Overview of the modular assembly process of the leucine zipper-based non-covalent association and transduction system. First a CPP (module 1) is 'clicked' to a leucine zipper peptide (module 2), which binds specifically to its complementary leucine zipper peptide linked to a proteinaceous cargo; here GFP-LZ (module 3). R = Ac or S0387.

8.2   Results and Discussion

The azide-functionalized TAT peptide azido-YGRKK-RRQRRR-GC(Acm)§ (module 1) was prepared by solid phase peptide synthesis (SPPS) and a subsequent on-resin diazotization of the *N*-terminus [41]. The azide-functionalized TAT peptide was cleaved from the resin using trifluoroacetic acid and purified by reversed-phase HPLC. The mass and purity of the purified product were verified by ESI mass spectrometry and analytical reversed-phase HPLC, respectively. The clickable leucine zipper (module 2) was prepared by coupling of propargylamine to an aldehyde resin *via* reductive amination, followed by standard SPPS using the resulting secondary amine as a starting point [42]. In this way the alkyne functionality was introduced at the *C*-terminus of the leucine zipper peptide (KIAALKE)₃. This allowed labeling of the *N*-terminus with carboxyl-S0387 (a commercially available Cy5 analog) by means of a HATU-mediated peptide coupling. Subsequently, the S0387-labeled, alkyne-functionalized (KIAALKE)₃ peptide was cleaved from the resin and analyzed as described above for module 1. Finally, S0387-labeled alkyne-functionalized (KIAALKE)₃ was 'clicked' to azido-TAT using CuSO₄/sodium ascorbate as a copper(I) source and lutidine as copper ligand. The resulting S0387-(KIAALKE)₃-triazolo-TAT (S0387-LZ-TAT) conjugate was purified by reversed-phase

HPLC and the mass and purity were verified by MALDI mass spectrometry and analytical HPLC, respectively. Unlabeled (KIAALKE)$_3$-TAT (LZ-TAT) was prepared in a similar way, except that this peptide was acetylated *N*-terminally instead of labeled with S0387. The GFP-leucine zipper, GFP-(EIAALEK)$_3$, (GFP-LZ, our model cargo) was cloned into a DNA plasmid as a fusion protein, expressed in and purified from *E. coli* by means of His-tag affinity chromatography [43]. The purity and mass were verified by SDS-PAGE electrophoresis and HR-ESI, respectively.

We first verified that the two leucine zippers were able to heterodimerize after linkage to TAT and GFP, respectively, by measuring their binding constant by means of isothermal titration calorimetry (ITC, Figure 8.2). The ITC data yielded a K_D of 181 nM ($K_D = K_A^{-1}$), which is similar to the dissociation constant of unfunctionalized leucine zippers (data not shown and ref. [44]). This demonstrates that the affinity of the leucine zippers for each other is not affected by GFP or TAT. The calculated stoichiometry of 1.14 supports a one-to-one heterodimerization.
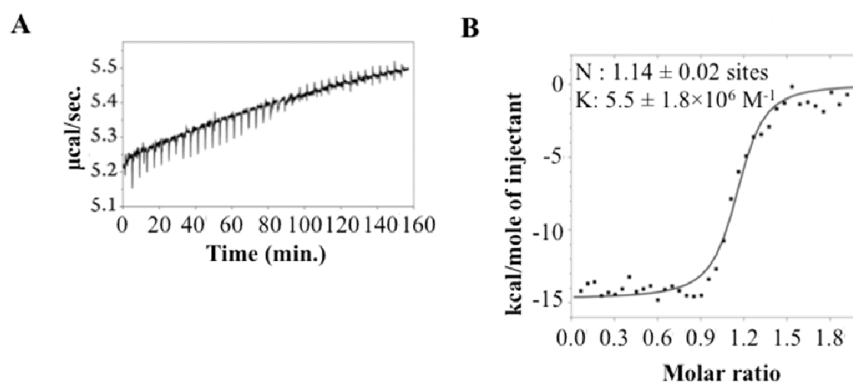
Figure 8.2. Isothermal titration calorimetry of LZ-TAT and GFP-LZ. (A) Raw heats acquired by titrating of LZ-TAT into a solution of GFP-LZ. (B) The integrals of the heat peaks were fitted to a one-site binding model, providing the association constant K_A and the stoichiometry N. Experiments were performed in 10 mM phosphate buffer pH 7.0.

The interaction between the leucine zippers was studied further by conducting dual-color fluorescence cross-correlation spectroscopy (FCCS) for GFP-LZ and S0387-LZ-TAT. FCCS extracts information on molecular interactions of differently labeled molecules from temporal fluctuations of fluorescence intensity in overlapping confocal detection volumes [45]. Since FCCS is a method especially suitable for detecting association at low nanomolar concentrations, GFP-LZ and S0387-LZ-TAT were first allowed to associate at 12.5 µM for 5 min at 4°C, after which they were diluted to 62.5 nM. A strong cross-

correlation was acquired for the two leucine zippers, whereas no cross-correlation was detected if one of the two leucine zippers was replaced by the corresponding free fluorophore (Figure 8.3A-D).

To quantify the fraction of associated particles, first, a double-labeled oligonucleotide was used as a positive reference showing maximal cross-correlation (Figure 8.3E). For S0387-LZ-TAT, almost complete association with GFP-LZ was observed, whereas over half of GFP-LZ species were associated with S0387-LZ-TAT species. Although these results seem to indicate a slightly altered stoichiometry, we could attribute the different values to differential affinities for the walls of the 384-wells plate used in the FCCS experiment, as a 3.3-fold excess of GFP-particles over S0387-labeled particles was detected in the solution, calculated on the basis of the estimated particle number in the confocal volume (1.8 for GFP and 1.1 for S0387) and the size of the confocal detection volume (0.3 fl for the GFP-channel and 0.6 fl for the S0387-channel) [46]. The FCCS measurements demonstrated that the non-covalent leucine zipper complexes were stable at concentrations below the K_D-value, which is indicative of a slow dissociation-rate.
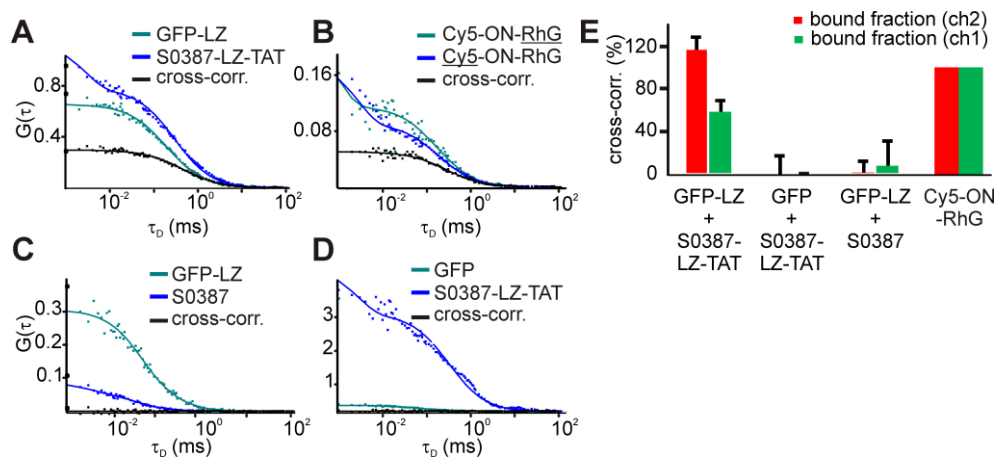
Figure 8.3. Interaction of leucine zippers as detected by FCCS. A) Association of GFP–LZ and S0387–LZ–TAT; B) a Rhodamine Green (RhG) and Cy5 double-labeled oligonucleotide (ON) served as positive control; C) GFP–LZ in the presence of S0387 or D) GFP in the presence of S0387–LZ–TAT. (C) and (D) were used as negative controls. E) The percentage of bound fraction of S0387 fluorophores (ch2) and GFP (ch1) was calculated by normalizing their cross-correlation amplitudes to those of Cy5 and RhG from the double-labeled ON, which were defined as 100% association. Errors bars represent the standard deviation of ten measurements of 10 s.

Having established the potential of the leucine zipper-tag as a non-covalent transduction system in a non-cellular context, we next investigated its transduction competence in living

cells. Hence, HeLa cells were incubated with GFP-LZ:LZ-TAT complexes and uptake was investigated by confocal laser scanning microscopy. As expected, intracellular transduction of GFP-LZ was profoundly stimulated when complexed with LZ-TAT; GFP was clearly visible in vesicular structures inside the cells (Figure 8.4A). Uptake was only observed for the complexes formed from GFP-LZ and TAT-LZ.

CellMask Deep Red was applied to stain the plasma membrane (after incubation with the leucine zippers) to verify that the punctate green structures were indeed localized inside cells and not fluorescent aggregates on the plasma membrane. GFP-LZ and CellMask Deep Red did not co-localize, thus establishing that the punctate green structures are predominantly localized intracellularly (Figure 8.4A). Washing with heparin to remove leucine zippers potentially bound to the cell surface did not change the appearance of the confocal images demonstrating that the GFP-LZ and LZ-TAT are indeed taken up by the cells (data not shown). Importantly, no intracellular delivery of GFP was observed when free GFP (no leucine zipper) was incubated with LZ-TAT, ruling out the possibility that cellular uptake could be a result of an unspecific interaction between LZ-TAT and GFP itself. To exclude the possibility that GFP-LZ internalization was enhanced through unspecific induction of macropinocytosis by TAT [13], GFP-LZ was also co-incubated with unlabeled free TAT (no leucine zipper) (Figure 8.4B). Indeed, no internalization of GFP-LZ was observed, confirming that a specific interaction between TAT-LZ and GFP-LZ is indeed the primary driving force for internalization.
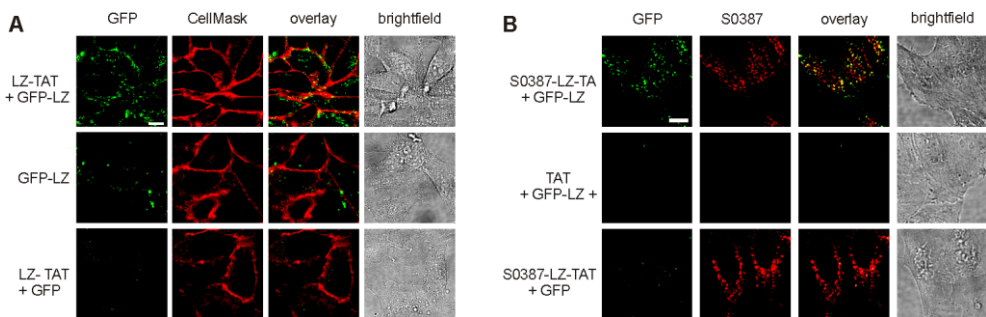
Figure 8.4. Confocal microscopy showing efficient transduction of GFP–LZ by LZ–TAT into HeLa cells. A) Leucine zippers (2.5 μM) were incubated with HeLa cells for 60 min at 37°C. The plasma membrane was stained with Cell-Mask Deep Red. B) HeLa cells were incubated with S0387-labeled LZ–TAT, GFP–LZ, TAT or GFP (1.25 μM each) for 60 min at 37°C. Yellow structures indicate colocalization, scale bars=10 μm.

After demonstrating that LZ-TAT is able to deliver GFP-LZ intracellularly through a specific non-covalent interaction, the next issue to be addressed was whether the leucine

zippers remain associated inside cells. In an attempt to answer this question, S0387-LZ-TAT was co-incubated with GFP-LZ (Figure 8.4B). The overlay of the confocal images from this experiment showed numerous yellow punctate dots indicating subcellular co-localization of the zippers. However, next to yellow dots, red and green dots were observed as well, indicating that the ratio of GFP-LZ and S0387-LZ-TAT differs widely between intracellular vesicles. Although elucidating the exact intracellular fate requires a more exhaustive study, which is beyond the scope of this communication, this observation suggests that the leucine zippers do not remain fully associated inside cells. One possibility is that the low endosomal pH promotes dissociation of leucine zippers [44].

In conclusion, by taking advantage of the specific binding of two complementary leucine zippers, we have developed a modular, non-covalent delivery system for leucine zipper-functionalized cargos. When a cell-penetrating peptide (CPP), TAT, was attached to one leucine zipper and mixed with its complementary leucine zipper bearing a GFP-cargo, the resulting non-covalent complex was transported into cells. Importantly, cells only took up the GFP-cargo when the complementary leucine zipper-TAT was added. Since the delivery system is modular, the leucine zipper-TAT can easily be altered either by varying the CPP or by adding functionalities to the leucine zipper such as labels. In this proof-of-concept study we have shown that GFP can be introduced into cells via a non-covalent and modular transduction system. This may pave the way for transduction of other (therapeutically active) proteins.

8.3   Materials and Methods

8.3.1   Experimental

Aldehyde resin was purchased from Novabiochem and Fmoc-*L*-amino acids were from Bachem or Novabiochem. S0387 was purchased from Few Chemicals (Bitterfeld-Wolfen, Germany). All other chemicals were purchased from Baker, Fluka or Sigma Aldrich and used as received. Mass spectra were recorded on a Bruker Biflex MALDI-TOF (high resolution 0-4000 and low resolution >4000, Bruker Daltronik, Bremen, Germany), a low resolution Thermo Finnigan LCQ ESI-ion trap (Thermo Fischer, Breda, The Netherlands) or a high resolution ESI-TOF JEOL AccuTOF (JEOL, Nieuw-Vennep, The Netherlands).

8.3.2   *General peptide synthesis and purification*

Peptides were synthesized on a Labortec640 (Labortec, Bubendorf, Schwitzerland) employing a standard Fmoc solid-phase peptide synthesis (SPPS) protocol. Semi-preparative RP-HPLC purification of peptides was performed using a C18 and a MeCN/water gradient containing 0.1% trifluoroacetic acid. The fractions were analyzed by ESI-ion trap mass spectrometry and analytical RP-HPLC using a C18 column.

8.3.3   *Infrared spectroscopy*

Infrared spectroscopy was performed on a Thermo Wattson IR300 spectrometer, fitted with a Harrick ATR unit (Thermo Fischer, Breda, The Netherlands). Dry samples were compressed on the ATR crystal with a pressure of 0.5 kg. Infrared spectra were recorded for 32 scans at 4 cm^{-1} resolution and a sample gain of 1, and background-subtracted.

8.3.4   *Isothermal titration calorimetry*

Isothermal titration calorimetry (ITC) was carried out on an ITC200 (MicroCal, Northhampton, MA, USA). Peptides and proteins were dissolved in 10 mM phosphate buffer pH 7.0. The titration experiment was carried out at 5°C and stirring at 500 rpm as a series of 39 injections of 1.0 μL with a duration of 2.0 s and a spacing of 240 s. The integrals of the measured heat peaks were fitted to a one-site binding model using Origin 7.0 with a MicroCal ITC plug-in and the binding stoichiometry (N), association constant (K), molar enthalpy (ΔH) and entropy (ΔS) of binding were extracted.

8.3.5   *Confocal laser scanning microscopy and fluorescence cross-correlation spectroscopy (FCCS)*

Confocal laser scanning microscopy and FCCS were performed on a TCS SP5 confocal microscope (Leica Microsystems, Mannheim, Germany) equipped with an HCX PL APO 63 x N.A. 1.2 water immersion lens and a fluorescence-correlation spectroscopy (FCS) unit. For confocal microscopy, cells were kept at 37°C on a temperature-controlled microscope stage. GFP was excited with a 488 nm argon ion laser. Emission of GFP was collected using a 500-550 nm detection range for confocal microscopy and with a 500-550 nm band-pass filter for FCCS measurements. S0387 and CellMask Deep Red were excited with a 633 nm HeNe laser. Emission for confocal microscopy was collected between 650

and 720 nm for S0387 and between 650 and 750 nm for CellMask Deep Red. For FCCS, emission of S0387 was collected with a 647-703 nm filterblock.

Autocorrelation and cross-correlation measurements for FCCS were performed in a 384-well plate (175 µm, lowbase design, MMI, Eching, Germany). Autocorrelation and cross-correlation functions were calculated with an ISS VISTA software package (ISS, Illinois, USA). Fitting was performed according to a 3D-Gaussian model containing a triplet component for GFP and S0387. The particle number obtained from the fit was corrected for uncorrelated background [47]:

$$G_{tot}(0) = 1 + 1/N_{app} = 1 + (1-CPS_b/CPS_t)_2/N_{corr}$$

A similar model without a triplet component was used for cross-correlation analysis. To correct for bleed-through effects of GFP into the S0387 channel, the true, corrected relative cross-correlation amplitude $\hat{G}_{0;x}/G_{0,g}$ (green channel) was calculated by the method described by Bacia *et al*. [48]:

Relative cross-correlation amplitude (green) = $\hat{G}_{0;x}/G_{0,g}$ = $((G_{0;x}/\ G_{0,g})$ - $k_{Gr}(CPS_g/CPS_r))/(1$ - $k_{Gr}(CPS_g/CPS_r))$

Where $G_{0;x}$ is the uncorrected cross-correlation amplitude at the diffusional autocorrelation time $(\tau)=0$ and $G_{0,g}$ the autocorrelation amplitude of GFP at $\tau=0$. k_{Gr} corresponds to the bleed-through ratio of GFP from the green into the red channel, determined by taking the ratio of the counts per second (CPS) values in the red (S0387) and green (GFP) channel (CPS_r/CPS_g). The relative cross-correlation amplitude for the red channel was determined by dividing the corrected cross-correlation amplitude $\hat{G}_{0;x}$ by the autocorrelation amplitude $G_{0,r}$ in the red channel:

Relative cross-correlation amplitude (red) = $\hat{G}_{0;x}/G_{0,g}$

Since the dimensions of confocal detection volumes are wavelength-dependent, the relative cross-correlation values never reach 1.0. Therefore, a double-labeled oligonucleotide, containing rhodamine green (RhG) and Cy5 as fluorophores, similar to an oligonucleotide published previously [49], was included as positive control. To calculate the number of particles in a complex, values obtained with the double-labeled oligonucleotide were used as a reference and defined as 100% association.

8.3.6 Cellular uptake experiments

Leucine zipper complexes were prepared in two steps. First, the leucine zippers (25 μM each) were mixed and incubated in phosphate buffer (10 mM, pH 7.0) at 4°C for at least 5 min. Subsequently, complexes were diluted in HBS (10 mM HEPES, 135 mM NaCl, 5 mM KCl, 1 mM $MgCl_2$, 1.8 mM $CaCl_2$, pH 7.4) containing 5 mM glucose to the indicated concentrations. Controls with GFP and TAT were prepared in the same way, *i.e.* by first mixing solutions of these molecules with S0387-LZ-TAT or GFP-LZ respectively, followed by a dilution into HBS with glucose. Likewise, when incubation was carried out with GFP-LZ only, GFP-LZ was also first diluted to 25 μM and then further diluted into glucose-containing HBS to the indicated concentration. All cellular experiments were conducted with HeLa cells, which were seeded two days before the experiment in 8-well microscopy chambers (Nunc, Wiesbaden, Germany) at a density of 20,000 cells/well. At the time of the experiment, cells had grown to 75% confluence. To determine whether cellular uptake of GFP-LZ was mediated by LZ-TAT, cells were first incubated with leucine zipper complexes (2.5 μM) or controls for 60 min at 37°C, washed with serum-containing medium, and incubated for 5 min with the plasma membrane stain CellMask Deep Red (5 μg/ml). Then, cells were washed three times with serum-containing medium and imaged immediately by confocal laser scanning microscopy. This experiment was also performed with two additional heparin washes included (2x5 min with heparin, 500 μg/ml in HBS supplemented with glucose) to remove cell surface-bound leucine zippers (data not shown). To determine colocalisation of leucine zipper-tagged molecules, HeLa cells were incubated with GFP-LZ and S0387- LZ-TAT (both 1.25 μM) for 60 min, washed three times with serum-containing medium and visualized by confocal laser scanning microscopy.

8.3.7 Expression and purification of GFP-(EIAALEK)₃ (GFP-LZ)

Expression of leucine zipper-tagged GFP: E. coli BLR (DE3) cells containing a pET-15b plasmid carrying GFP-(EIAALEK)₃ as a fusion gene with an *N*-terminal Histag [50] were used for protein expression. Expression was induced by addition of IPTG (0.5 mL, 1M) and protein was expressed for 5 h at 30°C.

Protein purification: The protein expression culture was pelleted at 4,000 rpm and 4°C for 15 min using a Sorvall RC-5 centrifuge (Thermo Fischer, Breda, The Netherlands). The supernatant was discarded and the pellet stored at -20°C. After thawing, the pellet was re-suspended in lysis buffer (25 mL, 50 mM $NaHPO_4$, 10 mM imidazole and 300 mM NaCl,

pH 8.0) on ice. To this suspension lysozyme (225 μL, 100 mg/mL in water) and PMSF (225 μL, 17 mg/mL in MeOH) were added. After gentle shaking at 4°C for 30 min the suspension was sonicated (2x3 min at output 6 and 40% duty cycle) using a Branson Sonifier 250 (Marius Instruments Nieuwegein, The Netherlands). The resulting cell lysate was spun at 1,000 rpm and 4°C for 30 min using a Sorvall RC-5 centrifuge (Thermo Fischer, Breda, The Netherlands). The pellet was discarded and the supernatant incubated with Ni-NTA agarose beads (washed twice with lysis buffer) at 4°C for 1 h. This suspension was added to a filter tube and the beads were allowed to settle on the filter. The flow-through was collected and re-incubated with Ni-NTA beads. The column was washed with 20 column volumes of washing buffer (10 mL, 50 mM phosphate, 20 mM imidazole, 300 mM NaCl, pH 8.0) and then 6 column volumes of elution buffer (3 mL, 50 mM phosphate, 250 mM imidazole, 300 mM NaCl, pH 8.0) to elute the GFP-LZ. Green fractions were combined and dialyzed against buffer (4x 500 μL 10 mM phosphate pH 7.0) using 10 kDa MWCO centrifugal filters (Millipore, Cork, Ireland). The mass was verified by ESI-TOF [M+H]+ *m/z*: 33371.8 (calcd. 33371.6) and the purity was checked by SDS-PAGE (10% acrylamide).

8.4   Acknowledgements

8.5   References

[1] R. Xiong, Z. Li, L. Mi, P.-N. Wang, J.-Y. Chen, L. Wang, W.-L. Yang, Study on the intracellular fate of Tat peptide-conjugated quantum dots by spectroscopic investigation., J. Fluoresc., 20 (2010) 551-556.
[2] H. Yukawa, Y. Kagami, M. Watanabe, K. Oishi, Y. Miyamoto, Y. Okamoto, M. Tokeshi, N. Kaji, H. Noguchi, K. Ono, M. Sawada, Y. Baba, N. Hamajima, S. Hayashi, Quantum dots labeling using octa-arginine peptides for imaging of adipose tissue-derived stem cells., Biomaterials, 31 (2010) 4094-4103.

[3] S.F.M. van Dongen, W.P.R. Verdurmen, R.J.R.W. Peters, R.J.M. Nolte, R. Brock, J.C.M. van Hest, Cellular integration of an enzyme-loaded polymersome nanoreactor., Angew. Chem. Int. Ed., 49 (2010) 7213-7216.

[4] M.M. Fretz, G.A. Koning, E. Mastrobattista, W. Jiskoot, G. Storm, OVCAR-3 cells internalize TAT-peptide modified liposomes by endocytosis., Biochim. Biophys. Acta, 1665 (2004) 48-56.

[5] L. Chaloin, P. Bigey, C. Loup, M. Marin, N. Galeotti, M. Piechaczyk, F. Heitz, B. Meunier, Improvement of porphyrin cellular delivery and activity by conjugation to a carrier peptide., Bioconjugate Chem., 12 (2001) 691-700.

[6] R. Fischer, M. Fotin-Mleczek, H. Hufnagel, R. Brock, Break on through to the other side-biophysics and cell biology shed light on cell-penetrating peptides., ChemBioChem, 6 (2005) 2126-2142.

[7] K.M. Stewart, K.L. Horton, S.O. Kelley, Cell-penetrating peptides as delivery vehicles for biology and medicine., Org. Biomol. Chem., 6 (2008) 2242-2255.

[8] N. Schmidt, A. Mishra, G.H. Lai, G.C.L. Wong, Arginine-rich cell-penetrating peptides., FEBS Lett., 584 (2010) 1806-1813.

[9] P. Järver, I. Mäger, Ü. Langel, In vivo biodistribution and efficacy of peptide mediated delivery., Trends Pharmacol Sci, 31 (2010) 528-535.

[10] O. Le Bihan, R. Chèvre, S. Mornet, B. Garnier, B. Pitard, O. Lambert, Probing the in vitro mechanism of action of cationic lipid/DNA lipoplexes at a nanometric scale., Nucleic Acids Res, 39 (2011) 1595-1609.

[11] J.S. Suk, J. Suh, K. Choy, S.K. Lai, J. Fu, J. Hanes, Gene delivery to differentiated neurotypic cells with RGD and HIV Tat peptide functionalized polymeric nanoparticles., Biomaterials, 27 (2006) 5143-5150.

[12] S. Veldhoen, S.D. Laufer, A. Trampe, T. Restle, Cellular delivery of small interfering RNA by a non-covalently attached cell-penetrating peptide: quantitative analysis of uptake and biological effect., Nucleic Acids Res, 34 (2006) 6561-6573.

[13] Y.-J. Lee, A. Erazo-Oliveras, J.-P. Pellois, Delivery of macromolecules into live cells by simple co-incubation with a peptide., ChemBioChem, 11 (2010) 325-330.

[14] J. Brugnano, B.C. Ward, A. Panitch, Cell penetrating peptides can exert biological activity, Biomol. Concepts, 1 (2010) 109-116.

[15] A. Honda, M.A. Moosmeier, W.R. Dostmann, Membrane-permeable cygnets: rapid cellular internalization of fluorescent cGMP-indicators., Front. Biosci., 10 (2005) 1290-1301.

[16] E.P. Diamandis, T.K. Christopoulos, The biotin-(strept)avidin system: principles and applications in biotechnology., Clin. Chem., 37 (1991) 625-636.

[17] M.A. Moosmeier, J. Bulkescher, J. Reed, M. Schnölzer, H. Heid, K. Hoppe-Seyler, F. Hoppe-Seyler, Transactin: a universal transmembrane delivery system for Strep-tag II-fused cargos., J Cell. Mol. Med., 14 (2010) 1935-1945.

[18] R.K. June, K. Gogoi, A. Eguchi, X.-S. Cui, S.F. Dowdy, Synthesis of a pH-sensitive nitrilotriacetic linker to peptide transduction domains to enable intracellular delivery of histidine imidazole ring-containing macromolecules., J Am Chem Soc, 132 (2010) 10680-10682.

[19] J. Rinne, B. Albarran, J. Jylhävä, T.O. Ihalainen, P. Kankaanpää, V.P. Hytönen, P.S. Stayton, M.S. Kulomaa, M. Vihinen-Ranta, Internalization of novel non-viral vector TAT-streptavidin into human cells., BMC Biotechnol., 7 (2007) 1.

[20] S. Futaki, M. Niwa, I. Nakase, A. Tadokoro, Y. Zhang, M. Nagaoka, N. Wakako, Y. Sugiura, Arginine carrier peptide bearing Ni(II) chelator to promote cellular uptake of histidine-tagged proteins., Bioconjug Chem, 15 (2004) 475-481.

[21] E. Hochuli, H. Döbeli, A. Schacher, New metal chelate adsorbent selective for proteins and peptides containing neighbouring histidine residues., J. Chromatogr., 411 (1987) 177-184.

[22] J. Israéli, M. Cecchetti, Complexes mixtes de l'histidine, J. Inorg. Nucl. Chem., 30 (1968) 2709-2716.

[23] R. Valiokas, G. Klenkar, A. Tinazli, R. Tampé, B. Liedberg, J. Piehler, Differential protein assembly on micropatterned surfaces with tailored molecular and surface multivalency., ChemBioChem, 7 (2006) 1325-1329.

[24] L. Schmitt, C. Dietrich, R. Tampe, Synthesis and characterization of chelator-lipids for reversible immobilization of engineered proteins at self-assembled lipid interfaces, J. Am. Chem. Soc., 116 (1994) 8485-8491.

[25] T. André, A. Reichel, K.-H. Wiesmüller, R. Tampé, J. Piehler, R. Brock, Selectivity of competitive multivalent interactions at interfaces., ChemBioChem, 10 (2009) 1878-1887.

[26] A.D. Keefe, D.S. Wilson, B. Seelig, J.W. Szostak, One-step purification of recombinant proteins using a nanomolar-affinity streptavidin-binding peptide, the SBP-Tag., Protein Expr Purif, 23 (2001) 440-446.

[27] A. Meinhart, T. Silberzahn, P. Cramer, The mRNA transcription/processing factor Ssu72 is a potential tyrosine phosphatase., J Biol Chem, 278 (2003) 15917-15921.

[28] H. Robson Marsden, N.A. Elbers, P.H.H. Bomans, N.A.J.M. Sommerdijk, A. Kros, A reduced SNARE model for membrane fusion., Angew. Chem. Int. Ed., 48 (2009) 2330-2333.

[29] J.R. Litowski, R.S. Hodges, Designing heterodimeric two-stranded alpha-helical coiled-coils. Effects of hydrophobicity and alpha-helical propensity on protein folding, stability, and specificity., J. Biol. Chem., 277 (2002) 37272-37279.

[30] B. Apostolovic, M. Danial, H.-A. Klok, Coiled coils: attractive protein folding motifs for the fabrication of self-assembled, responsive and bioactive materials., Chem. Soc. Rev., 39 (2010) 3541-3575.

[31] D.N. Woolfson, M.G. Ryadnov, Peptide-based fibrous biomaterials: Some things old, new and borrowed., Curr. Opin. Chem. Biol., 10 (2006) 559-567.

[32] E. Moutevelis, D.N. Woolfson, A periodic table of coiled-coil protein structures., J. Mol. Biol., 385 (2009) 726-732.

[33] F.H.C. Crick, The packing of-helices: simple coiled-coils, Acta Crystallogr., 6 (1953) 689-697.

[34] P. Lavigne, L.H. Kondejewski, M.E. Houston, F.D. Sönnichsen, B. Lix, B.D. Skyes, R.S. Hodges, C.M. Kay, Preferential heterodimeric parallel coiled-coil formation by synthetic Max and c-Myc leucine zippers: a description of putative electrostatic interactions responsible for the specificity of heterodimerization., J. Mol. Biol., 254 (1995) 505-520.

[35] E.K. O'Shea, R. Rutkowski, P.S. Kim, Mechanism of specificity in the Fos-Jun oncoprotein heterodimer., Cell, 68 (1992) 699-708.

[36] B. Apostolovic, S.P.E. Deacon, R. Duncan, H.-A. Klok, Hybrid polymer therapeutics incorporating bioresponsive, coiled coil peptide linkers., Biomacromolecules, 11 (2010) 1187-1195.

[37] J. Enbäck, P. Laakkonen, Tumour-homing peptides: tools for targeting, imaging and destruction., Biochem. Soc. Trans., 35 (2007) 780-783.

[38] P. Laakkonen, K. Vuorinen, Homing peptides as targeted delivery vehicles., Integr. Biol., 2 (2010) 326-337.

[39] E. Vivès, C. Granier, P. Prevot, B. Lebleu, Structure--activity relationship study of the plasma membrane translocating potential of a short peptide from HIV-1 Tat protein, Lett. Pept. Sci., 4 (1997) 429-436.

[40] E. Vivès, P. Brodin, B. Lebleu, A truncated HIV-1 Tat protein basic domain rapidly translocates through the plasma membrane and accumulates in the cell nucleus., J. Biol. Chem., 272 (1997) 16010-16017.

[41] E.D. Goddard-Borger, R.V. Stick, An efficient, inexpensive, and shelf-stable diazotransfer reagent: imidazole-1-sulfonyl azide hydrochloride., Org. Lett., 9 (2007) 3797-3800.

[42] H.T. Ten Brink, J.T. Meijer, R.V. Geel, M. Damen, D.W.P.M. Löwik, J.C.M. van Hest, Solid-phase synthesis of C-terminally modified peptides., J. Pept. Sci., 12 (2006) 686-692.

[43] I.J. Minten, L.J.A. Hendriks, R.J.M. Nolte, J.J.L.M. Cornelissen, Controlled encapsulation of multiple proteins in virus capsids., J. Am. Chem. Soc., 131 (2009) 17771-17773.

[44] B. Apostolovic, H.-A. Klok, pH-sensitivity of the E3/K3 heterodimeric coiled coil., Biomacromolecules, 9 (2008) 3173-3180.

[45] P. Schwille, F.J. Meyer-Almes, R. Rigler, Dual-color fluorescence cross-correlation spectroscopy for multicomponent diffusional analysis in solution., Biophys. J., 72 (1997) 1878-1886.

[46] H. Glauner, R.I. R, K. Hansen, B. Steemers, Y.D. Chung, F. Becker, S. Hannus, R. Brock, Simultaneous detection of intracellular target and off-target binding of small molecule cancer drugs at nanomolar concentrations, Br. J. Pharmacol., 160 (2010) 958-970.

[47] D.E. Koppel, Statistical Accuracy in Fluorescence Correlation Spectroscopy, Phys Rev A, 10 (1974) 1938-1945.

[48] K. Bacia, P. Schwille, Practical guidelines for dual-color fluorescence cross-correlation spectroscopy, Nat Protoc, 2 (2007) 2842-2856.

[49] N. Baudendistel, G. Muller, W. Waldeck, P. Angel, J. Langowski, Two-hybrid fluorescence cross-correlation spectroscopy detects protein-protein interactions in vivo, Chemphyschem, 6 (2005) 984-990.

[50] I.J. Minten, L.J. Hendriks, R.J. Nolte, J.J. Cornelissen, Controlled encapsulation of multiple proteins in virus capsids, J Am Chem Soc, 131 (2009) 17771-17773.

Summary and future directions

9 Summary and future directions

Despite a sharp increase in the understanding of diseases at the molecular level over the last decade and the concomitant validation of numerous therapeutically relevant drug targets, yearly drug approvals have not increased in number. In fact, most drug development efforts are currently still aimed at only a small percentage of disease-associated proteins that are considered suitable for drugging. One of the main reasons is that a substantial part of these target proteins needs to be targeted at sites that are involved in protein-protein interactions. For the foreseeable future, obtaining sufficient selectivity for pharmaceutical applications towards these targets with small molecules is going to remain a bottleneck. Therefore, the scientific and pharmaceutical community is shifting gears towards the development of biological molecules as alternatives to small molecules, as these so-called undruggable proteins can be targeted highly selectively with a variety of biological molecules. Although biologicals already represent a growing fraction of newly approved medicines, expected to reach 15-50% of the novel medicines in 2015, the application of biologicals for therapeutic purposes is currently limited to extracellular applications [1]. Nevertheless, increasing efforts are being undertaken to develop biomacromolecules that can be delivered into cells, where they can address the largely unexplored intracellular target space.

This thesis deals with a promising approach for delivery of biomacromolecules into cells: the application of cell-penetrating peptides (CPPs), which have a well-established capacity to induce the cellular uptake of a large variety of cargo molecules. More specifically, the main aim of this thesis was to gain a better mechanistic insight into the activity of CPPs, with the underlying goal of advancing the use of CPPs towards therapeutic applications. Towards this end, the **first chapter** gives a general introduction about the current state of affairs in drug development and also introduces the molecule class of CPPs with its main characteristics and its interactions with cellular components.

9.1 Side effects of drug carriers

Target selectivity and side effect profiles are of crucial importance for any drug. Traditionally, these topics are directly related to the properties of the drug. However, with the rise of molecular entities dedicated to drug delivery, it is of critical importance to realize that not just the macromolecule to be delivered needs to have a high selectivity and an acceptable side-effect profile, but that the delivery vehicle itself may also generate side effects. Though initially considered as Trojan horses, the question of vehicle-related side effects is receiving more and more attention also for CPPs, as reports about specific side

effects induced by CPPs, either *in vitro* or *in vivo*, have steadily accumulated over the last decade. Therefore, in the **second chapter,** an overview of the biological responses that are elicited by cationic drug carriers is given, in particular those elicited by CPPs. Ultimately, the identification of the mechanism of induction of these side effects may lead to the rational engineering of delivery vehicles that do not have these side effects. Additionally, a better understanding of the principles that govern cellular internalization may lead to hybrid peptides that both possess the ability to internalize into cells and exert a therapeutically relevant activity.

9.2   Understanding the activity of cell-penetrating peptides

Chapter three to five deal with distinct mechanisms by which these peptides enter cells. **Chapter three** provides a detailed mechanistic insight into a peptide entry mechanism that was described several years earlier, but for which little progress had been made on the understanding of the molecular basis of the mechanism [2]. The hypothesis that formed the basis of this chapter was that direct cytoplasmic uptake at high (>10 μM) peptide concentrations involved activation of the lipid remodeling enzyme acid sphingomyelinase. The hypothesis was based on observations that this protein could be a shared target of multiple drugs that were found to inhibit this uptake mechanism. A series of carefully designed experiments were conducted that provided experimental support for this hypothesis. In **chapter four**, data are reported showing that uptake of cationic CPPs is dependent on chirality in certain cell-types, which questions a long-standing paradigm on the receptor-independence of the uptake of these peptides. The results shown in this chapter strongly suggest that the endocytic uptake of cationic CPPs is a two-step process. Initially, peptides bind to heparan sulfates on the cell surface, a step independent of chirality, as could be confirmed *in vitro* by isothermal titration calorimetry. The second step, which is chirality dependent, is triggering the endocytic uptake of the peptides. It was also shown that this chirality-dependent trigger was not present in all cells, but correlated with the presence of heparan sulfates on the cell surface. For the nucleation zone-dependent uptake mechanism there was no clear role for amino acid chirality, as the somewhat higher uptake of D-R9 via this mechanism can be explained by the higher proteolytic stability of D-R9 as compared to L-R9. Alternatively, the difference might also be due to the fact that endocytosis preferentially depletes L-peptides from the cell surface.

Chapter five deals with an amphipathic CPP that is not dependent on arginines for activity, the chimeric transportan analog TP10. The CPP is composed N-terminally of residues derived from the neuropeptide galanin and C-terminally of residues derived from

the wasp venom peptide mastoparan. The two parts are linked via a lysine residue. The effect of epimerization of NMR labels at individual positions of the sequence on properties such as cytotoxicity, internalization efficiency and membrane binding was investigated. As with the arginine-containing peptides, strong effects of amino acid chirality on all of these properties were found. Unexpectedly, no clear correlation between their secondary structure and/or aggregation behavior in model systems and their properties in a cellular environment was found. When comparing the results with previous results obtained with the arginine-containing peptides R9 and penetratin (**chapter four**), it was found that, despite the absence of arginines in TP10, there were remarkable similarities in the dependence on heparan sulfate chains for membrane binding. In contrast, the induction of phosphatidylserine exposure of TP10 was much greater compared to R9. In suspension Jurkat cells, some, but not all, TP10 analogs were able to efficiently reach the cytosol through a pathway that could not be affected by a broad-range cysteine protease inhibitor. No such protease inhibitor-insensitive translocation at low concentrations was observed for the arginine-rich CPP R9, providing evidence that TP10 directly translocates across the plasma membrane.

To reach the cytosol after endocytic internalization, peptides still need to translocate across the endosomal membrane. Although internalization into endosomes can be achieved with high efficiency for most biomacromolecules, endosomal sequestration still remains a major impediment for the further development of these molecules towards clinically useful drugs. When sequestered in endosomes, cargo and vehicles will be exposed to an acidic and hydrolytic environment, which will severely damage the cargo. Assessing the integrity of cargo and/or delivery vehicle over time inside cells is therefore an important analytical aspect in the optimization of delivery constructs. To address this issue, a fluorescence correlation spectroscopy-based method to measure the intracellular stability of CPPs is described in the **sixth chapter**. Next to following degradation over time, the method is also suitable to investigate the specific enzymes that are involved in degradation, whenever specific inhibitors for these enzymes are available.

9.3   From biology to application

As alluded to before, CPPs have the capacity to carry a wide range of cargo into cells. The **seventh chapter** reports on the exploitation of the capacity of the HIV-1 derived CPP Tat to shuttle polymersomes inside cells. Polymersomes are spherical particles that self-assemble from amphiphilic block copolymers. The polymersomes that were applied consisted of polystyrene-polyisocyanopeptide (PS-PIAT), had an average diameter of 114

+/- 28 nm and were loaded with proteins. Conjugation of the Tat peptide to these polymersomes with a copper-free click reaction endowed the polymersomes with the capacity to efficiently enter various cell types. Intracellular trafficking studies indicated that polymersomes were internalized via macropinocytosis and that they were partially directed towards acidic compartments. However, even in these conditions, the polymeric bilayer protected the enzymatic activity, as illustrated by the longer maintenance of the activity of the model enzyme horse-radish peroxidase compared to results from a previous study using free horse-radish peroxidase trafficked to the lysosome. In **chapter eight**, a modular approach for the CPP-mediated delivery of proteins is reported. Also in this study, the model CPP Tat was applied, whereas green fluorescent protein was used as a model cargo. The modular approach consisted of two complementary leucine zippers, of which one was fused to the cargo protein and one to the CPP. The modularity of the approach is also underscored by the fact that CPPs are coupled to the leucine zipper via a copper-free click reaction, which enables the easy and rapid exchange of the CPP that is being employed.

9.4   Future directions

The near future in the field of CPPs and CPP mimics is certainly going to be highly exciting, as the first CPP-based medicines are moving closer to regulatory approval and more and more novel candidates of medicines employing CPP-based functionalities are entering clinical trials (see **chapter two**). It has now become clear that CPP or their evolved counterparts are not merely either 'good' or 'bad' delivery vehicles, but that the context in which they are applied is critical for the chance of success. Moreover, the insights into the general process of cell entry that have been generated over the last decade through the use of CPPs are tremendous. Emanating from this knowledge, several interesting trends can now be observed in the application of CPP and CPP mimics as drug delivery vehicles or in related fields stimulated by CPP research. Specifically, five promising areas of research can be distinguished. The first is the combination of the pharmacophore and the capacity to internalize in one domain. The most frequently used way to achieve this combination in a peptide is to apply quantitative structure-activity relationship-based algorithms for the identification of cell-permeant proteomimetic peptides [3]. The second trend is the use of the guanidinium group, of which the ability to drive internalization became evident through the field of CPPs, to decorate a variety of transporters, including peptoids, small molecules, carbohydrates or polymers [4-7]. Studies showing that these guanidinium-rich transporters also exploit heparan sulfates for their entry [8] and compete with poly-arginine peptides for internalization [9] support the

hypothesis that the internalization mechanism of CPPs has been successfully transferred to synthetic CPP mimics. The third trend is towards overcoming the relative lack of specificity of CPPs through targeting disease-specific interactions or characteristics. The approach is reminiscent of the use of small molecules, which also generally have a system-wide distribution and only achieve specificity through targeting molecules and/or molecular pathways implicated in disease. An example of this approach is the Tat-mediated delivery of siRNA against proteins involved in oncogenic pathways [10]. In this case, specificity was not obtained through selective delivery, but through targeting proteins that are overexpressed or constitutively active exclusively in tumors. A second example is the use of antisense oligonucleotides aimed at splice correction in Duchenne muscular dystrophy using Pip5 transduction peptides, leading to the production of a functional dystrophin protein [11]. In the last case, however, specificity was further enhanced through local intramuscular injections in a recent successful clinical I trial [12]. A fourth research area of active interest is the generation of stimuli-responsive CPPs. Here, the CPP functionality is exposed upon encountering a certain trigger. A prominent example of this approach is the use of a tissue- or tumor-specific protease activity to cleave a linker connecting a CPP and an anion stretch that forms an activity-inhibiting ionic interaction with the cationic CPP before cleavage [13]. A promising new direction in this field is the *in vivo* selection for the cleavage site using phage display, which obviates the need for any *a priori* knowledge on the nature of the tumor protease activity [13]. The last notable direction in which the CPP field is moving is towards tissue-specific CPPs. Various selection strategies have been developed or are now in development that aim to identify tissue-specific CPPs, with the promise to improve the selectivity and therefore potentially reduce side effects when conjugated with bioactive moieties [14-16].

9.5   Conclusion

In conclusion, much of what has been learned from CPPs, from the improved understanding of the pathways of cellular entry to the molecular determinants that are required for efficient cell entry, is driving progress and fostering innovation in drug delivery research far beyond the specific field of CPPs. Therefore, it is safe to say that the research into the biology of CPPs has already made important contributions to the fields of biology and medicine in general and drug delivery in particular, irrespective of whether the future will see many next-generation medicines entering the clinic in which the CPP as such is still recognizable. Against this background, I also hope that through generating key novel insights into the biology of CPPs, the relevance of this thesis is not just restricted to

the scientific field of CPPs, but that it represents a valuable contribution to the whole field of drug delivery.

9.6   References

[1] B. Leader, Q.J. Baca, D.E. Golan, Protein therapeutics: a summary and pharmacological classification, Nat Rev Drug Discov, 7 (2008) 21-39.

[2] F. Duchardt, M. Fotin-Mleczek, H. Schwarz, R. Fischer, R. Brock, A comprehensive model for the cellular uptake of cationic cell-penetrating peptides, Traffic, 8 (2007) 848-866.

[3] M. Hällbrink, K. Ilk, A. Elmquist, P. Lundberg, M. Lindgren, Y. Jiang, M. Pooga, U. Soomets, Ü. Langel, Prediction of Cell-Penetrating Peptides, International Journal of Peptide Research and Therapeutics, 11 (2005) 249-259.

[4] L. Elson-Schwab, O.B. Garner, M. Schuksz, B.E. Crawford, J.D. Esko, Y. Tor, Guanidinylated neomycin delivers large, bioactive cargo into cells through a heparan sulfate-dependent pathway, J Biol Chem, 282 (2007) 13585-13591.

[5] A. Membrino, M. Paramasivam, S. Cogoi, J. Alzeer, N.W. Luedtke, L.E. Xodo, Cellular uptake and binding of guanidine-modified phthalocyanines to KRAS/HRAS G-quadruplexes, Chem Commun (Camb), 46 (2010) 625-627.

[6] T.B. Potocky, J. Silvius, A.K. Menon, S.H. Gellman, HeLa cell entry by guanidinium-rich beta-peptides: importance of specific cation-cell surface interactions, Chembiochem, 8 (2007) 917-926.

[7] P.A. Wender, W.C. Galliher, E.A. Goun, L.R. Jones, T.H. Pillow, The design of guanidinium-rich transporters and their internalization mechanisms, Adv Drug Deliv Rev, 60 (2008) 452-472.

[8] A.V. Dix, L. Fischer, S. Sarrazin, C.P. Redgate, J.D. Esko, Y. Tor, Cooperative, heparan sulfate-dependent cellular uptake of dimeric guanidinoglycosides, Chembiochem, 11 (2010) 2302-2310.

[9] N.W. Luedtke, P. Carmichael, Y. Tor, Cellular uptake of aminoglycosides, guanidinoglycosides, and poly-arginine, J Am Chem Soc, 125 (2003) 12374-12375.

[10] H. Michiue, A. Eguchi, M. Scadeng, S.F. Dowdy, Induction of in vivo synthetic lethal RNAi responses to treat glioblastoma, Cancer Biol Ther, 8 (2009) 2306-2313.

[11] H. Yin, A.F. Saleh, C. Betts, P. Camelliti, Y. Seow, S. Ashraf, A. Arzumanov, S. Hammond, T. Merritt, M.J. Gait, M.J. Wood, Pip5 transduction peptides direct high efficiency oligonucleotide-mediated dystrophin exon skipping in heart and phenotypic correction in mdx mice, Mol Ther, 19 (2011) 1295-1303.

[12] H. Yin, H. Moulton, C. Betts, M. Wood, CPP-directed oligonucleotide exon skipping in animal models of Duchenne muscular dystrophy, Methods Mol Biol, 683 (2011) 321-338.

[13] M. Whitney, J.L. Crisp, E.S. Olson, T.A. Aguilera, L.A. Gross, L.G. Ellies, R.Y. Tsien, Parallel in vivo and in vitro selection using phage display identifies protease-dependent tumor-targeting peptides, J Biol Chem, 285 (2010) 22532-22541.

[14] E. Vives, J. Schmidt, A. Pelegrin, Cell-penetrating and cell-targeting peptides in drug delivery, Biochim Biophys Acta, 1786 (2008) 126-138.

[15] M. Zahid, X. Lu, Z. Mi, P.D. Robbins, Cationic and tissue-specific protein transduction domains identification, characterization, and therapeutic application, Adv Genet, 69 (2010) 83-95.

[16] M. Zahid, P.D. Robbins, Identification and characterization of tissue-specific protein transduction domains using peptide phage display, Methods Mol Biol, 683 (2011) 277-289.

Nederlandse samenvatting

Door het ontcijferen van het menselijke genoom is men veel meer over de biologie van ziektes te weten gekomen. Echter, tot nu toe heeft die kennis helaas nog niet geleid tot veel nieuwe medicijnen. Een voorname reden is dat het bijzonder moeilijk is om de manier waarop eiwitten met elkaar communiceren te blokkeren met 'klassieke' medicijnen zoals die tegenwoordig veelal door de farmaceutische industrie gemaakt worden. Gelukkig zijn er veel nieuwe ideeën voor andere soorten medicijnen, meestal gebaseerd op biologische moleculen zoals eiwitten of DNA. Hoewel men de laatste jaren aanzienlijke vooruitgang heeft geboekt met de ontwikkeling van deze 'next-generation' medicijnen, blijft het nog altijd moeilijk om de medicijnen op de juiste plek in het lichaam te krijgen. Met name bij het in de cel krijgen van grote moleculen van therapeutische waarde blijken veel factoren een rol te spelen.

Dit proefschrift gaat over een veelbelovende methode om de toekomstige biologische medicijnen in de cellen te krijgen: de toepassing van cel-penetrerende peptiden, die vanaf dit punt CPP's zullen worden genoemd. CPP's zijn zeer kleine eiwitten waarvan onderzoekers ongeveer 20 jaar geleden hebben aangetoond dat ze in staat zijn om veel grotere moleculen, waaronder grote eiwitten, de cel binnen te brengen. Het belangrijkste doel van dit proefschrift is om een beter inzicht te genereren in hoe deze kleine eiwitten het transport van grote moleculen in de cel bewerkstelligen, met het onderliggende doel om CPP's als bouwstenen in toekomstige medicijnen te gaan gebruiken. In het **eerste hoofdstuk** wordt een algemene inleiding gegeven over de huidige stand van zaken in medicijnontwikkeling. Daarnaast worden in het eerste hoofdstuk ook CPP's geïntroduceerd en worden hun belangrijkste eigenschappen uiteengezet.

Omdat bijwerkingen van essentieel belang zijn voor ieder medicijn, is het ook belangrijk om te weten of CPP's mogelijke bijwerkingen hebben. Gedurende de laatste tien jaar zijn er inderdaad een aantal studies gepubliceerd waarin duidelijk werd dat CPP's niet enkel potentiële medicijnen de cel binnen brengen door te functioneren als een zogeheten *Trojaans paard*, maar dat ze tevens belangrijke interacties aangaan met cellen die de basis kunnen vormen van bijwerkingen. Kennis over de aspecten van de CPP die verantwoordelijk zijn voor de bijwerkingen kan helpen bij de ontwikkeling van nieuwe varianten van CPP's die deze bijwerkingen niet hebben. Met deze overwegingen als basis is het **tweede hoofdstuk** geschreven. In dit hoofdstuk wordt een overzicht gegeven geven van de biologische effecten die CPP's en andere medicijntransporters kunnen hebben op cellen en in het lichaam.

Het derde tot en met het vijfde hoofdstuk behandelen mechanismes die de CPP's gebruiken om cellen binnen te komen. Het **derde hoofdstuk** beschrijft een mechanisme dat reeds enkele jaren eerder beschreven werd, maar waarover een onvoldoende begrip bestond wat betreft het onderliggende moleculaire werkingsmechanisme. De hypothese die ten grondslag lag aan deze studie was dat CPP's, mits aanwezig in hoge concentratie, het enzym zure sphingomyelinase kunnen activeren voor een opnamemechanisme dat werkzaam is bij hoge CPP concentraties. Dit actieve enzym catalyseert vervolgens de omzetting van het lipide sphingomyeline naar ceramide en fosforylcholine, waarbij ceramide een cruciale rol speelt bij het werkingsmechanisme dat leidt tot opname.

De aanleiding van het **vierde hoofdstuk** was de vergelijking van CPP's die opgebouwd zijn uit L-aminozuren met CPP's die opgebouwd zijn uit D-aminozuren. CPP's opgebouwd uit L-aminozuren kunnen worden afgebroken door enzymen in het lichaam, terwijl CPP's gemaakt met D-aminozuren volledig stabiel zijn. De conventionele gedachte was dat beide CPP's met gelijke efficiëntie de cel binnen gaan. Echter, de experimentele bevindingen laten zien dat dit niet het geval is. In de meeste cellen die getest zijn, zijn CPP's gemaakt van L-aminozuren duidelijk actiever. In het bijzonder zijn er duidelijke aanwijzingen dat opname van CPP's een proces is dat uit twee stappen bestaat. De eerste stap is dat ze binden aan suikers die vastzitten aan de membraan van de cel. De tweede stap is dat ze de cel binnen gaan. Bevindingen die worden beschreven in het **vierde hoofdstuk** laten zien dat enkel de tweede stap afhangt van het type aminozuur; de binding aan de suikers die vastzitten aan het membraan is vrijwel identiek.

In **hoofdstuk vijf** wordt een ander type CPP onderzocht dan wat gebruikt is in de voorgaande studies. Het betreft een chimeer CPP dat opgebouwd is uit een deel van het neuropeptide galanin en het wespengif mastoparan. Deze CPP gaat meer directe interacties aan met de celmembraan en is al bij lagere concentraties toxisch in vergelijking met andere typen CPP's. Diverse varianten van deze CPP zijn onderzocht die slechts op één punt van elkaar afwijken. Hierdoor was het mogelijk was om subtiele veranderingen in het peptide te koppelen aan het biologische gedrag. Deze studie laat zien dat kleine modificaties sterke effecten kunnen hebben op diverse CPP eigenschappen zoals opname-efficiëntie, binding aan de celmembraan en toxiciteit.

Wanneer CPP's de cel binnen gaan, zijn ze nog niet altijd op de plek van bestemming. Normaal gesproken worden ze via endosomen, hetgeen afgesloten compartimenten zijn, de cel binnen gebracht. De vloeistof waarin deze compartimenten zich bevinden, het cytosol, of de kern, waarin zich het DNA bevindt, is vaak de eindbestemming van de CPP-gebaseerde medicijnen. Om veelbelovende therapieën te kunnen optimaliseren is het

belangrijk om te weten in hoeverre CPP's of vergelijkbare constructen nog intact zijn nadat ze door de cel zijn opgenomen. Om dit te kunnen onderzoeken wordt in het **zesde hoofdstuk** een methode beschreven om te analyseren in hoeverre de CPP's die de cellen zijn binnengegaan nog intact zijn. Daarnaast worden ook methodes beschreven om te onderzoeken welke enzymen betrokken zijn bij de afbraak van de CPP's binnen de cel.

Hoofdstuk zeven is het eerste hoofdstuk van dit proefschrift dat een directe applicatie bevat van CPP's. In dit hoofdstuk wordt gebruik gemaakt van de capaciteit van CPP's om grote structuren de cel binnen te brengen. Een CPP afkomstig van het HIV virus, genaamd Tat, werd gebruikt om een artificieel organel, een soort plastic bol gevuld met enzymen, de cel binnen te brengen. Dit artificiële organel, ook wel polymersoom genoemd, heeft een gemiddelde diameter van 114 +/- 28 nm en was na koppeling met de CPP in staat om diverse celtypes binnen te komen. Doordat de eiwitten omringd waren door een plastic wand werden ze beschermd tegen schade die door cellulaire eiwitten aangebracht zou kunnen worden. Een tweede toepassing van CPP's in dit proefschrift wordt beschreven in **hoofdstuk acht**, hetgeen een modulair systeem betreft dat gebruikt kan worden om op eenvoudige wijze verschillende eiwitten naar cellen binnen te brengen. Het systeem maakt tevens gebruik van de HIV-afkomstige CPP Tat en was gekoppeld aan een leucine zipper. Een complementaire leucine zipper was gekoppeld met het fluorescente eiwit green fluorescent protein (GFP), dat als model eiwit fungeerde. Aangezien de twee complementaire leucine zippers sterk aan elkaar binden, wordt de transport functie van de CPP gebruikt om het eiwit de cel binnen te krijgen. Er is geen sprake van een directe koppeling tussen de CPP en het te transporteren eiwit. Daarom is het relatief gemakkelijk om het type eiwit dat moet worden afgeleverd uit te wisselen.

De nabije toekomst in het CPP veld zal een spannende periode worden, nu de eerste CPP-gebaseerde medicijnenkandidaten dichter bij goedkeuring komen om als medicijn gebruikt te worden. Het is nu ook duidelijk dat CPP's niet zonder meer 'goed' of 'slecht' zijn, maar dat hun waarde sterk afhangt van de specifieke applicatie. Ook is het duidelijk dat CPP's, onafhankelijk van hun eventuele toekomstige toepassing in de kliniek, al belangrijke inzichten hebben gegenereerd die van grote waarde zijn in het onderzoeksveld van het gericht afleveren van medicijnen. In het licht van deze overwegingen hoop ik dat de inzichten in de biologie van CPP's die in dit proefschrift beschreven worden niet slechts een waardevolle contributie zijn voor het CPP onderzoeksveld, maar tevens van waarde zullen zijn voor het veld van gerichte medicijnafgifte als geheel.

Curriculum Vitae

Wouter Verdurmen werd op 8 maart 1983 geboren te Hulst. In 2001 haalde hij zijn VWO-diploma aan het Reynaertcollege in Hulst. Een jaar later begon hij aan de studie Bedrijfscommunicatie in Nijmegen, waarvan hij in 2003 zijn propedeuse haalde. In datzelfde jaar switchte hij naar Biomedische Wetenschappen en in 2006 deed hij zijn bachelorstage bij dr. Fons van der Loo op het gebied van gentherapie bij reumatoïde artritis. In het eerste jaar van zijn Master Biomedische wetenschappen onderzocht hij tijdens een onderzoeksstage in de groep van professor Wim de Grip de activatie van G-eiwitten. Tijdens het tweede jaar ging hij naar de Universiteit van Oxford voor een stage in de groep van Tony Watts over de G-eiwit gekoppelde receptor de neurotensin receptor type 1. Na in 2008 zijn master cum laude behaald te hebben is hij direct begonnen met zijn promotie onder begeleiding van professor Roland Brock op het gebied van cell-penetrating peptides. De resultaten van zijn promotieproject staan in dit proefschrift beschreven. Aan het einde van zijn promotie heeft hij een Rubicon beurs van NWO gekregen waarmee hij vanaf 1 september 2012 een tweejarig onderzoek doet als postdoc aan de universiteit van Zürich onder begeleiding van professor Andreas Plückthun. In het kader van het onderzoeksproject zal getracht worden om eiwitten als medicijn te ontwikkelen voor toepassingen in cellen.

List of publications

Ruttekolk IR, Witsenburg JJ, Glauner, H, Bovee-Geurts PH, Ferro ES, Verdurmen WP, Brock R. The intracellular pharmacokinetics of terminally capped peptides. Mol Pharm. (2012). 9:1077-1086

Verdurmen WP, Bovee-Geurts P, Wadhwani P, Ulrich A, Hällbrink M, van Kuppevelt T, Brock. R. Preferential uptake of arginine-rich L- versus D-amino acid cell-penetrating peptides in a cell type-dependent manner. Chem Biol. (2011) 18:1000-1010.

Verdurmen WP, Brock R. Biological responses towards cationic peptides and drug carriers. Trends Pharmacol Sci. (2011) 32: 116-124

Hansen MB, Verdurmen WP, Leunissen, EH, Minten I, van Hest JC, Brock R, Löwik DW. A modular and non-covalent transduction system for leucine zipper-tagged proteins. Chembiochem. (2011) 12: 2294-2297

Ruttekolk IR+, Verdurmen WP+, Chung YD, Brock R. Measurements of the Intracellular Stability of CPPs. Methods Mol Biol. (2011) 683: 69-80.
+ these authors contributed equally

Lorenz C, Fotin-Mleczek M, Roth G, Becker C, Chau Dam T, Verdurmen WP, Brock R, Probst J, Schlake T. Protein expression from exogenous mRNA: Uptake by receptor-mediated endocytosis and trafficking via the lysosomal pathway. RNA Biol. (2011) 8: 627-636

Ruttekolk IR, Chakrabarti A, Richter M, Duchardt F, Glauner H, Verdurmen WP, Rademann J, Brock R. Coupling to polymeric scaffolds stabilizes biofunctional peptides for intracellular applications. Mol Pharmacol. (2011) 79: 692-700

Verdurmen WP, Thanos M, Ruttekolk IR, Gulbins E, Brock R. Cationic Cell-Penetrating Peptides Induce Ceramide Formation via Acid Sphingomyelinase: Implications for Uptake. J Control Release (2010) 147:171-179

Verdurmen WP+, van Dongen SF+, Peters RJ, Nolte RJ, Brock R, van Hest JC. Cellular Integration of an Enzyme-Loaded Polymersome. Angew Chem Int Ed Engl. (2010) 49: 7213-7216.
+ these authors contributed equally

Duchardt F, Ruttekolk IR, Verdurmen WP, Lortat-Jacob H, Bürck J, Hüfnagel, H, Fischer R, van den Heuvel, M, Löwik, DW, Vuister GW, Ulrich A, de Waard M, Brock R. A cell-penetrating peptide derived from human lactoferrin with conformation-dependent uptake efficiency. J Biol Chem. (2009) 284: 36099-36108

Dankwoord

Ondanks de hardnekkige perceptie bij sommigen, promoveren doe je niet alleen. Dit is in het bijzonder van toepassing op mijn promotie, want ik heb gedurende de afgelopen jaren het geluk gehad om met zéér veel mensen samen te werken, zowel kleinschalig als grootschalig. In mijn geval had ik dubbel geluk, want het waren stuk voor stuk erg fijne samenwerkingsverbanden! De volgende mensen wil ik in het bijzonder bedanken:

De keuze met wie ik moet beginnen om te bedanken is voor mij eenvoudig, dat is mijn promotor. Roland, bedankt voor het snel en adequaat beantwoorden van al mijn vragen, voor alle tijd die je in mijn ontwikkeling hebt gestoken, voor de kennis die ik van je heb opgedaan en voor het altijd positief en optimistisch blijven. Wat mij betreft heb je je taak als promotor duidelijk overstegen.

Daarnaast wil ik ook zeker mijn voorganger op het gebied van cell-penetrating peptides in onze groep, Ivo, bedanken. Gedurende de eerste periode van mijn promotie ben jij degene geweest die me op weg heeft geholpen in het lab. Binnen deze korte periode heb ik ontzettend veel van je geleerd, in het bijzonder confocale microscopie en fluorescentie correlatie spectroscopie.

Ook van de rest van de groep heb ik veel opgestoken. In het bijzonder zou ik daarvoor Jenny en Petra willen bedanken. Van jullie heb ik meer geleerd dan jullie je waarschijnlijk realiseren. Niettemin omdat ik ook al van jullie kennis gebruik mocht maken tijdens mijn masterstage enkele jaren eerder! En Merel en Theo, bijzonder bedankt voor het helpen bij het voorbereiden van het proefschrift.

Waar ik onze hele groep voor wil bedanken, is het feit dat er altijd een leuke sfeer in onze groep heerste. Er zijn heel wat mensen gekomen en gegaan tijdens de vier jaren die ik hier heb rondgelopen, maar de goede sfeer is gelukkig altijd gebleven. Dus daar wil ik jullie stuk voor stuk voor bedanken: Alokta, Giel, Ivo, Jenny, Joris, Judith, Marco, Merel, Michael, Petra, Rike, Sip, Theo, Wim en Yi-Da. Ook mijn studenten Jos, Lauke, Robyn en Sabine wil ik erg bedanken voor hun nuttige werk.

` Dat onderzoek leuk is, werd mij (onder andere) duidelijk uit de samenwerking met jou, Stijn. Er was maar één enthousiast telefoontje van mij nodig over mysterieuze blauwe

naalden die uit cellen kwamen en je stond al bij het NCMLS op de stoep om deze blauwe naalden samen te bewonderen én vast te leggen met de digitale camera. Jij wist me te vertellen dat het kristalnaalden waren. De leuke herinneringen aan dit experiment hebben me mede overtuigd om het op de cover te plaatsen. Het plezier wat ik had in de samenwerking op het gebied van de polymersomes heb ik gelukkig kunnen voortzetten met Ruud, en geldt in even zo grote mate voor het project met Morten en Dennis met de leucine zippers. Dus jullie ook bedankt voor de fijne samenwerking! In het bijzonder wil ik ook Jan noemen. Jou wil ik niet alleen bedanken voor de fijne samenwerking, maar natuurlijk ook voor de tijd en energie die je hebt gestoken in het meedenken over en mogelijk maken van de volgende stap in mijn carrière.

In addition, I would like to express my thanks for the nice collaboration on the R9-chimearas and the TP10 analogs with Parvesh and Anne. Currently, close to the end of my project, the project is even taking a very interesting twist, so I'm sure our collaboration on this topic will continue for at least a little while from the time of this writing.

Weer terug naar het Nederlands, wil ik verdergaan met het bedanken van diegenen die mij niet direct op de werkvloer hebben geholpen, maar zeker wel indirect met het opladen van de batterij. En dat kan op verschillende manieren: door het voeren van geanimeerde discussies, uiteraard onder het genot van een drankje, in café Jos; door het bijwonen van gezellige etentjes en feestjes, zowel binnens- als buitenshuis; door het kijken van de (alle) films uit de IMDB top 250, door het ophalen van oude herinneringen; en door samen stoom af te blazen tijdens het hardlopen, in het zwembad, op de fiets of in de bergen. Dus iedereen die één of meerdere van deze activiteiten met mij gedaan heeft: bedankt!

Ook wil ik diegenen bedanken die zonder twijfel de grootste bijdrage hebben geleverd aan het mij brengen waar ik nu ben: mijn ouders, Dennis, Erwin en Noël. Ik wil jullie bedanken voor de onvoorwaardelijke steun, mijn keuzevrijheid, en voor het geven van het goede voorbeeld.

Net zo makkelijk als de keuze met wie het dankwoord te beginnen is ook de keuze met wie het dankwoord te eindigen. Hoe kan het ook anders, dat ben jij, Sascha. Bedankt voor het zijn van de de reden dat ik na iedere werkdag, hoe leuk ik het ook vind om te werken, zelfs met nog meer plezier naar huis ga.